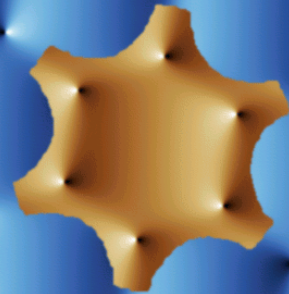


FisEs '23

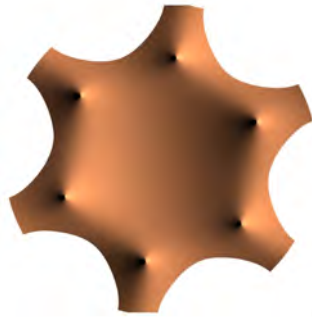


XXIV Congreso de Física Estadística

Pamplona
25-27 octubre de 2023

Departamento de Física
y Matemática Aplicada

Universidad de Navarra



XXIV Congreso de **Física Estadística**

Pamplona, 25 a 27 de octubre de 2023

Libro de resúmenes

Departamento de Física y Matemática Aplicada

Universidad de Navarra

Organismos patrocinadores



GEFENOL
Real Sociedad
Española de Física



Universidad de Navarra

Organiza



Departamento de Física y Matemática Aplicada
Universidad de Navarra
Irunlarrea s/n, E – 31080 Pamplona, Spain

© FisEs23, 2023.

Cubierta: Convección de Bénard-Marangoni
(Reconstrucción numérica)

Comité Científico

- Enrique Abad (U. de Extremadura)
- Rosa María Benito (U. Politécnica de Madrid)
- Javier Burguete (U. de Navarra)
- Alvaro Domínguez (U. de Sevilla)
- Eva González Noya (IQF Rocasolano, CSIC)
- Cristina Masoller (U. Politècnica de Catalunya)
- Manuel Matías (IFISC, UIB-CSIC)
- Juan José Mazo (U. Complutense de Madrid)
- Alberto Pérez-Muñuzuri (U. Santiago de Compostela)
- David Reguera (U. de Barcelona)
- Irene Sendiña (U. Rey Juan Carlos)
- Joaquín Torres (U. de Granada)

Comité Local

- J. Bragard
- J. Burguete (coord)
- R. Cruz Hidalgo
- A. Garcimartín
- W. González-Viñas
- D. Maza
- M. Maza-Cuello
- R. García-García
- I. Zuriguel

Programa

	Miércoles 25 Oct	Jueves 26 Oct	Viernes 27 Oct
9:00		S2.1 A. Galindo	S5.1 M. San Miguel
9:30		S2.2 C. Mejía-Monasterio	S5.2 J. López-Pedrares
10:00		S2.3 J.M. Romero Enrique	S5.3 H. Pérez-Martínez
10:30		S2.4 J.M. López	S5.4 S. Boccaletti
11:00		S2.5 M. Popescu	S5.5 A. Marín
11:30		Pausa Café	Pausa Café
12:00		S3.1 R. Zambrini	S6.1 V. Garzó
12:30		S3.2 P. Pirker-Díaz	S6.2 M. Aguilar-Janita
13:00		S3.3 J. Ojer	S6.3 L. Alonso Llanes
13:30		S3.4 R. Gutiérrez	S6.4 J. Térmens
14:00		Comida Comedores Universitarios	Comida Comedores Universitarios
14:30		P2 Pósters	S7.1 M. Castro
15:00		Vestíbulo Edif Biblioteca	S7.2 A. Lasanta
15:30	Inscripción y registro		S7.3 G.B. Morales
16:00	Inauguración		S7.4 G. Tirabassi
16:30	S1.1 M.A. Rubio		S7.5 J. Aguirre
17:00	S1.2 M. Maza-Cuello		S7.6 J. Moreno-Gordo
17:30	S1.3 A. Pérez-Cervera		S7.7 S.Varela
18:00	S1.4 M. Martínez-Barbeito		Clausura
18:30	S1.5 N. Ruiz-Pino	Café Despedida	
19:00	P1 Pósters Refresco		
19:30	Vestíbulo Edif Biblioteca	Tesis 3 minutos	
20:00			

Índice

I	Sesión 1. Miércoles 25 Tarde	1
II	Sesión 2. Jueves 26 Mañana, A	9
III	Sesión 3. Jueves 26 Mañana, B	17
IV	Sesión 4. Jueves 26 Tarde	23
V	Sesión 5. Viernes 27 Mañana, A	29
VI	Sesión 6. Viernes 27 Mañana, B	37
VII	Sesión 7. Viernes 27 Tarde	43
VIII	Sesión Póster 1. Miércoles 25 Tarde	53
IX	Sesión Póster 2. Jueves 26 Tarde	115
X	Asistentes al Congreso	179

Parte I

Sesión 1. Miércoles 25 Tarde

Interfacial Shear Rheology: Principles, Experimental techniques and Some Applications.

Miguel A. Rubio¹,

¹Dpto. Física Fundamental, Facultad de Ciencias, Universidad Nacional de Educación a Distancia, Avda. Esparta s/n, Las Rozas, E-28232, Spain

Interfaces appear everywhere in nature separating media or tissues with different constituents, properties, functions, and length scales. Examples of such interfaces are the cell membrane, which is essentially a phospholipid bilayer, the tear film external layer, or dividing surfaces appearing in industrial products such as emulsions, foams, etc.

Fluid-fluid interfaces allow for the preferential adsorption of chemical species, which may modify the physico-chemical properties of the interface. Such modifications are directly related to the interfacial micro-structure and the physico-chemical interactions between the different adsorbed species.

Changes in the surface mechanical properties (rheology) are crucial for the functionality of many industrial processes because they govern crucial aspects such as emulsion or foam stability. Unfortunately, experimental studies of interfacial rheology are difficult mainly due to two different aspects: i) to have a clear understanding of the results it is necessary to perturb the interface using a pure deformation mode, but this is not always easily accomplished in experiments, and ii) a probe at a planar interface feels the drag from both the interface and the bulk fluid phases, such that specific data analysis schemes have to be developed to decouple the interfacial and subphase contributions and extract the interfacial mechanical properties.

In this talk I will give a general description of interfacial rheology by: i) introducing the mathematical representation of interfacial rheological properties, ii) describing in detail the most recent developments in experimental techniques [1, 2, 3] and data analysis schemes [4] in interfacial shear rheology, and iii) presenting the application of such techniques to the study of the two-dimensional melting of fatty acid Langmuir monolayers.

-
- [1] J. Tajuelo, J.M. Pastor, F. Martínez-Pedrero, M. Vázquez, F. Ortega, R.G. Rubio, and M.A. Rubio, *Magnetic microwire probes for the magnetic rod interfacial stress rheometer*, *Langmuir*, **31**, 1410 (2015).
 - [2] J. Tajuelo, J.M. Pastor, and M.A. Rubio, *A magnetic rod interfacial shear rheometer driven by a mobile magnetic trap*. *J. Rheol.* **60**, 1095 (2016).
 - [3] Y. Tein, B.R. Thompson, C. Majkrzak, B. Maranville, D. Renggli, J. Vermant, and N.J. Wagner, *Instrument for measurement of interfacial structure–property relationships with decoupled interfacial shear and dilatational flow: “Quadrotrough”*, *Rev. Sci. Inst.* **93** 093903 (2022).
 - [4] P. Sánchez-Puga, J. Tajuelo, J. M. Pastor, and M.A. Rubio, *Flow field-based data analysis in interfacial shear rheometry*, *Adv. Coll. Interf. Sci.* **288**, 102332 (2021).

Dinámica *stick-slip* inducida por fricción

Martin Maza-Cuello¹, and Diego Maza¹

¹ Departamento de Física y Matemática Aplicada, Facultad de Ciencias, Universidad de Navarra, E-31080 Pamplona, Spain.

En este trabajo estudiamos experimentalmente la dinámica macroscópica de una masa (el “caminante”) sobre una base plana que oscila horizontalmente [1], como se muestra en la Fig. 1. En este sistema, la transición entre fricción estática y dinámica puede provocar que el caminante rectifique el movimiento oscilatorio de la base, generando un desplazamiento neto donde las no linealidades juegan un papel fundamental [2].

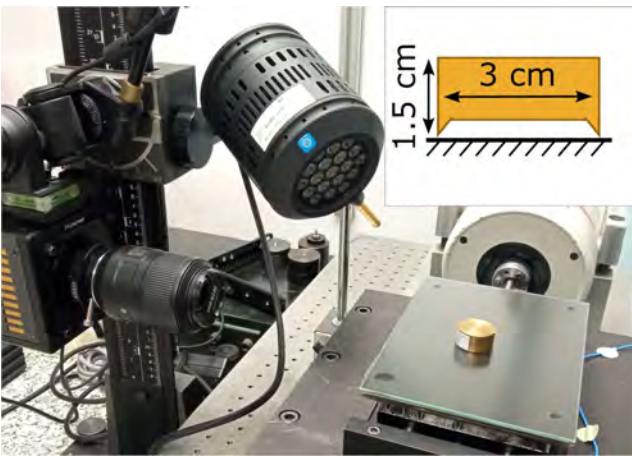


Fig. 1. Vista general del sistema experimental. El detalle muestra las dimensiones relevantes del caminante. La superficie es de vidrio esmerilado y el caminante, de latón.

Cuando la fuerza es sinusoidal, la simetría de la señal impide el transporte. Sin embargo, la dinámica *stick-slip* del caminante tiene una amplitud menor y está desfasada con respecto a la oscilación de la base. A partir de las ecuaciones dinámicas del sistema, se encuentran dos regímenes de oscilación distintos cerca y lejos de la aceleración umbral $\gamma^* = \mu_s g$. Experimentalmente se verifica la existencia de estos dos regímenes, permitiendo obtener buenas estimaciones de los coeficientes de fricción estática (μ_s) y dinámica (μ).

A continuación se estudió una fuerza biarmónica. Se fijó la frecuencia en $f = 20$ Hz y la misma amplitud para ambos armónicos, y se estudió la velocidad de deriva v_D variando dos parámetros: la fase relativa φ entre los armónicos y la aceleración máxima γ . Cuando γ está cerca del umbral, la modulación de la amplitud en función de φ hace que sólo se encuentre deriva para ciertos intervalos de φ . Para γ lejos del umbral, la velocidad de deriva v_D del caminante depende sinusoidalmente con φ como muestra la Fig. 2. La no linealidad del sistema permite además invertir el sentido de transporte para φ fija con tan sólo aumentar γ .

Extendiendo el análisis desarrollado para el caso de la señal sinusoidal pura, se obtuvo una expresión de la velocidad de deriva v_D en función de los parámetros del sistema a partir de una aproximación de *no-stick*. Esta expresión tiene como único parámetro de ajuste el coeficiente de fricción dinámico μ , que se midió previamente para el mismo sistema con la señal sinusoidal. El buen acuerdo con las medidas experimentales, como se muestra en la Fig. 2, valida esta aproximación y permite, para un cierto valor de γ , elegir la fase relativa φ de manera que se maximice v_D .

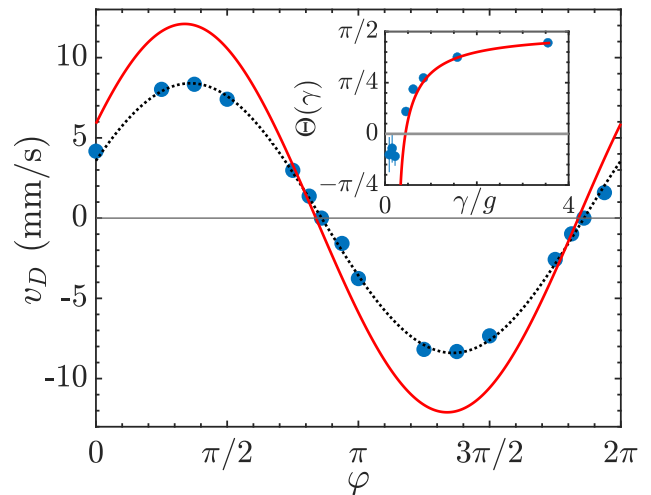


Fig. 2. Velocidad de deriva v_D para $\gamma = 0.62g$ en función de φ . Puntos azules: medidas experimentales (error menor que el tamaño del símbolo). Línea discontinua (en negro): ajuste a una función sinusoidal. Curva continua (en rojo): predicción de la aproximación *no stick*. Recuadro: fase Θ que satisface $v_D(\Theta) = 0$ (sin deriva), en función de la aceleración γ (símbolos como en el panel principal).

Este sistema permite, por tanto, una medida de los coeficientes de rozamiento y la determinación del conjunto de parámetros que maximizan el transporte. Las medidas aquí presentadas resultan un primer paso para caracterizar el transporte debido a otras fuerzas oscilantes o el efecto de la lubricación, además de abrir interrogantes acerca de la dinámica global de un sistema de muchos caminantes fabricados con el mismo o distinto material.

[1] M. Maza-Cuello, D. Maza, enviado a Phys. Rev. Applied.

[2] J. Nath, S. Das, A. Vishwakarma, and A. DasGupta, *Directed transport of a particle on a horizontal surface under asymmetric vibrations*, Physica D **440**, 133452 (2022).

A Universal Description of Stochastic Oscillators

Alberto Perez-Cervera¹, Boris Gutkin², Peter J. Thomas³, and Benjamin Lindner⁴

¹Department of Applied Mathematics & Instituto de Matemática Interdisciplinar. Universidad Complutense de Madrid, Spain

²Group for Neural Theory, LNC2 INSERM U960, DEC, Ecole Normale Supérieure - PSL University, Paris France

³Department of Mathematics, Applied Mathematics, and Statistics, Case Western Reserve University, Cleveland, Ohio

⁴Department of Physics & Bernstein Center for Computational Neuroscience, Humboldt University, Berlin, Germany

Many systems in physics, chemistry and biology exhibit oscillations with a pronounced random component. Such stochastic oscillations can emerge via different mechanisms, for example linear dynamics of a stable focus with fluctuations, limit-cycle systems perturbed by noise, or excitable systems in which random inputs lead to a train of pulses. Despite their diverse origins, the phenomenology of random oscillations can be strikingly similar. Here we introduce a nonlinear transformation of stochastic oscillators to a new complex-valued function $Q_1^*(\mathbf{x})$ that greatly simplifies and unifies the mathematical description of the oscillator's spontaneous activity, its response to an external time-dependent perturbation, and the correlation statistics of different oscillators that are weakly coupled. The function $Q_1^*(\mathbf{x})$ is the eigenfunction of the Kolmogorov backward operator with the least negative (but non-vanishing) eigenvalue $\lambda_1 = \mu_1 + i\omega_1$. The resulting power spectrum of the

complex-valued function is exactly given by a Lorentz spectrum with peak frequency ω_1 and half-width μ_1 ; its susceptibility with respect to a weak external forcing is given by a simple one-pole filter, centered around ω_1 ; and the cross-spectrum between two coupled oscillators can be easily expressed by a combination of the spontaneous power spectra of the uncoupled systems and their susceptibilities. Our approach makes qualitatively different stochastic oscillators comparable, provides simple characteristics for the coherence of the random oscillation, and gives a framework for the description of weakly coupled oscillators.

-
- [1] A. Perez-Cervera, B. Gutkin, P.J. Thomas and B. Lindner, *A Universal Description of Stochastic Oscillators*, Proceedings of the National Academy of Sciences (Accepted 2023)

Dynamical Model for Power Grid Frequency Fluctuations: Application to Islands with High Penetration of Renewables

María Martínez-Barbeito¹, Damià Gomila¹, and Pere Colet¹

¹Instituto de Física Interdisciplinar y Sistemas Complejos (IFISC, CSIC-UIB), Campus Universitat de les Illes Balears E-07122 Palma de Mallorca, Spain

As the transition towards a sustainable energy system accelerates, conventional power plants are progressively replaced by variable renewable energy sources (VRES). This reduces the overall flexibility of the grid, requiring additional control strategies to ensure stable operation.

We propose a model for the high-voltage grid including conventional and variable renewable generation, as well as demand variations [1]. By assimilating load and generation data, our model reproduces frequency fluctuations with the current power mix with a high degree of accuracy. Moreover, it allows to simulate the frequency dynamics for different scenarios with a very high penetration of renewable energy. As a case study, we analyze the power grids of Gran Canaria and the Balearic Islands. We characterize the frequency fluctuations and propose a method to estimate the control needed to keep frequency deviations within statutory limits (50 ± 0.15 Hz).

The model takes the demand and each plant's scheduled generation as input [2], and it gives the frequency and generation at each site. In Figure 1, we compare simulations to actual frequency measurements [3]. We see that the model correctly captures frequency deviations in accordance to power ramps, and it reproduces the frequency time series and the main statistical properties with reasonable accuracy. The discrepancies are mainly associated with the lack of power data with finer temporal and spatial resolution, as well as unknown power plant characteristics.

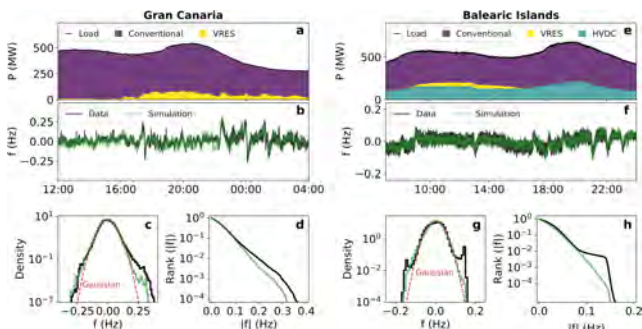


Fig. 1. Model validation. (a,e) Demand-generation balance. (b,f) Frequency-time series, (c,g) probability density, and (d,h) rank-size distribution of frequency fluctuations given by the model in comparison to the data.

Our model can be used as a test bench to study the power grid under different scenarios. In this work, we focus on the effects of a high penetration of VRES. Accordingly, we perform simulations for increasing amounts of VRES in the system. We take 2019 (Gran Canaria) and 2020 (Balearic Islands) as the reference cases, where VRES generation covers a small fraction of the demand, and frequency deviations stay close to the statutory limits.

For Gran Canaria, we increase wind capacity because it is a major resource in the island. As wind power ramps are

magnified, frequency deviations become larger, except for the time windows where the wind generation exceeds the demand. In these cases, we only introduce in the grid the demanded amount and the excess power is simply discarded. This is known as curtailment, which serves as another control mechanism showing benefits to some extent.

In Figure 2b, we show that increasing secondary control reduces the size of all frequency deviations. In [1], we estimated the control needs in winter and summer using a numerical and an analytical approach. As expected, the control needs increase with wind penetration. Up to a certain point, there is a linear relationship between the secondary control gain parameter κ and the installed wind power. However, for larger fractions of installed wind power, there is a plateau due to the curtailment. We obtained a good agreement between the analytical approach and the numerical simulation results for scenarios with up to 4 times the current wind capacity.

For the Balearic Islands, we increase solar photovoltaics, as wind is not viable. The Balearic grid has the peculiarity that it is connected to mainland via a high voltage direct current (HVDC) link. The link provides threshold-like frequency control when the frequency reaches its legal limits [4], leading to characteristic features in the shape of the frequency fluctuations. In scenarios with increasing solar generation, where all conventional power plants are completely disconnected from the grid, the control provided by the link is enough to keep the frequency deviations within the statutory limits [5]. Nonetheless, fluctuations are very fast in the control dead band due to lack of inertia. Having inertia or keeping one conventional plant operating at a minimum power to provide frequency regulation reduces this volatility (Figure 2d).

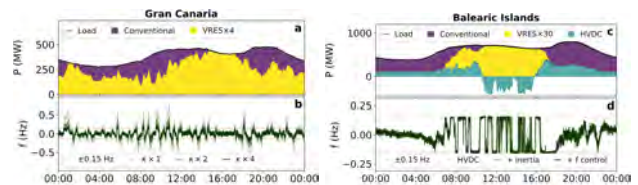


Fig. 2. Increasing VRES. (a,c) Demand-generation balance. (b,d) Frequency-time series for different control scenarios.

- [1] M. Martínez-Barbeito, D. Gomila, P. Colet, *IEEE Trans. Sustain. Energy* (2023). Published online. DOI: 10.1109/TSTE.2022.3231975
- [2] <https://demanda.ree.es/visiona/home>
- [3] <https://power-grid-frequency.org>
- [4] M. Martínez-Barbeito, D. Gomila, P. Colet, *ENERGY Int. Conf. Smart Grids, Green Commun. IT Energy-aware Technol.* (2021).
- [5] M. Martínez-Barbeito, D. Gomila, P. Colet, *Submitted* (2023).

Feedback flashing ratchet: Markovian description, H-theorem and second principle

Natalia Ruiz-Pino¹, and Antonio Prados¹

¹Física Teórica, Apartado de Correos 1065, Universidad de Sevilla, E-41080 Sevilla, Spain

Flashing ratchets are systems where a directed motion of a Brownian particle could be created just by switching on/off a periodic potential. The key is the alternation between two processes: the motion under the action of the potential (while it is on) and free diffusion (while it is off). The protocol for switching the potential can be (i) an open-loop protocol (periodic, random, etc.), where no information of the system is used in the switching, and (ii) a feedback protocol (or closed-loop protocol), for which the switching is based on the information extracted from the system. In the latter case, the directed movement may emerge even for symmetric potentials.

The system that we have focused on is a feedback flashing ratchet, in which the external control measures the position $x(t)$ of an overdamped Brownian particle at regular times t_k [1]. A schematic representation of the system is depicted in Fig. 1. Depending on the information extracted, i.e. the value of $x(t_k)$, the control takes the value $C = 1$ or $C = 0$ and a sawtooth periodic potential $V(x)$ is thus switched on/off in the time interval $I_k = (t_k, t_{k+1})$, i.e. the particle feels a force $-CV'(x)$ during that time interval.

The process of measurement entails an entropy reduction of the particle, since the information extracted by the control (and employed in the update of the potential) concentrates the probability distribution of the particle position in the microstates compatible with the result of the measurement. Very recently, it has been shown that this entropy reduction (i) can be accurately computed by measuring the entropy of long-enough sequences of control actions and (ii) it is essential to define a physically meaningful efficiency of the ratchet [2].

In this work, we present an alternative framework for the study of the feedback flashing ratchet. In particular, we show that (x, C) , i.e. the position of the particle together with the state of the control, is a Markovian stochastic process for which the joint probability $P(x, C, t)$ obeys a differential Chapman-Kolmogorov equation [3]. Specifically, one has

$$\partial_t P = \mathcal{L}_{FP}^{(C)} P + \sum_k \delta(t - t_k) [-\Theta_{1-C}(x) P(x, C, t) + \Theta_C(x) P(x, 1 - C, t)]. \quad (1)$$

where $\mathcal{L}_{FP}^{(C)}$ is the Fokker-Planck operator for the potential $CV(x)$, and $\Theta_C(x) = 1$ ($\Theta_C(x) = 0$) where x would make the control be switched to the value C . The second term on the rhs of Eq. (1), which only acts at the measurement times t_k , accounts from the transitions from $(x, 1)$ to $(x, 0)$ (or vice versa) when the control is switched off (on) at the times t_k .

The Markovian character of the (x, C) process can be intuitively understood, as shown in Fig. 1. At $t = t_k$, when

a measurement takes place, the control value is updated and its value for $t = t_k^+$ depends on the particle position just before the measurement, $x(t_k^-)$. Afterwards, the control value remains constant during the time interval $I_k = (t_k, t_{k+1})$, i.e. until the next measurement. In that time interval I_k , $x(t)$ evolves following an overdamped Langevin equation with potential $CV(x)$. This structure of measurement and Langevin evolution is periodically repeated, showing that the vector (x, C) at time t^+ just depends on its previous value at time t^- .

In this work, we analyse in depth some physical consequences arising from this Markovian description. In particular, we show that it is possible to derive an H -theorem for the differential Chapman-Kolmogorov equation, supporting the existence of a long-time regime in which the ratchet reaches a time-periodic state. We also discuss the implications of this result for the thermodynamic balance, in order to improve our understanding of the second principle—with the contribution of the information gathered by the control.

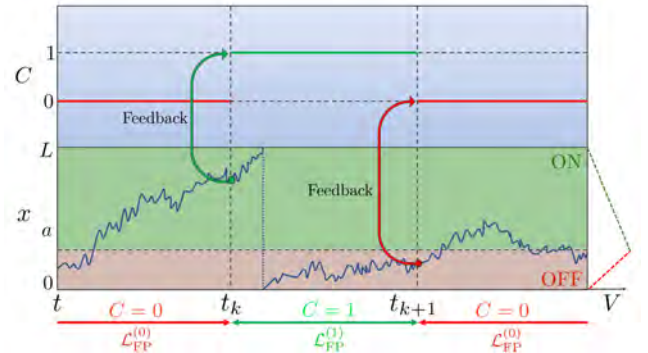


Fig. 1. Schematic evolution of the process (x, C) . In the considered interval, two measurements of the control at times t_k and t_{k+1} take place. By itself, $x(t)$ is not Markovian since, in addition to $x(t^-)$, one needs $C(t^-)$ —which determined whether the potential is on or off—to predict $x(t^+)$. Also, $C(t)$ is clearly non-Markovian, since it is determined by the value of $x(t)$ at the time of the last measurement. Finally, the joint process (x, C) is Markovian because $(x(t^-), C(t^-))$ univocally determines $(x(t^+), C(t^+))$, for all t^-, t^+ , as explained in the text.

-
- [1] F. J. Cao and M. Feito, *Physical Review E* **79**, 041118 (2009).
 [2] N. Ruiz-Pino, D. Villarubia, A. Prados, and F. J. Cao-García, arXiv:2303.16804 (submitted to *Phys. Rev. E*).
 [3] C. W. Gardiner, *Stochastic Methods: A Handbook for the Natural and Social Sciences*, Springer Series in Synergetics (Springer Berlin Heidelberg, 2009).

Parte II

Sesión 2. Jueves 26 Mañana, A

Thermodynamic perturbation theory: applications in coarse-graining and complex-fluid modelling

Amparo Galindo

Department of Chemical Engineering

Institute for Molecular Science and Engineering and Centre for Process Systems Engineering
Imperial College London, London SW7 2AZ, UK

The fundamental phase diagram of a pure substance exhibiting gas, liquid, and solid phases is reasonably well understood. As the pioneering work of van der Waals showed, the fluid phase behaviour of simple fluids can be understood in terms of the balance of spherical repulsive and attractive forces, and even the fluid-solid transition of such systems can be explained in terms of the freezing of a hard-sphere system. A challenge arises, however, when aiming to model accurately the properties and phase behaviour of complex molecules and mixtures such as surfactants, polymers, colloids, peptides, or proteins, which are commonly considered in modelling approaches now. Aiming to treat associating systems, in the thermodynamic perturbation theory of Wertheim an anisotropic intermolecular potential that incorporates short-ranged attractive interactions to form associated aggregates and networks was proposed which greatly enhanced the capability of analytical methods and has, over the years, been extended provide a tool that can be used to study a plethora of complex fluids. I will discuss some of the recent advances in this area; especially the recasting of the free energy expression into a group contribution method, and the advantage of incorporation of generalised Lennard-Jonesium potentials to improve accuracy and predictive ability. Furthermore, with this framework in place, the theory

can also be used to develop force-fields for use in computer simulation, and a link to coarse-grained force fields translatable over thermodynamic states and transferable over systems is possible.

-
- [1] M. S. Wertheim, *Fluids with highly directional attractive forces. I. Statistical thermodynamics*, J. Stat. Phys. **35**, 19 (1984).
 - [2] M. S. Wertheim, *Fluids with highly directional attractive forces. II. Thermodynamic perturbation theory and integral equations*, J. Stat. Phys. **35**, 35 (1984).
 - [3] M. S. Wertheim, *Fluids with highly directional attractive forces. III. Multiple attraction sites*, J. Stat. Phys. **42**, 459 (1984).
 - [4] M. S. Wertheim, *Fluids with highly directional attractive forces. IV. Equilibrium polymerization*, J. Stat. Phys. **42**, 477 (1984).
 - [5] V. Papaioannou, T. Lafitte, C. Avendaño, C. S. Adjiman, G. Jackson, E. A. Müller and A. Galindo, *Group contribution methodology based on the statistical associating fluid theory for heteronuclear molecules formed from Mie segments*, J. Chem. Phys. **140**, 477 (2014).

Dynamic phase transitions in stochastic clustering under confinement

Giulia Janzen¹, and Carlos Mejía-Monasterio²,

¹ Theory of Polymers and Soft Matter, Department of Applied Physics, Eindhoven University of Technology.

² School of Agricultural, Food and Biosystems Engineering, Polytechnic University of Madrid.

When a system of interacting particles is driven out of equilibrium, macroscopic long range correlations emerge even if the interactions are local. An instance exhibiting such behaviour is that of a stochastic lattice gas of interacting particles in which one of the particles is subject to an external field. This Biased Particle (BP) produces changes at the microstructure of the medium (the other particles) that depend on the strength of the external field F and on the density ρ of the medium itself. Bath particles accumulate in front of the BP, creating jamming. This produces a frictional force that compensates the dragging force applied on the probe. As a consequence of the equilibrium between these forces, in the steady state the BP reaches a terminal drift velocity V . In the limit of small field ($F < 1$), the system reaches a viscous regime in which the terminal velocity depends linearly on the field: $V = F/\xi$, with ξ the friction coefficient. Behind the BP, a depleted region appears, with a medium density that approaches the equilibrium density as a long-range power law $\sim x^{3/2}$, meaning that the medium remembers the passage of the BP on large spatial and temporal scales. In confined geometries, these long-range correlations induce a superdiffusive growth of the BP fluctuations [1, 2, 3]. Moreover, when two BPs exist, they interact forming a stable pair that moves together as dragging force is minimised [4, 5].

Here we study the stochastic dynamics of many BPs driven out of equilibrium by an external force and moving in a dense quiescent bath through narrow channels. As the number of these BPs increases, a transition from a mixed phase to a collective pattern of dense clusters and dilute phases sets in, similar to mobility induced phase separation observed for active particles. Clustering is mediated by the interaction with the bath and follows from a stochastic aggregation-fragmentation process. We show that the phase separation persists as confinement stabilises the thermal fluctuations, leading to large and long lived clusters that facilitate the formation of clogs. When the clogs are formed the BPs exhibit a dynamic phase transition from superdif-

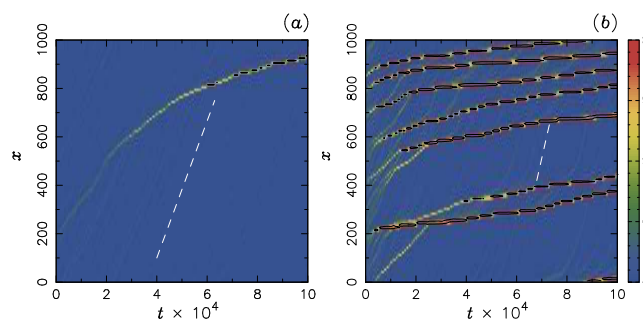


Fig. 1. Formation of clusters at *a*) low and *b*) high density of intruders in a long but narrow channel. Dashed lines indicate intruders evaporating between clusters.

fusion to single-file and entrain the whole system into an anomalous slow dynamics. As a result, dynamics exhibit negative differential mobility.

-
- [1] O. Bénichou, C. Mejía-Monasterio and G. Oshanin, *Anomalous field-induced growth of fluctuations in dynamics of a biased intruder moving in a quiescent medium*, Physical Review E (**87**, 020103 (2013).
 - [2] P. Illien, O. Bénichou and C. Mejía-Monasterio, G. Oshanin, R. Voituriez, *Active transport in dense diffusive single-file systems*, Phys. Rev. Lett. **111**, 038102 (2013).
 - [3] O. Bénichou, A. Bodrova, D. Chakraborty, P. Illien, A. Law, C. Mejía-Monasterio, G. Oshanin and R. Voituriez, *Geometry-induced superdiffusion in driven crowded systems*, Phys. Rev. Lett. **111**, 260601 (2013).
 - [4] C. Mejía-Monasterio and G. Oshanin, *Bias-induced interactions between driven particles in a quiescent medium*, Soft Matter **7**, 993 (2011).
 - [5] O.A. Vasilyev, O. Benichou, C. Mejía-Monasterio, E.R. Weeks and G. Oshanin *Cooperative behavior of biased probes in crowded interacting systems*, Soft Matter **13**, 7617 (2017).

Contribución de Casimir al Hamiltoniano interfacial para el fenómeno de mojado tridimensional

Alessio Squarcini¹, José M. Romero-Enrique^{2,3}, and Andrew O. Parry⁴

¹Institut für Theoretische Physik, Universität Innsbruck.

²Departamento de Física Atómica, Molecular y Nuclear, Universidad de Sevilla.

³Instituto Carlos I de Física Teórica y Computacional.

⁴Department of Mathematics, Imperial College London.

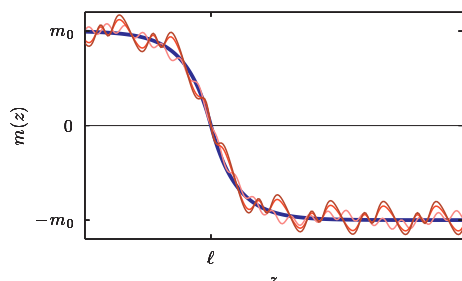


Fig. 1. Esquema del perfil de magnetización de campo medio constreñido $m_\pi(z; \ell)$ (línea azul gruesa) y pequeñas fluctuaciones alrededor de él (líneas delgadas rojas) que también satisfacen el criterio de cruce $m = 0$ para $z = \ell$.

El estudio teórico de las transiciones de mojado tridimensionales (3D) de corto alcance no consideran una contribución de Casimir entrópica o de baja temperatura al potencial efectivo que describe la interacción entre la interfaz y la pared. Esta la determinamos derivando exactamente el modelo interfacial para el mojado 3D a partir de un Hamiltoniano microscópico de tipo Landau-Ginzburg-Wilson Hamiltoniano. El término de Casimir cambia la interpretación de los efectos de fluctuación que ocurren en las transiciones de mojado, de modo que, por ejemplo, ya no se obtienen predicciones de campo medio cuando se ignoran las fluctuaciones interfaciales. Si bien la contribución de Casimir no altera el diagrama de fases superficial, aumenta significativamente la adsorción cerca de una transición de mojado de primer orden y cambia por completo las singularidades críticas predichas para el mojado tricrítico, incluyendo la no universalidad que ocurre en 3D

a partir las fluctuaciones interfaciales. Usando el grupo de renormalización numérico, mostramos que, para el mojado crítico, el régimen asintótico es extremadamente estrecho, observándose un régimen preasintótico en el que el crecimiento de la longitud de correlación paralela está caracterizada por un exponente efectivo en concordancia cuantitativa con las simulaciones del modelo de Ising bajo las mismas condiciones. Ello resuelve una discrepancia histórica entre las predicciones teóricas y los resultados obtenidos por simulación para el fenómeno de mojado crítico tridimensional bajo interacciones de corto alcance.

- [1] A. Squarcini, J. M. Romero-Enrique, and A. O. Parry Phys. Rev. Lett. **128**, 195701 (2022).
 [2] A. Squarcini, J. M. Romero-Enrique, and A. O. Parry Mol. Phys. doi: 10.1080/00268976.2023.2193654 (2023).

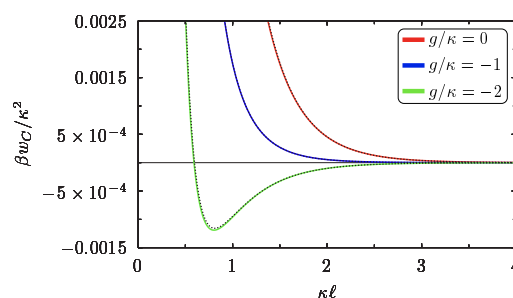


Fig. 2. La contribución de Casimir al potencial efectivo pared-interfaz para una capa de mojado con anchura uniforme ℓ ilustrada para mojado crítico ($g = -2\kappa$), tricrítico ($g = -\kappa$) y de primer orden ($g = 0$).

Lyapunov exponents at the liquid-vapor critical transition

Mauricio Romero-Bastida¹, José Alejandro², and Juan M. López³,

¹SEPI ESIME-Culhuacán, Instituto Politécnico Nacional, 04430 México D.F., México

²Departamento de Química, Universidad Autónoma Metropolitana, 09340, México D.F., México

³Instituto de Física de Cantabria (IFCA), CSIC-Universidad de Cantabria, E-39005 Santander, Spain

Fluids are a prototypical example of chaotic motion at molecular level. In fact, a fluid will generally have very many positive Lyapunov exponents (LEs) associated with the erratic evolution of the microscopic degrees of freedom (position and momenta) of its constituent molecules. Real fluids can be found in two different phases, vapor and liquid, which can also coexist in a certain region of the temperature-density (T, ρ) phase diagram, bounded by the coexistence line. Above the coexistence line the fluid has uniform density, while below the coexistence curve we find two well separated phases of very different density. The coexistence curve has a maximum and terminates at the liquid-vapor critical point (T_c, ρ_c) .

All this is very well-known and understood from basic equilibrium statistical mechanics. However, there is not currently a full understanding of the mechanical instability in the molecular motion at this critical point nor at the coexistence line. For instance, we do not still know how to characterize the liquid-vapor transition or its coexistence in terms of the underlying microscopic dynamics for simple 3D fluids

models. How do the LEs change at the transition? Can we establish a phase change in a fluid by looking only at microscopic dynamics? In other words, what are the fingerprints of a phase change in terms of LEs and Lyapunov vectors?

Here, we couple techniques from nonlinear dynamics and statistical physics to analyze the emergence of the phase of coexistence in the prototypical Lenard-Jones model of a 3D fluid. By means of numerical simulations we show that the largest LE exhibits a dramatic drop at the coexistence curve. Calculation of the inverse participation ratio shows that this LE drop is accompanied by a strong localization of the Lyapunov vector, marking a change in the dominant microscopic instability: from localized to spatially extended Lyapunov modes. We also show that the functional dependence of the LE with temperature (or density) allows to determine the spinodal curve that separates the phase coexistence region from the metastability (supercooled vapor) region. All these results are new and pave the way to understand the liquid-vapor transition in purely dynamical terms.

Self phoretic colloids near interfaces

Mihail N. Popescu

Dept. of Atomic, Molecular, and Nuclear Physics, University of Sevilla, Sevilla (SPAIN)

Chemically active colloids can achieve force- and torque-free motility (“self-propulsion”) via the promotion, on their surface, of catalytic chemical reactions involving the surrounding solution. Such systems are valuable both from a theoretical perspective, serving as paradigms for nonequilibrium processes, as well as from an application viewpoint, according to which active colloids are envisioned to play the role of carriers (“engines”) in novel lab-on-a-chip devices.

The motion of such colloids is intrinsically connected with a “chemical field”, i.e., the distribution near the colloid of the number densities of the various chemical species present in the solution, and with the hydrodynamic flow of the solution around the particle. In most of the envisioned applications, and in virtually all the reported experimental studies, the active colloids operate under spatial confinement (e.g., within a microfluidic channel, a drop, a free-standing liquid film, etc.). In such cases, the chemical field and the hydrodynamic flow associated with an active colloid are influenced by any nearby confining surfaces, and these disturbances couple back to the particle. Thus, an effective interaction with the spatial confinement arises. Consequently, the particle is endowed with means to perceive and to respond to its environment.

In this contribution I present several examples of complex behaviors exhibited by active particles near interfaces (see also the review [1]) and I discuss, by employing simple models of chemical activity and self-phoretic motion [2], the basic physical principles governing the phenomenology.

For Janus spheres (half of the surface is coated with the catalyst; e.g., silica spheres decorated with Pt which promotes decomposition of hydrogen peroxide in the surrounding aqueous solutions in which the particles are suspended) assumed to be moving via a self-phoretic mechanism, it has been often observed that during their motion near walls they exhibit a stable preference for orienting their symmetry axis parallel to the wall [3]. This “sliding” state, Fig. 1(a), can be rationalized as a stable attractor of the overdamped dynamics of a particle which moves, in the absence of external forces or torques acting on it, due to a “phoretic slip” hydrodynamic actuation, proportional to the local tangential gradient in the chemical composition of the solution, at its surface [4]. Based on the concept of sliding states it has been possible to explain the emergence of topographically-guided motion of chemically active particles, i.e., steady-state motion along the edges of patterns imprinted on a wall [3]. Upon further accounting for the emergence of osmotic flows at the walls (due to the same inhomogeneities in the chemical composition of the solution induced by the activity of the particles), additional spatially localized steady states, such as sliding along a chemical stripe or along the edge of chemical stripes, have been predicted [5].

For a Janus particle near a wall, in addition to the sliding state discussed above a second steady state (stable attractor of the dynamics) may exist: the particle hovers at a fixed distance from the wall, while stirring the fluid, Fig. 1(b).

For a Janus particle, this theoretically predicted state, which can exist even in the absence of gravity, has proved difficult to be evidenced experimentally. However, its equivalent for a heavy, uniformly active sphere near a wall turns out to provide the means for a new method of separation of similarly-sized, but surface-properties different, particles [6].

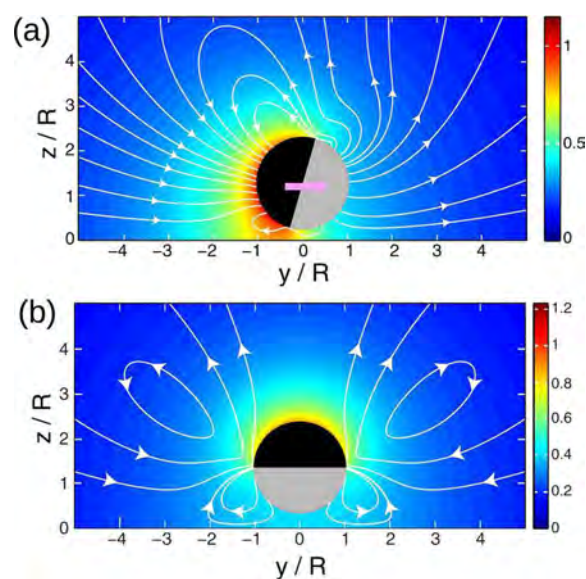


Fig. 1. A chemically active Janus particle in sliding (a) and hovering (b) states above a planar wall. The active part is indicated in black, and the magenta arrow shows the translational velocity of the particle. The white streamlines correspond to the flow field in the laboratory frame. The chemical field $c(r)$ (in units of a characteristic density) is color coded.

-
- [1] M.N. Popescu, W.E. Uspal, A. Domínguez, and S. Dietrich, *Effective Interactions between Chemically Active Colloids and Interfaces*, *Acc. Chem. Res.* **51**, 2991 (2018).
- [2] R. Golestanian, T. Liverpool, and A. Ajdari, *Designing phoretic micro- and nano-swimmers*, *New J. Phys.* **9**, 126 (2007).
- [3] J. Simmchen *et al*, *Topographical pathways guide chemical microswimmers*, *Nat. Commun.* **7**, 10598 (2016)
- [4] W.E. Uspal, M.N. Popescu, S. Dietrich, and M. Tasinkevych, *Self-propulsion of a catalytically active particle near a planar wall: from reflection to sliding and hovering*, *Soft Matter* **11**, 434 (2015).
- [5] W.E. Uspal, M.N. Popescu, M. Tasinkevych, and S. Dietrich, *Shape-dependent guidance of active Janus particles by chemically patterned surfaces*, *New J. Phys.* **20**, 015013 (2018).
- [6] M. Bekir *et al*, *Versatile Microfluidics Separation of Colloids by Combining External Flow with Light-Induced Chemical Activity*, *Soft Matter* **14**, 1002 (2018).
 https://doi.org/10.1002/adma.202300358 .

Parte III

Sesión 3. Jueves 26 Mañana, B

Complex quantum systems for machine learning

Roberta Zambrini

IFISC (CSIC-UIB), Campus UIB, Palma, Spain

In the last decades, Complex Systems have been explored in physical systems also in the quantum regime, with enormous advances both in their theoretical treatment as well as in the ability to detect and manipulate individual quantum objects and couple them under control. Experiments involving complex quantum systems are realized with ions, cold atoms, superconducting circuits, and optical modes, to mention some. Fundamental open questions in this context range from the characterization of novel regimes, like e.g. many-body localization, to the emergence of collective phenomena, like time crystals, to the effects of coherences and many-body correlations, with no classical analog, in processing information. Beyond the theoretical challenges in understanding Complex Quantum Systems, these are crucial also in many applications such as quantum computing, the quantum Internet, or quantum simulations. In this talk I will present some results on the use of complex quantum systems for machine learning purposes.

Non-conventional computing inspired by the brain, (classical) neuromorphic computing, is at present successful approach in a broad spectrum of applications, also burgeoning due to big data availability. Within this context, recently neuromorphic approaches have been proposed also in quantum substrates as non-conventional, mostly analog, forms of machine learning. In this talk we are going to present Quantum Reservoir Computing. The classical version of this approach has been developed in the last 20 years. The idea in a nutshell is to process an input injected into a (complex) physical system and to optimize only the output layer for a certain task, with a considerable advantage with respect to deep neural network settings. Several classical systems have been considered as classical reservoirs ranging from optical, to mechanical or even biological implementations [1]. Moving from classical to quantum physical reservoirs, however, opens a series of new challenging questions, related to fundamental as well as realization aspects. Examples are the identification of the best quantum regimes of operation, the role of statistics, or of quantum coherences and entanglement. Indeed quantum reservoir computing has the potential to remarkably boost the processing performance in temporal tasks by exploiting quantum coherences, not requiring error correction, and it is suited for fully quantum information processing (with quantum inputs).

After introducing the Quantum Reservoir Computing and

showing how memory and non-linearity arise in a quantum formalism, we will discuss the crucial aspect of quantum measurement in the online series processing and propose a solution based on weak measurement [2].

The use of complex (quantum) systems as reservoirs is strongly influenced by their operation regimes, as we will discuss in the context of dynamical phase transitions [3]. A common setting is based on a qubits network (Ising model in transverse field) as a reservoir. This exhibits phenomena like many-body localization or thermalization, which influence the spread and processing of information. Looking at reservoir in these dynamical phases, we establish that the thermal phase is naturally adapted to the requirements of quantum reservoir computing and report an increased performance at the thermalization transition.

Another aspect we will present is the possibility to perform reservoir computing with quantum fluctuations of light, considering Gaussian states of continuous-variable in a photonic network. While these quantum states are insufficient for universal quantum computing, they are nevertheless enough for universal reservoir computing. Tunable nonlinearity is achieved through the injection of the input quantum state [4]. Finally, to address non-trivial temporal tasks, we propose a photonic platform suitable for real-time quantum reservoir computing, and address the effect of statistical noise [5].

-
- [1] Kohei Nakajima, Ingo Fischer, *Reservoir Computing: Theory, Physical Implementations, and Applications* (Springer, 2021)
 - [2] P. Mujal, R. Martinez-Peña, G.L. Giorgi, M.C. Soriano, R. Zambrini, *Time Series Quantum Reservoir Computing with Weak and Projective Measurements*, NPJ Quantum Information 9, 16 (2023)
 - [3] R. Martinez-Peña, G.L. Giorgi, J. Nokkala, M.C. Soriano, and R. Zambrini, *Dynamical phase transitions in quantum reservoir computing* Physical Review Letters 127, 100502 (2021)
 - [4] J. Nokkala, R. Martinez-Peña, G.L. Giorgi, V. Parigi, M.C. Soriano, R. Zambrini, *Gaussian states of continuous-variable quantum systems provide universal and versatile reservoir computing*, Communications Physics 4, 53 (2021)
 - [5] J. Garcia-Beni et al., *Scalable Photonic Platform for Real-Time Quantum Reservoir Computing*, Phys. Rev. Applied 20, 014051 (2023)

Self-regulation of a network of Kuramoto oscillators

Paula Pirker-Díaz¹, Albert Díaz-Guilera^{1,2}, and Jordi Soriano^{1,2}

¹Universitat de Barcelona Institute of Complex Systems (UBICS), Universitat de Barcelona

²Departament de Física de la Matèria Condensada, Universitat de Barcelona

Synchronization is a prevalent phenomenon in nature, observed in various phenomena such as fireflies, pacemaker cells, and crowd clapping [1]. In neuroscience, synchronization plays a pivotal role, particularly in understanding information processing and normal/abnormal brain function. Disorders like epilepsy, Parkinson's, Alzheimer's, autism, and schizophrenia have been associated with alterations in neuronal synchrony. While global synchronization is often excessive in these pathologies, healthy brains exhibit a balance between global and local synchronization. Glial cells, especially astrocytes and oligodendrocytes, influence neuronal oscillations and regulate network activity, contributing to the desired level of synchronization. For instance, glial cell loss in Parkinson's disease can lead to uncontrollable global synchronization [2].

Here we employ numerical simulations to investigate the role of glial cells in synchronization. Although synchronization in networks of oscillators has been extensively studied [3], but recent interest has focused on developing methods to control the behavior of these systems. In this paper, a network of glial cells and neurons is considered, where glial cells regulate the synchronization of the neuronal network they support [4]. The study utilizes a self-regulation model to control global and local synchronization, employing Kuramoto oscillators to represent neuronal populations. The modular structure of the network, inspired by real neuronal networks, is crucial for interesting phenomena to emerge.

The proposed model demonstrates that global synchronization can be significantly reduced while maintaining stable and high levels of local synchronization (see Fig. 1). The study highlights the importance of non-random network structures and their effects on emergent phenomena. The interaction among modules in the network is also examined, revealing interesting patterns that arise and persist during the dynamic evolution of the system. It should be noted that the model is a highly simplified representation of biological neuronal networks, but the obtained results are still intriguing. The findings contribute to the understanding of synchronization and emphasize the significant role played by glial cells in maintaining the desired level of synchronization in the brain.

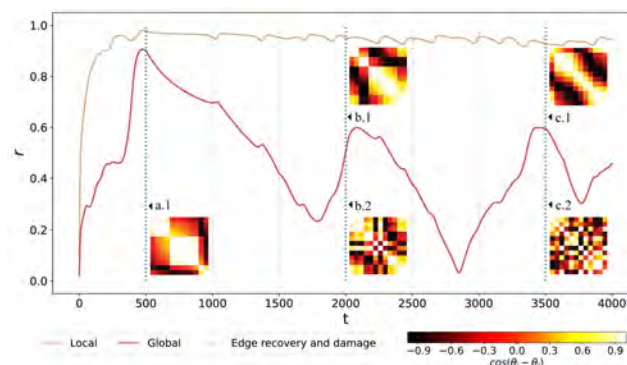


Fig. 1. Time evolution of the global and the local order parameters of a single realization of the model. The plot includes $\cos(\bar{\theta}_i - \bar{\theta}_j)$ matrices at $t = 500$ (case *a*), $t = 2000$ (case *b*) and $t = 3500$ (case *c*). For case *a*, only the plot with the best arrangement for detecting the present communities is shown (*a.1*). For cases *b* and *c* we also show the plots of the matrices conveniently rearranged for each case (*b.1* and *c.1*), but we also include the same matrices rearranged following the same rows and columns order than *a.1* (figs. *b.2* and *c.2*).

- [1] S. H. Strogatz, *Sync: how order emerges from chaos in the universe, nature, and daily life*, 1st. ed. New York, NY, USA: Hyperion, 2003.
- [2] G. Carola, D. Malagarriga, C. Calatayud, et al. "Parkinsons disease patient-specific neuronal networks carrying the LRRK2 G2019S mutation unveil early functional alterations that pre-date neurodegeneration." *npj Parkinsons Dis.* vol. 7, no. 55, 2021.
- [3] A. Arenas, A. Díaz-Guilera, J. Kurths, Y. Moreno and C. Zhou, "Synchronization in complex networks", *Physics Reports*, vol. 469, no. 3, pp. 93-153, 2008.
- [4] E. Bullmore and O. Sporns, "Complex brain networks: graph theoretical analysis of structural and functional systems.", *Nat. Rev. Neurosci.*, vol. 10, pp. 186198, 2009.

Modeling Explosive Opinion Depolarization in Interdependent Topics

Jaume Ojer¹, Michele Starnini^{1,2}, and Romualdo Pastor-Satorras¹

¹Departament de Física, Universitat Politècnica de Catalunya, Campus Nord, 08034 Barcelona, Spain

²CENTAI Institute, 10138 Turin, Italy

Opinion polarization is on the rise, causing concerns for the openness of public debates. Thus, modeling the process of reducing opinion polarization, or *depolarization*, has been the object of recent work. In most cases, such modeling efforts address the simplest case of one-dimensional opinions with respect to a single topic. However, the process of opinion formation may invest multiple interdependent topics at the same time, leading to correlations between opinions that can easily be observed [1]. Here, we propose an analytically tractable model of opinion dynamics, which we name the *social compass model* [2], in a space of two interdependent topics. We observe that this model exhibits a first- or second-order phase transition from polarization to consensus depending on the correlations between opinions.

Let us consider a system of N agents. Each agent i holds opinions towards two distinct topics X and Y , represented by $x_i, y_i \in [-1, 1]$, respectively. We represent these opinions in the polar plane, where the angle θ_i represents the orientation of an individual with respect to both topics, and the radius ρ_i expresses the attitude strength or conviction. For instance, two agents i and j holding extreme and opposite opinions, $x_i = y_i = 1, x_j = y_j = -1$, will be represented in the polar plane by opposite orientations, separated by an angle π . Note that a polar representation of opinions is not novel in political science, where individuals can lay in a plane defined by two major axes, e.g. libertarian vs authoritarian and left vs right [3].

Focusing on the time evolution of the orientation $\theta_i(t)$, a consensus will be reached in the population when all agents will converge towards a similar orientation with respect to the two topics. We model the opinion dynamics with two key assumptions: i) each agent i has a tendency to maintain their initial opinion $\theta_i(0) = \varphi_i$ proportional to their conviction ρ_i (i.e., agents with high conviction are more stubborn and less prone to change their opinion), and ii) agents exert a certain degree of social influence on their peers. We operationalize this simple theoretical framework in the following set of N ordinary differential equations,

$$\dot{\theta}_i(t) = \rho_i \sin[\varphi_i - \theta_i(t)] + \frac{\lambda}{N} \sum_{j=1}^N \sin[\theta_j(t) - \theta_i(t)], \quad (1)$$

where λ is a coupling constant that quantifies the strength of social influence, and where each individual can interact with all other individuals. Furthermore, we assume that their conviction ρ_i will not change over time. By means of a mean-field approach, we find that the nature of the phase transition from a polarized state (agents' opinions are aligned to their initial value) to a depolarized one (agents converge to a consensus as a function of the social influence) depends on the distribution of the polarized initial opinions $P(\varphi)$. Indeed,

correlated opinions represented in the polar plane by a bimodal distribution trigger a second-order –or continuous– transition, whereas uncorrelated opinions represented by a quadrimodal distribution lead to a first-order –or explosive– transition.

We tested our theoretical framework by using real data of initial opinions from the American National Election Studies (ANES) with respect to polarized and interdependent topics. Fig. 1 (a) shows that for correlated opinions regarding religion and same-sex couples (approximately bimodal $P(\varphi)$) we obtain a continuous transition, while Fig. 1 (b) shows that for uncorrelated opinions regarding immigration and military diplomacy (quadrimodal $P(\varphi)$) we obtain an explosive transition with hysteresis.

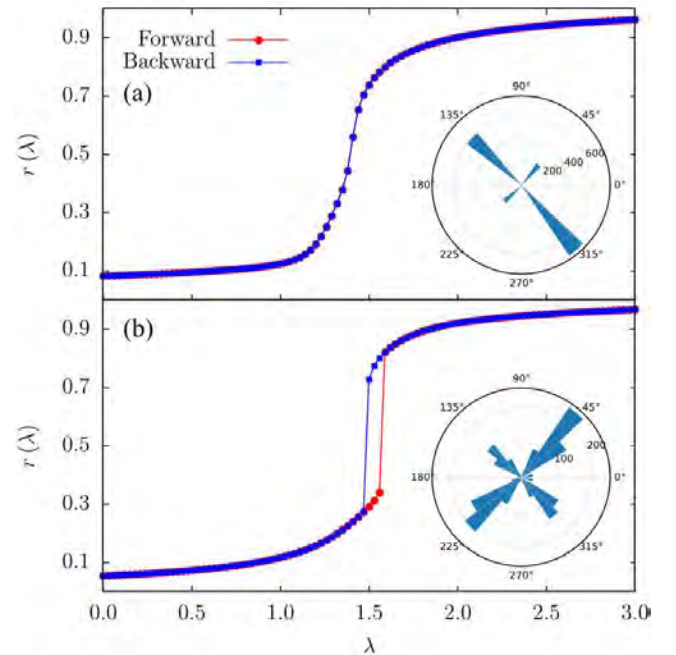


Fig. 1. Main: Order parameter $r(\lambda) = \frac{1}{N} \left| \sum_j e^{i\theta_j(\lambda)} \right|$ including both forward (red) and backward (blue) continuations in λ . Inset: Initial orientation distributions $P(\varphi)$ represented in polar coordinates. We considered correlated (a) and uncorrelated (b) empirical opinions from ANES data regarding two polarized topics.

[1] F. Baumann, P. Lorenz-Spreen, I.M. Sokolov, and M. Starnini, *Phys. Rev. X* **11**, 011012 (2021).

[2] J. Ojer, M. Starnini, and R. Pastor-Satorras, *Phys. Rev. Lett.* **130**, 207401 (2023).

[3] <http://www.politicalcompass.org>

Non-equilibrium criticality in the synchronization of self-sustained oscillators

Ricardo Gutiérrez, and Rodolfo Cuerno

Grupo Interdisciplinar de Sistemas Complejos (GISC), Departamento de Matemáticas,
Universidad Carlos III de Madrid, 28911 Leganés, Madrid, Spain

Synchronization is a pervasive collective phenomenon frequently displayed by systems of scientific interest across disciplines, from neurons and circadian rhythms to lasers and qubits [1]. The study of synchronous dynamics has traditionally focused on the identification of threshold parameter values for the transition to synchronization, and on the nature of such transition. The dynamical process whereby systems of self-sustained oscillators synchronize, however, has been devoted much less attention. The fact that one might reasonably expect this process to be strongly system-dependent probably explains why such an important aspect of synchronization remains poorly understood.

In a recent contribution [2], we have shown that, in fact, the synchronization process displays robust universal features, some of which have been previously studied in the literature on kinetic roughening of interfaces. This is another active branch of contemporary statistical physics that studies universal properties in non-equilibrium growth processes, covering also a great diversity of cases, including, for instance, coffee ring formation, bacterial growth and natural and artificial deposition processes [3]. The overlap between the two fields originates in a mathematical connection between synchronization models and the equations of surface growth, which has been discussed in the literature [1], but whose dynamical implications do not seem to have been investigated until now. Indeed, starting from a system of phase oscillators (i.e. idealized dissipative dynamical systems with an attracting limit cycle) at the sites of a lattice, and performing a continuum approximation, for a relatively slow spatial variation of the phase field $\phi(\mathbf{x}, t)$, as occurs for coupling strengths well into the synchronized regime, the dominant contributions yield

$$\partial_t \phi(\mathbf{x}, t) = \omega^*(\mathbf{x}) + \nu \nabla^2 \phi(\mathbf{x}, t) + \frac{\lambda}{2} [\nabla \phi(\mathbf{x}, t)]^2. \quad (1)$$

Eq. (1), which features the same deterministic derivative terms as the standard Kardar-Parisi-Zhang (KPZ) equation, is known the KPZ equation with columnar noise [4].

In Ref. [2], by means of a detailed numerical study of one-dimensional systems of phase oscillators coupled through a function containing just one Fourier component, we provide strong evidence indicating that the synchronization process in these systems is characterized by forms of generic scale invariance associated with the universality classes of kinetically rough interfaces with columnar disorder. Specifically, for Kuramoto coupling the relevant universality class is that of the Edwards-Wilkinson equation with columnar noise, while for generic couplings it is that of the KPZ equation with columnar noise. Moreover, the phase fluctuations around the average growth follow a ubiquitous Tracy-Widom (TW) probability distribution, which is frequently associated with the KPZ nonlinearity, in the latter case, see Fig. 1. For the highly-symmetric Kuramoto case, the fluctuations are simply Gaussian.

More recent results will be discussed where this connection is shown to be generalized in a straightforward way to phase oscillators with an arbitrary number of harmonics, and also to actual two-dimensional systems featuring a stable limit cycle in their phase space, including Stuart-Landau oscillators and van der Pol oscillators. As in general in such systems the odd symmetry of the Kuramoto (sine) coupling never holds, the critical behavior is consistently that of the KPZ equation with columnar noise, with TW fluctuations, in agreement with the observation made in Ref. [2]. Synchronization and surface growth processes with columnar noise thus seem to be much more closely related than previously anticipated; they are both instances of generic scale invariance with anomalous scaling forms.

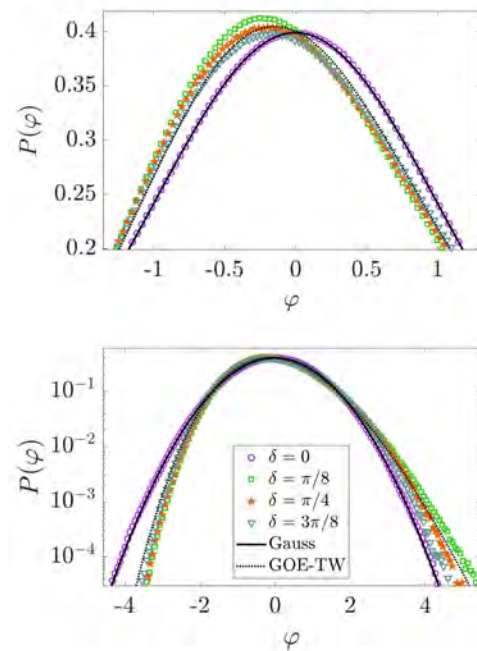


Fig. 1. Fluctuations around the average growth of the synchronization process for Kuramoto coupling ($\delta = 0$), which follows a Gaussian distribution, and for other (non-odd) couplings ($\delta \neq 0$), which follow a TW distribution.

-
- [1] A. Pikovsky, M. Rosenblum, and J. Kurths, *Synchronization: A Universal Concept in Nonlinear Sciences* (Cambridge University Press, Cambridge, 2001).
 - [2] R. Gutiérrez and R. Cuerno, *Nonequilibrium criticality driven by Kardar-Parisi-Zhang fluctuations in the synchronization of oscillator lattices*, Phys. Rev. Research **5**, 023047 (2023).
 - [3] A. -L. Barabási and H. E. Stanley, *Fractal Concepts in Surface Growth* (Cambridge University Press, Cambridge, 1995).
 - [4] I. G. Szendro, J. M. López and M. A. Rodríguez, *Localization in disordered media, anomalous roughening, and coarsening dynamics of faceted surfaces*, Phys. Rev. E **76**, 011603 (2007).

Parte IV

Sesión 4. Jueves 26 Tarde

Explosive synchronization of higher-order Kuramoto oscillators

Ana P. Millán^{1,2}, Joaquín J. Torres^{1,3}, G. Bianconi^{4,5}

¹Department of Electromagnetism and Matter Physics, University of Granada (Spain)

²Department of clinical neurophysiology, Amsterdam UMC (The Netherlands)

³Institute Carlos I for Theoretical and Computational Physics

⁴School of Mathematical Sciences, Queen Mary University of London (United Kingdom)

⁵The Alan Turing Institute (United Kingdom)

From social interactions to the human brain, networks and their high-order counterpart are key to describing the underlying structure and dynamics of complex systems. While it is well known that network structure strongly affects its function, the role that the underlying geometry and topology play on the emergent dynamical properties of a system is yet to be clarified (figure 1). Here I consider the synchronization of higher-order topological signals, associated not only with the nodes of a system but in general with any of its higher-dimensional components or simplices: links, triangles, tetrahedra, and so on. Whereas nodes interact only through links, higher-order simplices in general may interact both through their lower or higher dimensional faces. For instance, links may interact through the nodes and also the triangles that they share. These interactions are captured by the n -dimensional ($n > 1$) Hodge Laplacian \mathcal{L}_n :

$$\mathcal{L}_n = \mathcal{B}_n^\top \mathcal{B}_n + \mathcal{B}_{n+1} \mathcal{B}_{n+1}^\top = \mathcal{L}_n^{\text{up}} + \mathcal{L}_n^{\text{down}}, \quad (1)$$

where \mathcal{B}_n is the incidence matrix projecting a simplicial complex of dimension n to its $n - 1$ -dimensional boundary, and $\mathcal{L}_n^{\text{up}}$ and $\mathcal{L}_n^{\text{down}}$ encode respectively the interaction through the upper and lower dimensional faces.

Following the definition of the Hodge Laplacian, we propose the generalization of the Kuramoto dynamics including coupling between higher-order simplices as [1]:

$$\dot{\theta} = \omega - \sigma \mathcal{B}_{n+1} \sin \mathcal{B}_{n+1}^\top \theta - \sigma \mathcal{B}_n^\top \sin \mathcal{B}_n \theta, \quad (2)$$

where θ and ω indicate respectively the vectors of phases and intrinsic frequencies associated with each simplex. By using the Hodge decomposition (separating a vector into its harmonic, irrotational and solenoidal components), one can see that the projections of θ on the upper and lower dimensional phases, i.e. $\theta^{[+]} = \mathcal{B}_{n+1}^\top \theta$ and $\theta^{[-]} = \mathcal{B}_n \theta$, decouple. Remarkably, the dynamics on both of these projections displays a continuous phase transition on the associated Kuramoto order parameter, R^+ and R^- , with a critical point $\sigma_c = 0$, as shown in figure 2 (blue points).

We propose an alternative definition of the higher-order Kuramoto model, in which now the dynamics associated with the lower and higher dimensional faces are coupled:

$$\dot{\theta} = \omega - \sigma R^- \mathcal{B}_{n+1} \sin \mathcal{B}_{n+1}^\top \theta - \sigma R^+ \mathcal{B}_n^\top \sin \mathcal{B}_n \theta. \quad (3)$$

In this formulation, the higher-order Kuramoto dynamics displays projected on the upper and lower dimensional phases display an explosive phase transition, as shown in figure 2 (orange points).

In summary, the higher-order Kuramoto dynamics can lead to either a continuous or explosive synchronization transition, depending on the existence or not of coupling between the solenoidal and irrotational components of the dynamics. The topological transition cannot be observed via

the standard Kuramoto order parameter, but it requires the application of *topological filters* to retain only the solenoidal or irrotational components of the data.

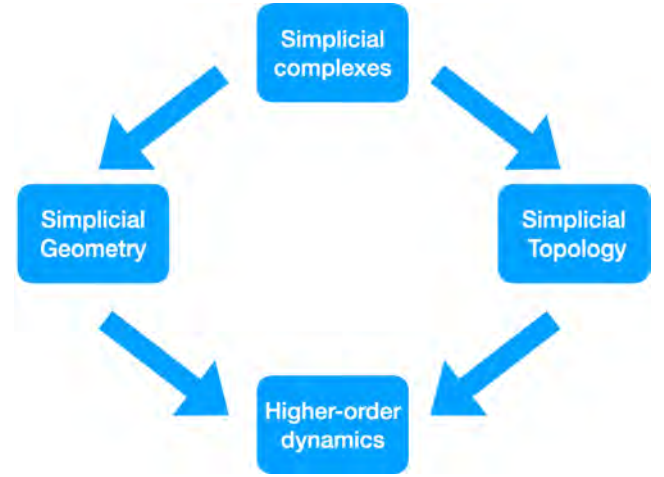


Fig. 1. Simplicial complexes encode the geometry and topology of the data, which strongly affect higher-order dynamics. Figure extracted from [2].

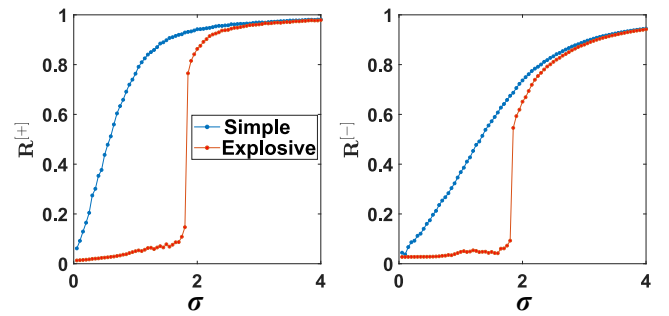


Fig. 2. The order parameters R^+ and R^- reveal the synchronization transition of topological signals defined on links ($n = 1$) and coupled with the continuous (blue line) and explosive (red line) versions of the higher-order Kuramoto model, respectively.

[1] Ana P. Millán, Joaquín J. Torres and Ginestra Bianconi, *Explosive higher-order Kuramoto dynamics on simplicial complexes*, Physical Review L **124**.21, 218301 (2021).

[2] Ana P. Millán, Juan G. Restrepo, Joaquín J. Torres and Ginestra Bianconi, *Geometry, topology and simplicial synchronization in Higher-Order Systems* (pp. 268-299) (Springer International Publishing, 2022).

Maximum weight-dependent navigability on human brain connectomes

Laia Barjuan^{1,2}, Jordi Soriano^{1,2} and M.Ángeles Serrano^{1,2,3}

¹Departament de Física de la Matèria Condensada, Universitat de Barcelona, Martí i Franquès 1, E-08028 Barcelona, Spain

²Universitat de Barcelona Institute of Complex Systems (UBICS), Universitat de Barcelona, Barcelona, Spain

³ICREA, Passeig Lluís Companys 23, E-08010 Barcelona, Spain

The brain exists in a 3D Euclidean space and, therefore, connectomes are spatially embedded networks whose architecture has not only been shaped by communication needs throughout evolution, but also by physical constraints. As a result, geometry is a crucial factor to consider when studying communication processes on brain networks.

Historically, brain network communication has focused on optimal routing, which proposes that information travels through topological shortest paths. However, this approach requires each element of the nervous system to have full knowledge of the topology of the network and this assumption is highly unlikely in a physiological system [1]. Alternatively, more decentralized routing protocols that take advantage of the geometric nature of the brain have been proposed. One of these methods is the greedy routing, which is guided by a local rule that sends information to the connected region closest in distance to a desired destination. Several studies have used geometric distances to guide navigation on brain networks [2, 3] and have shown that combining topology and geometry can lead to near-optimal decentralized communication.

In this work, we introduce a framework to explore decentralized routing protocols that combine the weighted topology of the human connectome and its spatial embedding. More specifically, we explored a continuous spectrum of stochastic routing protocols, having the greedy routing strategy and a weight-biased random walk at the opposite extremes, on two cohorts of real human connectome networks.

In our framework, messages are preferentially sent along paths with larger connection weights and to nodes closer in space to the target node. This accounts for the expectations that messages have more chances to go through channels with more nerve fibers and that nearby nodes are connected with higher probability. We implemented a probability of transition in which distances obtained from weights and Euclidean distances are balanced using a tuning parameter λ [4]. Namely, the transition probability from node i to its neighbour j when going to target t is

$$P_\lambda(j | i t) = \exp(-(\lambda \cdot d_{jt}^e + (1 - \lambda) \cdot d_{ij}^w)) \frac{1}{Z_i^t}, \quad (1)$$

where $Z_i^t = \sum_j \exp(-(\lambda \cdot d_{jt}^e + (1 - \lambda) \cdot d_{ij}^w))$ is the normalization factor, d^e is the Euclidean distance between the centers of the regions, and $d_{ij}^w = \ln(1/w_{ij})$, where w_{ij} is the weight of the connection.

Since probabilistic procedures can take excessively long paths before reaching the destination we applied a time-out (measured in maximum number of steps) after which we suppose the message has faded before reaching the target. We studied two standard metrics widely employed to assess the efficiency of greedy routing navigation: the success rate

–proportion of paths that reach the target successfully, when considering all possible source/target pairs– and the average stretch –ratio between the number of links in the path and the number of links in the topological shortest path between the source and the target, averaged over all successful paths.

We found that there is an intermediate region in this spectrum, a sweet spot, in which connectomes become maximally navigable, achieving full communication efficiency. Moreover, we found that in this region weights, topology and distances are coupled in such a way that information transmission not only is maximally efficient but also robust even under severe perturbation.

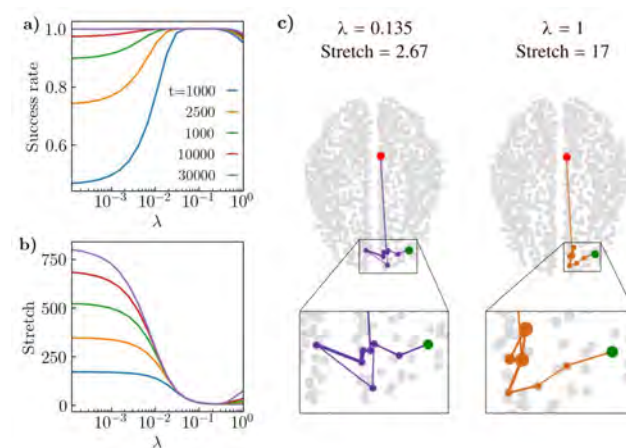


Fig. 1. **a, b**) Success rate and stretch respectively. Each curve shows the outcome for a specific value of time-out. **c**) Path taken from ROI 154, in red, to ROI 20, in green, for a value of λ in the sweet-spot region (in purple), and when considering only distances (in orange). In the insets the size of the nodes is proportional to the number of times the message visits them.

- [1] A. Avena-Koenigsberger, B. Misic, and O. Sporns *Communication dynamics in complex brain networks* Nat. Rev. Neurosci. **19**, 17 (2018).
- [2] C. Seguin, M.P. van den Heuvel and A. Zalesky *Navigation of brain networks* Proc. Natl. Acad. Sci. U.S.A. **115**, 6297 (2018).
- [3] A. Allard and M.Á. Serrano *Navigable maps of structural brain networks across species* PLoS Comput. Biol. **16**, 1 (2020).
- [4] A. Avena-Koenigsberger, X. Yan, A. Kolchinsky, M.P. van den Heuvel, P. Hagmann and O. Sporns *A spectrum of routing strategies for brain networks* PLoS Comput. Biol. **15**, e1006833 (2019).

The architecture of Multifunctional Ecological Networks

Mar Cuevas-Blanco¹, Sandra Hervas-Parejo¹, Isabel Donoso¹, Anna Traveset¹,
Lucas Lacasa¹ and Victor M. Eguiluz¹

¹IFISC (CSIC-UIB), Edifici Instituts Universitaris de Recerca Campus UIB E-07122 Palma, Mallorca, Spain

²IMEDEA (CSIC-UIB), C/ Miquel Marqués, 21 07190 Esporles Illes Balears, Spain

The importance of species and their interactions has been the focus of analysis due to their role in maintaining biodiversity and ecosystem functioning. Ecosystem interactions are inherently multidimensional and quantifying such multifunctionality is a major challenge nowadays [1]. However, the identification and quantification of keystone species from a holistic multifunctional perspective remain unknown [2]. To our knowledge, only one study has estimated the weight of edges between layers by quantifying the role of the same individual in two ecological processes [3].

Here, we bridge this gap by developing a framework for data standardization and post-processing analysis via mathematical modeling, inspired by the resource (plant species)-consumer (animal/fungi species) paradigm. We apply such framework by focusing on six ecological functions and capitalize on an unprecedented sampling effort based on direct observations on the islet Na Redona in the Balearic Islands, in Mediterranean Sea, that encompasses 1537 weighted interactions between 695 plant, animal/fungal species. Incorporating the functional dimension, the complete relational dataset is formalized in terms of a rank-3 tensor that we call the Resource-Consumer-Function tensor (RCF).

We interpret the architecture of this tensor as a weighted, multipartite, multilayer network and visualise it as a multipartite edge-colored weighted network (Figure 1). The network displays two types of nodes: resources and consumers, with interactions (links) taking place between groups but no direct intragroup links. Each layer of the network represents a specific function and the strength of each interaction is represented by a link weight that measures the fraction of plants of the species that has been observed participating in the function. Consumers (animals, fungi) are often centered around a single plant species and thus form clusters.

A first question worth addressing is to quantify the relationship between the resources of the ecosystem and the functions the system embodies. This is achieved by integrating out the consumer index and thereby building a Resource-Function Matrix (RFM), which is the adjacency matrix of our Multifunctional Ecological Network. The nested pattern observed suggests the existence of both multifunctional species and multispecies function keystone, a new concept we coined here. Just as keystone species encode, among other properties, robustness and resilience of entire communities the response of the ecosystem to disturbances may also occur in the functional dimension.

To further understand the multifunctional species keystone and the role of plant species as ecosystem assemblers, we project the RFM into the function class and extract a Function-Function Interaction Network (FFIN). We quantify the ecosystem robustness against perturbations (extinctions) of plant species by sequentially pruning edges in FFIN. Additionally, we rank plant species, based on their

multifunctional keystone, by conditioning the FFIN to each single plant species and rank based on the specific role of resources as brokers of functions.

The dual concept of function keystone can be addressed by following a similar mathematical manipulation: initially starting again from RFM we project now on the plant class and thus construct a Resource-Resource interaction network. We address two complementary questions: (i) how robust is the ecosystem against perturbations of functions? And (ii) how to quantify the heterogeneous roles and impacts of each function in the ecosystem?

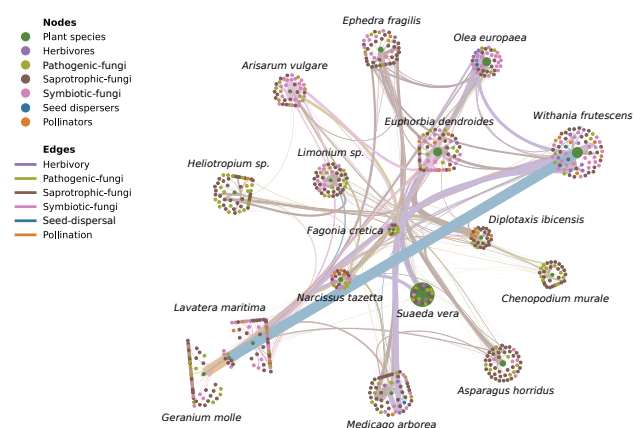


Fig. 1. Network visualization of the Resource-Consumer-Function tensor from the Na Redona dataset. The RCF is composed of two groups of nodes: (resource) plant species (labeled) and (consumers) animal/fungus species. Node and edges colors account for plant species (green) and animal/fungus species according to the functional interaction type. The sizes of plant-nodes represent their observed abundance. Edges represent function connections and their widths quantify the weight of interaction. Species are clustered via Infomaps community detection algorithm.

[1] Bianconi, G., *Multilayer networks: structure and function*, Oxford university press (2018).

[2] Manning, P., van der Plas, F., Soliveres, S. et al. Redefining ecosystem multifunctionality. *Nat Ecol Evol* 2, 427436 (2018). <https://doi.org/10.1038/s41559-017-0461-7>.

[3] Hervas-Parejo, S., Tur, C., Heleno, R., Nogales, M., Timteo, S., and Traveset, A., Species functional traits and abundance as drivers of multiplex ecological networks: first empirical quantification of inter-layer edge weights. *Proceedings of the Royal Society B*, 287(1939), 20202127 (2020).

Acknowledgement: We acknowledge support from the Spanish Agency of Research (AEI) through Research and Development Projects Program (Grant PID2020-114324GB-C22 funded by MCIN/AEI/10.13039/501100011033). In particular, MCB thanks financial support Grant PID2020-114324GB-C22 funded by MCIN/AEI/10.13039/501100011033 and by ESF Investing in your future. Sesión 4, S4.3

Procesos de reacción-difusión y diseño de estrategias de control epidemiológico

Pablo Valgañón^{1,2}, A. Arenas³, D. Soriano-Paños^{2,4} and Jesús Gómez-Gardeñes^{1,2}

¹Departamento de Física Materia de la Condensada, Universidad de Zaragoza, 50009 Zaragoza, España.

²GOTHAM Lab - Instituto de Biocomputación y Física de Sistemas Complejos, Universidad de Zaragoza, 50018 Zaragoza, España.

³Departamento de Ingeniería Informática y Matemáticas, Universidad Rovira i Virgili, 43007 Tarragona, España.

⁴Instituto Gulbenkian de Ciencia (IGC), Oeiras, Portugal.

El análisis de los procesos de contagio-difusión en metapoblaciones es una poderosa herramienta teórica para estudiar cómo influye la movilidad humana en la propagación de enfermedades transmisibles [1] y, en particular, analizar el impacto que los patrones recurrentes de movilidad y la distribución espacial de agentes tienen en el desarrollo de epidemias en grandes áreas urbanas [2, 3]. Asimismo, este tipo de modelos es especialmente valioso para diseñar estrategias de control y mitigación de brotes epidémicos con intervenciones no farmacológicas [4] o que hagan uso de recursos limitados [5].

En este trabajo proponemos un marco metapoblacional en el que incorporamos la naturaleza distinguible de los agentes en lo que respecta tanto a su residencia como a su destino habitual [6]. El modelo propuesto permite tanto un cálculo rápido del patrón espacio-temporal de la trayectoria epidémica como el cálculo analítico del umbral epidémico. Este umbral se calcula como el radio espectral de una matriz de mezcla que engloba la distribución residencial y los patrones específicos de desplazamiento de los agentes. Demostramos que la simplificación de individuos indistinguibles sobreestima el valor del umbral epidémico. Finalmente, mostraremos la utilidad que la adición de la distinguibilidad tiene a la hora de diseñar estrategias de control y vigilancia epidemiológica en entornos urbanos en los que es preciso identificar aquellos puntos de control que maximicen nuestra capacidad de detección mediante recursos limitados.

- [1] D. Soriano-Paños, W. Cota, S.C. Ferreira, G. Ghoshal, A. Arenas, and J. Gómez-Gardeñes, *Modeling communicable diseases, human mobility and epidemics: a review*, *Annalen der Physik* **2022**, 2100482 (2022).
- [2] J. Gómez-Gardeñes, D. Soriano-Paños, and A. Arenas, *Critical regimes driven by recurrent mobility patterns of reaction-diffusion processes in networks*, *Nature Physics* **14**, 391-395 (2018).
- [3] D. Soriano-Paños, L. Lotero A. Arenas, and J. Gómez-Gardeñes, *Spreading processes in multiplex metapopulations containing different mobility networks*, *Physical Review X* **8**, 031039 (2018).
- [4] A. Arenas, W. Cota, J. Gómez-Gardeñes, S. Gómez, C. Granell, J.T. Matamalas, D. Soriano-Paños, and B. Steinegger, *Modeling the Spatiotemporal Epidemic Spreading of COVID-19 and the Impact of Mobility and Social Distancing Interventions*, *Physical Review X* **10**, 041055 (2020).
- [5] A. Reyna-Lara, D. Soriano-Paños, J.H. Arias, H.J. Martínez, and J. Gómez-Gardeñes, *A metapopulation approach to identify targets for Wolbachia-based Dengue control*, *CHAOS* **32**, 041105 (2022).
- [6] P. Valgañón, D. Soriano-Paños, A. Arenas, and J. Gómez-Gardeñes, *Contagion-diffusion processes with recurrent mobility patterns and distinguishable agents*. *CHAOS* **32**, 043102 (2022).

Parte V

Sesión 5. Viernes 27 Mañana, A

Mechanisms behind collective social phenomena

Maxi San Miguel

IFISC (UIB-CSIC) Institute for Crossdisciplinary Physics and Complex Systems,
Campus Universitat Illes Balears, E-07122 Palma, Spain

Collective social phenomena can be modelled considering a set of agents in different possible states which are located at the nodes of a complex network of interactions. I will give an overview of some relevant mechanisms in the modelling of paradigmatic collective phenomena such as the consensus and social contagion problems. These mechanisms include dyadic interaction vs. group interaction, co-evolution dynamics of the topology of the network of interactions and the state of the agents, and aging introduced as non-poissonian distributions of the interaction interevent times.

I will illustrate these mechanisms in the Voter Model of opinion formation [1, 2], the Granovetter-Watts model of complex contagion [3, 4] and the Coordination Game [5, 6]. I will also discuss the problem of social polarization and social balance through a general homophily-heterophily coevolution model [7].

-
- [1] O. Artime, A.F. Peralta, J. Ramasco, M. San Miguel, and R. Toral *Aging-induced continuous phase transition*, Phys. Rev. E **98**, 032104 (2018).
 - [2] A.F. Peralta, A. Carro, M. San Miguel, and R. Toral *Analytical and numerical study of the non-linear noisy voter model on complex networks*, CHAOS **28**, 075516(2018).
 - [3] D. Abella, M. San Miguel, and J. Ramasco, *Aging in binary-state models: The threshold model for complex contagion*, Phys. Rev. E **107**, 024101 (2023).
 - [4] B. Min, and M. San Miguel, *Threshold cascade dynamics on coevolving networks*, Entropy. **25**, 929 (2023).
 - [5] T. Raducha, and M. San Miguel, *Coordination and equilibrium selection in coordination: the role of local effects*, Sci. Rep. **12**, 373 (2022).
 - [6] M.A. Gonzalez-Casado, A. Sanchez, and M. San Miguel, *Network coevolution drives segregation and enhances Pareto optimal equilibrium selection in coordination games*, Sci. Rep. **13**, 28663 (2023).
 - [7] M. Saeedian, M. San Miguel, and R. Toral, *Absorbing transition in a coevolution model with node and link states in an adaptive network: Network fragmentation transition at criticality*, New J Phys. **22**, 113001 (2020).

Modelos de competición y mutación en redes complejas

Javier López-Pedrares^{1,2}, and Alberto P. Muñuzuri^{1,2}

¹Group of Nonlinear Physics, Universidade de Santiago de Compostela, 15782 Santiago de Compostela, Spain.

²Universidade de Santiago de Compostela, 15782 Santiago de Compostela, Spain.

Los humanos y los animales determinamos redes complejas de interacción. Dichas redes han visto modificada su estructura con el paso de los años. En los últimos siglos basta observar el crecimiento poblacional y la forma de comunicarse para ver dicha modificación estructural.

Por otra parte, los virus necesitan organismos huésped para poder proliferar y sobrevivir. Así los humanos y los animales son en general los organismos huésped que emplean los virus para poder reproducirse.

Aquí surge el interés de acoplar modelos de competición viral y epidemiológicos a través de redes complejas, que

nos permitan estudiar y predecir el comportamiento de pandemias. Es clave, además, tener en cuenta la mutación continua que sufren los virus. Es por eso que se presentan modelos acoplados que predicen además en que forma modificar la estructura de una red puede o no determinar la mutación de los organismos patógenos.

[1] López-Pedrares, Javier, Vázquez-Cendón, M. Elena and Muñuzuri, Alberto P., *Interactions between hosts affect virus competition mechanism within an infectious strain*, Chaos, Solitons & Fractals **170**, 113344 (2023).

Emergence of opinion polarization in weighted contact structures

H. Pérez-Martínez^{1,2}, F. J. Bauzá^{2,3}, D. Soriano-Paños^{2,4}, J. Gómez-Gardeñes^{1,2} and L. M. Floría^{1,2}

¹Department of Condensed Matter Physics, University of Zaragoza, 50009 Zaragoza (Spain).

²GOTHAM lab, Institute for Biocomputation and Physics of Complex Systems (BIFI), University of Zaragoza, 50018 Zaragoza (Spain).

³Department of Theoretical Physics, University of Zaragoza, 50009 Zaragoza (Spain).

⁴Institute Gulbenkian of Science (IGC), 2780-156 Oeiras (Portugal).

Opinion polarization has become widespread in modern societies. Its emergence is usually linked to the advent of social networks, as the dynamical aspect of online interactions and the homophily in social contacts can generate echo chambers that isolate people from opposing perspectives. However, recent studies suggest that echo chambers in online interactions might be less common than previously thought, and in general, real-world relationships are not solely dependent on ones opinion about certain issues, but also on friendship, kinship, professional ties and the like, usually featuring cross-cutting interactions with disagreeing peers: the effect these relationships have over ones opinion lies on the importance assigned to the others' points of view.

To take these facts into account, we adapt an opinion model previously applied to temporal graphs [1] to weighted graphs with static contact patterns. In our model, agents always interact with the same set of neighbors, being influenced by their opinions and giving more importance to like-minded individuals by changing the weights of the links.

Mathematically, the opinion change of an agent i is governed by the equation:

$$\dot{x}_i = -x_i + K \sum_{j=1}^N A_{ij} w_{ij} \tanh(x_j), \quad (1)$$

where the influence that each neighbor has over the agent's opinion is weighted by w_{ij} following:

$$w_{ij} = \frac{(|x_i - x_j| + \delta)^{-\beta}}{\sum_{l=1}^N A_{il} (|x_i - x_l| + \delta)^{-\beta}}. \quad (2)$$

It depends on the parameter β , and the higher it is, the stronger the homophily effect become.

We find that polarization is indeed possible under this formalism in a wide parameter range and network structures (see Figure 1a, right panel). Moreover, in these polarized configurations agents can follow a broad range of opinions between the most extreme ones, similar to what occurs in reality. Depending on the parameters, the agents environment can vary from high heterogeneity, meaning that the agents have multiple cross-cutting relationships with disagreeing neighbors, to low heterogeneity, in which agents tend to interact with many like-minded neighbors reproducing a scenario of very high homophily. In general, highly heterogeneous environments give rise to less polarized configurations, in which agents usually take milder points of view.

In addition, the polarized configurations obtained over a certain range of parameters mimic those obtained in surveys about typically polarized issues like LGBTQ+ rights or other partisan topics (see Figure 1a, left panel). Comparing our distributions with those obtained in the 2016 American National Election Studies (ANES) Survey [2], we infer

some optimal combination of parameters that give rise to the most similar opinion distributions, which allows us to classify multiple issues by their degree of polarization based on the inferred optimal parameters (see Figure 1b).

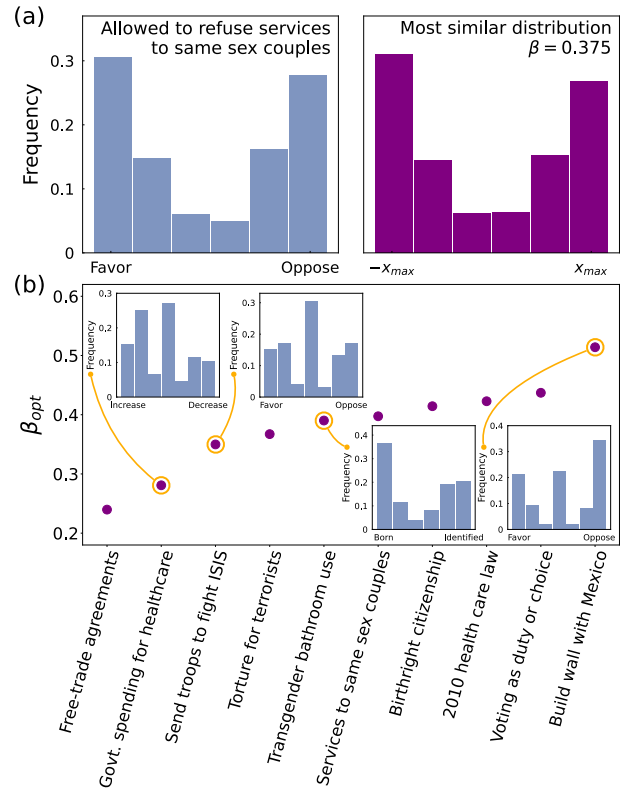


Fig. 1. **Comparison with real-world data.** (a) Left: Frequency of responses regarding the question: 'Do you think business owners who provide wedding-related services should be allowed to refuse services to same-sex couples if same-sex marriage violates their religious beliefs?', obtained from the ANES survey of 2016 (codes V161227 and V161227a, aggregated in V161227x). Right: most similar opinion distribution obtained in our simulations. (b) β_{opt} estimated for multiple polarized issues of the ANES 2016 survey. Inset figures show some of their distributions. An ErdsRnyi graph with $\langle k \rangle = 10$ and $N = 10^4$ nodes is used to generate the results of the figure.

[1] F. Baumann, P. Lorenz-Spreen, I. M. Sokolov, and M. Starnini, *Phys. Rev. Lett.*, *Modeling Echo Chambers and Polarization Dynamics in Social Networks*, **124**, 048301 (2020).

[2] The American National Election Studies (www.electionstudies.org). These materials are based on work supported by the National Science Foundation under grant numbers SES 1444721, 2014-2017, the University of Michigan, and Stanford University.

Why are there six degrees of separation in a social network?

S. Boccaletti

¹⁶*CNR - Institute of Complex Systems, Via Madonna del Piano 10, I-50019 Sesto Fiorentino, Italy*

In the short story "Chains" (1929), the Hungarian writer Frigyes Karinthy described a game where a group of people was discussing how the members of the human society were closer together than ever before. To prove this point, one participant proposes that any person out of the entire Earth population (around 1.8 billion at that time) could be reached using nothing except each personal network of acquaintances, betting that the resulting chain would be of no more than five individuals. The story coined the expression 'six degrees of separation' to reflect the idea that all people of the world are six or fewer social connections apart from each other. The concept was later generalized to that of "small world" networks, where the maximal social distance (the diameter of the network) scales logarithmically, rather than linearly, with the size of the population.

After early studies on the structure of social networks by Michael Gurevich and Manfred Kochen, Stanley Milgram performed his 1967 famous set of experiments on social distancing where, with a limited sample of a thousand individuals, it was shown that people in the United States are indeed connected by a small number of acquaintances. Later on, Duncan Watts recreated Milgram's experiments with Internet email users by tracking 24,163 chains aimed at 18 targets from 13 countries and confirmed that the average number of steps in the chains was around six. Furthermore, many experiments conducted at a planetary scale on various social networks verified the ubiquitous character of this feature: 1) a 2007 study by Jure Leskovec and Eric Horvitz (with a data set of 30 billion conversations among 240 million Microsoft Messenger users) revealed the average path length to be 6, 2) the average degree of separation between two randomly selected Twitter users was found to be 3.435, and 3) the Facebook network in 2011 (721 million users with 69 billion friendship links) displayed an average distance between nodes of 4.74.

Such abundant and consistent evidence points to the fact that the structure of these networks radically differs from either that of regular networks (where the diameter scales linearly with the size) and that of classical small-world networks (where, instead, the scaling law is logarithmic). A clear explanation of the mechanisms through which social networks organize into ultra-small world states (where the diameter does not depend on the system size over several orders of magnitude) is, however, still missing. Why does

such a collective property emerge? What are its fundamental mechanisms? Why is the common shortest path length between units of a social network six, rather than five or seven or any other number, implying an average distance which is also not far from six?

So far, the few available studies on ultra-small world states have focused on finding the relationship between the scaling properties of distances in a graph and those of the node's degree distribution. It was indeed proved that scale-free networks with degree distribution $p(k) \sim k^{-\gamma}$ and $2 < \gamma < 3$ (as it is observed in all real-world networks) display a scaling of the diameter as $D \sim \ln \ln N$, which departs from the classic logarithmic scaling of small-world networks and yet maintains an explicit dependence on the network size N . On the other hand, scale-free networks featuring an asymptotically invariant shortest path (called Mandala networks) may be synthesized, which however have an associated value of γ strictly equal to 2 and therefore do not match any case observed in the real world.

Rather than being dependent on global (i.e., degree distribution) scaling properties, I will show that the mechanism behind such observed regularity can be found, instead, in a dynamic evolution of the network. Precisely, I will rigorously demonstrate that, when a simple compensation rule between the cost incurred by nodes in maintaining connections and the benefit accrued by the chosen links is governing the evolution of a network, the asymptotic equilibrium state (a Nash equilibrium where no further actions would produce more benefit than cost), features a diameter which does not depend on the system's size, and is equal to 6. In other words, we theorematically prove that any network where nodes strive to increase their centrality by forming connections if and only if their cost is smaller than the payoff tends to evolve into an ultra-small world state endowed with the 'six degree of separation' property, irrespective of its initial structure. Our study points out, therefore, that evolutionary rules of the kind traditionally associated with human cooperation and altruism can in fact account also for the emergence of this attribute of social networks. Furthermore, we show that such a global network feature can emerge even from situations where individuals have access to only partial information on the overall structure of connections, which is indeed the case in almost all social networks.

The interrupted nature of constricted dense suspension flows

Alvaro Marin¹ and Mathieu Souzy²,

¹Physics of Fluids, University of Twente, Enschede, Netherlands.

²INRAE, Aix-Marseille Univ, Aix-en-Provence, France

When people, animals, or particles are forced through a constriction, the flow may become intermittent due to the development of clogs that obstruct the constriction. Despite the diverse nature and scale of these systems – including hungry sheep herds [1, 2], pedestrian crowds trying to escape a room in a life-and-death situation [3], discharge of dry granular silos or suspended hydrated particles transported through pipelines, sand hourglass, or mice escaping a water pool – a distinctive phenomenology of particles or bodies flowing in erratic bursts is observed, separated by short period of arrest. The analogy does not seem to be only qualitative: in all cases the number of escapees per burst follow an exponential distribution, and the probability distribution of time lapses separating the passage of consecutive bodies seems to exhibit a power-law tail with characteristic exponents that depend on diverse system parameters.

We follow this statistical approach, which require high time- and space-resolution experiments to obtain probability distributions of arrest times between successive bursts, which display power-law tails with characteristic exponents. We will show that dense non-cohesive particle suspensions going through a constriction exhibit intermittent flow behavior with a striking similarity as in dry granular matter, human crowds, or animal herds [1, 4, 5], both for pressure or volume-controlled driving. Nonetheless different flow drive leads to subtle and non-trivial results that will be discussed in the presentation [6]. Our results will also be compared with approximated computational fluid dynamics simulations and discrete particle simulations [7], illustrating the crucial role of the interparticle liquid flow.

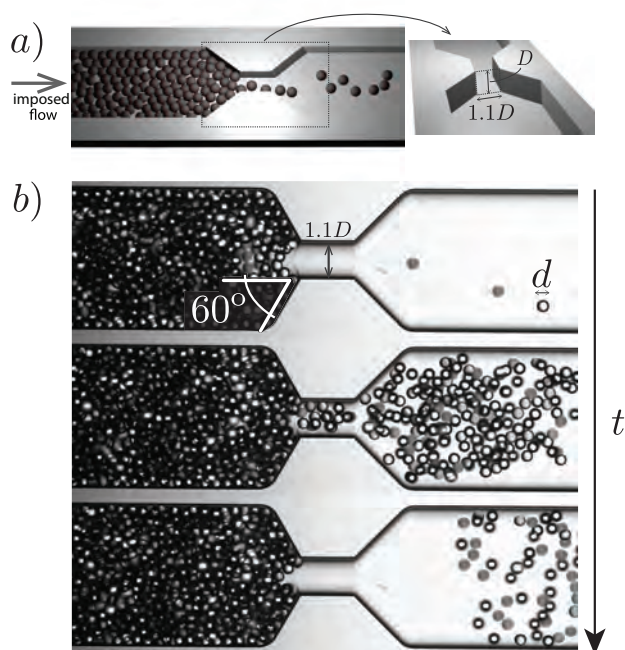


Fig. 1. a) The experimental setup consists on a glass channel with rectangular sections that transitions through a conical section to a constriction with an almost squared cross-section, characterized by the neck-to-particle size ratio D/d , where $D = 100 \mu\text{m}$ is the constriction width and d is the particle size diameter ($d = 33 \mu\text{m}$ in this case). b) Sequence of events during a burst of particles in an intermittent flow regime.

-
- [1] I. Zuriguel, D. R. Parisi, R. C. Hidalgo, *et al.* *Clogging transition of many-particle systems flowing through bottlenecks*, Scientific Reports, **4** 7324 (2014).
- [2] A. Garcimartín, J.M. Pastor, L.M. Ferrer, J.J. Ramos, C. Martín-Gómez, & I. Zuriguel. *Flow and clogging of a sheep herd passing through a bottleneck*, Physical Review E, **91**(2) 022808 (2015).
- [3] D. Helbing, I. Farkas & T. Vicsek. *Simulating dynamical features of escape panic*, Nature **407** (6803):487-490 (2000)
- [4] A. Marin, H. Lhuissier, M. Rossi, & C. J. Kähler. *Clogging in constricted suspension flows*, Physical Review E, **97**(2), 021102 (2018).
- [5] M. Souzy, I. Zuriguel & A. Marin. *Transition from clogging to continuous flow in constricted particle suspensions*, Physical Review E **101**.6: 060901 (2020).
- [6] M. Souzy & A. Marin. *Role of liquid driving on the clogging of constricted particle suspensions*, Journal of Fluid Mechanics, **953**: A40 (2022)
- [7] T. Weinhart *et al.* *Fast, flexible particle simulations an introduction to MercuryDPM*, Computer Physics Communications **249**107129 (2020).

Parte VI

Sesión 6. Viernes 27 Mañana, B

On the application of kinetic theory to granular gases

Vicente Garzó¹,

¹Departamento de Física and Instituto de Computación Científica Avanzada (ICCAEx),
Universidad de Extremadura, E-06006 Badajoz, Spain

It is well established that when granular matter is externally excited, the external work done on the system provides kinetic energy to the grains that compensate for energy dissipated by collisions and the effects of gravity. In this regime (rapid-flow conditions), the motion of grains resembles the random motion of atoms or molecules in an ordinary or molecular gas and hence, they admit a hydrodynamic-like type of description [1]. The corresponding hydrodynamic equations can be derived from a fundamental point view by extending the conventional kinetic theory of classical gases (which can be considered as a mesoscopic description intermediate between statistical mechanics and hydrodynamics) to dissipative dynamics. This approach has been widely employed in the past few years to obtain the granular hydrodynamic Navier–Stokes equations with explicit forms of the transport coefficients [2].

In this talk, I will consider the inelastic version of the Enskog kinetic equation (which applies to moderate densities) for a simple model of granular gases: a gas of *smooth* hard spheres where the inelasticity in collisions is accounted for via a (positive) constant coefficient of normal restitution. In contrast to previous theoretical attempts [1], the dynamic properties of the granular gas will be obtained for the whole range of values of the coefficient of restitution and the remaining parameters of the system [3]. The study will cover not only monocomponent systems, but also multicomponent granular systems. The knowledge of the dynamic properties will allow us to address some interesting applications, such

as the stability of the homogeneous cooling state and the hydrodynamic description of vibrating steady states. The reliability of the theoretical results will be confronted against Monte Carlo and molecular dynamics simulations as well as real experiments. Since the comparison shows in general good agreement (even for strong inelasticity and/or moderately high densities), one can conclude that kinetic theory can be considered as a reliable tool for describing granular flows in rapid-flow conditions. Finally, a recent connection with the random walk description of the diffusion properties of an intruder in a granular gas will be also provided [4, 5].

-
- [1] I. Goldhirsch, Rapid granular flows, *Annu. Rev. Fluid Mech.* **35**, 267–293 (2003).
 - [2] N. Brilliantov and T. Pöschel, *Kinetic Theory of Granular Gases* (Oxford University Press, Oxford, 2004).
 - [3] V. Garzó, *Granular Gaseous Flows* (Springer Nature, Cham, 2019).
 - [4] E. Abad, S. Bravo Yuste, and V. Garzó, On the mean square displacement of intruders in freely cooling granular gases, *Granular Matter* **24**, 111 (2022).
 - [5] R. Gómez González, E. Abad, S. Bravo Yuste, and V. Garzó, Diffusion of intruders in granular suspensions: Enskog theory and random walk interpretation, *Phys. Rev. E* **108**, 024903 (2023).

Mean-field description of a non-imitative evolutionary game

M. Aguilar-Janita ¹, N. Khalil ¹, I. Leyva ^{1 2} and I. Sendiña-Nadal ^{1 2}

¹Complex Systems Group, Universidad Rey Juan Carlos, 28933 Móstoles, Madrid, Spain

²Center for Biomedical Technology, Universidad Politécnica de Madrid, Pozuelo de Alarcón, 28223 Madrid, Spain

The origin of cooperation in human societies remains an unresolved question. According to the principle of "survival of the fittest," defection should prevail over cooperation since the former provides individuals with the highest benefits.

Evolutionary Game Theory offers a theoretical framework to address this issue and that allows us to leverage techniques developed in the field of statistical physics. Within this framework, social dilemmas are formulated as two-person games, wherein each player chooses to cooperate or defect, and the game is iteratively played over multiple rounds. Mathematically, these games are described by a payoff matrix:

$$\begin{array}{c|cc} & C & D \\ \hline C & R & S \\ D & T & P \end{array} \quad (1)$$

Different values of the game parameters R , S , T and P describe different classical games such as *Prisoner's Dilemma*, *Harmony*, *Snowdrift*, and *Stag Hunt*. The dynamics of Evolutionary Game Theory heavily rely on how players adapt their strategies in each round of the game. Typically, the adaptation process follows imitative rules, where each player adjusts their strategy based on the outcomes of other players. The long-term stable strategies of games employing these imitative rules are significantly influenced by the population structure, characterized by the network topology connecting the players. However, recent experiments involving humans playing the *Prisoner's Dilemma* have demonstrated that the final outcome is independent of the network structure [1]. Moreover, empirical evidence suggests that humans do not take into account their neighbors' payoffs when making decisions [2]. Consequently, the community has started considering update strategies that eschew information about other players and solely depend on internal variables specific to each player [3].

In our study, we propose a novel model of non-imitative dynamics wherein agents possess an internal parameter called aspiration, denoted as m , against which they compare their payoffs. We investigate this model in a fully connected, mean-field network and determine the stationary values of the mean cooperation fraction ρ , both theoretically and through simulations based on the Gillespie algorithm. Furthermore, we introduce a mathematical framework that allows us to simplify the complexity of the parameter space to just two new parameters that encapsulate all the relevant information. These parameters are defined as follows:

$$\sigma = \frac{S - m}{|R - m|}, \quad (2)$$

$$\tau = \frac{T - m}{|P - m|}. \quad (3)$$

values of R , P , S , T , and m . Additionally, we introduce an effective temperature θ which modulates the transition probabilities between cooperation and defection for each agent, introducing a stochastic component. Our investigation reveals a wide variety of stable system behaviors. Particularly, we focus on the critical behavior of the system during transitions between different states under parameter variations, including changes in the effective temperature. Furthermore, we specifically examine parameter values that correspond to classical games and draw novel conclusions within these scenarios.

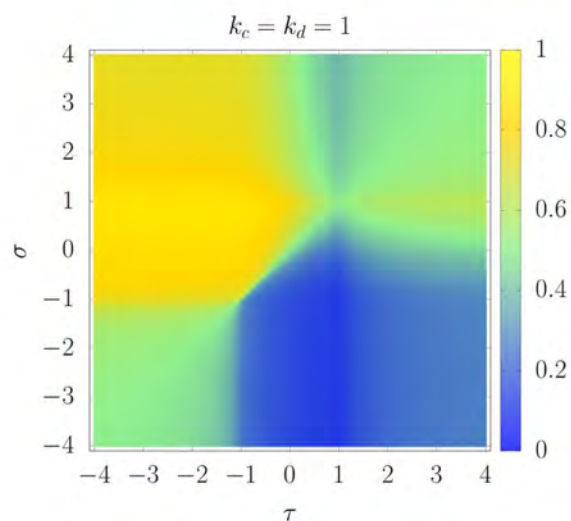


Fig. 1. Phase diagram for the two relevant parameters σ and τ for the case $R, P > m$ and an effective temperature of $\theta = 0.5$. The mean cooperation fraction ρ is codified with colors.

-
- [1] C. Gracia-Lazaro, A. Ferrer, G. Ruiz, A. Tarancon, J. Cuesta, A. Sanchez and Y. Moreno, *Heterogeneous networks do not promote cooperation when humans play a Prisoners Dilemma*, Proc. Natl. Acad. Sci. USA **109**, 10922-20926 (2012).
- [2] J. Grujić, C. Gracia-Lázaro, M. Milinski et al. *A comparative analysis of spatial Prisoner's Dilemma experiments: Conditional cooperation and payoff irrelevance*, Sci Rep **4**, 4615 (2014)
- [3] G. Cimini and A. Sanchez, *How evolution affects network reciprocity in Prisoner's Dilemma*, Journal of Artificial Societies and Social Simulation **18**, 22 (2015)
- [4] Nagi Khalil, I. Leyva, J. A. Almendral, and I. Sendiña-Nadal, *Deterministic and stochastic cooperation transitions in evolutionary games on networks*, Phys. Rev. E **107**, 054302 (2023)

Traffic Flows and Evacuations in Robotic Systems: an experimental exploration

L. Alonso-Llanes^{1,2}, I. Zuriguel¹ and A. Garcimartin¹

¹Physics and Applied Mathematics Department, Science Faculty, University of Navarra, 31080 Pamplona, Spain.

²Group of Complex Systems and Statistical Physics, Physics Faculty, University of Havana, 10400 Havana, Cuba.

This research work presents an experimental study of traffic flows in a single line circular road using line-follower robots. Inspired by the Nagel-Schreckenberg model [1], the study aims to reproduce its key elements and explore the emergent behavior of the system of robots.

The experimental setup consists of a circular track with line-following robots capable of autonomous movement (Fig. 1). Robots are programmed to mimic the behavior of vehicles in a traffic system, incorporating features such as obstacle detection, braking and acceleration. By varying parameters such as robot density and maximum speed, we investigate the dynamics of traffic flow and the occurrence of phase transitions between free-flowing and congested traffic states. Through extensive data collection and analysis, various macroscopic observables, including traffic density, average velocity, and flow rate, are measured and compared with theoretical predictions from the Nagel-Schreckenberg model.

The results shed light on the system's collective behavior, highlighting the impact of density on traffic congestion, the role of fluctuations in traffic flow, and the influence of interactions on overall traffic performance.

In addition to studying traffic flows on the circular road, the research aims to explore the robots' behavior in evacuation scenarios through a narrow exit, both competitively and cooperatively. The findings contribute to our understanding of collective movement and decision-making processes in complex systems, with implications for various fields, including transportation planning, swarm robotics, and crowd management.

[1] K. Nagel and M. Schreckenberg *A cellular automaton model for freeway traffic*, J. Phys. I France. **2**, 2221 (1992).

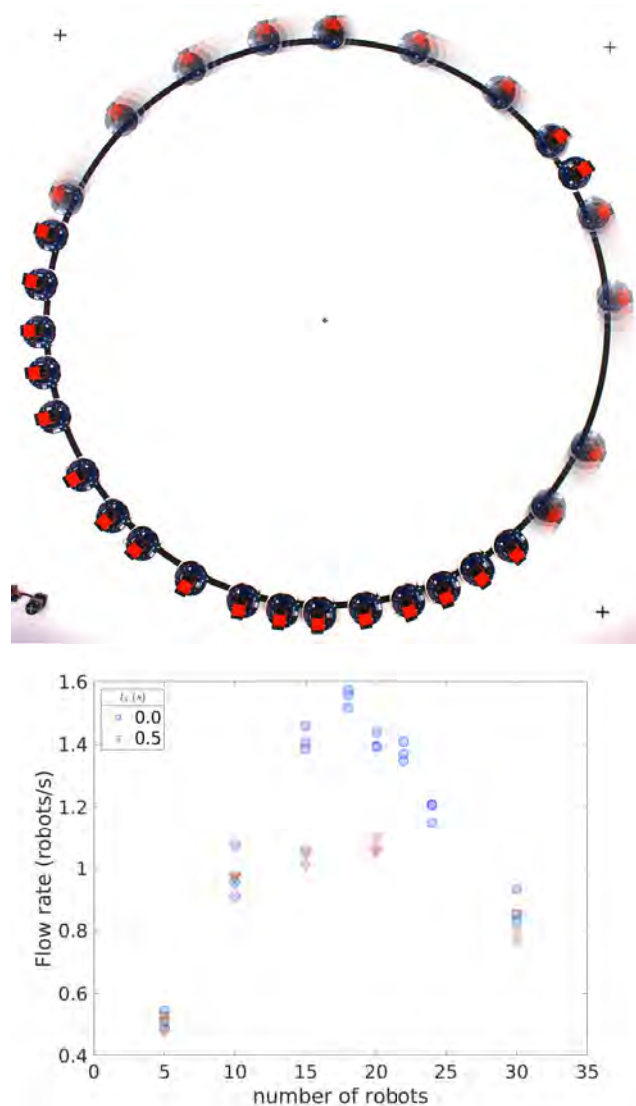


Fig. 1. (a) Top view of the circular road. Image shows a 15-frame overlay (0.75s) of an experiment with 30 robots. (b) Flow rate vs. number of robots for different stopping times t_s , i. e., time that robots wait after an obstacle detection.

Morphological symmetry-breaking and spontaneous motility of cell clusters

Joan Térmens^{1,2}, Ido Lavi^{1,2,3}, and Jaume Casademunt^{1,2}

¹Departament de Física de la Matèria Condensada, Universitat de Barcelona

²Universitat de Barcelona Institute of Complex Systems (UBICS)

³Center for Computational Biology, Flatiron Institute (Simons Foundation)

Collective cell migration is a hallmark of the tissue remodeling events that underlie embryonic morphogenesis, wound repair, and cancer invasion. The coordinated motion of groups of cells in cohesive tissues results from the combination of cell-cell and cell-substrate interactions. As for isolated cells, it requires appropriate guidance that breaks symmetry in the form of chemical or mechanical gradients, allowing for a directional response. An alternative way of inducing a symmetry breaking in an isolated cell cluster is by means of changes in the cluster shape. While the interplay between shape and motion in cells has been established, showing that a morphological symmetry breaking can generate spontaneous motility [1], this possibility seems far less obvious in cell clusters, given that cell polarization in clusters is controlled by the proximity to the edge, which polarizes cells outwards regardless of the edge shape. Here, we unveil a deep connection between morphology and collective migration in clusters that are not globally polarized, showing that cells can self-organize to flow coordinately without external guidance. We base our study on a continuum description of the tissue as an active polar fluid, where traction forces on the substrate compete with contractile cell-cell forces. This model has been previously validated in various experiments with epithelial tissues [2, 3]. Here we focus on the free-boundary problem associated with shape evolution. We study under what conditions a spontaneous symmetry breaking of the circular shape may give rise to sustained motion and what shapes are attained by the traveling clusters (see Fig. 1). Two key length scales control this possibility. The screening length quantifies the extent of the hydrodynamic interactions, and the nematic correlation length defines the extent of the polarization alignment in neighboring cells. We find that spontaneous collective cell migration emerges for asymmetric shapes when the nematic length is sufficiently large compared to the smallest radii of curvature of the edge contour, and the screening length is sufficiently large compared to the system size. The first condition assures that the polarizing effect of the edge propagates sufficiently inside the cluster in an asymmetric way. The second makes the problem essentially nonlocal, assuring a response of the cluster as a whole. Then, the travel-

ing clusters do not relax to a circle and show sustained velocities that depend on shape and parameters in nontrivial ways. Depending on the tissue contractility, the clusters can significantly accelerate due to positive feedback associated with the velocity-shape coupling. We also show that chiral shapes generate the rotation of the cluster. From previous calibrations of our model from experimental data, we have estimates of all parameters for different cell lines of epithelial tissues. Our numerical simulations show that the predicted speeds are remarkably large and should be easily observable in epithelial monolayers prepared with prescribed shapes and sizes. We will also report on work in progress in the experimental verification of these results.

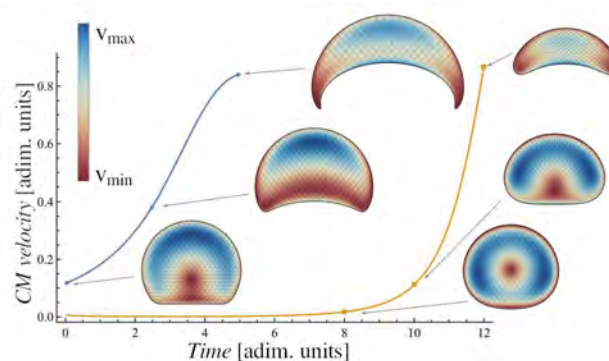


Fig. 1. Center of mass velocities and spontaneous evolutions of two traveling clusters with different initial shapes.

-
- [1] C. Blanch-Mercader, and J. Casademunt, *Spontaneous Motility of Actin Lamellar Fragments*, Phys. Rev. Lett. **110**, 078102 (2013).
- [2] C. Pérez-González, et al. *Active wetting of epithelial tissues*, Nat. Phys. **15**, 79 (2019).
- [3] M.E. Pallarès, et al. *Stiffness-dependent active wetting enables optimal collective cell durotaxis* Nat. Phys. **19**, 279289 (2023)

Parte VII

Sesión 7. Viernes 27 Tarde

Apología de la vaca esférica: modelos sencillos para sistemas complejos

Mario Castro^{1,2}

¹Instituto de Investigación Tecnológica (IIT), Universidad Pontificia Comillas, Madrid, Spain

²Grupo Interdisciplinar de Sistemas Complejos (GISC).

El éxito de la Ciencia de la Complejidad se debe, fundamentalmente, a su capacidad de explicar comportamientos emergentes y universales a partir de modelos relativamente sencillos. Por contra, en áreas afines como la Biología matemática o la Ecología, existe una tendencia creciente hacia la formulación de modelos detallados que tratan de capturar matemática decenas de mecanismos microscópicos y que dan lugar a una multitud de parámetros libres. Muchos de estos parámetros no se pueden medir experimentalmente y, en el mejor de los casos, los valores estimados divergen en un uno o dos órdenes de magnitud.

En esta charla trataré de argumentar que el concepto de *vaca esférica* (es decir un modelo simple, pero no demasiado) no es solo una manera conveniente de atacar problemas complejos sino que, en muchos casos, es la única manera honesta pero a la vez constructiva de avanzar en esas disciplinas afines.

Avances recientes en conceptos metodológicos como la *identificabilidad* [2] o los llamados modelos *sloppy* [1] permiten construir, de una manera sistemática y basada en datos, modelos sencillos que capturan los ingredientes esenciales de modelos más sofisticados pero imposibles de falsificar experimentalmente.

Utilizando ejemplos tomados de la Inmunología de sis-

temas [3], la Epidemiología [4] o la Ecología, mostraré algunos problemas comunes en su modelado y varias posibles soluciones complementarias: la construcción de modelos *top-down*, la reducción sistemática de modelos, y el modelado de nuestra ignorancia mediante el uso de distribuciones de probabilidad.

En definitiva, mi intención es resolver la tensión entre la complejidad que imponen las ciencias afines y la sorprendente eficacia de los modelos sencillos.

-
- [1] Transtrum, Mark K., et al. "Perspective: Sloppiness and emergent theories in physics, biology, and beyond." *The Journal of chemical physics* **143** (1) (2015).
 - [2] Castro, Mario, and Rob J. de Boer. "Testing structural identifiability by a simple scaling method." *PLOS Computational Biology* **16** (11), e1008248 (2020).
 - [3] Castro, Mario, et al. "Fusion and fission events regulate endosome maturation and viral escape." *Scientific Reports* **11** (1), 7845 (2021).
 - [4] Castro, Mario, et al. "The turning point and end of an expanding epidemic cannot be precisely forecast." *Proceedings of the National Academy of Sciences* **117** (42), 26190-26196 (2020).

Anomalous relaxation in systems far from equilibrium

Antonio Lasanta¹,

¹Departamento de Álgebra. Facultad de Educación, Economía y Tecnología de
Universidad de Granada, Cortadura del Valle, s/n, 51001 Ceuta, Spain. and
CarlosI Institute for Theoretical and Computational Physics, University of Granada, E-18071 Granada, Spain.

In this talk I will present very recent theoretical and experimental results about the relaxation of systems subject to one or several quenches. In particular, I will show that during the transient evolutions, before reaching an equilibrium or stationary state and under some particular conditions, the studied systems show surprising and counterintuitive effects. Namely, the Mpemba effect [3, 2, 1], the Kovacs effect [4] and an asymmetry between equidistant and symmetric heating and cooling processes. The ME happens when two identical systems, but with different initial temperatures, are put instantly in contact with a heat bath at a colder-than-both temperature, and the system that is further from equilibrium reaches it faster than the system that is initially closer to equilibrium and the opposite, the Inverse Mpemba effect, the cooler heats up before the heater and the Kovacs effect can take place when a thermalization process is suddenly interrupted by a change of the bath temperature, leading to a nonmonotonic evolution of the energy of the system. Finally we will show that heating was predicted to be faster than cooling, which we experimentally confirmed using an optically trapped colloidal particle. More strikingly, we show with both experiments and theory that between any pair of temperatures, heating is not only faster than cooling but the

respective processes in fact evolve along fundamentally distinct pathways, which we explain with a new theoretical framework we coin "thermal kinematics" [5].

-
- [1] JANUS, *The Mpemba effect in spin glasses is a persistent memory effect*, PNAS **116**,153501(2019).
 - [2] Lasanta, Antonio and Vega Reyes, Francisco and Prados, Antonio and Santos, Andrés, *When the Hotter Cools More Quickly: Mpemba Effect in Granular Fluids*, Phys. Rev. Lett.. **119**, 148001(2017).
 - [3] Carollo, Federico and Lasanta, Antonio and Lesanovsky, Igor, *Exponentially accelerated approach to stationarity in Markovian open quantum systems through the Mpemba effect* Phys. Rev. Lett.. **127**, 060401(2021).
 - [4] Militaru, Andrei and Lasanta, Antonio and Frimmer, Martin and Bonilla, Luis L and Novotny, Lukas and Rica, Ral A, *Kovacs memory effect with an optically levitated nanoparticle* Phys. Rev. Lett.. **127**, 130603(2021).
 - [5] Ibez, Miguel and Dieball, Cai and Lasanta, Antonio and Godec, Alja and Rica, Ral A, *Heating and Cooling are Fundamentally Asymmetric and Evolve Along Distinct Pathways*, arXiv preprint arXiv:2302.09061(2023).

Scale-invariance and near-critical behavior in neural systems

Guillermo B. Morales¹, Serena di Santo¹, and Miguel A. Muñoz¹

¹Departamento de Electromagnetismo y Física de la Materia, Universidad de Granada

The brain is in a state of perpetual reverberant neural activity, even in the absence of specific tasks or stimuli. Shedding light on the origin and functional significance of such a dynamical state is essential to understanding how the brain transmits, processes, and stores information. An inspiring, albeit controversial, conjecture proposes that some statistical characteristics of empirically observed neuronal activity can be understood by assuming that brain networks operate in a dynamical regime with features, including the emergence of scale invariance, resembling those seen typically near phase transitions.

Here, we present a data-driven analysis based on simultaneous recordings of the activity of thousands of individual neurons in various regions of the mouse brain [1]. To analyze these data, we construct a unified theoretical framework that synergistically combines a phenomenological renormalization group approach and techniques that infer the general dynamical state of a neural population, while designing complementary tools. This strategy allows us to uncover strong signatures of scale invariance that are quasiuniversal across brain regions and experiments, revealing that all the analyzed areas operate, to a greater or lesser extent, near the edge of instability. These results are then replicated on a minimal computational model to uncover the essential ingredients involved in the emergence of this scale-invariance phenomenon. To wrap-up, we move beyond biological systems to show that even artificial neural networks operating near the edge-of-instability, where optimal performance is achieved for an image-classification task, show similar

scaling behavior when subject to the aforementioned phenomenological renormalization group analysis.

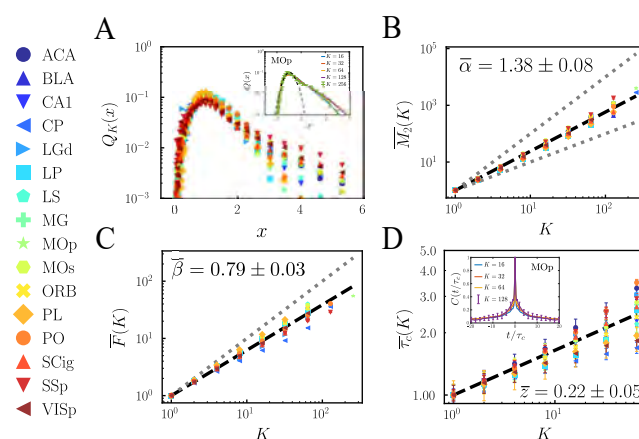


Fig. 1. Results of the phenomenological RG analyses of brain activity measured in 16 different mouse brain areas, showing the existence of a non-trivial quasi-universal scaling across regions.

[1] G. B. Morales, S. di Santo, and M. A. Muñoz, *Quasiuniversal scaling in mouse-brain neuronal activity stems from edge-of-instability critical dynamics*, Proceedings of the National Academy of Sciences **120(9)** (2023).

Entropy-Based Early Detection of Critical Transitions in Spatial Vegetation Fields

Giulio Tirabassi¹, and Cristina Masoller¹

¹Departament de Física, Universitat Politècnica de Catalunya, Rambla St. Nebridi 22, Terrassa 08222, Spain

In semi-arid regions, vegetated ecosystems can display abrupt and unexpected changes, i.e., transitions to different states, due to drifting or time-varying parameters, with severe consequences for the ecosystem and the communities depending on it. Despite intensive research, the early identification of an approaching critical point from observations is still an open challenge. Many data analysis techniques have been proposed, but their performance depends on the system and on the characteristics of the observed data (the resolution, the level of noise, the existence of unobserved variables, etc.). Here, we propose an entropy-based approach to identify an upcoming transition in spatio-temporal data. We apply this approach to observational vegetation data and simulations from two dynamical models of vegetation dynamics to infer the arrival of an abrupt shift to an arid state.

Permutation entropy (PE) is a popular complexity measure for time-series analysis [1], as it is very simple to implement and robust to noise. It has also been adapted to the analysis of two-dimensional (2D) images by defining 2D ordinal patterns (2D-OPs) [2], a technique that is useful to characterize the complexity of simulated cardiac arrhythmia data [3], as well as statistical properties of textures in images [4].

Formally, spatial PE is defined as the normalized Shannon entropy:

$$H = -\frac{1}{\log M} \sum_i^M p_i \log p_i, \quad (1)$$

where p_i are the probabilities of the 2D-OPs and M is the number of possible 2D-OPs. In the case of a continuous field, if the 2D-OPs are calculated with rectangles of $X \times Y$ pixels, then we have $M = (XY)!$. In the case of binary fields, instead, we have $M = 2^{XY}$. To examine properties at different spatial scales, one can use a lag and, in this case, the 2D-OPs are formed by non-neighboring data points.

For this study we use satellite tree cover data from the Moderate Resolution Imaging Spectroradiometer (MODIS) at 250m resolution (MOD44B) [5]. Each pixel represents a continuous variable: the proportion of tree coverage in a $250\text{m} \times 250\text{m}$ patch. We selected transects displaying tree coverage bistability with respect to rainfall. The transects have 200×4800 pixels; pixels occupied by rivers or water bodies have been disregarded in the calculations [6].

Figure 1 displays the results of the analysis of the first transect among those selected. The average tree cover shows two clearly different states that overlap in a bistability region, where the rainfall ranges from 2900 to 3100 mm/year. Starting in the upper branch, when the mean annual rainfall decreases, both entropy and spatial correlation decrease, with the entropy rising back right before the transition. The rise of the entropy before the transition seems to be a robust indicator of the approaching tipping point as it occurs in the six transects studied, as well as in a high-resolution transect

($3\text{m} \times 3\text{m}$) and in spatially extended models displaying critical slowing down [6] (not shown).

Like other spatial early-warning indicators, the spatial permutation entropy does not need a time series of the system dynamics, and it is suited for spatially extended systems evolving on long time scales, like vegetation plots.

Our results suggest that the spatial PE can be a good indicator of an abrupt shift in vegetation, and we believe that it has promising applications in the remote monitoring of ecosystems [6].

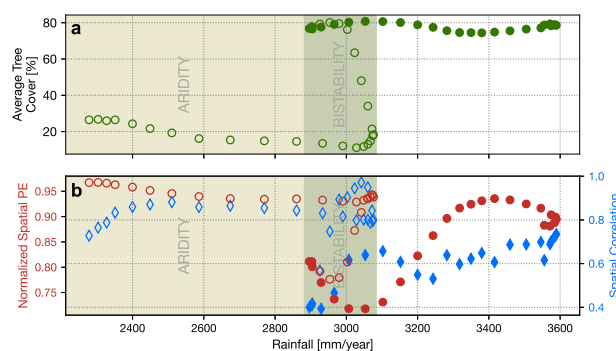


Fig. 1. Analysis of satellite vegetation data (transect 1). **a.** Average tree cover as a function of the mean annual rainfall; solid and empty symbols are used to differentiate the upper and lower branches. **b.** Spatial entropy (red) and spatial correlation (blue) of the tree cover field. These quantities have been computed using a 50km-wide window and a 12.5km step.

- [1] C. Bandt and B. Pompe, *Permutation Entropy: A Natural Complexity Measure for Time Series*, Phys. Rev. Lett. **88**, 174102 (2002).
- [2] H. V. Ribeiro et al., *Complexity-Entropy Causality Plane as a Complexity Measure for Two-Dimensional Patterns*, PLoS ONE **7**, e40689 (2012).
- [3] A. Schlemmer et al., *Spatiotemporal Permutation Entropy as a Measure for Complexity of Cardiac Arrhythmia*, Front. in Phys. **6**, 39 (2018).
- [4] H. Y. D. Sigaki et al., *Complexity-Entropy Causality Plane as a Complexity Measure for Two-Dimensional Patterns*, Phys. Rev. E. **99**, 013311 (2019).
- [5] C. DiMiceli et al., *MOD44B MODIS/Terra vegetation continuous fields yearly L3 global 250m SIN grid V006 [data set]. NASA EOSDIS land processes DAAC (2015).* <https://doi.org/10.5067/MODIS/MOD44B.006>
- [6] G. Tirabassi and C. Masoller, *Entropy-based early detection of critical transitions in spatial vegetation fields*, Proc. Natl. Acad. Sci. **120** (1), e2215667120 (2023).

Network science to study the emergence of complexity in the origin of life

Jacobo Aguirre^{1,2}, Izaskun Jiménez-Serra¹, Fernando Puente-Sánchez³ and Miguel García-Sánchez⁴.

¹Centro de Astrobiología CSIC-INTA, Madrid, Spain

²Grupo Interdisciplinar de Sistemas Complejos (GISC), Madrid, Spain

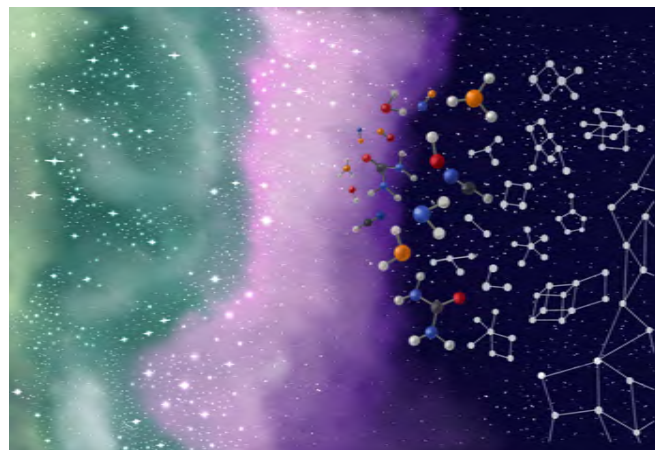
³Department of Aquatic Sciences and Assessment, Swedish University of Agricultural Sciences, 76551 Uppsala, Sweden

⁴Instituto de Investigacin Tecnológica, Universidad Pontificia Comillas, 28015 Madrid, Spain;

The road to life is punctuated by transitions toward complexity, from astrochemistry to biomolecules and eventually, to living organisms. Disentangling the origin of such transitions is a challenge where the application of complexity and network theory has not been fully exploited. Encouraged by this idea, we present a theoretical and computational framework, NetWorld, to model the evolution of simple networked structures toward complexity [1, 2].

In our computational environment, simple networks simulate the most basic building bricks of life and interact to form complex structures. The framework unveils the emergence of a drastic transition from simple structures toward complexity when the parameter representing the environment reaches a critical value. Notably, although our system does not attempt to model the rules of real chemistry nor is dependent on external input data, the results describe the emergence of complexity in the evolution of chemical diversity in the interstellar medium, where the original blocks of life could have been produced before being introduced in the early Earth by asteroids and meteorites during the Late Heavy Bombardment that took place between 4.1 and 3.8 billion years ago.

In particular, our results describe the real abundance distributions of chemical compounds detected in four interstellar clouds, and where a transition towards complexity takes place when the amount of interstellar dust (or extinction, playing the role of the environment parameter of our model) reaches a critical value and protects the cloud from the external interstellar UV radiation [3]. Furthermore, our work reveals an as yet unknown relationship between the abundances of molecules in dark clouds and the potential number of chemical reactions that yield them as products, supporting the ability of the framework presented here to shed light on real scenarios.



In summary, our work builds a bridge from complexity to astrobiology and reinforces the notion that some of the properties that condition the extremely complex journey from the chemistry in space to prebiotic chemistry and finally, to life could show relatively simple and universal patterns.

[1] M. García-Sánchez, I. Jiménez-Serra, F. Puente-Sánchez and J. Aguirre, *The emergence of interstellar molecular complexity explained by interacting networks*, PNAS **119** (30), e2119734119 (2022).

[2] <https://github.com/MiguelGarciaSanchez/NetWorld>

[3] M. Agúndez and V. Wakelam, *Chemistry of dark clouds: Databases, networks, and models*, Chem. Rev. **113**, 12, 8710 (2013).

Memory and rejuvenation phenomena in spin glasses, a computational approach for a thirty year open problem.

Javier Moreno-Gordo^{1,2,3,4} on behalf of the Janus Collaboration

¹ Departamento de Física Teórica, Universidad de Zaragoza, 50009 Zaragoza, Spain

² Instituto de Biocomputación y Física de Sistemas Complejos (BIFI), 50018 Zaragoza, Spain

³ Departamento de Física, Universidad de Extremadura, 06006 Badajoz, Spain

⁴ Instituto de Computación Científica Avanzada (ICCAEx)

Spin glasses are magnetic systems whose low-temperature phase is frozen and disordered and they are often seen as paradigmatic examples for the study of glassy behavior. The experimental study of spin glasses is plenty of interesting phenomena such as the *aging* phenomenon [1]. In our work [2], however, we will focus on the *memory* and *rejuvenation* phenomena [3].

Unfortunately, despite more than thirty years of theoretical efforts following the experimental discovery of memory and rejuvenation, these effects have thus far been impossible to simulate reliably.

Yet, recent developments convinced us to accept this challenge. First, the custom-built Janus II supercomputer makes it possible to carry out “numerical experiments” in which the very same quantities that can be measured in experiments are computed from the simulation, allowing for parallel analysis of the simulation/experiment data. Second, recent numerical results for the off-equilibrium study of spin glasses [4, 5], have allowed us to compare experimental and numerical results.

All these aspects together have allowed us to simulate a protocol in which we can numerically reproduce the memory and rejuvenation phenomena, as can be shown in Figure 1.

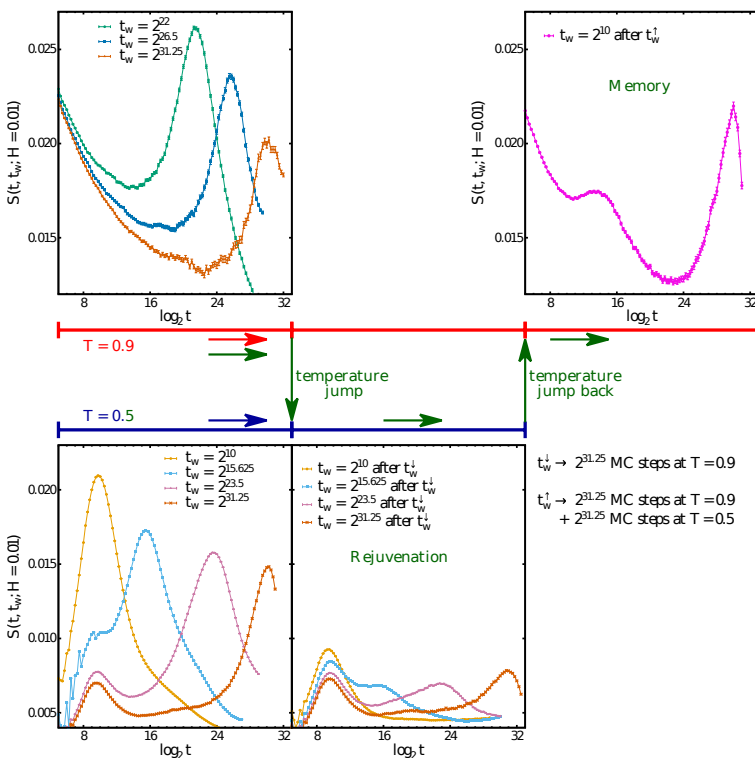


Fig. 1. Magnetic response of simulated spin glass in different moments of the thermal protocol shows the rejuvenation and memory phenomena.

25-27 de octubre de 2023, Pamplona

- [1] Gruber, E. L. G. E. (1978). LGE Struik: Physical Aging in Amorphous Polymers and Other Materials. Elsevier Sci. Publ. Comp., AmsterdamOxfordNew York 1978. 229 Seiten, 141 Abbildungen, Preis: US \$42, 50, Holl. Gulden 97, 50.
- [2] Baity-Jesi, M., & Janus Collaboration. (2023). Memory and rejuvenation in spin glasses: aging systems are ruled by more than one length scale. Nature Physics, 1-8, 2023.
- [3] Jonason, K., Vincent, E., Hammann, J., Bouchaud, J. P., & Nordblad, P. (1998). Memory and chaos effects in spin glasses. Physical Review Letters, 81(15), 3243.
- [4] Zhai, Q., .. & Yllanes, D. (2020). Scaling law describes the spin-glass response in theory, experiments, and simulations. Physical Review Letters, 125(23), 237202.
- [5] Baity-Jesi, M., ... & Yllanes, D. (2021). Temperature chaos is present in off-equilibrium spin-glass dynamics. Communications Physics, 4(1), 74.

Physics meets biology: Organ-on-a-chip

Sylvana Varela^{1,2}, Elías Ferreiro² and Bruno K. Rodiño²

¹Department of Mechanical Engineering, Universitat Rovira i Virgili, 43007, Tarragona, España

²BFlow,15706, Santiago de Compostela, España

Los sistemas organ-on-a-chip (OoaC) son dispositivos tridimensionales que imitan la fisiología humana en pequeños chips. Tienen la posibilidad de ser cultivados con células y aplicar condiciones dinámicas de flujo, permitiendo discriminar con mayor eficacia qué moléculas funcionarán en el organismo vivo (etapa crítica en la fase preclínica del desarrollo de fármacos). Se estima que la aplicación de esta tecnología supone ahorros en tiempo del 40% en fase preclínica y ahorros económicos entre el 10% y el 26% por fármaco lanzado al mercado, además de reducir el número de experimentos necesarios en animales [1]. Con los modelos 2D actuales no es posible reproducir la disposición 3D de las células de los vasos sanguíneos y el flujo sanguíneo que soportan. La aplicación de la tecnología OoaC es especialmente interesante para la réplica de vasos sanguíneos, por esta razón se ha desarrollado un chip Vessel-on-a-chip (Voac). La necesidad de los Voac desarrollados (3D) proviene de que los sistemas disponibles en el mercado no pueden reproducir características tan relevantes de la biología vascular como canales de un calibre de milímetros o con sección circular. En el caso de las enfermedades cardiovasculares, los modelos Voac tienen un alto interés, ya que estas enfermedades están estrechamente relacionadas con la disfunción endotelial (pérdida de las funciones de las células endoteliales que recubren las paredes de los vasos sanguíneos). Más concretamente, los modelos Voac refuerzan dos características interesantes para estudiar la biología vascular:

- Modelos celulares en 3D superior al modelo 2D estático.
- Modelos bajo flujo controlado que reproducen las características biológicas del endotelio.

En cuanto a estas dos características de los Voac (cultivo en 3D y control de las condiciones de flujo, Fig. 1), el modelo de BFlow supera al resto de competidores en el mercado [5, 6, 7].

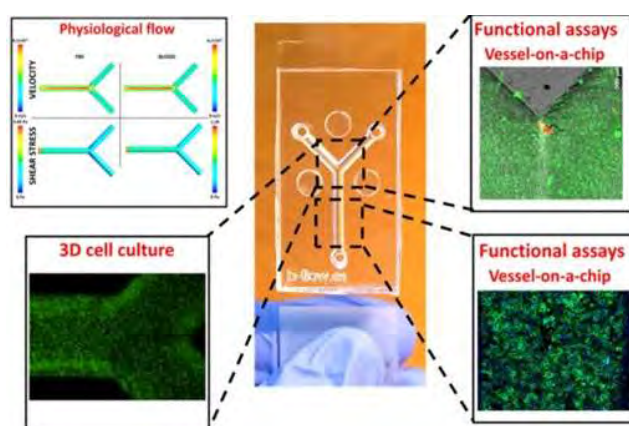


Fig. 1. Características de los Voac de Bflow [5, 6, 7].
25-27 de octubre de 2023, Pamplona

El abordaje desde el punto de vista físico de los diferentes modelos de OoaC permite mejorar los diseños antes de llegar a las pruebas biológicas mediante la optimización de las geometrías y el estudio mediante simulaciones numéricas de los diferentes modelos.

-
- [1] Franzen N, van Harten WH, Retél VP, Loskill P, van den Eijnden-van Raaij J, IJzerman M, *Impact of organ-on-a-chip technology on pharmaceutical R&D costs*, Drug Discovery Today **24(9)**, 1720-4 (2019).
- [2] Aymerich M, Ivarez E, Bao-Varela C, Moscoso I, Gonzalez-Juanatey JR, Flores-Arias MT, *Laser technique for the fabrication of blood vessels-like models for preclinical studies of pathologies under flow conditions*, Biofabrication. **9(2):025033** (2017)
- [3] Casas-Arozamena C, Otero-Cacho A, Carnero B, Almenglo C, Aymerich M, Alonso-Alconada L, *Haemodynamic-dependent arrest of circulating tumour cells at large blood vessel bifurcations as new model for metastasis*, Sci Rep **9(2):025033** (2017)
- [4] Otero-Cacho A, Aymerich M, Flores-Arias MT, Abal M, Ivarez E, Prez-Muuzuri V, *Determination of hemodynamic risk for vascular disease in planar artery bifurcations*, Sci Rep. **8(1):2791** (2018)
- [5] Turpin C, Apalama ML, Carnero B, Otero-Cacho A, Munuzuri AP, Flores-Arias MT, *Impact of Enhanced Phagocytosis of Glycated Erythrocytes on Human Endothelial Cell Functions*, Cells. **11(14):2200** (2022)
- [6] Kim S, Lee H, Chung M, Jeon NL, *Engineering of functional, perfusable 3D microvascular networks on a chip*, Lab Chip. **13(8):1489** (2013)
- [7] Tvan Duinen V, Stam W, Mulder E, Famili F, Reijkerker A, Vulto P, *Robust and Scalable Angiogenesis Assay of Perfused 3D Human iPSC-Derived Endothelium for Anti-Angiogenic Drug Screening*,IJMS. **21(13):4804**. (2020)

Parte VIII

Sesión Póster 1. Miércoles 25 Tarde

The simplest complex dynamics under friction

Martin Maza-Cuello¹, and Diego Maza¹

¹ Departamento de Física y Matemática Aplicada, Facultad de Ciencias, Universidad de Navarra, E-31080 Pamplona, Spain.

Under its seemingly trivial nature, the dynamics of a mass over an oscillating, horizontal surface hides a rich set of non-linear behaviors in the presence of dry friction and/or viscous forces, where friction may become a driving force [1].

In this study, we present experimental measurements of the dynamics of a free, rigid body—a “walker”—over a base that oscillates sinusoidally. The setup is shown in Fig. 1. Even in this fundamental configuration, at least three dynamic regimes can be found depending on the maximum acceleration and the friction coefficients between walker and surface: i) stick, ii) stick-slip, and iii) no-stick (continuous slipping). The first transition is characterized by the crossover from static to dynamic friction, while the second one arises from a dynamical constraint on the time intervals over which the walker may slip.

Although the walker performs a periodic motion with the same frequency as the base, the dynamics is characterized by an amplitude A_W smaller than that of the base, together with a time lag τ between base and walker maxima, cf. Fig. 2.

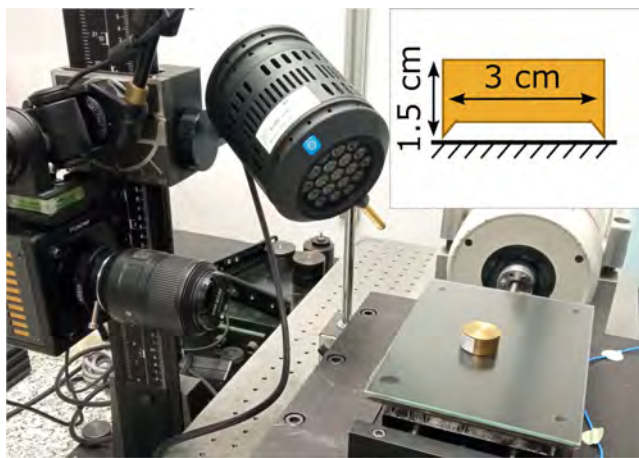


Fig. 1. Experimental setup: a walker is free to move on top of an oscillating base. The inset shows the relevant dimensions of the walker. The contact between walker and base is a ring with width ~ 0.3 mm. For the particular case of the image, the walker is made out of brass and the surface is frosted glass.

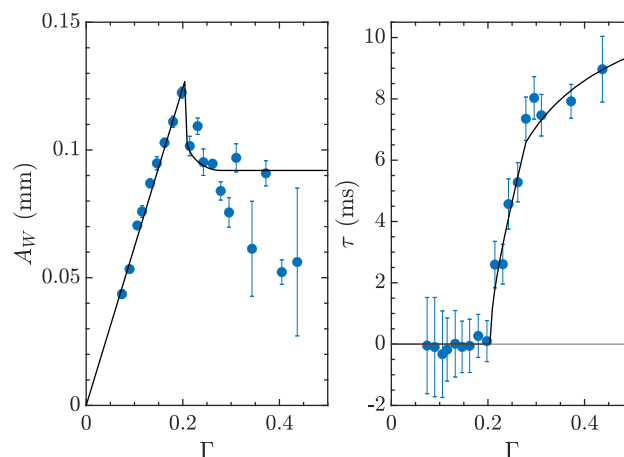


Fig. 2. Amplitude A_W of the walker’s oscillations and time lag τ between the maxima of the walker and the base, for a brass walker over a quartz surface at 57°C , as a function of the dimensionless acceleration $\Gamma \equiv A\omega^2/g$ (A : base amplitude, ω : frequency of the base, g : gravitational acceleration). Points are data averaged over 20 periods, black lines are fits to a minimal model with $\mu_s = 0.21$ and $\mu = 0.12$.

These quantities can be theoretically described from a minimal model of dry friction where the only fitting parameters are the static and dynamic friction coefficients, denoted μ_s and μ respectively. As a result, the latter can be quantified from the measurement of the walker’s dynamics, allowing us to obtain values of μ_s and μ for several combinations of materials.

[1] M. Nicolas, *A comprehensive study on the behavior of a rigid block on an oscillating ground with friction, elastic and viscous forces*, *Inter. J. Non-Linear Mech.* **93** (2017) 21–29.

Mathematical Analysis of the competition among different Variants of SARS-CoV-2 in European Countries

Vctor L de Rioja ¹, Sergio Alonso ¹, Enrique Alvarez-Lacalle ¹, Mart Catal ², and Clara Prats ¹

¹Department of Physics, Universitat Politècnica de Catalunya,

²Center for Statistics in Medicine, NDORMS. University of Oxford, United Kingdom

Countries across Europe suffered different waves of COVID-19 during the pandemic [1]. Such countries experienced similar variants of the SARS-CoV-2 virus as the pandemic evolved over time, including pre-Alpha, Alpha, Delta, and Omicron, with various lineages such as BA1, BA2, BA5 and BQ.1.

We employ a mathematical modeling approach based on non-interactive epidemics of the different variants to analyze the transmissibility of these variants in Europe over a period of more than two years, from late 2020 to early 2023. Weekly sequencing data from 28 European countries were used to estimate the difference on the transmission rate $\Delta\beta$ between different variants of SARS-CoV-2, specifically between pre-Alpha vs Alpha, Alpha vs Delta, and Delta vs Omicron. Sub-lineages of Omicron (BA1, BA2, BA5 and BQ.1) were also analyzed within 16 European countries. An example of such analysis is shown in Fig.1 for the particular case of France. The number of samples analyzed in France is shown in the top panel, and the resulting variants are shown with a different color code. The fraction of each variant with respect the total is shown in middle panel, which permit us to define the substitution model and calculate the increase of the trasmissibility between two variants. Finally, the dynamics among the variants can be compared with the total number of cases and the corresponding reproductive number of the epidemics, see botton panel

The study found that the transmission rate of SARS-CoV-2 increases as the virus evolves, $\Delta\beta_\alpha < \Delta\beta_\delta < \Delta\beta_o$. Furthermore, the transmission rate tends to be higher in smaller countries than in larger ones, thats why multiple substitution, spatially, and temporally separated are also studied.

Analyzing the transmission rates of different variants can provide insights into factors that influence the spread of the virus and it can be compared with hospitalization rates to

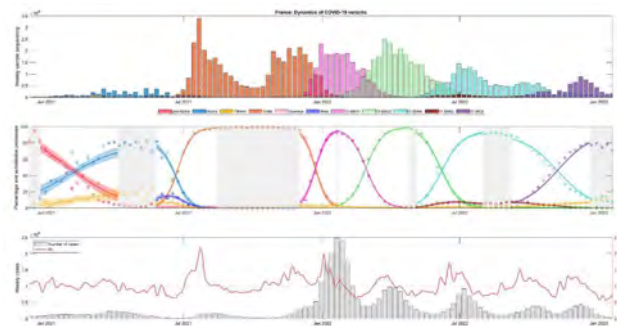


Fig. 1. Dynamical evolution of the differnt variants of SARS-CoV-2 in France over time. Weekly sample sequencing of the differnt variants (top); real percentage data of eahc variant compared with the mathematical substitution model (middle); and weekly total cases together with the associated effective reproduction number (bottom).

assess the decrease of the severity of the differnt variants [2].

[1] M Catal, S Alonso, E Alvarez-Lacalle, D Lpez, PJ Cardona, C Prats *Empirical model for short-time prediction of COVID-19 spreading*, Plos computational biology **16** (12), e1008431 (2010).

[2] M Catal, E Coma, S Alonso, C Andrs, I Blanco, A Antn, AE Bordoy, P.J. Cardona, F. Fina, E. Martr, M. Medina, N. Mora, V. Saludes, C. Prats, D. Prieto-Alhambra, E. Alvarez-Lacalle *Transmissibility, hospitalization, and intensive care admissions due to omicron compared to delta variants of SARS-CoV-2 in Catalonia: A cohort study and ecological analysis*, Frontiers in public health, 2490 (2022).

Collective motion of virtual amoebae: interactions among deformable swimmers

Eduardo Moreno ¹, Robert Grossmann ², Carsten Beta ², and Sergio Alonso ¹,

¹Department of Physics, Universitat Politècnica de Catalunya,

²Biological Physics Group, Univesität Potsdam

The coupling of the internal mechanisms of cell polarization to cell shape deformations and subsequent cell crawling poses many interdisciplinary scientific challenges. Several mathematical approaches have been proposed to model the coupling of both processes, where one of the most successful methods relies on a phase field that encodes the morphology of the cell, together with the integration of partial differential equations that account for the polarization mechanism inside the cell domain as defined by the phase field [1]. This approach has been previously employed to model the motion of single cells of the social amoeba *Dictyostelium discoideum*, a widely used model organism to study actin-driven motility and chemotaxis of eukaryotic cells [2].

Besides single cell motility, *Dictyostelium discoideum* is also well-known for its collective behavior. We extend the previously introduced model for single cell motility [2] to describe the collective motion of large populations of interacting amoebae by including repulsive interactions between the cells [3]. We performed numerical simulations of this model, first characterizing the motion of single cells in terms of their polarity and velocity vectors, see Fig.1(A,B). We then systematically studied the collisions between two cells that provided the basic interaction scenarios also observed in larger ensembles of interacting amoebae, see Fig.1(C). Finally, the relevance of the cell density was analyzed, revealing a systematic decrease of the motility with density, associated with the formation of transient cell clusters that emerge in this system even though our model does not include any attractive interactions between cells.

This model is a prototypical active matter system for the investigation of the emergent collective dynamics of deformable, self-driven cells with a highly complex, nonlinear coupling of cell shape deformations, self-propulsion and repulsive cell-cell interactions. Understanding these self-organization processes of cells like their autonomous ag-

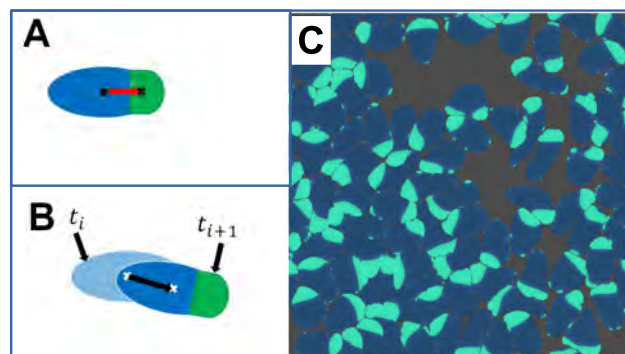


Fig. 1. A) Definition of the polarization vector of a single polarized cell. B) Definition of the velocity vector after the motion of the cell. C) Set of 81 cells moving and colliding with the other cells in a square domain with periodic boundary conditions.

gregation is of high relevance as collective amoeboid motility is part of wound healing, embryonic morphogenesis or pathological processes like the spreading of metastatic cancer cells.

-
- [1] D. Shao W.J. Rappel, H. Levine, *Computational model for cell morphodynamics*, Physical Review Letters. **105** (10), 108104 (2010).
- [2] S. Alonso, M. Stange, C. Beta, *Modeling random crawling, membrane deformation and intracellular polarity of motile amoeboid cells*, PloS one **13** (8), e0201977 (2018).
- [3] E. Moreno, R. Gromann, C. Beta, S. Alonso, *From single to collective motion of social amoebae: a computational study of interacting cells*, Frontiers in Physics **9**, 850 (2021).

Complex rheology of a pedestrian evacuation

Dariel Hernández-Delfin¹, Ander García^{1,2}, and Marco Ellero^{1,3,4}

¹ BCAM, Basque Center for Applied Mathematics, 48009 Bilbao, Spain

² Department of Mathematics, University of the Basque Country UPV/EHU, Bilbao, 48080, Spain

³ Zienkiewicz Center for Computational Engineering (ZCCE), Swansea University, United Kingdom

⁴ IKERBASQUE, Basque Foundation for Science, 48013, Vizcaya, Spain

This study revisits the evacuation of pedestrians through a bottleneck from a rheological perspective. Pedestrian crowd dynamics exhibit complex behavior with the variation of the competitiveness of pedestrians forming part of the crowd. When pedestrians possess high competitiveness, the desire to escape rapidly leads to higher evacuation times. Besides the anecdotal experience, this is an outcome that has been previously corroborated through numerical[1] and experimental[2] investigations and has given the name of *faster-is-slower phenomenon* (FIS).

In the field of suspension rheology, a similar effect is obtained when non-Brownian suspensions are submitted to an external perturbation. Namely, the system's viscosity increases as the shear rate or shear stress upon the suspension increases. This effect is known as *shear thickening* and can occur smoothly or abruptly, being denoted as *continuous shear thickening* (CST) and *discontinuous shear thickening* (DST)[3], respectively. *Shear thickening* is explained on the basis of the transition that might emerge in the nature of the dominant forces, passing from frictionless (lubricated) interactions to frictional contacts. A similar transition experiences pedestrians systems when the competitiveness of pedestrians is increased, causing a system transition from purely-repulsive social long-range to frictional contact short-range forces.

Based on numerical simulations employing the Social Force Model (SFM)[4], we evaluate a pedestrian egress from a room across a constriction formed by the room door. The numerical setup employed here is a steady-state version of the geometry assessed by Helbing et al. in Ref. [1]. We find that the viscosity of the pedestrian flow depends on the desired velocity, showing discontinuous shear thickening close to the values where FIS is observed (see Fig. 1). The study find that both social force and shear force are necessary to trigger the frictionless-friction transition that leads to FIS. Contact forces alone cannot activate FIS, and social force interaction is necessary for avoiding contact at low speeds.

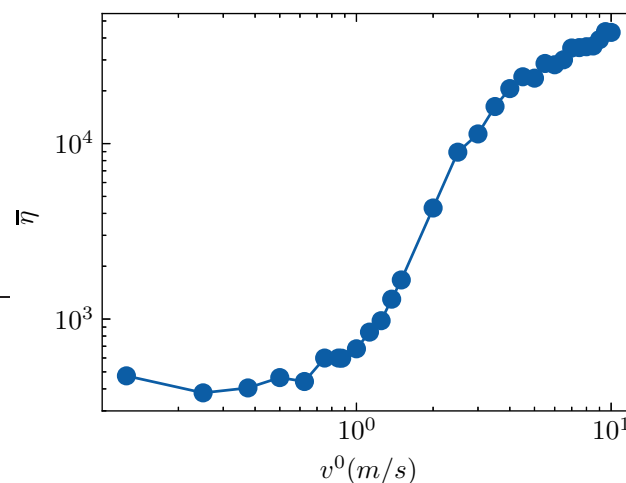


Fig. 1. Viscosity of the pedestrian flow as a function of the desired speed.

Suspension systems may be better for mimicking pedestrian dynamics than dry granular systems.

-
- [1] Helbing, D., Farkas, I. & Vicsek, T. Simulating dynamical features of escape panic. *Nature*. **407**, 487-490 (2000)
 - [2] Garcimartín, A., Zuriguel, I., Pastor, J., Martín-Gómez, C. & Parisi, D. Experimental evidence of the "faster is slower" effect. *Transportation Research Procedia*. **2** pp. 760-767 (2014)
 - [3] Wyart, M. & Cates, M. Discontinuous shear thickening without inertia in dense non-Brownian suspensions. *Physical Review Letters*. **112**, 098302 (2014)
 - [4] Helbing, D. & Molnr, P. Social force model for pedestrian dynamics. *Physical Review E*. **51**, 4282 (1995)

Optimization of number and location of solar plants and storage in a power grid with high penetration of renewables

Benjamín A. Carreras^{1,2}, Pere Colet¹, José M. Reynolds-Barredo², and Damià Gomila¹

¹Instituto de Física Interdisciplinar y Sistemas Complejos, IFISC (CSIC-UIB)

Campus Universitat de les Illes Balears, E-07122 Palma de Mallorca, Spain.

²Departamento de Física, Universidad Carlos III de Madrid, 28911 Leganés, Madrid, Spain.

We analyze the risk of blackouts with high penetration of variable renewable energy sources (VRESs) using a model for the long-term evolution of the power grid including propagation of cascading failures, day-to-day fluctuations of renewable generation and moderate use of storage [1]. As a case study, we consider the replacement of conventional power plants by solar photovoltaic generation combined with storage in the power grid of the Balearic Islands. We analyze grid resilience and stress as VRESs are progressively incorporated and evaluate the VRES performance as the average fraction of daily demand covered by renewables. We find that VRES intrinsic variability typically increases the grid stress and the blackout risk. However, if VRESs are implemented in a distributed way, the spatial spreading of the generation may have a positive effect on grid resilience.

Futhermore we propose a method to find the optimal number and location of solar plants while minimizing the amount of storage needed to keep the risk and performance at levels comparable to a power grid with only conventional plants [2].

[1] B.A. Carreras, P. Colet, J.M. Reynolds-Barredo, and D. Gomila, *Assessing blackout risk with high penetration of variable renewable energies*, IEEE Access **9**, 132663 (2021).

[2] B.A. Carreras, P. Colet, J.M. Reynolds-Barredo, and D. Gomila, *Optimization of number and location of solar plants and storate in a power grid with high penentation of renewables*, submitted for publication.

Graph alignment across connectomes using Bayesian Inference

Teresa Lázaro¹, Roger Guimerà¹, and Marta Sales-Pardo¹

¹URV, teresa.lazaro@urv.cat

The graph alignment problem refers to the task of finding the correspondence mapping between two or more equivalent graphs, i.e. finding the right permutation between their node labels. This is an active research area used in several interdisciplinary fields, including, for instance, the comparison of protein structures or the identification communities in a social network. In our study, we have developed a Bayesian inference-algorithm to align N graphs simultaneously.

In particular, our objective is to align four experimental connectomes obtained from the brains of *C.elegans* at different developmental stages [1]. Since individuals that belong to the same species share common brain features, it is meaningful to search for the mappings between their connectomes: We can consider their brains as variations of a common "brain template", also called the blueprint. Therefore, our aim is to infer the right permutations between the node labels of the four brain graphs, as well as identifying the most likely blueprint that generates these connectomes.

In the bayesian framework, we first must to formalize a generative process (with q the copy error probability of an edge/neuronal connection) for the different networks we observe, (\mathbf{A}^k are the observed adjacency matrices). The graph alignment problem in this case is then to match each network to the latent matrix, or, in other words, to find the permutation of network indices π^k for each network \mathbf{A}^k that match the underlying blueprint. In what follows, we will call this blueprint as the latent (directed) adjacency matrix \mathbf{L} .

Finally, our goal will be then to find the set of permutations $\{\pi^k\}$ and the latent matrix \mathbf{L} that maximize the posterior probability $p(\mathbf{L}, \{\pi^k\}|\{\mathbf{A}^k\})$, Eq. (1).

$$p(\mathbf{L}, q, \{\pi^k\}|\{\mathbf{A}^k\}) = \frac{p(\{\mathbf{A}^k\}|\mathbf{L}, q, \{\pi^k\})p(\mathbf{L})p(q)p(\{\pi^k\})}{p(A)} \quad (1)$$

To maximize this Bayesian probability (the best solution), we have developed a Parallel Monte Carlo algorithm that incorporates biological assumptions about the nodes, such as the knowledge of the neuroblast group to which each neuron belongs or the *a priori* knowledge of certain node labels (called the anchors).

This probabilistic approach allows us to recover with good accuracy the alignment of the four *C.elegans* connectomes. Until now these kinds of alignments were done only for pairs [2], in easier problems and without our possibilities of fitting the generative model to other problems. Additionally, we are able to infer the group label of some neurons in cases where their neuroblast groups is unknown.

[1] Joshua T. Vogelstein, John M. Conroy, et al. *Fast Approximate Quadratic Programming for Graph Matching.*, PLOS ONE, 10(4):e0121002, April 2015.

[2] Daniel Witvliet, Ben Mulcahy, James K. Mitchell, et al. *Connectomes across development reveal principles of brain maturation.*, Nature, 596(7871):257261, August 2021

Inferring the connectivity of complex networks using ordinal transition methods

Juan A. Almendral^{1,2}, I. Leyva^{1,2} and Irene Sendiña-Nadal^{1,2}

¹ Complex Systems Group & GISC, Universidad Rey Juan Carlos, 28933 Móstoles, Madrid, Spain

² Center for Biomedical Technology, Universidad Politécnica de Madrid, 28223 Pozuelo de Alarcón, Spain

Time series analysis has garnered significant research attention in recent decades. However, the exponential growth in data generation from various social, technological, and natural sources observed in the last years has posed a challenge for researchers seeking to extract valuable information from these datasets. Among the set of new tools developed for this purpose, the ordinal methods derived from the seminal work of Bandt and Pompe [1] have emerged as particularly intriguing for analyzing correlated data series [2, 3, 4]. However, using these methods to understand the information exchange in networks of dynamical systems and uncover the interplay between dynamics and structure during the synchronization process remains relatively unexplored. Here, we compare the ordinal permutation entropy, a standard complexity measure in the literature, and the entropy of the ordinal transition probability matrix that describes the transitions between the ordinal patterns derived from a time series.

Our findings, using networks of coupled chaotic Rössler systems [5], demonstrate that ordinal transition methods outperform conventional ordinal patterns' statistics when it comes to detecting subtle dynamical changes and discriminating nodes based on their topological roles [6]. In particular, to assess the methods validity in a more realistic environment with available ground truth structural information, we analysed the experimental datasets of networks of nonlinear electronic circuits downloadable in Ref. [7]. These datasets comprise the time series of the output voltage of $N = 28$ electronic circuits coupled in 20 different network configurations and monitored along their synchronization process for 100 coupling levels, ranging from disconnection (isolated nodes) to values producing a network state of complete synchrony. These experimental datasets provide the ideal testbed for our inference method and to predict the circuits connectivity by means of the network permutation entropy of each timeseries circuit as shown in Fig. 1.

These initial results illuminate new possibilities for using ordinal methods in various applications, including functional brain data analysis, power grids, mobility networks, or any arbitrary real-world time series exhibiting correlations originating from an existing underlying unknown network structure. Many methods focused on the structurefunction relationship are primarily intended to infer the detailed connectivity network, down to the level of the individual links, from time series. However, in many cases, knowledge of centrality roles alone is sufficient for designing successful interventions in the dynamics. Therefore, we anticipate that our results, which do not rely on pairwise correlations between time series, will be of particular interest in the context

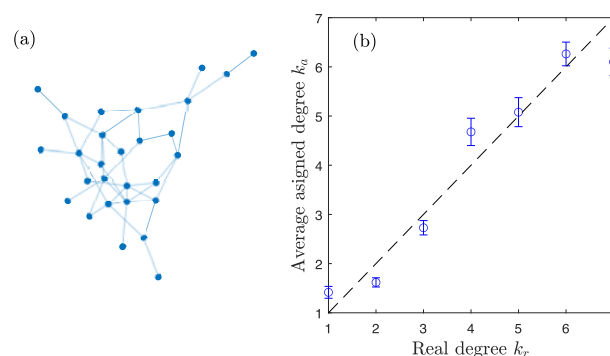


Fig. 1. Inference of the nodes' degree of networks of electronic circuits based on the network permutation entropy of the timeseries reported in Ref. [7]. (a) Structure connectivity of the electronic circuit network used as a ground truth. (b) Average assigned degree k_a versus the real degree k_r obtained when using a single network as a training reference.

of functional networks and other scenarios in which the underlying structural information is inaccessible.

-
- [1] Christoph Bandt, and Bernd Pompe. *Permutation entropy: A natural complexity measure for time series*, Phys. Rev. Lett. **88**,174102 (2002).
- [2] Inmaculada Leyva, Johann H Martínez, Cristina Masoller, Osvaldo A Rosso, and Massimiliano Zanin, *20 years of ordinal patterns: Perspectives and challenges*, Europhysics Letters **138**, 31001 (2022).
- [3] A. Tlaie, I. Leyva, R. Sevilla-Escoboza, V. P. Vera-Avila, and I. Sendiña Nadal, *Dynamical complexity as a proxy for the network degree distribution*, Phys. Rev. E **99**, 012310 (2019).
- [4] A. Tlaie, L.M. Ballesteros-Esteban, I. Leyva, and I. Sendiña-Nadal, *Statistical complexity and connectivity relationship in cultured neural networks*, Chaos, Solitons & Fractals **119**, 284–290 (2019).
- [5] O. E. Rössler, *An equation for continuous chaos*, Physics Letters A **57**, 397–398 (1976).
- [6] J.A. Almendral, I. Leyva, and I. Sendiña-Nadal. *Unveiling the Connectivity of Complex Networks Using Ordinal Transition Methods*, Entropy **25**, 1079 (2023).
- [7] V. Vera-vila, R. Sevilla-Escoboza, A. Lozano-Sánchez, R. Rivera-Durn, J.M. Buld, *Experimental datasets of networks of nonlinear oscillators: Structure and dynamics during the path to synchronization*, Data in Brief **28**, 105012 (2020).

Opportunistic gambling versus conservative bet-hedging in populations evolving in fluctuating environments

Rubén Calvo^{1,2}, Miguel A Muñoz^{1,2}, and Tobias Galla³

¹Departamento de Electromagnetismo y Física de la Materia, Universidad de Granada E-18071, Granada, Spain

²Instituto Carlos I de Física Teórica y Computacional, Universidad de Granada E-18071, Granada, Spain

³Instituto de Física Interdisciplinar y Sistemas Complejos IFISC (CSIC-UIB), 07122 Palma de Mallorca, Spain

Living organisms often have to struggle with the variability of their surroundings. When environmental fluctuations are unpredictable, lineages of individuals can prevail if genotypes ‘hedge their bets’ [1]. The theory of bet hedging states that evolutionary success is determined not only by the mean fitness of a certain population but rather by a trade-off between such an average fitness (first moment of the distribution, denoted as μ) and the fitness variation across environmental conditions (second moment of the distribution, denoted as σ^2). However, higher order moments of the distribution of fitness have not yet been taken into account, and the impact of asymmetry on the success of bet-hedging strategies remains unknown.

Here, we aim to study precisely the effect that the shape of the distribution of fitness has on the benefits of adopting a bet-hedging strategy. For that, we propose a Stochastic Evolutionary Game Theory approach [2] and use an individual-based model for a finite population, considering the situation in which a single mutant needs to thrive in an established existing resident population. The dynamics unfolds through a series of stochastic birth-death events, where the reproduction rates of residents and mutants are controlled by their payoffs, that fluctuate stochastically according to a certain distribution (see Figure 1). With these ingredients, the population dynamics are such that the mutant will eventually either go extinct or take over the population. Hence, the success of a newly introduced mutant can be quantified in terms of the probability of fixation, denoted as ϕ_1 .

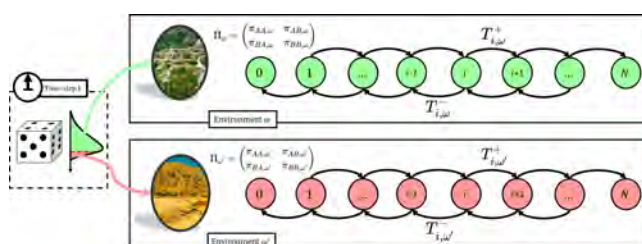


Fig. 1. **Illustration of the model.** A Stochastic Evolutionary Game in which the payoffs are drawn, at each birth-death event, out of a certain distribution. The environment is denoted as ω . The payoff matrix is an environment-dependent function denoted as Π_{ω} . The state of the system is characterized by the number of individuals adopting the strategy A , i . The transition probabilities $T_{i,j}^{\pm}$ denote the probabilities of each birth-death event. N denotes the total size of the population.

Using this simple model, we were able to prove, both numerically and analytically that the Evolutionary Stable Strategy (that is, the strategy that cannot be invaded with a probability bigger than $1/N$) is determined not only by the mean fitness and its variance but also by the shape of the distribution

and, more specifically, by its degree of asymmetry, quantified by the skewness μ_3 . The simplest case comes when we suppose that the payoff of the individual adopting strategy A is a_1 with probability p_1 and a_2 with probability p_2 , while the individual adopting strategy B always receives a payoff equal to 1 (because the outcome of the game only depends on payoff differences, one of the payoffs can always be set to 1). For this scenario, the fixation probability in terms of the first three moments is depicted in Figure 2. In this case, we can observe the existence of bet-hedging strategies in which the values of σ and μ are reduced and the fixation probability ϕ_1 increases; together with what we have named ‘opportunistic gambling strategies’, being those in which the evolutionary success is increased by increasing the variance of the fitness distribution, rather than reducing it.

This work stands as an initial point to study the relevance of the asymmetry on the distribution of payoffs to determine the evolutionary success of bet-hedging strategies. A more sophisticated model would include the separation of time scales for the evolutionary process and the stochastic switching of the environment.

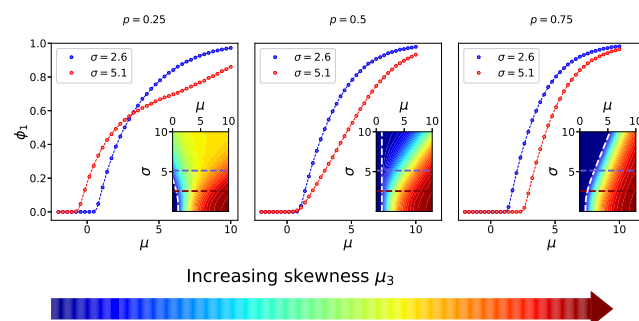


Fig. 2. **Results for a dichotomous distribution of payoffs:** The graphs show the fixation probability in terms of the first moment μ for two different values of σ (circles are the results of the simulations, the lines come from the theory), each for a certain value of the probability p_1 (and hence, a certain skewness). The insets show the fixation probability in the space (μ, σ) . The white dotted line in the inset stands for the frontier of the Evolutionary Stable Strategy.

[1] Starrfelt, Jostein and Kokko, Hanna, *Bet-hedging-a triple trade-off between means, variances and correlations*, Biological Reviews 87, 14647931 (2012).

[2] P. Ashcroft, P. M. Altrock, and T. Galla, *Fixation in finite populations evolving in fluctuating environments*, J. R. Soc. Interface., vol. 11, no. 100, p. 20140663, Nov. 2014, doi: 10.1098/rsif.2014.0663.

How does a polymer stretch?

Alessandro Fiasconaro^{1,2}, and Fernando Falo^{1,2,3},

¹Dpto. Física de la Materia Condensada, Universidad de Zaragoza.

²Instituto de Biocomputación y Física de Sistemas Complejos (BIFI), Universidad de Zaragoza.

³Institute of Biophysics, National Research Council (CNR) - Palermo Unit, Italia.

Based on classical statistical mechanics, we calculate the exact partition function of the length extension of a discrete extensible wormlike polymer under a stretching force. The bonds extensibility is modeled with harmonic springs, and the links present the transversal bending recoil typical of the wormlike chain (WLC) model.

The evaluation has followed two methods: From the one hand by using the Transfer Matrix procedure to calculate numerically the extension/force curve of the polymer, whose outcomes have been double checked with numerical experiments given by Langevin simulations. On the other hand, by calculating some approximated analytical extension/force functions, the most accurate at the date, that can reproduce with high precision the numerical curves also at low values of the longitudinal elastic constant where the common phenomenological proposals differ considerably

- [1] S.B. Smith, L. Finzi, and C. Bustamante, *Direct mechanical measurements of the elasticity of single DNA molecules by using magnetic beads*. Science **258** 1122 (1992).
- [2] J.F. Marko and E.D. Siggia, *Stretching DNA*. Macromolecules **28** 8759 (1995).
- [3] A. Rosa, T.X. Hoang, D. Marenduzzo, A. Maritan, *Elasticity of semiflexible polymers with and without self-interactions*. Macromolecules **36** 10095 (2003).
- [4] A. Rosa, T.X. Hoang, D. Marenduzzo, A. Maritan, *A new interpolation formula for semiflexible polymers*. Biophys. Chem. **115** 251 (2005).
- [5] A. Fiasconaro, F. Falo, *Analytical results of the extensible freely jointed chain model*. Physica A **532** 121929 (2019).
- [6] A. Fiasconaro, F. Falo, *Elastic traits of the extensible discrete wormlike chain model*. Physical Review E **107** 024501 (2023).

Collective motion of Nafion-based micromotors in water

David Reguera^{1,2}, Jordi Fraxedas³ and María J. Esplandiu³,

¹Departament de Física de la Matèria Condensada, Universitat de Barcelona, C/Martí i Franquès 1, 08028 Barcelona, Spain.

²Universitat de Barcelona, Institute of Complex Systems (UBICS), C/Martí i Franquès 1, 08028 Barcelona, Spain.

³Catalan Institute of Nanoscience and Nanotechnology (ICN2), CSIC and BIST, Campus UAB, Bellaterra, 08193 Barcelona, Spain.

Ion exchange is one of the most interesting processes occurring at the interface between aqueous solutions and polymers, such as the well-known Nafion. If the exchanged ions have different diffusion coefficients, this interchange generates local electric fields which can be harnessed to drive fluid motion. In this work, we show how it is possible to design and fabricate self-propelling microswimmers based on Nafion, driven by ion-exchange, and fueled by innocuous salts. These Nafion micromotors are made using colloidal lithography by micro/nanostructuring Nafion in the form of asymmetric rods. These microswimmers exhibit fascinating collective motion in water driven by the interplay of their self-generated chemical/electric fields and their capability to pump matter nearby towards the collective motile structure. The pumping activity of the microswimmers induces the formation of growing mobile clusters, whose velocity

increases with size. Such dynamic structures are able to trap nearby micro/nano-objects while purifying the liquid, which acts both as the transport media and as fuel. Such phenomenology opens the door to potential applications in water remediation that are currently under development.

-
- [1] M. J. Esplandiu, K. Zhang, J. Fraxedas, B. Sepulveda, and D. Reguera, *Acc. Chem. Res.* **51**, 1921 (2018).
 - [2] M. J. Esplandiu, D. Reguera, and J. Fraxedas, *Soft Matter* **16**, 3717 (2020).
 - [3] M. J. Esplandiu, D. Reguera, D. Romero-Guzmán, A. M. Gallardo-Moreno, and J. Fraxedas, *Nat. Commun.* **13**, 2812 (2022).
 - [4] J. Fraxedas, D. Reguera, M. J. Esplandiu, accepted in *Faraday Discussions*.

Collective behaviour of a suspension of energy depot repulsive disks

Juan Pablo Miranda^{1,2,3}, Demian Levis^{3,4}, and Chantal Valeriani^{1,2}

¹ Departamento de Estructura de la Materia, Física Térmica y Electrónica, Universidad Complutense de Madrid, 28040 Madrid, Spain

² GISC-Grupo Interdisciplinar de Sistemas Complejos, 28040 Madrid, Spain

³ Departament de Física de la Matèria Condensada, Universitat de Barcelona, Martí i Franquès 1, 08028 Barcelona, Spain

⁴ UBICS University of Barcelona Institute of Complex Systems, Martí i Franquès 1, 08028 Barcelona, Spain

Active matter systems are made of self-driven units active particles each capable of converting stored or ambient energy into systematic motion. This features leads the system in an out-of-equilibrium state, giving rise to a very interesting phenomenology, such as a unexpected collective behaviour or rich spatio-temporal self-organisation.

In this work [1], we study structural and dynamical features of a two dimensional system of active repulsive disks able to take energy from their environment, store it into an internal energy depot and convert it into kinetic energy [2]. The Langevin equations of the model reads:

$$\dot{\mathbf{v}} = -\gamma(\mathbf{v})\mathbf{v} - \frac{1}{m}\nabla U(\mathbf{r}) + \mathcal{F}(t), \quad (1)$$

$$\gamma(\mathbf{v}) = \gamma_0 - \frac{qd}{c + d\mathbf{v}^2}. \quad (2)$$

Where the parameters q , d and c express the properties of the energy depot. This model uses a velocity dependent friction $\gamma(\mathbf{v})$, in which activity is encoded. Varying the parameters of the model, we study suspensions at different activities.

Unexpectedly, despite the model has no explicit alignment, it displays collective behaviour in the form of a transition between an ordered (flocking) and a disordered state, depending on the system's densities and values of the activity. This transition is studied also from an structural point of view, where we differentiate a band and a homogeneous phase of flocking, similar to what happens in some Active Matter models with orientational alignment.

To unravel the origin of this transition, we suggest a simple argument based on particles' collisions.

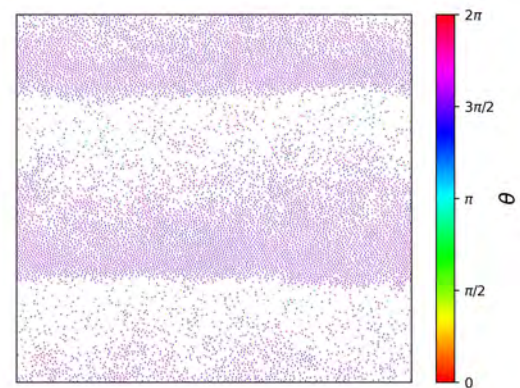
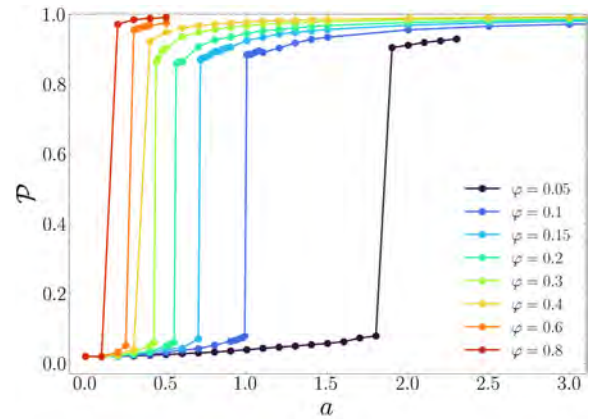


Fig. 1. Top picture: Polar order parameter for different activities a and surface fractions φ . Bottom picture: Snapshot of a system with 10000 particles showing orientational order in the form of a band flock.

[1] Miranda-Lopez, J. P., Levis, D. & Valeriani, C. (2023). Collective behaviour of energy depot repulsive disks, *In Preparation* (2023),

[2] Schweitzer, F., Ebeling, W., & Tilch, B. (1998). Complex motion of Brownian particles with energy depots. *Physical Review Letters*, 80(23), 5044.

Polymer translocation under end-pulling time-dependent forces.

Alejandro Sáinz-Agost^{1,2}, Fernando Falo^{1,2}, and Alessandro Fiasconaro^{1,2,3}

¹Dpto. de Física de la Materia Condensada, Universidad de Zaragoza, Spain

²Instituto de Biocomputación y Física de los Sistemas Complejos, Universidad de Zaragoza, Spain

³Istituto di Biofisica, Consiglio Nazionale delle Ricerche. Palermo, Italy

Polymer translocation has long been a topic of interest in the field of biological physics given its relevance in both biological (protein and DNA/RNA translocation through nuclear and cell membranes) and technological processes (nanopore DNA sequencing, drug delivery) [1, 2]

In this work, we simulate the translocation of a semiflexible homopolymer through an extended pore, driven by both a constant and a time-dependent end-pulled force, employing a model introduced in previous studies [3], illustrated in Fig. 1. The time dependence is simplistically modeled as a cosine function, and we distinguish between two scenarios for the driving – longitudinal force and transversal force – depending on the relative orientation of the driving, parallel or perpendicular, with respect to the pore axis.

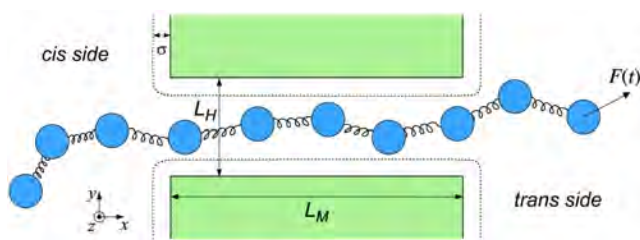


Fig. 1. Section of the polymer translocating through a nanopore in the 3d space. The pore has a square section of width L_h and its length is L_M , with the same repulsive walls as the whole membrane. The polymer is pulled through the pore with a time dependent force $F(t)$.

We investigate the effects of this periodic driving on the translocation times. We find a large minimum region of the mean translocation times as function of the frequency of the force that is typical of the Resonant Activation effect [4], with key differences between the two considered driving regimes, as shown in Fig. 2. This minimum is present independently of the physical characteristics of the polymeric chains considered and reveals a linear relation between the optimum translocation time and the corresponding period of the driving. We propose an explanation for the mechanism behind this relation, its connection to the driving regime considered, as well as the values of the coefficients involved.

The behavior of the translocation times when changing parameters of the chains were recorded, finding key differences in the responses between both driving regimes. We proposed a scaling law for the evolution of the translocation times of identical chains of different lengths, relating

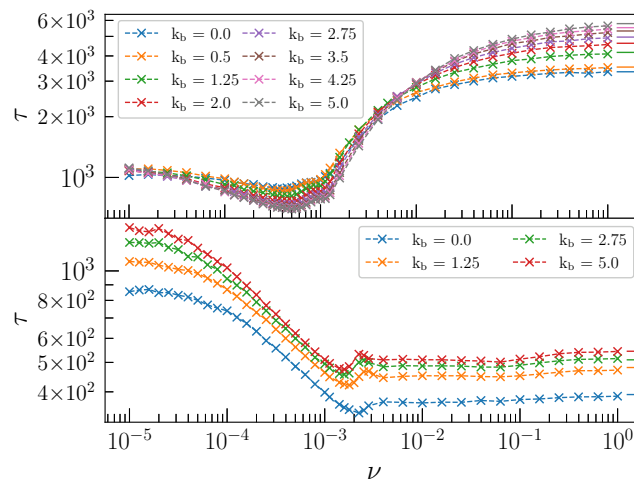


Fig. 2. Translocation curves for chains of $N = 30$ and different bending parameters k_b for transversal (top) and longitudinal (bottom) driving regimes. The three frequency regimes can be clearly distinguished, as well as the differences between the two driving schemes.

the changes of the translocation times to an effective size affected by the pore length and the Flory exponent of the chains, reflecting the rigidity of the polymers.

Lastly, an analytical expression for the low frequency range of the translocation curves is proposed, stemming from the use of a square wave as the driving mechanism. The validity of this expression is proven for both the square wave and our sinusoidal drivings, the analytical curves in clear agreement with the simulation results.

-
- [1] Kasianowicz, J., Brandin, E., Branton, D. & Deamer, D. Characterization of individual polynucleotide molecules using a membrane channel. *Proceedings Of The National Academy Of Sciences* **93**, 13770-13773 (1996)
 - [2] Lee, K., Park, K., Kim, H., Yu, J., Chae, H., Kim, H. & Kim, K. Recent Progress in Solid-State Nanopores. *Advanced Materials* **30**, 1704680 (2018)
 - [3] Fiasconaro, A., Mazo, J. & Falo, F. Active polymer translocation in the three-dimensional domain. *Physical Review E* **91**, 022113 (2015)
 - [4] Doering, C. & Gadoua, J. Resonant activation over a fluctuating barrier. *Phys. Rev. Lett.* **69**, 2318-2321 (1992)

Information dynamics in a model of EEG brain rhythms

Gustavo Menesse¹, and Joaquin J. Torres¹

¹Department of Electromagnetism and Matter's Physics - Faculty of Science - University of Granada, 18071 Granada, Spain

²Institute Carlos I for Theoretical and Computational Physics - University of Granada, 18071 Granada, Spain.

In recent years, several new information theory tools were developed to study complex systems. One of them is information dynamics (ID), which studies how a complex system locally stores, transfers, and modifies information. Another tool is Partial Information Decomposition (PID), which analyses the information between random variables by decomposing it into three types of information “atoms”: unique, redundant, and synergistic, each of them capturing different fundamental relations between variables. A recently developed framework called Integrated Information decomposition (Φ -ID)[4] is constructed using ideas from Integrated Information Theory (IIT) [3] and both ID and PID, providing a more general framework for exploring information dynamics in complex systems. In this study, we apply Φ -ID to explore the behavior of a neuronal network with a rich and well-known phase diagram [5] with different emerging dynamical phases associated with familiar brain waves observed in EEG recordings (see 1). Our analysis shows that: i) the system has the maximum integrated information Φ^R in a region where excitatory neurons exhibit the maximum variance, in a transition between intermediate neuronal activity with clear dominant rhythms β and high activity where γ oscillations dominates (see 2); ii) local information transfer appears to be maximum in a metastable region where δ and β waves dominates (not shown); iii) at short time scales, the inhibitory population has maximum information storage close to a first-order transition (not shown). In conclusion, in our model, the emergence of EEG-like rhythms at the collective level encompasses a rich information dynamics. This simple model can help to better understand the relationship between different brain rhythms and local information dynamics.

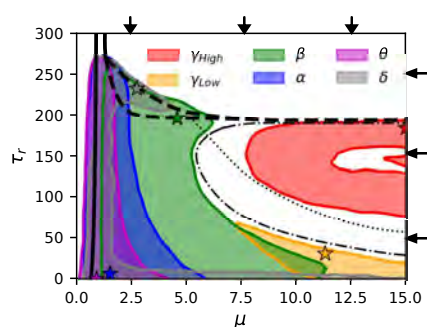


Fig. 1. **Phase diagram of rhythms in the model.** Rhythms observed in the excitatory population across the phase diagram by power spectrum analysis of average membrane potential. Each color shows a specific band of brain rhythms. The colored stars indicate the maximum of maximums for each rhythm.

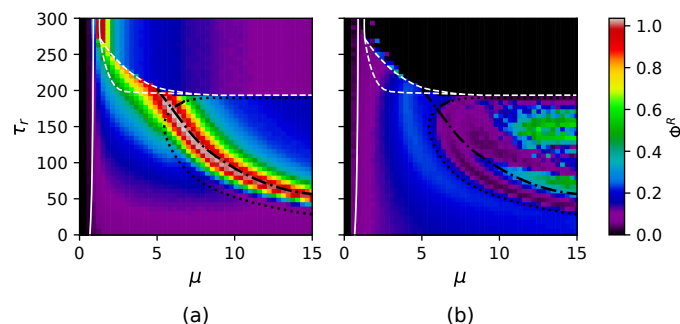


Fig. 2. **Integrated information ϕ^R across phase diagram.** The solid(dashed) white line describes a second-order(first-order) phase transition. The dotted (dash-dotted) white line indicates the maximum variance in the states of the I (E) neurons. (a) Φ^R in the excitatory group of 12E. (b) Φ^R in the inhibitory group of 9I.

-
- [1] Lizier, J. T. (2013). *The Local Information Dynamics of Distributed Computation in Complex Systems*. Springer Berlin Heidelberg.
- [2] Barrett, A. B. (2015). Exploration of synergistic and redundant information sharing in static and dynamical Gaussian systems. *Physical Review E - Statistical, Nonlinear, and Soft Matter Physics*, 91(5).
- [3] Tononi, G., Boly, M., Massimini, M., & Koch, C. (2016). Integrated information theory: From consciousness to its physical substrate. In *Nature Reviews Neuroscience* (Vol. 17, Issue 7, pp. 450-461). Nature Publishing Group.
- [4] Mediano, P. A. M., Rosas, F. E., Farah, J. C., Shanahan, M., Bor, D., & Barrett, A. B. (2022). Integrated information as a common signature of dynamical and information-processing complexity. *Chaos*, 32(1).
- [5] Pretel, J., Torres, J. J., Marro, J., Mirasso, C. R., & Valizadeh, A. (2021). EEGs Disclose Significant Brain Activity Correlated with Synaptic Fickleness.

Rational and accidental design of patchy colloids assembly into complex ordered structures

Eva G Noya¹, Enrique Lomba¹, Daniel Tracey², Jonathan Doye², Francesco Sciortino³

¹Instituto de Química-Física Rocasolano, CSIC, Calle Serrano 119, Madrid, Spain

²Chemistry Department, University of Oxford, UK

³ University of Rome, Italy

Advances in the synthesis of nanoparticles with ever increasing control over the particles interactions have led material scientists to envision a new class of smart, responsive materials which assemble spontaneously from appropriately designed nanoparticles [1]. Thus understanding the effect of the particles shape and interactions on their assembly behaviour is not only an interesting fundamental question, but also one that can have important practical implications. In spite of much effort, designing models that assemble into a desired ordered structure is still challenging, both due to the appearance of competing structures and the tendency of these systems to get stuck in kinetic bottlenecks [2]. In this contribution, we will analyse a few relatively simple cases to exemplify these difficulties.

Firstly, we will present two cases in which the assembled structure from simple patchy models challenges our intuition. In the first of these examples we examine the phase behaviour of a simple model of three-patch particles under planar confinement. One would expect that this system forms a honey-comb lattice at low temperature and pressure, but, instead, if the patches are narrow enough, the system organizes into an exotic solid phase consisting of a honey-comb lattice whose voids can be continuously filled without crossing a phase transition [3]. In the second example, we consider the assembly of tetrahedral patchy particles. Our simulations predict that clathrate structures are assembled when the patches are narrower than a given threshold size, a result

that again is not intuitively obvious[5].

Secondly, we will introduce a simple scheme to design model systems that assemble into complex ordered structures, such as, e.g. clathrate crystals. Our results show that incorporation of specificity and/or torsional contributions to the interactions can be exploited both to design models for which the target crystal is the global free energy minimum and to favour the kinetics of crystallization [4]. What is the minimal amount of information required to assemble complex periodic or aperiodic ordered structures will also be discussed.

-
- [1] S. C. Glotzer, *Assembly engineering: Materials design for the 21st century*, Chem. Eng. Sci. **131**, 3 (2015).
 - [2] S. Ravaine and E. Duguet, *Synthesis and assembly of patchy particles: Recent progress and future prospects*, Curr. Opin. Colloid Interface Sci. **30**, 45 (2017).
 - [3] E. G. Noya, N. G. Almarza, and E. Lomba, *Assembly of trivalent particles under confinement: from an exotic solid phase to a liquid at low temperature*, Soft Matter **13**, 3221 (2017).
 - [4] D. F. Tracey, E. G. Noya and J. P. K. Doye, *Programming patchy particles to form complex periodic structures*, J. Chem. Phys. **151**, 224506 (2019).
 - [5] E. G. Noya, I. Zubieta, D. J. Pine and F. Sciortino, *Assembly of clathrates from tetrahedral patchy colloids with narrow patches*, J. Chem. Phys. **151**, 094502 (2019).

Finite-size scaling of human-population distributions over fixed-size cells and relation to fractal spatial structure

Montserrat García del Muro¹ and Ivaró Corral²

¹Departament de Física de la Materia Condensada, Universitat de Barcelona

² Centre de Recerca Matemàtica, Barcelona

Using demographic data of high spatial resolution for a region in the south of Europe, we study the population over fixed-size spatial cells. We find that, counterintuitively, the distribution of the number of inhabitants per cell increases its variability when the size of the cells is increased. Nevertheless, the shape of the distributions is kept constant, which allows us to introduce a scaling law, analogous to finite-size scaling. The scaling of the moments of the distribution is found to be related with the multifractal properties of the spatial pattern formed by the population. The agreement between theory and empirical data is satisfactory, yielding that only two exponents are necessary to describe the human-

population pattern: $d_f = 1.29$ and $\tau_2 = 1.69$. These results have been published in Ref. [1].

We acknowledge PGC-FIS2018-099629-B-I00 from the Spanish MICINN and CEX2020-001084-M from the Spanish State Research Agency, through the Severo Ochoa and Mara de Maeztu Program for Centers and Units of Excellence in R&D.

-
- [1] A. Corral and M. Garcia del Muro, *Finite-size scaling of human-population distributions over fixed-size cells and its relation to fractal spatial structure*, Phys. Rev. E **106**, 054310 (2022).

Endemic infectious states below the epidemic threshold and beyond herd immunity

Javier Aguilar^{1,2}, Beatriz Arregui García¹, Raúl Toral¹, Sandro Meloni¹ and José J. Ramasco¹

¹Instituto de Física Interdisciplinar y Sistemas Complejos IFISC (CSIC-UIB), Campus UIB, 07122 Palma de Mallorca, Spain.

²Instituto Carlos I de Física Teórica y Computacional, Universidad de Granada, Granada, Spain.

In the recent COVID-19 pandemic, we have witnessed a sequence of epidemic waves intertwined with anomalous fade-outs, characterized by periods of low but persistent epidemic prevalence. These long-lasting epidemic states complicate epidemic control because it becomes difficult to assess when control measures should be relaxed, as their lifting may result in new major outbreaks. Furthermore, this phenomenon challenges current modeling approaches, as classical epidemic models fail to explain its emergence. Inspired by this phenomenon, we propose a simple mechanism in [1] that is capable of reproducing several features observed in real data. Specifically, we introduce a modification of the Susceptible-Infected-Recovered (SIR) model within a meta-population framework, where a small inflow of infected individuals accounts for undetected internal or imported cases. By focusing on a regime where this external seeding is so small that it cannot be detected from the analysis of epidemic curves, we find that outbreaks of finite duration percolate over time, resulting in overall low but long-lasting epidemic states both below and above the epidemic threshold.

By employing a two-state description of the local dynamics, we can derive analytical predictions for the duration of outbreaks at global scales (Fig. 1-(a)). Our analysis reveals that outbreaks with extremely long durations, on the order of thousands of days as observed in Fig. 1-(a), can occur within an extended parameter range. This finding challenges the assumption that the total fade-out of the disease is guaranteed, even in cases of sub-critical spreading or when herd immunity is attained. We believe that the coarse-graining approach utilized to extract analytical information from the local dynamics holds further potential for exploring the intricate relationship between local and global dynamics inherent in any meta-population structure.

This work is specially pertinent as the current literature is struggling to find explanations to criticality signatures found in the COVID-19 spread (uninterrupted-yet-small prevalence, linear growth of the recoveries, high susceptibility to changes in mobility restrictions and social distancing, etc). Our model is capable of reproducing the persistence of the COVID-19 disease between waves in the census areas of England. We can also explain empirical features such as the exponential distribution of the time between outbreaks (Fig. 1-(b)), the linear growth of the recoveries and the near-critical values of the effective reproductive number. These results are remarkable given the simplicity of our assumptions and the lack of fine-tuning.

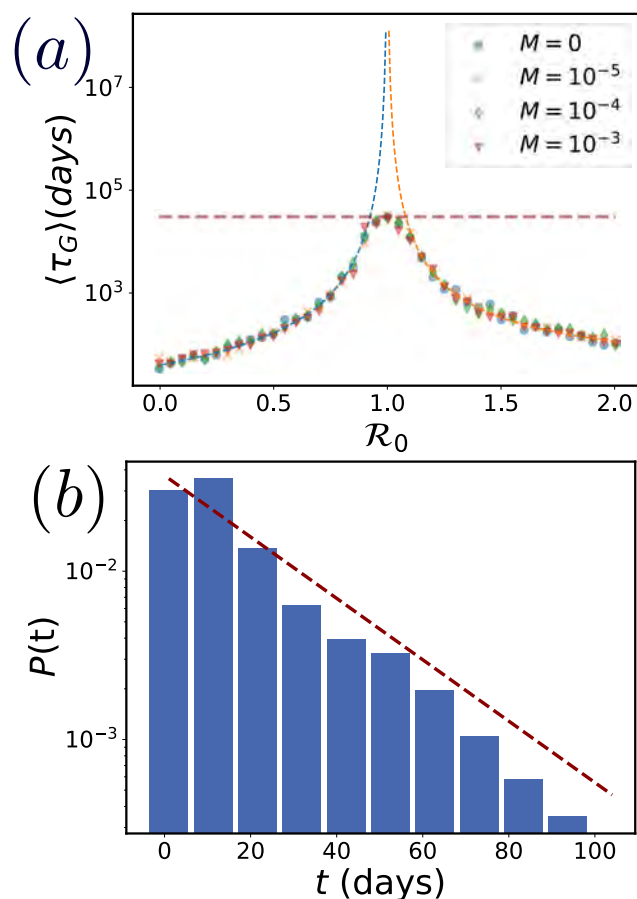


Fig. 1. In (a), dots show the duration of the first global outbreak averaged over 100 simulations for different values of the basic reproductive number \mathcal{R}_0 and mobility M . All simulations are stopped either at time $t_{\max} = 4 \times 10^4$ (days) (horizontal dotted line) or when the total prevalence reaches zero. Dashed curved lines show our analytical estimations. There is a region below and above the epidemic threshold for which the duration of epidemic outbreaks is much longer than the epidemic survival times in the classical SIR model. In (b), empirical distribution of times for which the regions in England have zero prevalence. As predicted by our theory, it is well-fitted by an exponential distribution. The value of the exponent of the best fit is 0.041(8), and can be used as a proxy for the rate at which infected individuals enter the region under study from outside per unit of time.

[1] Aguilar, J., Arregui García, B., Toral, R., Meloni, S., and Ramasco, J. J. . *Endemic infectious states below the epidemic threshold and beyond herd immunity*. Communications Physics. 6 (1), 187.

Interplay of inertia and damping in power grids

María Martínez-Barbeito¹, Julian Fritzsche^{2,3}, Damià Gomila¹, Pere Colet¹, and Philippe Jacquod^{2,3}

¹Instituto de Física Interdisciplinar y Sistemas Complejos (IFISC, CSIC-UIB), Campus Universitat de les Illes Balears E-07122 Palma de Mallorca, Spain

²Department of Quantum Matter Physics, University of Geneva, 1211 Geneva, Switzerland

³School of Engineering, University of Applied Sciences of Western Switzerland HES-SO, 1951 Sion, Switzerland

Inertia and damping play a crucial role in power grid operation. In the event of a disturbance, such as a sudden change in load or the loss of a generator, the inertia from rotating masses slows down the rate of change of frequency (RoCoF), allowing time for other control mechanisms to respond. These mechanisms are responsible for damping and controlling frequency oscillations, returning the grid to a stable state.

In this work, we analyze the interplay of inertia and damping in the propagation of frequency disturbances. We run simulations using a dynamical model for the high-voltage power grid of Continental Europe [1, 2]. We examine different inertia and damping distributions, assessing the response of the system to varying fault locations. Specifically, we analyze the frequency of the grid close to the fault and at other locations within the initial seconds following the fault.

As expected, we observe that having inertia near the fault reduces the RoCoF and frequency nadir in its proximity,

while damping simply reduces the amplitude of the oscillations. However, inertia also favors the propagation of inter-area oscillations, i.e., coherent oscillations recorded in distant areas. These oscillations live in the slowest modes of the network Laplacian matrix [3], which are located in the Iberian Peninsula and Balkan region in the European grid. As a consequence, in the event of a fault in the Iberian Peninsula, oscillations propagate to the Balkan region as the slowest modes are excited, and vice versa. We show that increasing damping in these specific areas, rather than homogeneously, is more effective to reduce inter-area oscillations.

[1] L. Pagnier and P. Jacquod, *PLoS One* (2019).

[2] M. Tyloo, L. Pagnier, and P. Jacquod, *Science advances* (2019).

[3] J. Fritzsche, M. Tyloo, and Ph. Jacquod, *60th IEEE Conference on Decision and Control (CDC)* (2021).

Un Modelo Basado en Agentes para comprender los procesos que estructuran las redes mutualistas en Doñana

Blanca Arroyo-Correa¹, Javier Galeano², Ignasi Bartomeus¹ and Pedro Jordano¹

¹Estación Biológica de Doñana, CSIC

²Grupo de Sistemas Complejos, Universidad Politécnica de Madrid

Las interacciones polinizador-planta tienen una enorme importancia en la ecología, siendo uno de los tipos de interacciones bióticas más importantes en nuestro planeta. En ecología se realizan una gran cantidad de estudios de campo para recabar información sobre dichas comunidades y se utilizan redes complejas para generar una imagen global que represente la comunidad polinizador-planta y analizar sus propiedades globales.

Una vez caracterizada la comunidad, el siguiente paso en el estudio sería tener un modelo matemático para poder predecir la imagen global de las interacciones a partir de unas hipótesis sencillas de trabajo. Para ello, las simulaciones de modelos basados en agentes pueden ser un primer paso para entender cuales son los elementos básicos que nos pueden dar esa compleja comunidad ecológica. Este tipo de modelos tienen la desventaja de la difícil generalización de los resultados pero la ventaja de que con reglas sencillas en las interacciones de los agentes se pueden obtener comportamientos emergentes que muestran una imagen ecológica compleja. Además permiten modelizar sobre las entidades que realmente interactúan en la naturaleza, los individuos.

En el trabajo que se presenta se han recogido datos de las interacciones polinizador-planta se obtuvieron en un estudio que se realizó en una zona del Parque Nacional de Doñana, en la costa atlántica del suroeste de España [1]. Nuestra área de estudio se localiza en las laderas de dunas de arena estabilizadas, donde la vegetación está compuesta principalmente por matorral esclerófilo mediterráneo. Seleccionamos seis parcelas de 1200 m², que estaban separadas por 300 m de distancia, que incluían 11 especies de arbustos polinizados por insectos. Se realizaron censos para registrar las visitas de polinizadores en las parcelas de estudio durante el período de máxima floración de la comunidad vegetal (164 días entre principios de febrero y mediados de julio de 2021). Para cada especie de planta, se seleccionó un número variable de individuos de plantas (muestreo aleatorio estratificado) dependiendo de la abundancia local dentro de cada parcela, totalizando 700 individuos de plantas. Realizamos encuestas semanales de cada planta con flores usando cámaras de video junto con censos visuales a lo largo de transectos aleatorios. A partir de los datos obtenidos se construyeron las redes de interacciones individuales, que son redes de tipo pesadas y bipartitas, para posteriormente generar las redes por especie que nos iban a servir de comparación con los modelos basados en agentes.

Los modelos basados en agentes se hicieron desde cero programándose en python. Se definieron dos clases diferen-

tes de agentes para modelizar individuos de plantas y polinizadores, respectivamente. Se diseñaron diferentes escenarios donde se variaron las distribuciones espaciales de las plantas: aleatoria, posición real gps y regular y para los polinizadores las distribuciones se realizaron de manera aleatoria dentro de cada uno de los plots estudiados. Las abundancias iniciales de los agentes que representan a las plantas se obtuvieron de los datos reales, mientras que las abundancias de los polinizadores se realizaron definiendo dos tipos de roles: generalistas, más abundantes y con mayor campo de búsqueda, y especialistas, con menor abundancia y radio de alcance pequeño. El movimiento de los polinizadores se simuló con dos tipos de movimientos: movimiento browniano y Levy walks. Y se utilizó como parámetro de interacciones el radio, r , al que los polinizadores podían observar una planta.

La red se calculaba de la siguiente manera: de manera aleatoria se selecciona un polinizador, se mueve y se buscan los vecinos que puede encontrar dentro de su radio de alcance, r . Dentro de dichos vecinos se elige uno al azar. A partir de esta interacción se generaba un enlace entre la planta y el polinizador.

Los resultados de las redes complejas utilizando estas sencillas reglas prometen excelentes resultados (Fig. 1) En esta figura se muestran las comparaciones entre el grado y el strength de las redes reales y las redes construidas a partir de los modelos basados en agentes especificando la posición espacial real de cada planta individual en la comunidad.

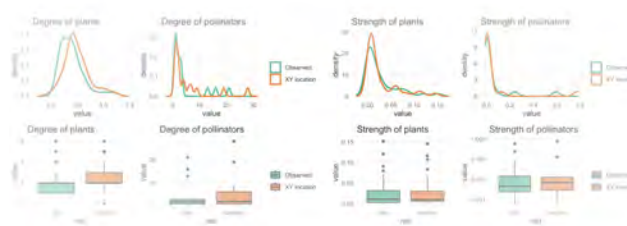


Fig. 1. Distribuciones de grado y strength de las redes reales y las redes generadas con los modelos basados en agentes para un plot específico del área de estudio.

[1] B. Arroyo-Correa, P. Jordano, and I. Bartomeus, *Intraspecific variation in species interactions promotes the feasibility of mutualistic assemblages*, E. Letters **26**, 448 (2023).

Stretching an extensible discrete wormlike chain (EDWLC)

Fernando Falo^{1,2} and Alessandro Fiasconaro^{1,2,3}

¹ Department of Condensed Matter Physics, University of Zaragoza, Spain.

² Institute for Biocomputation and Physics of Complex Systems, University of Zaragoza, Spain.

³ Institute of Biophysics, National Research Council (CNR) - Palermo Unit, Italy.

Based on classical statistical mechanics, we calculate the exact partition function of the length extension of a discrete extensible wormlike polymer under a stretching force [1, 2, 3, 4]. The bonds extensibility is modeled with harmonic springs with elastic constant k , and the links present the transversal bending recoil typical (with bending constant k_b) of the wormlike chain (WLC) model.

The evaluation has followed two methods: From the one hand by using the Transfer Matrix procedure to calculate numerically the extension/force curve of the polymer, whose outcomes have been double checked with numerical experiments given by Langevin MD simulations [6]. On the other hand, by calculating some approximated analytical extension/force functions, the most accurate at the date, that can reproduce with high precision the numerical curves also at low values of the longitudinal elastic constant where the usual phenomenological proposals differ considerably.

ticity of semiflexible polymers with and without self-interactions. Macromolecules 36, 10095 (2003).

[4] A. Rosa, T.X. Hoang, D. Marenduzzo, A. Maritan. *A new interpolation formula for semiflexible polymers.* Biophys. Chem. 115, 251 (2005).

[5] A. Fiasconaro, F. Falo. *Analytical results of the extensible freely jointed chain model.* Physica A 532, 121929 (2019).

[6] A. Fiasconaro, F. Falo. *Elastic traits of the extensible discrete wormlike chain model.* Physical Review E 107, 024501 (2023)

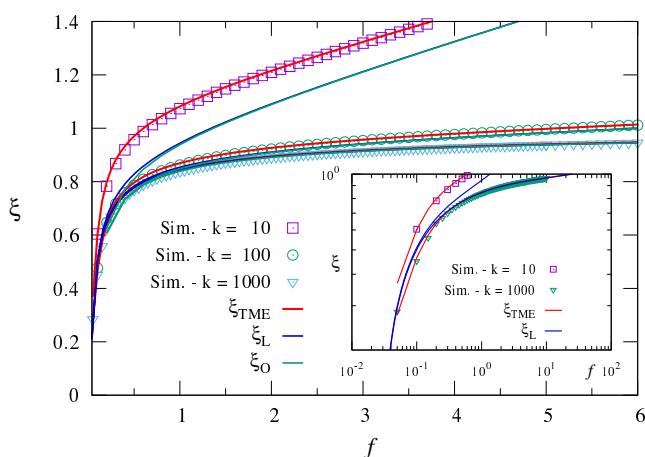


Fig. 1. Normalized end-to-end distance ξ as a function of the force f = the extensible discrete WLC model, for different elastic constant k , with the bending constant $k_b = 10$ and $l_0 = 1$. The symbols represents the Langevin simulations, the curves which superimpose with the symbols are the transfer matrix evaluation. ξ_L and ξ_O are the naïve extensible generalization (with f/kl_0) to the discrete inextensible and WLC formulas by Rosa *et al.* at high forces from references 3 and 4, respectively.

[1] S.B. Smith, L. Finzi, and C. Bustamante. *Direct mechanical measurements of the elasticity of single DNA molecules by using magnetic beads.* Science 258, 1122 (1992).

[2] J.F. Marko and E.D. Siggia. *Stretching DNA.* Macromolecules 28, 8759 (1995).

[3] A. Rosa, T.X. Hoang, D. Marenduzzo, A. Maritan. *Elastic traits of the extensible discrete wormlike chain model.* Physical Review E 107, 024501 (2023), Pamplona

Degree-day-based model to predict egg hatching of *Philaenus spumarius*, the main vector of the bacterium *Xylella fastidiosa* in Europe

Clara Lago¹, Àlex Giménez-Romero², Marina Morente¹, Manuel A. Matías², Aránzazu Moreno¹, Alberto Fereres¹

¹ Instituto de Ciencias Agrarias (ICA-CSIC), Serrano 115b, E-28006, Madrid, Spain

² Instituto de Física Interdisciplinar y Sistemas Complejos, IFISC (CSIC-UIB), Campus UIB, E-07122 Palma de Mallorca

The meadow spittlebug *Philaenus spumarius*, with a body length of 5-7 mm, is a polyphagous insect belonging to the spittlebug family *Aphrophoridae* that is the main vector transmission in Europe of the diseases induced by the bacterium *Xylella fastidiosa*. Among them one can mention the Olive Quick Syndrome Disease (OQSD) that has devastated the olive tree plantations in Apulia (Italy), the Almond Leaf Scorch Disease (ALSD) that devastated almond-tree plantations in Mallorca and Alicante, and Pierce's Disease that is a threat to Mediterranean European vineyards.

P. spumarius is a univoltine species that overwinters in the egg stage, with its nymphs emerging in late winter or spring. Predicting the time of egg hatching is essential for determining the precise times for deploying control strategies against insect pests, and in our case it is the most effective strategy to manage the diseases produced by *X. fastidiosa*. In this work we have built a tool to forecast egg hatching in the Iberian Peninsula through a growing degree-day (GDD) model. In order to fit the model we monitored eggs from oviposition to egg hatching, together with environmental conditions, at four field locations that were located at different altitudes in

central Spain.

The model was then used as a decision-support tool to calculate the optimum timing for applying control actions against *P. spumarius*. So we simulated controls at different times and our results [1] suggest that controlling nymphs at two different dates would target the highest percentages of nymphal populations present in the field. The predictions of the model can be checked in an easy way in this web page [2], that implements the GDD model using semihourly temperature data from Aemet stations. Our model represents a first step for predicting the emergence of nymphs and adopting timely control actions against *P. spumarius*. These actions could limit disease spread in areas where *X. fastidiosa* is present.

[1] C. Lago, À. Giménez-Romero, M. Morente, M.A. Matías, A. Moreno, and A. Fereres, *Environmental Entomology*, nvad013 (2023). <https://doi.org/10.1093/ee/nvad013>

[2] <http://pseggs.ifisc.uib-csic.es/>

Helium in liquid alkali metals: solubility and nucleation

Edgar Alvarez-Galera^{1,2}, Jordi Martí^{1,2}, and Lluís Batet^{1,3}

¹Department of Physics, Polytechnic University of Catalonia-Barcelona Tech

²B4-B5 Northern Campus UPC, 08034 Barcelona, Catalonia, Spain

³Diagonal 647, 08028 Barcelona, Catalonia, Spain

The easiest reaction to produce in a fusion reactor involves deuterium and tritium, producing helium (He) and one neutron (n)[1]. While the first isotope is stable and naturally present in water, the second must be obtained as a product from neutron captures by any of the two natural lithium isotopes, ⁶Li and ⁷Li[2]. He is also a by-product of the last reactions and, due to its very low solubility in lithium[3], may nucleate and form bubbles.

We investigate the possible formation of those bubbles using the molecular dynamics method. A mixture of Li and He atoms is described by a Hamiltonian composed by the Belashchenko embedded atom model (BEAM)[4] for Li-Li interactions and the Toennies-Tang-Sheng potentials (TTS) [5] for Li-He and He-He pairs.

The solubility of He is studied using Li, Na, K, Rb and Cs in their liquid state as solvents. We use the set of BEAM+TTS for the 5 alkali metals. We compute the Henry's constant, which is the ratio between the saturation pressure and concentration, from the work related to insert a single solute atom to a pure alkali metal system,

$$k_H = p^{\text{sat}}/x^{\text{sat}} = \rho k_B T \exp\{\beta \Delta\mu^{\text{excess}}\}. \quad (1)$$

The excess chemical potential $\Delta\mu^{\text{excess}}$ is determined increasing gradually a control parameter $0 < \xi < 1$ that multiplies the alkali-He potential, and adding an artificial potential $V_{\text{cav}}(r; \lambda) = Ae^{-r/B+\lambda}$ that creates a void space (cavity) among the solvent atoms. This procedure was proposed by Li et al. [6] and is required because of the divergent behaviour of TTS ($V(r) \sim r^{-1}$ for $r \rightarrow 0$) we need to ensure finite forces during the whole simulation. The excess chemical $\Delta\mu^{\text{excess}}$ is the sum of the free energy change during the growth, insertion and shrinkage stages:

$$\begin{aligned} \Delta\mu^{\text{excess}} &= \int_{\lambda_1}^{\lambda_2} d\lambda \langle V_{\text{cav}}(\lambda) \rangle_{V_{\text{cav}}(\lambda)} \\ &+ \int_0^1 d\xi \langle V_{\text{He-X}} \rangle_{V_{\text{cav}}(\lambda_2) + \xi V_{\text{He-X}}} \\ &+ \int_{\lambda_2}^{\lambda_1} d\lambda \langle V_{\text{cav}}(\lambda) \rangle_{V_{\text{cav}}(\lambda) + V_{\text{He-X}}} \quad (2) \end{aligned}$$

Then, we compare the temperature dependence of k_H from the model against experimental data[3]. Both results are in very good agreement and, as observed in Fig. 1, the logarithm of k_H turns out to be inversely linear to the temperature.

The results of k_H are employed in the study of the nucleation of He in Li. Simulations lead to highly stable clusters of He even for small nuclei. The critical radius is estimated from the Gibbs free energy (see Fig. 2), obtained as a sum of a bulk and a surface term. The first includes the reported values of k_H , and the second is computed based on the Thompson et al. method[7]. Bubbles formed by more than 100 He atoms (5-27 Å) can be stably maintained.

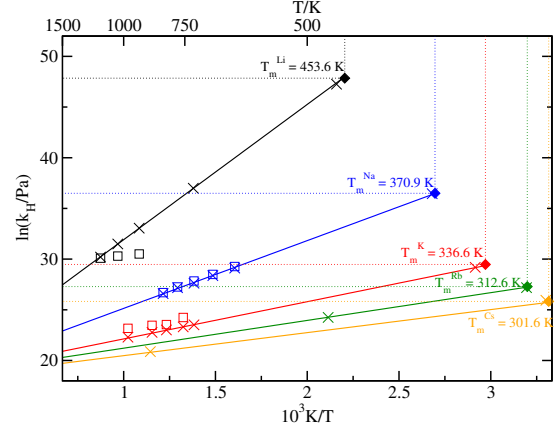


Fig. 1. Henry's constants for He in Li (black), Na (blue), K (red), Rb (green) and Cs (orange) at several temperatures. Crosses stand for experimental data.

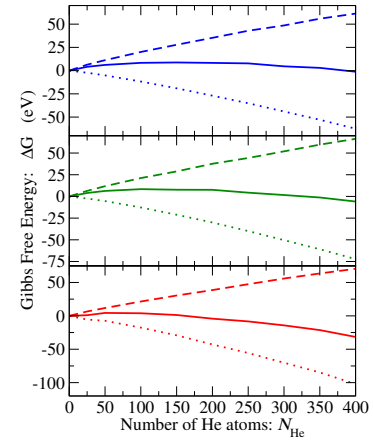


Fig. 2. Gibbs free energy of the He bubbles at temperatures of 470 K (blue), 657 K (green) and 843 K (red).

- [1] M. Korda and L. Koek, *Fusion Engineering and Design* **124**, 700 (2017).
- [2] M. Rubel, *Journal of Fusion Energy* **38**, 315 (2019).
- [3] H. U. Borgstedt, C. Guminski, H. U. Borgstedt, and C. Guminski, *Journal of Physical and Chemical Reference Data* **30**, 835 (2001).
- [4] D. Belashchenko, *Inorganic Materials* **48**, 79 (2012).
- [5] X. Sheng and K. Tang, *Physical Chemistry Chemical Physics* **23**, 7748 (2021).
- [6] L. Li, T. Totton, D. Frenkel, *The Journal of chemical physics* **146**, 214110 (2017).
- [7] S. Thompson, K. Gubbins, J. Walton, R. Chantry, and J. Rowlinson, *The Journal of chemical physics* **81**, 590 (1984).

Active wetting and collective durotaxis: speed, diffusion and super-diffusion of cellular clusters

Irina Pi Jaumà^{1,2}, Ricard Alert^{3,4}, and Jaume Casademunt^{1,2}

¹Física de la Matèria Condensada de la Universitat de Barcelona, Carrer de Martí i Franquès 1-11, 08028, Barcelona, Spain.

²Universitat de Barcelona Institute of Complex Systems (UBICS), Carrer de Martí i Franquès 1-11, 08028, Barcelona, Spain.

³Max Planck Institute for the Physics of Complex Systems (MPI-PKS), Noethnitzer Str. 38, 01187 Dresden, Germany.

⁴Center for Systems Biology Dresden (CSBD), Pfotenhauer Strasse 108, 01307, Dresden, Germany.

Collective migration of cohesive groups of cells underlies a variety of processes in embryonic morphogenesis, wound healing, and cancer invasion. Migration may respond to a variety of chemical and mechanical stimuli. Here we focus on the phenomenon of collective durotaxis [1, 2, 3], which refers to the migration of large groups of cells toward stiffer environments. We analyze this problem through the concept of active wetting [4], recently introduced to describe the spreading and retraction of cell clusters as a nontrivial competition between traction forces on the environment and tissue contractility. Since traction forces depend on substrate stiffness, the wetting properties, and the durotactic response must necessarily be related.

Experiments show that, generically, clusters dewet soft substrates and wet stiff ones, becoming maximally motile at an intermediate stiffness [5]. In particular, they show a nonmonotonic dependence of the durotactic velocity with the substrate stiffness. To elucidate the complex interplay between active wetting and collective durotaxis, we developed a continuum active wetting model that extends a previous one [4] from monolayers to 3D clusters, combining in-plane active traction and tissue contractility on the contact monolayer and out-of-plane surface tension [5]. In this model, the polarity field follows relaxational dynamics $\partial_t p_\alpha \propto -\delta F / \delta p_\alpha$, being

$$F = \int \left[\frac{a}{2} p_\alpha p_\alpha + \frac{K}{2} (\partial_\alpha p_\beta) (\partial_\alpha p_\beta) \right] d^2 r \quad (1)$$

the Frank free energy. By force balance, the stress tensor and the external force density originated at the tissue-substrate interface are related by $\partial_\beta \sigma_{\alpha\beta} + f_\alpha = 0$, and both quantities can be decomposed in a passive (viscosity η and friction ξ) and an active term (contractility ζ and active traction ζ_i),

$$\sigma_{\alpha\beta} = \eta (\partial_\alpha v_\beta + \partial_\beta v_\alpha) - \zeta p_\alpha p_\beta, \quad (2)$$

$$f_\alpha = -\xi v_\alpha + \zeta_i p_\alpha, \quad (3)$$

where v_α is the velocity field. The surface tension of the clusters enters as a boundary condition in the stress, $n_\alpha \sigma_{\alpha\beta} n_\beta = -\frac{\gamma}{R} \cos \theta$, being R the contact radius and θ the contact angle of the cluster with the substrate. Solving this model, we find that the durotactic velocity grows as the cluster spreads and achieves a maximum speed when the dynamic contact angle reaches approximately neutral wetting (90°) (see Fig. 1). After that, the saturation of traction and the growth of the friction coefficient with stiffness imply a decrease in the durotactic speed.

We have also generalized our theory to account for the biased random walks observed for cell clusters. Our stochastic model includes field-Langevin equations with both additive and multiplicative noises. Analyzing real data of local fluctuations of traction forces in cell monolayers, we can check which is the dominant noise source in the system and estimate temporal and spatial correlations of fluctuations of

the physical parameters. The model provides explicit predictions for diffusion coefficients so that unknown model parameters can be obtained from experiments. From experimental data, we show that fluctuations in the traction force in some relevant parameter regimes satisfy an effective fluctuation-dissipation theorem with a nonequilibrium temperature. Finally, some experiments [5] show that clusters undergo long hops that could be described as Levy flights, which we model within a stick-slip framework resulting from a nontrivial dependence of the friction coefficient with the relative direction of velocity and polarization.

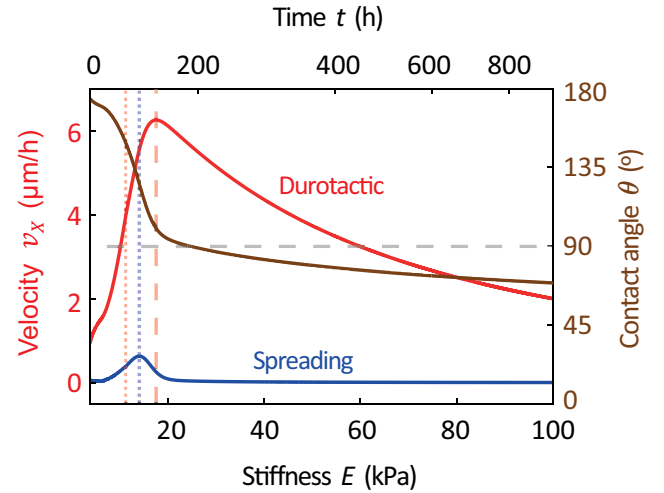


Fig. 1. Representative example of the velocity and shape dynamics of a migrating cluster with a constant volume, showing the nonmonotonic dependence of v_x with stiffness (in red), the spreading velocity (in blue) and the decrease in the contact angle (in brown).

- [1] R. Sunyer, et al., *Collective cell durotaxis emerges from long-range intercellular force transmission*, *Science* **353**, 1157 (2016).
- [2] R. Alert, and J. Casademunt, *Role of Substrate Stiffness in Tissue Spreading: Wetting Transition and Tissue Durotaxis*, *Langmuir* **35**, 75717577 (2019).
- [3] I. Pi-Jaumà, R. Alert, and J. Casademunt, *Collective durotaxis of cohesive cell clusters on a stiffness gradient*, *Eur. Phys. J. E* **45**, 7 (2022).
- [4] C. Pérez-González, et al., *Active wetting of epithelial tissues*, *Nat. Phys.* **15**, 7988 (2019).
- [5] M-E. Pallarès, I. Pi-Jaumà, et al., *Stiffness-dependent active wetting enables optimal collective cell durotaxis*, *Nat. Phys.* **19**, 279289 (2023).

Emerging topology and arrested states in defect-free active turbulence

Ido Lavi^{1,2}, Ricard Alert³, Jean-Francois Joanny⁴ and Jaume Casademunt^{1,2}

¹ Departament de Física de la Matèria Condensada, Universitat de Barcelona (Spain)

² UBICS - Universitat de Barcelona Institute of Complex Systems (Spain)

³ Max Planck Institute for the Physics of Complex Systems, Dresden (Germany)

⁴ Collège de France, Paris (France)

Active nematic turbulence is broadly described as being strongly mediated by topological defects [1]. However, it has been shown that defect-free active nematics can sustain turbulent flows that feature the same universal scaling properties [2]. To shed light on the role of topology in active turbulence, here we examine the physics of active nematic turbulence in the strict absence of defects. We find that the dynamic behavior transitions between two distinct and surprising scenarios that challenge our current understanding of active turbulence.

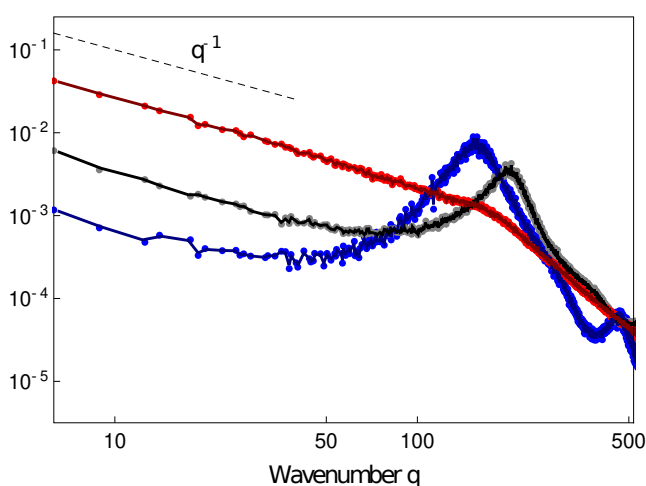


Fig. 1. Velocity-velocity correlations. Universal scaling for low- q . Blue corresponds to extensile aligning active nematics (arrested state); black corresponds to zero flow alignment coefficient; red corresponds to contractile aligning active nematics (spatiotemporal intermittency).

For contractile aligning nematics, the quiescent state undergoes a nonlinear instability that leads to strong self-similar turbulence compatible with a scenario of spatiotemporal intermittency. In contrast, for extensile aligning nematics, the initial turbulence is dynamically arrested due to topological frustration, as both the nematic field and the flow field get frozen into a self-avoiding tree structure of domain walls. This state of gridlock takes the form of unicursal labyrinthine patterns that are disordered but globally organized through paths that span the entire system while exhibiting residual, slow aging dynamics. We discuss the nature of this emerging topology and the origin of the restrictive rules that control the dynamics of domain walls. These lead to local structural motifs that explain the dynamical arrest and the nonlinear wavelength selection. Our results pose new challenges to the fundamental understanding of active

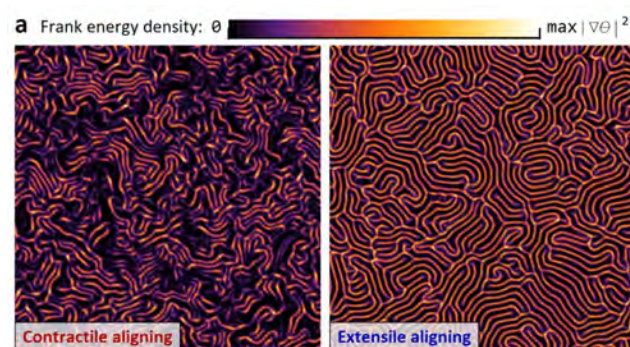


Fig. 2. Snapshots of two characteristic regimes: left, spatiotemporal intermittency for contractile aligning nematics; right, arrested turbulence for extensile nematics, showing unicursal labyrinthine gridlock. The color code shows the elastic energy distribution.

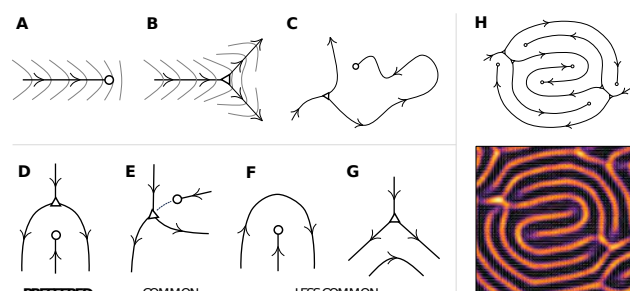


Fig. 3. Network motifs for the labyrinth graph in the arrested states. A and B, two unique building blocks of the self-avoiding tree of domain walls; C, an example of branching; D, primary anchoring motif responsible for gridlock; E, secondary anchoring motif; F and G, possible but unfavoured motifs; H, graph corresponding to a "Cretan" motif.

turbulence and, in particular, of the role of topological defects in this problem.

[1] R. Alert, J. Casademunt, and J.-F. Joanny, *Active turbulence*, *Annu. Rev. Cond. Mat. Phys.* **13**, 143 (2022).

[2] R. Alert, J.-F. Joanny, and J. Casademunt, *Universal scaling of active nematic turbulence*, *Nat. Phys.* **16**, 682 (2020).

Dinámica en fases nemáticas biaxiales inducidas por un campo para cristales líquidos cuboidales

Álvaro Rodríguez-Rivas¹, Alessandro Patti^{2,3}, and Alejandro Cuetos¹

¹Department of Physical, Chemical and Natural Systems, Pablo de Olavide University, 41013, Sevilla, Spain

²Department of Chemical Engineering, The University of Manchester, Manchester, M13 9PL, UK

³Department of Applied Physics, University of Granada, Fuente Nueva s/n, Granada, 18071, Spain

Los cristales líquidos nemáticos biaxiales (N_B , por sus siglas en inglés) han sido identificados como candidatos prometedores para el diseño de pantallas de próxima generación con propiedades electro-ópticas novedosas y tiempos de conmutación más rápidos. Aunque su existencia a nivel molecular aún está en debate, evidencia experimental respaldada por teoría y simulación ha demostrado de manera inequívoca que partículas coloidales adecuadas pueden formar fluidos N_B bajo condiciones específicas. Si bien este descubrimiento ha despertado un gran interés en la caracterización del comportamiento de fase de los cristales líquidos nemáticos biaxiales, se ha prestado significativamente menos atención al estudio de sus propiedades de transporte.

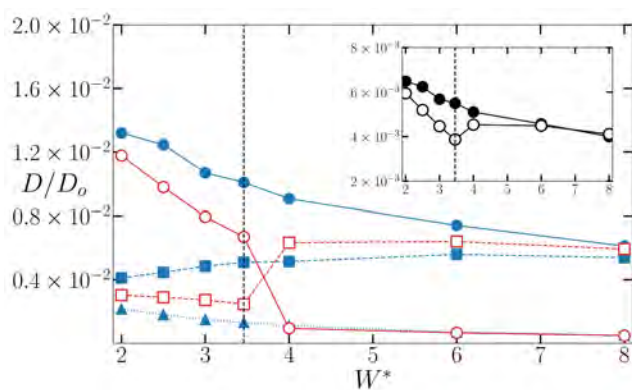


Fig. 1. Coeficientes de autodifusión a $\eta = 0.340$, en función del ancho de partícula y reducidos por D_0 . Los círculos y cuadrados vacíos corresponden, respectivamente, a los coeficientes de autodifusión calculados en la fase N_U a lo largo del director nemático y perpendicularmente a él. Los círculos sólidos, cuadrados y triángulos se refieren a los coeficientes de autodifusión obtenidos en la fase N_B a lo largo de los directores nemáticos \hat{n} , \hat{m} y \hat{p} , respectivamente. El gráfico adjunto muestra los coeficientes de autodifusión totales (isotrópicos) para las fases uniaxiales (círculos vacíos) y biaxiales (círculos sólidos). Las líneas verticales punteadas indican la transición de formas de partículas prolatas a oblatas.

Para llenar este vacío, hemos investigado la dinámica de equilibrio de fases N_B inducidas por campo mediante simulaciones de Monte Carlo dinámico, utilizando

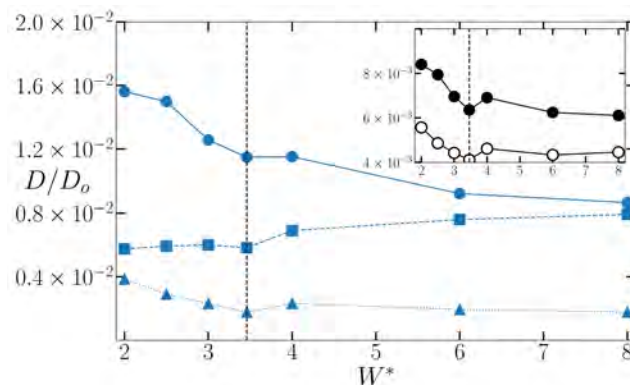


Fig. 2. Coeficientes de autodifusión reducidos por D_0 , en la fase biaxial inducida N_B^I a una fracción de empaquetamiento entre 0.220 y 0.307. Los círculos sólidos, cuadrados y triángulos se refieren a los coeficientes de autodifusión obtenidos a lo largo de los directores nemáticos \hat{n} , \hat{m} y \hat{p} , respectivamente. Los círculos vacíos y sólidos en el gráfico adjunto se refieren, respectivamente, a los coeficientes de difusión totales en las fases parental I y la fase inducida por campo N_B^I .

cuboides duros monodispersos[1]. En particular hemos calculado los coeficientes de autodifusión a largo plazo de los cuboides en un amplio rango de anisotropías, que abarcan geometrías prolatas a oblatas. Además, hemos comparado estas difusividades con las medidas en las fases isotrópicas o nemáticas uniaxiales termodinámicamente estables, a la misma densidad, cuando el campo externo se desactiva.

Nuestros resultados indican que, si bien los cuboides prolatas difunden significativamente más rápido en los nemáticos biaxiales que en los fluidos menos ordenados, no observamos un aumento similar con los cuboides oblatos a altas fracciones de empaquetamiento. Mostramos que estos cambios se deben muy probablemente a la congelación inducida por campo de los ejes perpendiculares al director nemático, junto con un aumento sustancial en el ordenamiento de la fase N_B resultante.

[1] A. Rodríguez-Rivas, A. Patti, A. Sengupta, and A. Cuetos, *Dynamics in field-induced biaxial nematic liquid crystals of board-like particles*, *J. Mol. Liq.* **367**, 120371 (2022).

Colisiones en etapas tempranas de la formación de biofilms: la influencia de la frontera

Álvaro Rodríguez-Rivas¹, Marta Pulido-Sánchez², Alessandro Patti^{3,4}, Fernando Govantes^{2,5}, and Alejandro Cuetos¹

¹Department of Physical, Chemical and Natural Systems, Pablo de Olavide University, 41013, Sevilla, Spain

²Centro Andaluz de Biología del Desarrollo

(Universidad Pablo de Olavide, Consejo Superior de Investigaciones Científicas y Junta de Andalucía)

³Department of Chemical Engineering, The University of Manchester, Manchester, M13 9PL, UK

⁴Department of Applied Physics, University of Granada, Fuente Nueva s/n, Granada, 18071, Spain

⁵Departamento de Biología Molecular e Ingeniería Bioquímica, Universidad Pablo de Olavide, Sevilla, Spain

Las colonias bacterianas o biofilms abundan en superficies vivas e inertes y se sabe que median en una amplia gama de procesos en ecología, procesos metabólicos, medicina e industria. Aunque se ha investigado ampliamente un rango de escala que va desde las células individuales hasta escalas demográficas, un emergente interés ha surgido en la obtención de una imagen biomecánica completa que destaque la dinámica célula-colonia[1]. En situaciones cotidianas, esta dinámica se ve profundamente modificada cuando nos encontramos diferentes biofilms bacterianos colisionando conforme crecen, y sus efectos en el desarrollo colectivo es de gran interés. Un ejemplo muy cercano y de gran interés lo encontramos en la microbiota intestinal.

En este trabajo realizamos un estudio exhaustivo de la evolución temporal de estas colisiones, sus propiedades estructurales y correlaciones, así como la influencia de la frontera sobre dichas propiedades y su alcance. Para ello, hacemos uso de simulaciones por ordenador con base en células individuales mediante la técnica de Dynamic Monte Carlo, y también el análisis de imágenes de microscopía durante la formación temprana de biofilms bidimensionales generadas por la bacteria Gram-negativa *Pseudomonas putida*[2, 3].

Partiendo inicialmente de dos bacterias generadoras para los dos biofilms que colisionan, hemos conseguido clasificar y caracterizar los distintos tipos de frontera generados. Para ello, hemos dispuesto las bacterias iniciales a distancias y orientaciones mutuas diferentes, así como distintos valores en los tiempos de difusión y crecimiento individuales, englobados estos dos últimos valores en un único parámetro Γ , que nos permite fijar la dinámica evolutiva de ambos biofilms bacterianos[2].

Hemos utilizado diversas mediciones, como la tortuosidad de la frontera, los perfiles de densidad, los perfiles del parámetro de orden nemático S_2 y los perfiles de los biotipos bacterianos con respecto a sus primeros vecinos, para poder cuantificar dos aspectos importantes de los biofilms bacterianos. Por un lado, hemos podido determinar que estos biofilms mantienen una alta integridad. Por otro lado, también hemos observado que la influencia de la frontera tiene efectos internos en las configuraciones estructurales de

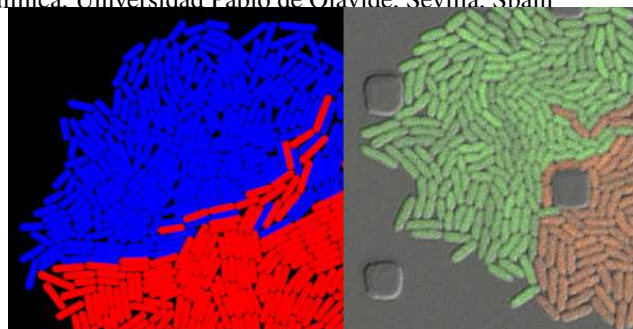


Fig. 1. Se presentan dos ejemplos de fronteras generadas en colisiones de biofilms. En la imagen de la izquierda, se muestra la configuración final de una simulación DMC. A la derecha, se muestra una imagen de microscopía donde se observa la zona de colisión entre dos biofilms que presentan diferentes colores de fluorescencia para la bacteria *Pseudomonas putida*. Podemos apreciar la similitud entre ambas fronteras y cómo estas afectan las orientaciones individuales de las bacterias cercanas en sus respectivas zonas de influencia.

los biofilms. De hecho, se observa un claro efecto sobre las orientaciones individuales de las bacterias, con disposiciones paralelas a la frontera y a lo largo de ésta. Esta correlación angular se extiende internamente por los biofilms en la zona de influencia de la frontera, lo que dificulta o impide el desarrollo normal de microdominios bacterianos que típicamente observados en los biofilms individuales[1] (ver Fig.1).

-
- [1] Z. You, D.J.G. Pearce, A. Sengupta, and L. Giomi, *Geometry and Mechanics of Microdomains in Growing Bacterial Colonies*, Phys. Rev. X **8**, 31065 (2018).
- [2] R.D. Acemel, F. Govantes, and A. Cuetos, *Computer simulation study of early bacterial biofilm development*, Sci. Rep. **8**, 5340 (2018).
- [3] A. Delgado-Campos and A. Cuetos, *Influence of homeostatic mechanisms of bacterial growth and division on structural properties of microcolonies: A computer simulation study*, Phys. Rev. E **106**, 034402 (2022)

Integrating conflicting seasonal light and thermal cues in the control of *Arabidopsis* elongation

Pablo Catalán¹, Gabriel Rodríguez-Maroto^{1,2}, Cristina Nieto,³ Salomé Prat⁴ and Saúl Ares⁵

¹Grupo Interdisciplinar de Sistemas Complejos (GISC) and Departamento de Matemáticas, Universidad Carlos III de Madrid, Leganés, Spain

²Max Planck Institute for Plant Breeding Research, Cologne, Germany

³Centro de Recursos Fitogenéticos y Agricultura Sostenible (CRF-INIA), CSIC, Alcalá de Henares, Spain

⁴Centro de Investigación en Agrigenómica (CRAG), CSIC-IRTA-UAB-UB, Cerdanyola, Spain

⁵GISC and Centro Nacional de Biotecnología (CNB) - CSIC, Madrid, Spain

As the summer approaches, plants experience enhanced light inputs and warm temperatures, two environmental cues with an opposite morphogenic impact: temperature stimulates growth, while light inhibits it, since growth occurs mostly during dark periods. Key components of this response are PHYTOCHROME B (phyB), EARLY FLOWERING 3 (ELF3), and CONSTITUTIVE PHOTOMORPHOGENIC 1 (COP1). Here, we used single and double mutant/overexpression lines of the model plant *Arabidopsis thaliana* to study the growth of the hypocotyl under different light and temperature conditions. The hypocotyl is the stem-like part of a plant embryo or seedling. It is located between the cotyledons (seed leaves) and the primary root.

We used this data to fit a mathematical model incorporating known interactions of these regulators [1]. The fitted model recapitulates thermal growth of all lines used, Fig. 1A, and correctly predicts thermal behavior of others not used in the fit, Fig. 1B. While thermal COP1 function is accepted to be independent of diurnal timing, our model shows that it acts at temperature signaling only during daytime. Our thermal model provides a unique toolbox to identify best allelic combinations enhancing climate change resilience of crops adapted to different latitudes.

Our model was fitted using data at two temperatures: 22° and 28°C. We have extended the model introducing an Arrhenius dependence in its parameters. From the values $k(T_1)$ and $k(T_2)$ of a parameter at two different temperatures, we can calculate its value at a temperature T as:

$$k(T) = e^{\frac{T_2 \ln(k(T_2)) - T_1 \ln(k(T_1))}{T_2 - T_1}} e^{-\frac{T_1 T_2}{T_2 - T_1} \ln\left(\frac{k(T_2)}{k(T_1)}\right)} \quad (1)$$

This extension of the model in [1] allows the study of plant growth around the world under current and potential future conditions. We have calculated the growth of *Arabidopsis*' hypocotyls for the average day lengths and temperatures registered around the world for every month of year 2022, Fig. 1C shows the results for September. Since day lengths is in principle less sensible to climate change than temperature, we have used our model to predict the thermomorphogenic response: the increase in growth as a result of an average increase of 1°C; Fig. 1D shows the results for September 2022. In [1] we have shown that the thermomorphogenic response significantly depends on the temperature interval and the activity levels of genes in the network. We can now use this information to obtain a more nuanced understanding of how plants integrate conflicting environmental cues to optimize growth.

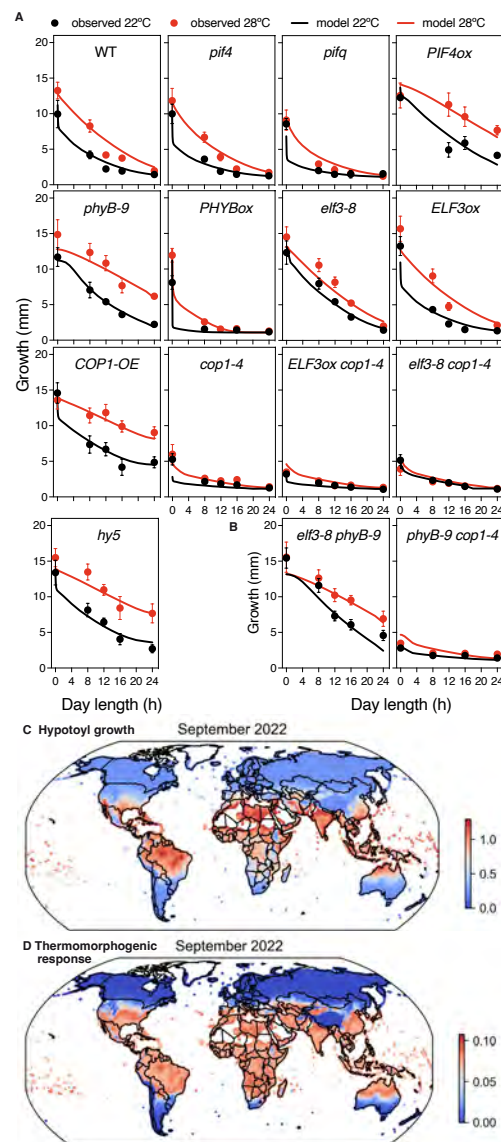


Fig. 1. A: Hypocotyl lengths of the various *Arabidopsis* backgrounds grown at either 22° or 28°C and different day lengths. Curves are model results. In B, the curves are pure predictions: these backgrounds were not used to fit the model. C: hypocotyl growth (mm) in 24 hours predicted by the model with the average day length and temperature conditions around the world in September 2022. D: predicted thermomorphogenic response: growth increase as response to a temperature increase of 1°C.

dynamics integrate conflicting seasonal light and thermal cues in the control of Arabidopsis elongation, Science Advances, **8**, eabp8412 (2022).

[1] C. Nieto, P. Catalán, L.M. Luengo, M. Legris, V. López-Salmerón, J.M. Davière, J.J. Casal, S. Ares, and S. Prat, *COP1*

Feedback control of organ size precision in the *Drosophila* eye

T. Navarro¹, A. Iannini¹, M. Neto¹, A. Campoy-Lopez^{1,2}, J. Muñoz-García^{3,4}, S. Ares^{3,5*}, and F. Casares^{1*}

¹CABD, CSIC/Universidad Pablo de Olavide. 41013 Sevilla

²ALMIA, CABD, CSIC/Universidad Pablo de Olavide. 41013 Sevilla

³Grupo Interdisciplinar de Sistemas Complejos (GISC)

⁴Departamento de Matemáticas, Universidad Carlos III de Madrid. 28911 Leganés

⁵Centro Nacional de Biotecnología (CNB), CSIC. 28049 Madrid

Biological processes are intrinsically noisy and yet, the result of development like the species-specific size and shape of organs is usually remarkably precise. This precision suggests the existence of mechanisms of feedback control that ensure that deviations from a target size are minimized. Still, we have very limited understanding of how these mechanisms operate. Here, we investigate the problem of organ size precision using the *Drosophila* eye. The size of the adult eye depends on the rates at which eye progenitor cells grow and differentiate. We first find that the progenitor net growth rate results from the balance between their proliferation and apoptosis, with this latter contributing to determining both final eye size and its variability. In turn, apoptosis of progenitor cells is hampered by Dpp, a BMP2/4 signaling molecule transiently produced by early differentiating retinal cells.

Our genetic experiments show how the status of retinal differentiation is communicated to progenitors through the differentiation-dependent production of Dpp which, by adjusting the rate of apoptosis, exerts a feedback control over the net growth of progenitors to reduce final eye size variability.

To dissect the dynamics of eye growth and differentiation, we have devised a theoretical model that captures the essential biological processes involved. This model is defined by three key variables: the width of the progenitor cell region (G), the width of the differentiated retinal cell region (R), and an intermediary strip of recently differentiated retinal cells (R_n) that produce Dpp. These variables collectively encapsulate the transformative stages of cellular development in the eye.

The dynamics of these variables are governed by the interplay of progenitor cell proliferation, apoptosis, and cellular differentiation, with transitions from progenitor cells to newly differentiated cells ($G \rightarrow R_n$) and from newly differentiated to fully differentiated retinal cells ($R_n \rightarrow R$). To account for the intrinsic stochasticity in biological systems, we have incorporated this interplay into a set of three Langevin equations. These equations, with noise terms modeling the fluctuations related to each of the basic processes in play, effectively capture the fluctuations inherent in the biological processes.

Our model faithfully reproduces the observed dynamics of eye growth and differentiation in experimental settings. Moreover, it provides a means to investigate the contribution of each process's fluctuations to the asymmetry typically seen between the two eyes of a single fly. Through linear stability analysis, we further demonstrate the stabiliz-

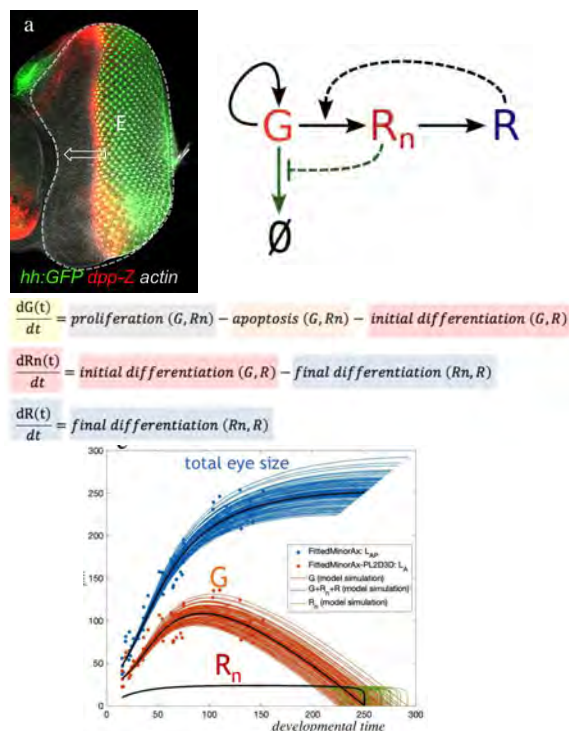


Fig. 1. The eye primordium of the developing fly embryo showing dividing progenitor cells (G) cells to the left and differentiated retinal cells (R) to the right; in between a narrow strip of newly differentiated retinal cells (R_n) produce Dpp. Dpp produced by newly differentiated cells inhibits apoptosis of progenitors, *hedgehog* produced in retinal cells activates differentiation. These processes are modeled through a set of differential equations, when including stochastic terms, they reproduce the dynamics and variability of eye development.

ing role of apoptosis in arresting eye growth. Consequently, our model not only captures the dynamics of eye development but also provides a framework for exploring the complex interplay of the constituent processes and their roles in developmental robustness.

[1] T. Navarro, A. Iannini, M. Neto, A. Campoy-Lopez, J. Muñoz-García, S. Ares, and F. Casares, *Feedback control of organ size precision is mediated by BMP2-regulated apoptosis in the Drosophila eye*, submitted to PLoS Biology, second round of review (2023).

Network Inference and Dimensionality Reduction in Biome-Specific Virus Data

Gorka Buenvarón-Campo¹, Mar Cuevas-Blanco¹, Carlos M. Duarte², and Victor M. Eguíluz^{3,4}

¹Institute for Cross-Disciplinary Physics and Complex Systems, E-07122 Palma, Mallorca, Spain

²Red Sea Research Center, King Abdullah University of Science and Technology, Kingdom of Saudi Arabia

³Basque Centre for Climate Change (BC3), Scientific Campus of the University of the Basque Country, 48940 Leioa, Spain

⁴IKERBASQUE, Basque Foundation for Science, 48009 Bilbao, Spain

Viruses play vital roles in diverse ecosystems, influencing dynamics and genetic diversity through their interactions with host organisms. Investigating the structure and distribution of viruses in across biomes is crucial for understanding their ecological significance and the potential impacts on ecosystem functioning. In this study, we analyze virus data provided by the KAUST Metagenomic Analysis Platform (KMAP) [1]. We aim to unravel taxonomic relationships and occurrences of viruses, shedding light on their role in different environments.

The data consists of files associated with different PFAM domains containing measurements of virus taxa at various biomes. By aggregating virus families and combining these files, we constructed a comprehensive dataset encompassing a wide range of virus taxa and their occurrences across biomes. The participation of viruses across PFAM domains and biomes exhibits significant heterogeneity, ranging from generalist viruses that occur in multiple domains and biomes, to highly specific or even exclusive viruses that are confined to particular PFAM domains and reported biomes. For the analysis of this complex dataset, we employed two distinct approaches that share similar conceptual foundations, providing complementary insights into the taxonomic relationships and distributions of viruses in different ecosystems. The first approach involved **inferring networks**, and the second utilized clustering algorithms, specifically **UMAP** (Uniform Manifold Approximation and Projection) [2], for data visualization and exploration.

We employed a two-step approach for network inference. Firstly, we combined the individual data frames associated with every PFAM domain. Pairwise similarity Eq. (1) between viruses were then calculated using a metric derived from the **Jensen-Shannon divergence** [3]. Significance was assessed through randomization, and a network was constructed, with virus families represented as nodes and edge weights determined by similarity measures. Additionally, a multilayer network analysis was conducted, treating each PFAM dataset as a separate layer. Using the Infomap algorithm [4], we perform community detection on both networks to unveil modular structures across diverse biomes.

As an alternative approach to network inference, we employed **UMAP** for data visualization and exploration. Using the combined data frame described earlier, we applied UMAP with the Jensen-Shannon distance as the metric. By iteratively adjusting the parameters, we aimed to strike a balance between capturing global and local structure, ultimately obtaining a visualization, shown in Fig. 1, that revealed clustering patterns and provided insights into the overall structure of the virus data.

$$s_{PQ} = 1 - \frac{1}{\sqrt{2}} \left[\sum P \log \frac{2P}{P+Q} + \sum Q \log \frac{2Q}{P+Q} \right]^{\frac{1}{2}}. \quad (1)$$

Here we present two figures (Fig. 1) showcasing the out-

comes of UMAP analysis. These visualizations depict the embedding of virus families in a two-dimensional space, allowing us to observe the formation of clusters and the relative distances between viruses. Each virus is represented by its name. Fig. 1A shows the color-coding of viruses based on the communities detected in the multilayer network, while Fig. 1B represents the color-coding based on the communities detected in the combined network. The spatial distribution of the virus families is better explained by the communities found at the joint network, while they do not match completely.

This study investigates the taxonomic relationships and occurrences of viruses in diverse environments. The results demonstrate the potential of network inference in capturing the underlying structure of virus communities. Additionally, various avenues, including embedding projection, statistical analysis, and bipartite network construction, are being pursued to further elucidate the complexity and dynamics of viral ecosystems.

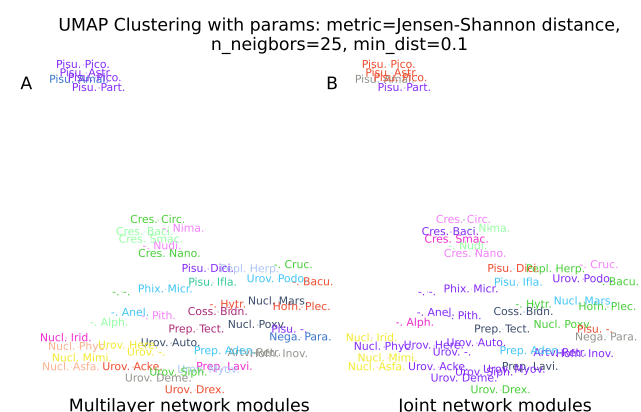


Fig. 1. UMAP results after embedding the virus space in 2 dimensions. The color of names refers to the communities detected in the multilayer (A) and joint (B) networks

[1] I. Alam, A. A. Kamau, D. K. Ngugi, et al., *KAUST Metagenomic Analysis Platform (KMAP), enabling access to massive analytics of re-annotated metagenomic data*, *Scientific Reports* **11**, 11511 (2021), <https://doi.org/10.1038/s41598-021-90799-y>.

[2] L. McInnes, J. Healy, and J. Melville, *UMAP: Uniform Manifold Approximation and Projection for Dimension Reduction*, arXiv preprint arXiv:1802.03426 (2018).

[3] J. Lin, *Divergence measures based on the Shannon entropy*, *Information Theory, IEEE Transactions on* **37**(1), 145-151 (1991).

[4] D. Edler, A. Holmgren, and M. Rosvall, *The MapEquation software package*, <https://mapequation.org>, 2023.

Active particles stabilise emulsions of phase-separating mixtures

Javier Díaz Brañas¹, and Ignacio Pagonabarraga¹

¹ Departament de Física de la Matèria Condensada, Universitat de Barcelona, Spain

Binary mixtures (BMs) that phase separate *via* Ostwald ripening exhibit a monotonic droplet growth following the power law[1] $R(t) \sim t^\alpha$, with the equilibrium morphology achieved in macrophase separation. Active particles (APs), are intrinsically out-of-equilibrium, consuming energy to produce work, commonly self-propulsion. Using a hybrid discrete/continuous diffusive simulation model, it is found that non-surfactant APs can arrest phase separation, inducing an activity-stabilised emulsification of the BM and preventing complete demixing. The rich steady-state phase behaviour includes isotropic droplets with a well-defined characteristic size, and hexatic order (see Fig. 1).

The mechanism of emulsification is found to be due to the global active pressure exerted by the APs onto the BM interface. Despite APs being completely solvable in one of the BM phases, activity leads to their accumulation at interfaces, where the competition between the active pressure and the surface tension of the BM leads to the arrest in the droplet size growth. A rich reentrant phase behaviour is found for higher activity rates leading firstly to unstable droplets with anisotropic shape, and finally to de-coupling between APs and the BM dynamics.

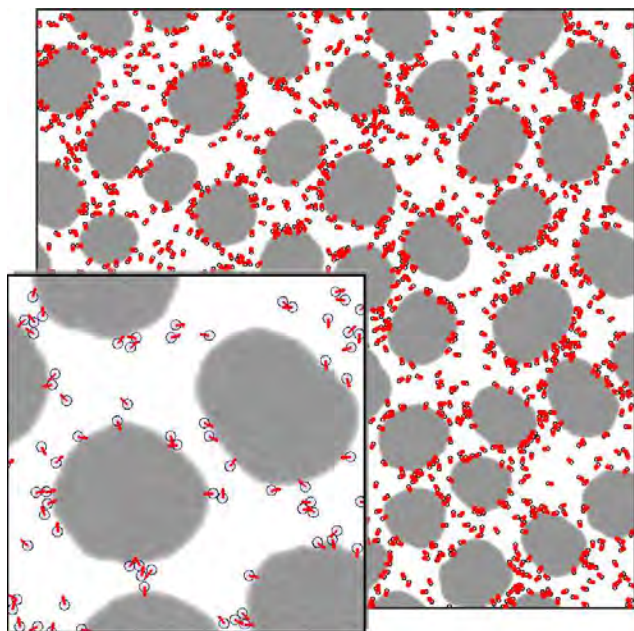


Fig. 1. Active particles accumulate at the binary mixture interface and exert active pressure, stabilising the emulsion morphology.

Conversely, APs can destabilise macrophase-separated BMs. The active energy provided by the APs' work can drive an equilibrated BM away from its equilibrium configuration, resulting in the same steady state morphologies as BM phase-separating after a quench. This highlights the rich emergent behavior of systems composed of active and passive elements and its relationship with the equilibrium morphologies[2].

[1] Lifshitz, I.M. and Slyozov, V.V., 1961. The kinetics of precipitation from supersaturated solid solutions. *Journal of physics and chemistry of solids*, 19(1-2), pp.35-50.

[2] Bechinger, C., Di Leonardo, R., Lwen, H., Reichhardt, C., Volpe, G. and Volpe, G., 2016. Active particles in complex and crowded environments. *Reviews of Modern Physics*, 88(4), p.045006.

Patrones de condensación en sustratos con distintas densidades de sitios de nucleación

Ruddy Urbina and Wenceslao González-Viñas

Depto. de Física y Matemática Aplicada, Universidad de Navarra, Pamplona, España

Las figuras de aliento (BF, del inglés Breath Figures) son los patrones en forma de gotas que aparecen sobre una superficie por la condensación de vapor de agua [1]. Este fenómeno puede ocurrir cuando el aire del entorno está sobresaturado de humedad a la temperatura de la superficie, y se producirá mientras se mantenga la condición de saturación. Cuando la condensación ocurre sobre una superficie limpia, homogénea e hidrofóbica, las BF pueden mostrar hasta seis etapas: 1) Nucleación inicial. 2) Crecimiento de gotas aisladas debido a la absorción de vapor, cuando la distancia entre gotas es mucho mayor que sus radios. En esta etapa el radio de las gotas crece como $t^{1/2}$. 3) Crecimiento por absorción de vapor con solapamiento de los perfiles de concentración alrededor de cada gota. En esta situación, la interacción entre gotas a través de la atmósfera reduce la absorción de gotas individuales y el radio promedio de la población aumenta como $t^{1/3}$. 4) Crecimiento dominado por coalescencias. Cuando dos o más gotas entran en contacto, coalescen formando una nueva gota de mayor tamaño y, a medida que estos eventos se vuelven más frecuentes el radio promedio de las gotas crecerá como t^1 . 5) Nuevas nucleaciones de gotas, en los espacios vacíos que dejan las coalescencias. 6) Deformación y/o desprendimiento de gotas grandes por efecto de la gravedad. Algunas de estas etapas pueden superponerse o estar ausentes dependiendo de las condiciones experimentales concretas.

En este trabajo, reportamos resultados experimentales sobre la condensación de vapor de agua en sustratos con diferentes densidades iniciales de núcleos de condensación. Los sustratos son vidrios, limpios o recubiertos mediante inmersión en una solución de octadeciltriclorosilano en hexametildisiloxano que deja a la superficie con un comportamiento hidrofóbico acompañado de impurezas que pro-

mueven la nucleación [2]. Los resultados del sustrato limpio y tres casos con recubrimientos con distintas densidades de sitios de nucleación se comparan empleando la densidad superficial de gotas y el radio promedio. Observamos que densidades iniciales altas producen dinámicas de crecimiento rápidas, pero con gotas en promedio más pequeñas.

La dinámica observada en todos los casos ha sido racionalizada empleando un modelo de crecimiento que parte de la idea de que en los primeros instantes se forman gotas diminutas distribuidas aleatoriamente. La validez de esta hipótesis ha sido verificada comprobando que las posiciones de los núcleos de condensación muestran una aleatoriedad espacial completa a distintas escalas, mediante el uso de la función L de Ripley-Besag. Para cada sustrato, se calculó una densidad inicial y un tiempo característico, que fueron usados para adimensionalizar las variables espaciales y temporales. Tras reescalar, las curvas correspondientes a cada sustrato colapsan entre sí (excepto para tiempos adimensionales muy largos, donde ocurren nuevas nucleaciones). En conclusión, la evolución del patrón de condensación queda determinada por la densidad inicial de núcleos, y las constantes de escalamiento (aunque hayan sido calculadas para tiempos cortos) describen lo que ocurre a escalas de tiempo mayores [3].

[1] D. Beysens, *Dew water* (River Publishers, Denmark, 2018).

[2] R. Seco-Gudiña, J. Guadarrama-Cetina, y W. González-Viñas, *Dynamics of water condensation over arrays of hydrophilic patches*, *Eur. Phys. J. Spec. Top.*, **226**, (2017).

[3] R. Urbina, y W. González-Viñas, *Unified description over time of drop-wise condensation with quenched disorder*, enviado a *Phys. Rev. E*.

Linear Response Theory in hard colloids

F. Orts¹, M. Maier², M. Fuchs², G. Ortega¹, E.M. Garzón¹, and A. M. Puertas³

¹ Fachbereich Physik, Universität Konstanz, 78457 Konstanz, Germany

² Departamento de Informática, Universidad de Almería, 04.120 Almería, Spain

³ Departamento de Química y Física, Universidad de Almería, 04.120 Almería, Spain

In microrheology, a colloidal tracer is inserted in a soft matter system and its dynamics is monitored. This tracer bead can be subjected to an external force, in so-called active microrheology. In passive microrheology, on the other hand, the tracer moves in response to the bath equilibrium thermal or density fluctuations. In active microrheology, the effective friction coefficient shows three regimes as a function of the external force: a linear regime at low forces, a non-linear force thinning regime, and a high force regime, dominated by the ballistic collisions with bath particles, that can be linear or non-linear. The connection between passive microrheology and (the linear low-force regime of) active microrheology is provided by linear response theory, which provides both the transient and stationary response of the tracer particle to the external force based on the equilibrium fluctuations:

$$\langle z(t) \rangle = \frac{\beta F_{ext}}{6} \langle \delta r^2(t) \rangle_{eq} \quad (1)$$

where $z(t)$ is the tracer displacement when force F_{ext} is applied, and $\langle \delta r^2(t) \rangle_{eq}$ is the equilibrium mean squared displacement.

In this work, simulations of passive and active microrheology in a system of quasi-hard spheres will be presented.

The tracer is pulled with a constant force, and its radius is varied from a to $8a$, where a is the radius of the bath particles. The tracer diffusion coefficient (in passive microrheology) and friction coefficient at low forces (in active microrheology) fulfill the Stokes-Einstein relation, and the tracer velocity autocorrelation function (VACF) correctly predicts the transient tracer velocity upon application of the external force. Both results, and further tests, confirm the validity of the linear response theory in this system. The friction coefficient and inverse diffusion coefficient are also interpreted using the Brinkman model, although our interpretation of the parameters is different from the original formulation. Finally, the effects of the moving tracer on the bath are presented.

A model based on the mode coupling description of the bath and tracer particles (as a binary mixture) is also presented to comprehend the physical mechanisms in passive microrheology. The theory requires the tracer-bath cross structure factor, which is calculated within the Percus-Yevick approximation for mixtures, with excellent agreement with the simulations, and the model correctly predicts frequency dependence of the tracer VACF, which implies the transient tracer response, as mentioned above.

Spherical bacteria, re-identification of parameters in complex systems.

Rafael Vida^{1,4}, Mario Castro^{1,3}, Jose Cuesta^{1,4} and Javier Galeano^{2,5}

¹Grupo Interdisciplinar de Sistemas Complejos ²Grupo de Sistemas Complejos ³Universidad Pontificia de Comillas

⁴ Universidad Carlos III de Madrid ⁵ Universidad Politécnica de Madrid

Population dynamic models are valuable tools when combined with time series data of species abundances as they enable the inference of interactions. In the realm of microbiome research, comprehending microbial interactions is essential for achieving various objectives. These objectives include predicting population changes over time, assessing the impact of microbiome manipulations on dynamics, and designing synthetic microbiomes for specific tasks. Understanding the emergent behavior of complex systems, arising from the interactions among their constituent elements, presents a formidable yet crucial challenge in scientific exploration. Current model reduction techniques either have limited applicability or result in "black boxes" that lack a connection to the underlying microscopic physics.

In order to understand these models, parameter estimation from observational data is a typical problem, often approached through nonlinear least-squares minimization.

In this study, we examine a generalized Lotka-Volterra ecological model to assess the suitability of different approaches for parameter estimation. Firstly, synthetic data is generated using models with known parameters, and these parameters are then estimated using least square techniques to compare them with the original values. Additionally, a Bayesian model analysis is conducted. Although the model is structural identifiable[1], namely, all the parameters can be estimated *in principle*, we show that it is not practically identifiable (conditioned data).

Furthermore, we perform a Model Reduction by Manifold Boundaries to identify parameter sets whose relationship makes re-identification impossible [2]. The parameter values of a model create a manifold within the space of data predictions. The goal of the minimization problem is to find the point on this manifold that best fits the experimental data. Using the model manifolds of Lotka-Volterra based models, we provide evidence that parameter inference in this type of models is not feasible, even in the case of 3 species. Moreover, it is important to note that the accurate capture of the sign of the interactions is generally impossible.

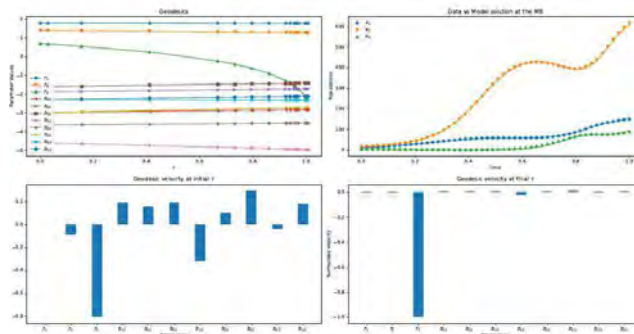


Fig. 1. In order to find the least relevant parameter combination, we identify the eigendirection of Fishers information matrix with smallest eigenvalue. We numerically construct a geodesic[4] from the initial parameters in this irrelevant direction until a boundary is identified. In the top left graph, we illustrate the evolution of geodesics for a 3-species LV model, which involves twelve parameters. By following a geodesic path towards the boundary of the manifold, it can be revealed a limiting behavior. Top right, the graph represents the data and the solution of the model. On the bottom, the geodesic velocity at the initial and final time is depicted.

- [1] Remien, C. H., Eckwright, M. J., & Ridenhour, B. J. *Parameter Identifiability of the Generalized Lotka-Volterra Model for Microbiome Studies*. **bioRxiv**, 463372. (2018)
- [2] Transtrum, M. K., Machta, B. B., & Sethna, J. P. . *Geometry of nonlinear least squares with applications to sloppy models and optimization*. **Physical Review E**, 83(3), 036701. (2011)
- [3] Gutenkunst, R. N., Waterfall, J. J., Casey, F. P., Brown, K. S., Myers, C. R., & Sethna, J. P. *Universally sloppy parameter sensitivities in systems biology models*. **PLoS computational biology**, 3(10), e189.(2007)
- [4] Transtrum, M. K., & Qiu, P. *Model reduction by manifold boundaries*. **Physical review letters**, 113(9), 098701, (2014).

Unveiling the airspace structure and aircraft mobility in Europe: a complex network perspective

Pau Esteve¹ and Massimiliano Zanin¹

¹Instituto de Física Interdisciplinar y Sistemas Complejos (IFISC), CSIC-UIB, 07122 Palma, Spain

Air transport constitutes a key socio-technical infrastructure of our society in terms of mobility. When it comes to modelling it, the most common representation is that of airport networks; that is, nodes correspond to airports pairwise connected whenever flights exist between them. However, flights do not necessarily follow a geodesic path between two airports; instead, they are restricted to fly following certain airways or pre-defined routes. This route networked structure constitutes the backbone of airspace, serving as the primary channel for aircraft flow.

In this contribution, we analysed an extensive dataset from EUROCONTROL's Data Archive [2], focusing on the European route structure and its evolution between 2015 and 2019. These routes are constituted by sequences of waypoints, navigational markers whose function is to guide aircraft on the right track. Fig. 1 displays a piece of this route structure in the Iberian Peninsula, revealing a higher density of waypoints near the major airports. Overall, the European route network encompasses more than 17,000 nodes and 31,000 edges.

While usually perceived as an almost static entity, the results reveal a highly dynamic structure. Notably, the network undergoes significant topological changes and experiences a remarkable increase in size of approximately 28% over the period from 2015 to 2019. A more in-depth discussion about the network's topological characteristics, evolution and spatial vulnerability can be found in [1].



Fig. 1. Route structure of the Iberian Peninsula. Nodes correspond to waypoints, navigational markers used to guide aircraft; airways are formed as sequences of waypoints.

Before departure, each flight is required to provide its flight plan, which outlines the sequence of waypoints the aircraft is expected to follow. While the flight plan acts as a reference for actual trajectories, there is a certain degree of flexibility that allows deviations from the plan. These deviations are commonly referred to as *directs* in air traffic

management. Directs occur when an air traffic controller instructs an aircraft to bypass one or more waypoints and proceed directly to the subsequent waypoint, minimizing flight distance and fuel consumption.

By integrating the route network with spatiotemporal flight trajectories, we can analyze the average number of directs taken per trajectory, as illustrated in Fig. 2. We observe a quite heterogeneous spatial distribution, with the FIR region of Riga standing out as particularly flexible, followed by Madrid, Milan, and Barcelona, regions known for managing a huge amount of traffic. To sum up, the present framework allows us to effectively characterize the flow of aircraft through the airspace and quantify actual flight deviations, offering valuable insights for air traffic management.

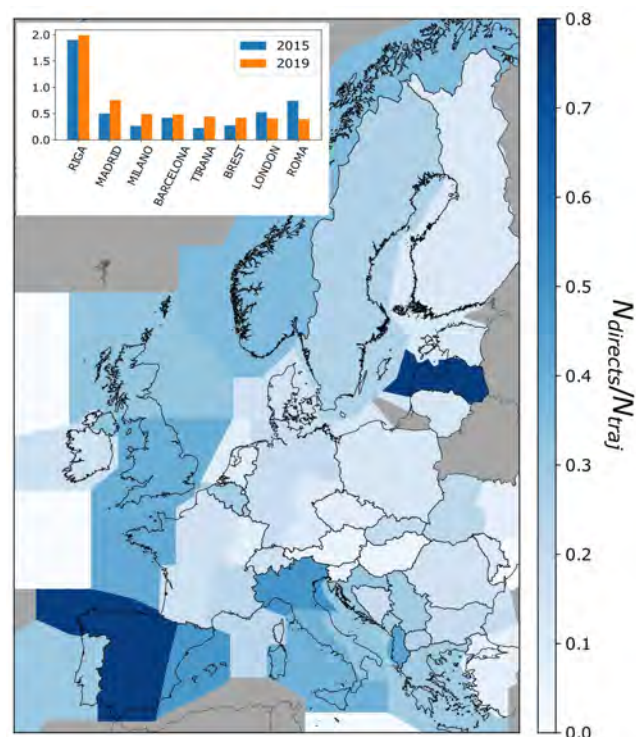


Fig. 2. Spatial distribution of the average number of directs taken per trajectory in 2019. The map is divided into the different Flight Information Regions (FIR) of the European airspace. The inset highlights the top 8 regions exhibiting a higher number of directs per trajectory, allowing a comparison of data between 2015 and 2019.

[1] P. Esteve, J.J. Ramasco, and M. Zanin, *Structure, resilience and evolution of the European Air Route Network from 2015 to 2018*, IEEE Transactions on Network Science and Engineering, 2023.

[2] <https://www.eurocontrol.int/dashboard/mtd-data-archive>

Numerical evidence for a phase transition in the six-dimensional Ising spin glass on a field

M. Aguilar-Janita¹, V. Martín-Mayor^{2,3}, J. Moreno-Gordo^{3,4,5} and J. J. Ruiz-Lorenzo^{5,3}

¹ Complex Systems Group, Universidad Rey Juan Carlos, 28933 Móstoles, Madrid, Spain.

² Departamento de Física Teórica, Universidad Complutense, 28040 Madrid, Spain.

³ Instituto de Biocomputación y Física de Sistemas Complejos (BIFI), 50018 Zaragoza, Spain.

⁴ Departamento de Física Teórica, Universidad de Zaragoza, 50009 Zaragoza, Spain.

⁵ Departamento de Física and ICCAEx, Universidad de Extremadura, 06006 Badajoz, Spain.

Spin glasses are disordered magnetic systems that exhibit randomness and frustration, making them an example not only of glassy systems, but also of complex systems more broadly.

However, despite considerable effort, the effect of an external magnetic field ($h \neq 0$) on finite-dimensional systems is not yet fully understood. It is unclear whether there is a phase transition to a spin glass phase at all. Some results from droplet theory suggest that there is no phase transition, regardless of the finite dimension of the system [1]. Other droplet model supporters believe that it only exists above six dimensions [2]. Numerical simulations are inconclusive for $D = 3$ [3] and suggest a positive answer for $D = 4$ [4]. Further confusion is added by the failure of the standard field-theoretical approach, as no stable one-loop perturbative fixed point on the renormalization group has been found below or at $D = 6$. Finally, a two-loop computation does find a non-trivial stable fixed point at $D = 6$ [5], the Gaussian one still being unstable. This non-trivial fixed-point would lie in the non-perturbative region, being unclear whether or not the fixed point would survive beyond the two-loop computation.

Even within the field-theoretical framework, the value of the upper critical dimension D_u^h for spin glasses in a field is an open question. The classical result from replica field theory states $D_u^h = 6$, but a recent work suggests a different value, $D_u^h = 8$ [6].

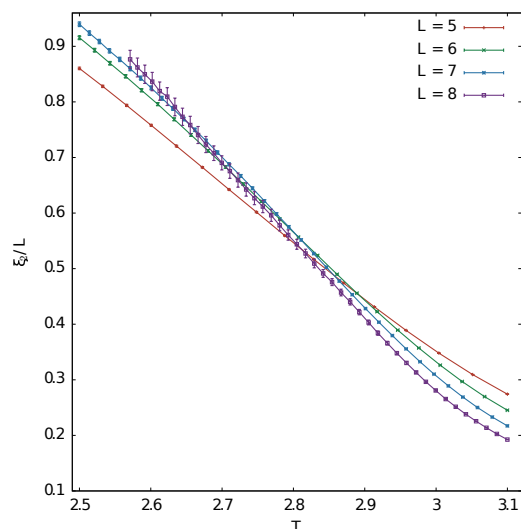


Fig. 1. Behavior of the correlation length in lattice units as a function of the temperature for the different simulated lattices. The crossing points indicate the presence of a phase transition in a field ($h = 0.075$).

In this work, we present results from massive numerical simulations of the Ising spin glass in six dimensions in a field using advanced computational and statistical techniques, such as Multi-Spin Coding, Parallel Tempering, and

a thermalization protocol based on the monitoring of the temperature random walk.

In Fig. 1 we show the behavior of the correlation length, ξ_2/L in lattice units, as a function of temperature for the four lattice sizes simulated. This behavior, with crossing points, marks the presence of phase transition. Furthermore, this conclusion is supported with the study of a cumulant which avoid the use of the zero modes in its definition (see Fig. 2).

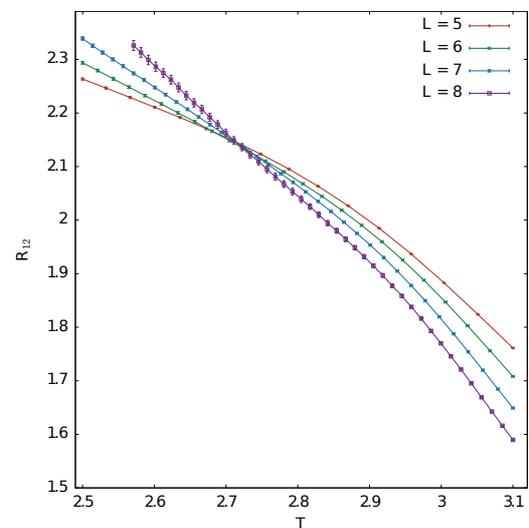


Fig. 2. Behavior of the R_{12} cumulant (defined avoiding the zero modes) as a function of the temperature for the different simulated lattices. The crossing points show the presence of a phase transition.

Finally, we show that the phase transition is correctly described by a replica-symmetric Hamiltonian and that the effective critical exponents are compatible with the Gaussian ones, suggesting that the upper critical dimension is $D_u^h = 6$. [7]

-
- [1] D. S. Fisher and D. A. Huse, Phys. Rev. Lett. **56**, 1601 (1986). Phys. Rev. B. **38**, 373 (1988).
- [2] J. Yeo and M. A. Moore, Phys. Rev. B. **91**, 104432 (2015).
- [3] J. M. Baitty-Jesi *et al.* (Janus Collaboration), Phys. Rev. B. **89**, 032140 (2014).
- [4] R. A. Baos *et al.* (Janus Collaboration), Proc. Natl. Acad. Sci. U.S.A. **109**, 6452 (2012).
- [5] P. Charbonneau and S. Yaida, Phys. Rev. Lett. **118**, 215701 (2017). P. Charbonneau *et al.*, Phys. Rev. E **99**, 022132 (2019).
- [6] M. C. Angelini, C. Lucibello, G. Parisi, G. Perrupato, F. Ricci-Tersenghi, and T. Rizzo, Phys. Rev. Lett. **128**, 075702 (2022).
- [7] M. Aguilar-Janita, V. Martín-Mayor, J. Moreno-Gordo and J. J. Ruiz-Lorenzo. Sesion Póster 1, 234. <https://arxiv.org/abs/2306.00569>.

Estimating Entropy of Correlated Discrete Sequences: Performance Analysis and a New Estimator

Juan De Gregorio¹, David Sánchez¹, and Raúl Toral¹

¹Institute for Cross-Disciplinary Physics and Complex Systems IFISC (UIB-CSIC),
Campus Universitat de les Illes Balears, E-07122 Palma de Mallorca, Spain

The Shannon entropy of a random variable, which measures its intrinsic uncertainty, is widely used in a variety of fields, such as statistical physics, biology, neuroscience, cryptography and linguistics, among many others.

Estimating the entropy of discrete sequences can be challenging due to limited available data. Moreover, there is currently no known unbiased estimator for the entropy [1], making the task even more difficult, especially in an undersample regime, in which the size of the sequence N is smaller than the number of possible outcomes L .

While numerous entropy estimators have been proposed in the literature (refer to, e.g., [1, 2]), their performance when considering the bias and standard deviation vary significantly depending on the specific system under study and the size of the available data. Most of these entropy estimator are designed particularly considering that the sequence is generated by independent events. To address possible correlations within the sequence, we propose a new entropy estimator that takes into account the order in which the elements appear in the sequence, as well as a Horvitz-Thompson correction [3] to address the issue of potential missing outcomes in a short sequence ($N < L$) [4].

Since entropy estimators are typically evaluated and compared only considering independent sequences [5], we have conducted a detailed analysis of the performance of some of the mostly used entropy estimators, when applied to correlated data. Specifically, we present the results for i) binary Markovian sequences (Fig. 1) and ii) Markovian systems in the undersample regime. In addition, we have also included our new estimator into this analysis (red crosses in Fig. 1) and we have found that it performs remarkably well in terms of the bias although showing a large dispersion.

- [1] Paninski, L., *Estimation of entropy and mutual information*, *Neural Computation* **15**, 1191-1253, 2003.
- [2] Chao, A.; Shen, T., *Nonparametric estimation of Shannons diversity index when there are unseen species in sample*, *Environmental and Ecological Statistics* **10**, 429-443, 2003.
- [3] Horvitz, D. G.; Thompson, D. J., *A generalization of sam-*

pling without replacement from a finite universe, *Journal of the American Stat. Assoc.* **47**, 66385 (1952).

- [4] De Gregorio, J.; Sánchez, D.; Toral, R., *An improved estimator of Shannon entropy with applications to systems with memory*, *Chaos, Solitons & Fractals* **165**, 112797, 2022.
- [5] Contreras Rodriguez, L.; Madarro-Cap, E.J.; Legn-Prez, C.M.; Rojas, O.; Sosa-Gmez, G., *Selecting an Effective Entropy Estimator for Short Sequences of Bits and Bytes with Maximum Entropy*, *Entropy* **23**, 561, 2021.

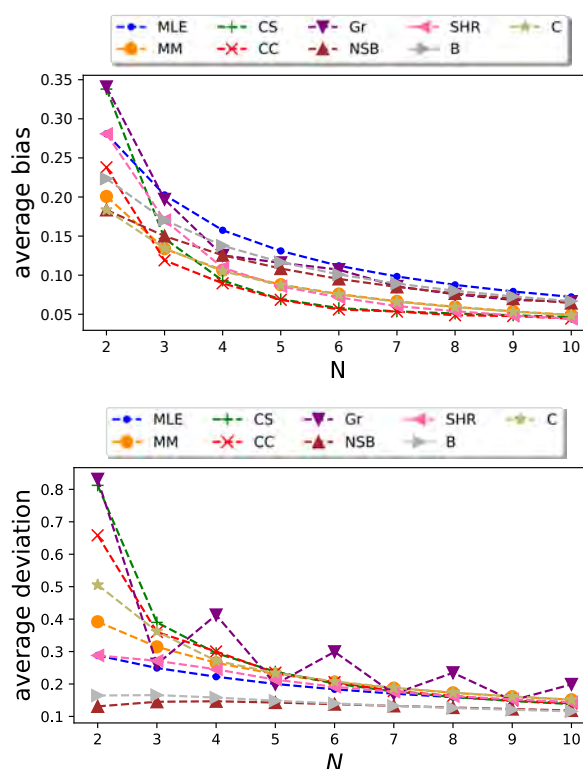


Fig. 1. Average bias (top) and deviation (bottom) of the entropy estimators when applied to Markovian, binary sequences for different sequence size N . The red line corresponds to our proposed estimator.

Spatial Memory in Rats under non Life-Threatening Conditions

J.M. Hernández¹, A.P. Segura², L. Lacasa¹, C.Mirasso¹, S.Canals², and Víctor M. Eguíluz¹

¹Institute for Cross-Disciplinary Physics and Complex Systems IFISC (CSIC-UIB), 07122 Palma de Mallorca, Spain.

²Laboratory of Plasticity of Brain Networks, Instituto de Neurociencias (CSIC-UMH), Alicante, Spain.

The *Morris water navigation task*, also known as the *Morris water maze*, is a commonly used behavioral procedure for studying spatial learning and memory in rodents. In this experiment, a rat is placed in a large circular pool and must find an invisible platform to escape the water. However, this situation puts the rats under high stress, which can be perceived as life-threatening by them. Our goal is to evaluate spatial memory formation in a setting closer to the rat’s daily life (a circular arena in the ground) with a softer, more natural reward: switching off the lights when the target is found. Since rats prefer dark environments, it has the potential to motivate rats to complete the task, without causing too much anxiety. Specifically, we measure memory formation within a single day of experimentation (*short-term memory*) and between two consecutive days (*long-term memory*), as well as analyze the relation between both.

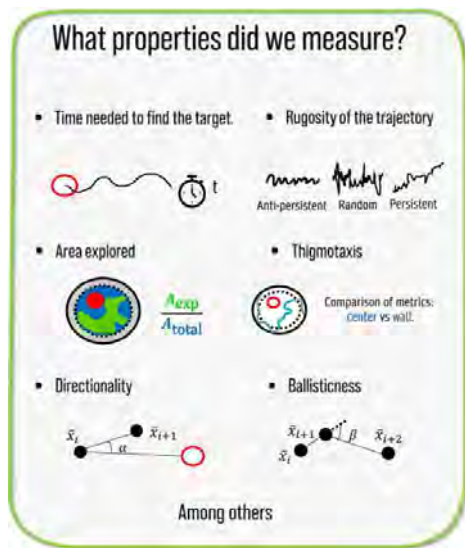


Fig. 1. Measured properties for spatial memory analysis.

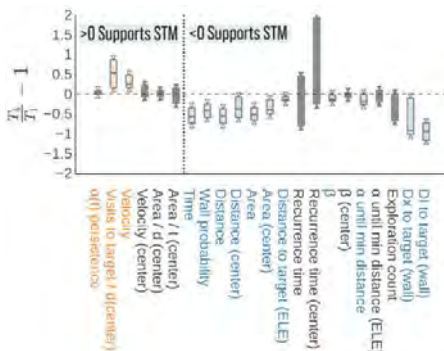


Fig. 2. **Strong evidence of STM.** Equally tailed, 95% C.I. for the median ratio change between trial 1 and trial 4. Metrics expected to increase (decrease) in the presence of STM are located at the left (right) of the dashed line. Statistically significant results are plotted in blue (decrease) and orange (increase).
25-27 de octubre de 2023, Pamplona

During an experiment, the rat tries to find the (initially unknown) target for four trials, and is expected to learn its location. By comparing the metrics (Fig. 1) between the first and last trial, we can estimate the existence of memory. Our findings provide strong evidence of STM formation, as the metrics that are expected to increase or decrease in the presence of memory align with the expected patterns (Fig. 2).

Moreover, we observe strong indications of LTM formation. Our main test relies on a *decision model*. If a rat shows LTM, it tends to prioritize visiting the target from the previous day (“preROI”) during T1 of any given day. This behavior is statistically significant and not merely influenced by chance or the proximity of preROI to the rat’s initial position compared to the current day’s target (“ROI”). To assess the absence of LTM, we establish a *null model*: a binary classifier predicting whether the rat finds the target (ROI or preROI) closer to its initial location within the crop. The null model is evaluated against the actual outcomes (preROI or ROI found first at each T1) across rats and days. If a *blind classifier*, predicting the majority class without using any data, outperforms the null model with 95% confidence based on the F1 score, we reject the null model and conclude the *detection* of LTM.



Fig. 3. Null model scheme for the LTM decision model.

The rat consistently reaches the previous day’s target with 95% confidence, ruling out proximity as the sole explanation. The blind classifier’s F1 score outperforms the null model with 99% confidence. Additionally, LTM is quantified using the same metrics as STM (Fig. 1).

[1] R. Morris, *Developments of a Water-Maze Procedure for Studying Spatial Learning in the Rat*, J. Neurosci. Methods **11**, 1984.

[2] J. Bergstra, D. Yamins, and D.D. Cox. *Making a Science of Model Search: Hyperparameter Optimization in Hundreds of Dimensions for Vision Architectures*, 30th International Conference on Machine Learning, 2013. Sesión Póster 1, P1.36

Quantum memories for squeezed and coherent superpositions in a driven-dissipative nonlinear oscillator

Adrià Labay-Mora¹, Roberta Zambrini¹, Gian Luca Giorgi¹
 Institute for Cross Disciplinary Physics and Complex Systems (IFISC) UIB-CSIC,
 Campus Universitat Illes Balears, Palma de Mallorca, Spain.

Quantum oscillators with nonlinear driving and dissipative terms have gained significant attention due to their ability to stabilize cat-states for universal quantum computation [1, 2, 3]. Recently, superconducting circuits have been employed to realize such long-lived qubits stored in coherent states [4]. We present a generalization of these oscillators, which are not limited to coherent states, in the presence of different nonlinearities in driving and dissipation, exploring different degrees. The master equation describing the time evolution of such oscillators is given by

$$\rho_t = -i[H_n, \rho] + \gamma_1 D[\rho] + \gamma_m D^{[m]}\rho \equiv \mathcal{L}\rho, \quad (1)$$

where in the Liouvillian superoperator \mathcal{L} we distinguish three different terms. First, the unitary evolution described by the Hamiltonian, which in the rotation frame and after the parametric approximation is

$$H_n = \Delta + i\eta_n [n e^{i\theta_0 n} - ()^n e^{-i\theta_0 n}]. \quad (2)$$

This models an n -photon drive with $n \geq 1$, where the detuning between the natural oscillator frequency ω_0 and the frequency of the driving force ω_s is denoted by $\Delta = \omega_0 - \omega_s$. This n -photon parametric process produces squeezing effects for $n > 1$ and will be called the squeezing term in the following. The parameter η_n controls the driving strength and ϕ represents its phase.

Specifically, we present an extensive analysis of the asymptotic dynamical features and of the storage of squeezed states. We demonstrate that coherent superpositions of squeezed states are achievable in the presence of a strong symmetry, thereby allowing for the storage of squeezed cat-states. In the weak symmetry regime, accounting for linear dissipation, we investigate the potential application of these nonlinear driven-dissipative resonators for quantum computing and quantum associative memory [5] and analyze the impact of squeezing on their performance [6].

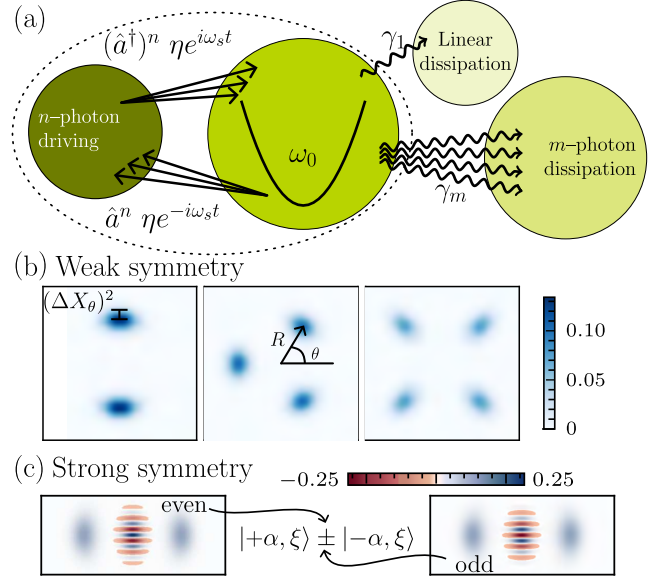


Fig. 1. (a) Sketch of the driven-dissipative nonlinear oscillator with the three processes involved in the master equation: nonlinear periodic driving with degree n , linear dissipation with rate γ_1 and nonlinear dissipation of degree m . The driving force pushes the system with strength η and frequency ω_s that may deviate from the natural oscillator frequency ω_0 . The dissipative terms emit photons out of the system at rates γ_1 and γ_m for the single- and multi-photon processes respectively. (b) Wigner distribution of the steady states generated in the weak symmetry regime with $\gamma_1 > 0$. From left to right: $(n, m) = \{(2, 3), (3, 4), (4, 3)\}$. (c) Wigner distribution of the two steady states (corresponding to even and odd parity eigenstates) present in the strong symmetry regime with $\gamma_1 = 0$ and $(n, m) = (2, 4)$.

- [1] B M Terhal, J Conrad, and C Vuillot. Towards scalable bosonic quantum error correction. *Quantum Science and Technology*, 5(4):043001, jul 2020.
- [2] Weizhou Cai, Yuwei Ma, Weiting Wang, Chang-Ling Zou, and Luyan Sun. Bosonic quantum error correction codes in superconducting quantum circuits. *Fundamental Research*, 1(1):50–67, 2021.
- [3] Mazyar Mirrahimi, Zaki Leghtas, Victor V Albert, Steven Touzard, Robert J Schoelkopf, Liang Jiang, and Michel H Devoret. Dynamically protected cat-qubits: a new paradigm for universal quantum computation. *New Journal of Physics*, 16(4):045014, 4 2014.

- [4] Raphaël Lescanne, Marius Villiers, Théau Peronnin, Alain Sarlette, Matthieu Delbecq, Benjamin Huard, Takis Kontos, Mazyar Mirrahimi, and Zaki Leghtas. Exponential suppression of bit-flips in a qubit encoded in an oscillator. *Nature Physics*, 16(5):509–513, May 2020.
- [5] Adrià Labay-Mora, Roberta Zambrini, and Gian Luca Giorgi. Quantum associative memory with a single driven-dissipative nonlinear oscillator. *Phys. Rev. Lett.*, 130:190602, May 2023.
- [6] Adrià Labay-Mora, Roberta Zambrini, and Gian Luca Giorgi. Quantum memories for squeezed and coherent superpositions in a driven-dissipative nonlinear oscillator, 2023.

A compartmental model for *Xylella fastidiosa* diseases with explicit vector seasonal dynamics

Àlex Giménez-Romero¹, Eduardo Moralejo² and Manuel A. Matías¹,

¹Instituto de Física Interdisciplinar y Sistemas Complejos, IFISC (CSIC-UIB), Campus UIB E-07122 Palma de Mallorca, Spain

²Tragsa, Passatge Cala Figuera 6, 07009 Palma de Mallorca, Spain

The bacterium *Xylella fastidiosa* (Xf) is mainly transmitted by the meadow spittlebug *Philaeus spumarius* in Europe, where it has caused significant economic damage to olive and almond trees. Understanding the factors that determine disease dynamics in pathosystems that share similarities can help to design control strategies focused on minimizing transmission chains.

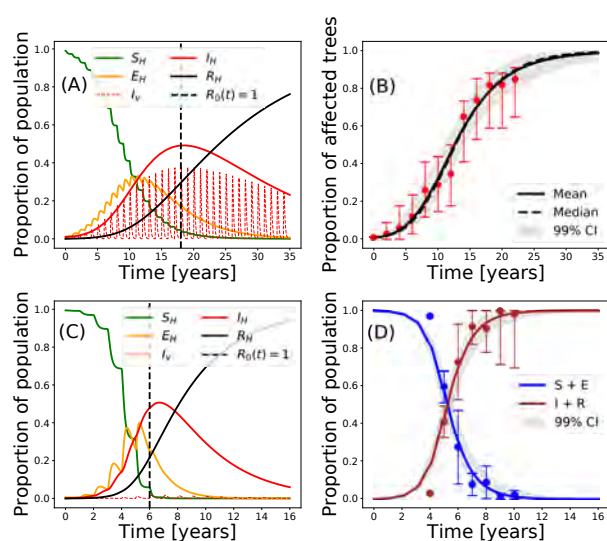


Fig. 1. (A) Simulation of the model with the best-fit parameters for ALSD. (B) Model fit to field data by means of the mean and median values of the posterior distributions of the parameters for ALSD. (C) Simulation of the model with the best-fit parameters for OQDS. (D) Model fit to field data by means of the mean and median values of the posterior distributions of the parameters for OQDS. The gray-shaded area corresponds to the 99% confidence interval. The error bars for the field data correspond to their 95% confidence interval obtained with a bootstrapping technique.

Several epidemic models have been already developed for Xf-diseases, but they lack a realistic description of some relevant processes [1]. Some of these models assume a simple general form for infected host dynamics or use a simplified S-I compartmental scheme for hosts, disregarding important features such as the latent period or the host mortality rate. Models that do take these features into account, however, do not explicitly model the population of vectors responsible for disease transmission [2]. Other more recent models have taken a step further in explicitly modeling the vector popu-

lation [3], but the characterization of its dynamics is still relatively simple, as it overlooks the known seasonal patterns of vector abundance. Several recent studies have provided new insights into the ecology and temporal dynamics of the transmission of Xf by *P. spumarius* in olive plants. However, these experimental data of the pathosystem have not been yet integrated at the population level. Thus, there is a need to continue advancing in the modeling of Xf diseases by developing more realistic models that can elucidate the fundamental processes involved in vector-host-pathogen interactions and help to design effective control strategies.

Here we introduce a compartmental model for Xf-caused diseases in Europe that accounts for the main relevant epidemiological processes, including the seasonal dynamics of *P. spumarius* [4, 5]. The model was confronted with epidemiological data from the two major outbreaks of Xf in Europe, the olive quick disease syndrome (OQDS) in Apulia, Italy, caused by the subspecies *pauca*, and the almond leaf scorch disease (ALSD) in Mallorca, Spain, caused by subspecies *multiplex* and *fastidiosa*. Using a Bayesian inference framework, we show how the model successfully reproduces the general field data in both diseases (Fig. 1). In a global sensitivity analysis, the vector-to-plant and plant-to-vector transmission rates, together with the vector removal rate, were the most influential parameters in determining the time of the infectious host population peak, the incidence peak and the final number of dead hosts. We also used our model to check different vector-based control strategies, showing that a joint strategy focused on increasing the rate of vector removal while lowering the number of annual newborn vectors is optimal for disease control.

- [1] Jeger, M. J. and C. Bragard, *Phytopathology* **109**, 200-209 (2019)
- [2] White, S. M., J. A. Navas-Corts, J. M. Bullock, D. Boscia, and D. S. Chapman, *Plant Pathology* **69**, 1403-1413 (2020).
- [3] Brunetti, M., V. Capasso, M. Montagna, and E. Venturino, *Ecological Modelling* **432**, 109204 (2020).
- [4] Gimnez-Romero, A., Flaquer-Galms, R., Matas, M.A. *Physical Review E*, **106**, 054402 (2022).
- [5] Gimnez-Romero, A., Moralejo, E., Matas, M.A. *Phytopathology* (2023).

Epidemic outbreaks reconstruction from the metric backbone

David Soriano-Paños^{1,2}, Felipe Xavier Costa^{3,1,4}, Rion Brattig-Correia^{3,1} and Luis M. Rocha

¹ Instituto Gulbenkian de Ciência, 2780-156 Oeiras (Portugal).

² GOTHAM lab, Institute for Biocomputation and Physics of Complex Systems, University of Zaragoza, 50018 Zaragoza (Spain).

³ Systems Science and Industrial Engineering Department, Binghamton University, Binghamton, NY 13902, USA.

⁴ Department of Physics, State University of New York at Albany, Albany, NY 12222, USA.

The interplay between network sparsification and spreading phenomena constitutes an important challenge in the Big Data Era. Specifically, the interest of this problem is two-fold: pruning the large set of redundant connections usually included in high resolution databases reduces the computational cost of the simulations but also unveils the primary subgraphs sustaining the spread of a pathogen. Mounting evidence in the literature suggest that network sparsification relying on global information allows for a better retrieval of spreading dynamics than just removing the weakest connections. For instance, Mercier et al. [1] show how using the effective resistance, which accounts for the relevance of a given edge in the ensemble of paths connecting their two nodes, outperforms weight thresholding in preserving SIR dynamics. Recently, Correia et al. [2] also show that the metric backbone, constructed as the union of all the shortest paths in the network, provides more solid foundations for network sparsification than relying on local information.

Despite the relevance of the metric backbone, determining the network features limiting the reconstruction of epidemic outbreaks from the union of shortest paths remains an open problem. In this talk, we will introduce a new method to construct synthetic metric backbones which will allow us to tackle this problem. We will show how both the relative size of the backbone and the semi-metric distortion values, quantifying the redundancy of the removed paths, play an important role for the reconstruction of outbreaks generated by the SI model. Building on this result, we will propose a new sparsification process relying on the semi-metric distortion distribution. Figure 1 shows that this method allows for a better retrieval of the dynamics on the original network while not disrupting its functionality in comparison to other methods studied in the literature such as the effective resistance or the weights thresholding. Finally, we will generalize to other epidemic dynamics such as the SIS or SIR models, showing that shortest paths fail in reconstructing dynamics for localized epidemic states close to the epidemic threshold.

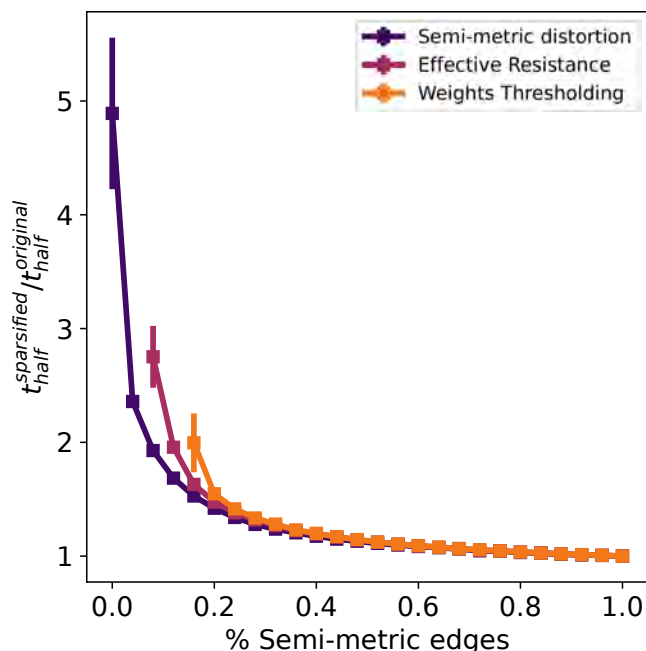


Fig. 1. Ratio between the time for a SI dynamics to reach half of the network in the sparsified configuration $t_{half}^{sparsified}$ and the original network $t_{half}^{original}$ as a function of the number of edges removed during sparsification. Note that this number of edges is indicated in terms of fraction of semi-metric edges, which are those not belonging to any shortest path in the network. Three different sparsification methods relying on three different properties of edges: semi-metric distortion (blue), effective resistance (purple) and weights (orange). Curves are interrupted when sparsification breaks the giant component of the network. The results are obtained by averaging 200 realizations for 50 different infectious seed for an infectivity $\beta = 0.5$ in a network constructed from face-to-face interactions in a school[3].

[2] R.B. Correia, A. Barrat and L.M. Rocha. PLOS Computational Biology **19**, e1010854 (2023).

[3] DJA Toth et al. Journal of The Royal Society Interface **12**(108), 20150279 (2015).

[1] A. Mercier, S. Scarpino and C. Moore. PLOS Computational Biology **18**(11), e1010650 (2022).

Partisan Voter Model: Stochastic description and noise-induced transitions

Jaume Llabres¹, Maxi San Miguel¹, and Raul Toral¹

¹Instituto de Física Interdisciplinar y Sistemas Complejos IFISC (CSIC-UIB), Campus UIB, 07122 Palma de Mallorca, Spain.

The paradigmatic *voter model* (VM) [1] is a stochastic binary state model of opinion formation in a population of interacting agents that imitate each other at random. The imitation mechanism accounts for the herding phenomena observed in many social systems. The Partisan Voter Model (PVM) [2] is a variation of the VM in which every agent has a fixed preference for one of the two states.

We consider here a mean field version of the PVM in a fully connected network. Voter $i \in [1, N]$ holds a binary state variable $s_i \in \{-1, +1\}$ and a preference for one of the two states. We consider that a fraction q of agents prefer to be in the state $+1$, and the rest are neutral. The preference is quantified with the parameter $\varepsilon \in [0, 1]$, which has been chosen to be the same for all voters which show a preference. An agent will copy another agent's agent with probability $\frac{1+\varepsilon}{2}$ when this state coincides with its preference, or with probability $\frac{1-\varepsilon}{2}$ otherwise. As in the VM, the PVM presents two absorbing states corresponding to the two configurations in which all agents are in the same state, either $+1$ or -1 .

Due to the preference of the voters, two variables are needed for the macroscopic description of the system. They have been chosen to be the sum Σ and the difference Δ of the densities of agents that are in their preferred state. An analysis of the dynamical equations shows that, for small ε , Σ is a fast dynamical variable while Δ is a slow one. This allows us to apply an adiabatic elimination technique where, at long time scales, we describe approximately the behavior of the system by slaving the dynamics of the fast variable, Σ , to the slow one, Δ .

With this reduced model, we have been able to determine analytically the following observables:

1. Exit probability $P_q(\Delta)$, defined as the probability of reaching the absorbing state $+1$ starting from an initial condition $\Delta_0 = \Delta$. In the thermodynamic limit it tends to 1 (resp. 0) if $q > \frac{1}{2}$ (resp. $q < \frac{1}{2}$). In the symmetric case $q = \frac{1}{2}$ it is equiprobable to end up in any of the absorbing states.

2. Fixation time $\tau(\Delta)$, defined as the average time to reach any consensus state starting from an initial condition $\Delta_0 = \Delta$ and whose expression in the thermodynamic limit becomes

$$\lim_{N \rightarrow \infty} \tau(\Delta) = \begin{cases} \exp N, & \text{if } |2q - 1| < \varepsilon, \\ \log N, & \text{otherwise,} \end{cases} \quad (1)$$

3. Quasi-stationary distribution $P_{\text{qst}}(\Delta)$, defined as the conditioned probability of the process to non-extinction, which captures the long term behavior of a process that has not yet reached the absorbing state. It exists only if $|2q - 1| < \varepsilon$. All the analytical results agree with simulations of the full, two variable, model.

Similarly to the Noisy Voter Model (NVM) [3], we introduce the Noisy Partisan Voter Model (NPVM) which in-

cludes idiosyncratic behavior with spontaneous changes of state. As in the NVM there is a competition between the herding, with rate h , and the idiosyncratic behavior, with rate a . We focus our work on the study of the stationary probability distribution examining the alterations of the noise-induced transition of the NVM. In the NVM the system switches from a bimodal to an unimodal distribution passing through a flat distribution for a critical value of the ratio $\frac{a}{h}$. In the NPVM there is a rich phase diagram with continuous and discontinuous noise-induced transitions depending on the values of q , ε and $\frac{a}{h}$. In Fig. 1, we display the parameter diagram $\varepsilon - \frac{a}{h}$ for $q = \frac{1}{2}$. For general $\varepsilon > 0$, the system exhibits three distinct regimes characterized by a different shape of the stationary distribution. In regions I and II the steady state is trimodal. The absolute maximum changes abruptly when crossing $(\frac{a}{h})_c$. The system goes from two maxima at the borders to one central maximum. Along the line $(\frac{a}{h})_c^*$, the lateral maxima disappear and in region III the distribution is unimodal. Additionally, the inset of Fig. 1 demonstrates that both transition lines decrease its value as the system size increases, indicating that they are finite-size transitions. In the thermodynamic limit $N \rightarrow \infty$, regions I and II disappear and the system only presents a unimodal distribution located at the center of the interval $\Delta = 0$.

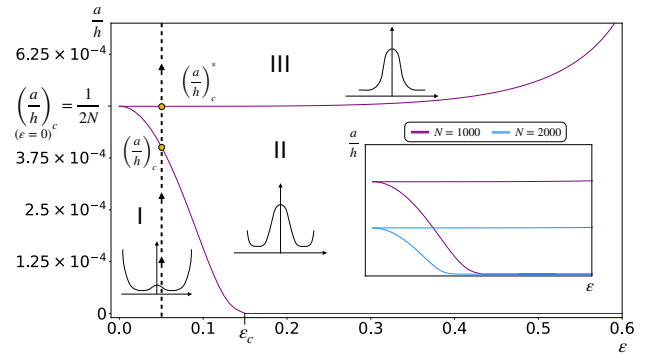


Fig. 1. Parameter diagram $\varepsilon - \frac{a}{h}$ for the different regimes of the stationary probability distribution $P_{\text{st}}(\Delta)$ for a system size $N = 1000$. Inset: Comparison of the parameter diagram $\varepsilon - \frac{a}{h}$ for system sizes: $N = 1000, 2000$ as indicated. Parameter values: $N = 1000, q = 0.5, \varepsilon = 0.05$.

[1] R. A. Holley, T. M. Liggett, *Ergodic Theorems for Weakly Interacting Infinite Systems and the Voter Model*, The Annals of Probability **3**, 643 (1975).

[2] N. Masuda, N. Gibert, S. Redner, *Heterogeneous voter models*, Physical Review E **82** (2010).

[3] A. F. Peralta, A. Carro, M. San Miguel, R. Toral, *Stochastic pair approximation treatment of the noisy voter model*, New Journal of Physics **20**, 103045 2018

Random walk interpretation of kinetic theory for intruders in freely cooling and driven granular gases

E. Abad¹, R. Gómez González², S. B. Yuste², and V. Garzó²

¹Departamento de Física Aplicada, Instituto de Computación Científica Avanzada (ICCAEx),
Universidad de Extremadura, 06800 Mérida (Spain),

²Departamento de Física, Instituto de Computación Científica Avanzada (ICCAEx),
Universidad de Extremadura, Avda. de Elvas s/n, 06006 Badajoz (Spain),

The Enskog kinetic theory has a longstanding tradition as a successful approach for the computation of transport properties in granular gases [1]. However, its relation with random walk approaches for the computation of such properties remains widely unexplored; the present work aims to shed further light on this relation to pave the way for future research in this field.

To illustrate the aforementioned relation, in a first stage we employ the (inelastic) Enskog-Lorentz kinetic equation in tandem with DSMC simulations to compute the mean square displacement (MSD) of intruders immersed in a granular gas of smooth inelastic hard spheres (grains). We consider the cases where the intruder-grain system includes (lacks) an interstitial molecular gas that plays the role of a thermal bath (background).

In the absence of such an interstitial fluid, there is no mechanism in this freely cooling granular gas to compensate for the continuous energy loss of the grains due to the dissipative collisions between them. Consequently, the random kicks experienced by an intruder upon collisions with grains also become less and less energetic in the course of time, and the intruder's motion is strongly slowed down with respect to the case of standard Brownian motion (as a matter of fact, the intruder's MSD exhibits a logarithmic time growth [2] instead of a linear one, and there is e.g. no longer equivalence between ensemble-averaged and time-averaged MSD among other peculiarities of this ultraslow anomalous diffusion).

We then incorporate the interstitial fluid, which has a two-fold effect; on the one hand, it induces a viscous drag force acting on intruders and grains; on the other hand, it feeds both particle species with energy, this supply being modeled via a stochastic Langevin-like force defined in terms of the background temperature T_b . As a result, in this driven granular gas the linear time growth of the intruder's MSD is restored (normal diffusion). However, the calculation of the associated intruder's diffusivity D proves a technically challenging task which has recently been tackled in the so-called first and second Sonine approximation [3].

In a second step, we invoke an effective random walk picture of the intruder's motion to obtain an intuitive interpretation of the intricate dependence of the diffusion coefficient on the main system parameters, both with and without the interstitial fluid [2, 3]. Despite the obvious differences in the time dependence of the MSD, for a proper parameter choice one observes in both cases a nonmonotonic behaviour of the MSD at a given time t as a function of the restitution coefficient α for grain-grain collisions (see Fig. 1 for the case with interstitial fluid and intruders mechanically equivalent to grains [selfdiffusion]). The idea underlying the random

walk approach is to decompose the MSD into a product of the number of intruder-grain collisions $N(t)$ and the square of an effective mean free path ℓ_e^2 between collisions. This latter quantity differs from the actual mean free path because of the persistence of the (strongly anisotropic) collision rules for hard spheres. While $N(t)$ increases with α , ℓ_e^2 decreases with this quantity because of the increased backscattering of intruder-grain collisions. The competition between the two effects then explains the aforementioned non-monotonic behaviour of the MSD. We anticipate that the overarching random walk approach presented here very likely applies to other types of driven systems lacking interstitial fluids, and in this sense the random walk interpretation is deemed to be very general.

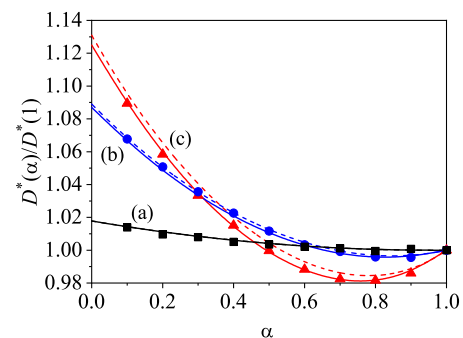


Fig. 1. Plot of the (adimensionalized) self-diffusion coefficient $D^*(\alpha)/D^*(1) \equiv D(\alpha)/D(1)$ versus the coefficient of restitution α for a system with (adimensionalized) background temperature $T_b^* = 1$ and three different values of the volume fraction ϕ occupied by grains: (a) $\phi = 0.01$ (black lines and squares); (b) $\phi = 0.1$ (blue lines and circles); and (c) $\phi = 0.25$ (red lines and triangles). The symbols refer to the DSMC results, while the solid (dashed) lines correspond to the theoretical results obtained from the second (first) Sonine approximation. Here, $D^*(1)$ is the elastic-limit value of the self-diffusion coefficient consistently obtained in each approximation.

-
- [1] V. Garzó, *Granular Gaseous Flows* (Springer, Cham, 2019).
- [2] E. Abad, S. B. Yuste, and V. Garzó, *On the mean square displacement of intruders in freely cooling granular gases*, *Granular Matter* **24**, 1–19 (2022).
- [3] R. Gmez-Gonzalez, E. Abad, S. B. Yuste, and V. Garzó, *Diffusion of intruders in granular suspensions: Enskog theory and random walk interpretation*, arXiv:2305.09259v1.

Machine learning for modeling mobility flows between locations

Oriol Cabanas¹, Lluís Danús¹, Esteban Moro^{3,4}, Roger Guimerà^{1,2} and Marta Sales-Pardo¹

¹Dept. Chemical Engineering, Universitat Rovira i Virgili, 43007 Tarragona

²ICREA, 08007 Barcelona

³Connection Science, Institute for Data Science and Society, MIT, Cambridge, United States

⁴Department of Mathematics, Universidad Carlos III de Madrid, Spain

Modeling human mobility and understanding the main features involved have inspired many studies. In this work, we analyze the number of persons moving from one city to another, regardless of the transportation or reason. Due to the large number of variables we can use to describe an urban region, models can be arbitrarily complex. The simplest approaches, the Gravity model[1] and the Radiation model[2], only use the distance and the population. However, more sophisticated deep learning approaches, such as the Deep Gravity model[4] can use 39 features.

The aim of this project is to use a symbolic regression method to recover closed-form mathematical models from the data, the Bayesian Machine Scientist(BMS)[?]. The only constraint we impose is that the variables that can appear in the model are the distance and the origin-destination populations. We use data from 6 states of the United States to train and test the models. Each state is trained with a sample of flows between a subset of cities and the same symbolic expression but with different parameters. To test the models we use the flows between a subset of cities different from the train set. To compare the performance of the BMS models, we train the mentioned reference models including a Random Forest with 39 features. To evaluate the predictions, we use the following metrics: Common Part of Commuter, Median Absolute Error, Median Relative Error, and Median Log-Ratio.

Our results show that the metrics Common Part of Commuters and Median Relative Error only capture the performance for high values of the flow. If we compare models, is difficult to distinguish a good performance from an over-fitted model. We state relative metrics are more useful since we have data with different orders of magnitude. If we compare the results for the Median Log-Ratio, we see that BMS models with three variables perform similarly or better than complex models with up to 39 features.

-
- [1] George Kingsley Zipf, *The P1 P2/D Hypothesis: On the Inter-city Movement of Persons*, American Sociological Review **11** (1946).
 - [2] Simini, Filippo, González, Marta C., Maritan, Amos, Barabási, Albert-László, *A universal model for mobility and migration patterns*, Nature **484** (2012).
 - [3] Simini, Filippo, Barlacchi, Gianni, Luca, Massimiliano, Pappalardo, Luca, *A Deep Gravity model for mobility flows generation*, Nature Communications **12** (2021).
 - [4] Roger Guimer, Ignasi Reichardt, Antoni Aguilar-Mogas, Francesco A. Massucci, Manuel Miranda, Jordi Pallars, Marta Sales-Pardo, *A Bayesian machine scientist to aid in the solution of challenging scientific problems*, Science Advances **6** (2020).

Multistability and stochastic effects in the dynamics of coupled cardiac gap junctions

Jean Bragard¹, Pau Lopez², Blas Echebarria²,

¹Dept Física y Matemática Aplicada, Universidad de Navarra

²Dept Física, Universitat Politècnica de Catalunya

Gap junctions are intercellular channels that allow electrical coupling through the cell to cell transfer of ions. They play an important role in the transmission of electrical impulses in nerve and muscle excitable tissue. In this contribution, we present results regarding the propagation of the cardiac action potential in a one-dimensional fiber, where cells are electrically coupled through gap junctions (GJs). Instead of considering a constant conductance between cells, we consider first deterministic gap junctional gate dynamics that depend on the intercellular potential

$$\frac{dg}{dt} = \frac{g_{\infty}(\Delta\phi) - g}{\tau_g(\Delta\phi)} \quad (1)$$

where $\Delta\phi$ is the difference in transmembrane potential between two adjacent cells. Once we include the dynamics, we find that, after a large number of stimulations, different GJs in the tissue can end up in two different states [1]: a low conducting state and a high conducting state (see Fig. 1). The conductance dispersion usually occurs on a large time scale, i.e., hundreds or thousands of heartbeats.

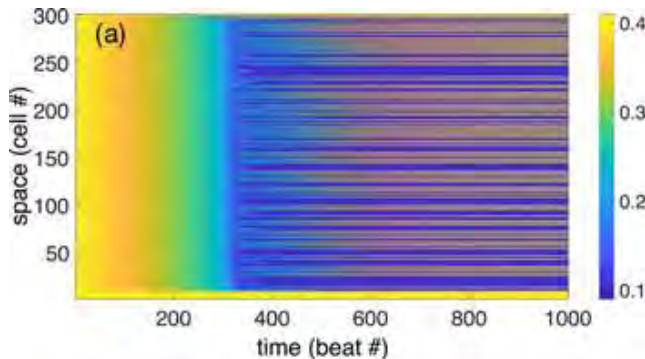


Fig. 1. Evolution of the intercellular conductivity as a function of the stimulation number, showing a final state with up and down states.

We first present evidence of the dynamical multistability that occurs by setting specific parameters of the GJ dynamics [2]. Subsequently, we explain how the multistability is a direct consequence of the GJ stability problem by reducing the dynamical systems dimensions.

Then, we study the effect of stochasticity in the dynamics of the gap junctions. The deterministic description of the gap junctional dynamics in Eq. (1) can be considered as the limit of a large set of GJs, where is of them behaves as a two-state system with transition rates depending on the intercellular potential difference. When the number of GJs becomes small (typically there are of the order of 50-100 in each junction) stochastic effects can become relevant and affect the multistability of the system.

[1] C. Hawks, J. Elorza, A. Witt, D. Laroze, I. R. Cantalapiedra, A. Pearanda, B. Echebarria, and J. Bragard, *Gap Junction Dynamics Induces Localized Conductance Bistability in Cardiac Tissue*, International Journal of Bifurcation and Chaos **29**, 1930021 (2019).

[2] J. Bragard, A. Witt, D. Laroze, C. Hawks, J. Elorza, I.R. Cantalapiedra, A. Pearanda, B. Echebarria, *Conductance heterogeneities induced by multistability in the dynamics of coupled cardiac gap junctions*, Chaos **31**, 073144 (2021).

Computational Study of Gram-positive Conjugation: from Single Cell Signaling to Colony Behavior

Álvaro López-Maroto^{1,2,3}, Christian Cortés^{1,3}, Wilfried J. Meijer⁴, Javier Buceta² and Saúl Ares^{1,3}

¹Centro Nacional de Biotecnología (CNB) - CSIC, Madrid, Spain.

²Institute for Integrative Systems Biology (I²SysBio), CSIC-UV, Valencia, Spain.

³Grupo Interdisciplinar de Sistemas Complejos (GISC).

⁴Centro de Biología Molecular Severo Ochoa (CSIC-UAM), Madrid, Spain.

Conjugation is a Horizontal Gene Transfer (HGT) phenomenon in which genetic information -coded in plasmids or integrative elements- is mobilized among individuals. Conjugation is well characterized in Gram negative (G-) bacteria. However, in spite of the clinical relevance of Gram positive (G+) species, and the issue of antibiotic resistance dissemination through HGT; little is known about the regulation of conjugation in G+. This work focuses on the study of population-level principles of G+ conjugative regulatory networks, taking the pLS20 plasmid from *Bacillus subtilis* as a model [1]. For this purpose, the Individual Based Model (IBM) Gro was applied to simulate the dynamics of pLS20 dissemination over a *B. subtilis* population growing in a solid surface. The analysis was performed from an epidemiology viewpoint, in which the pLS20 plasmid is considered an infectious agent being spread over the bacterial population. Thus, bacterial conjugation can be used as an experimental epidemiology model to extract principles and test strategies regarding agent transmission. The results of this study show the effect of the spatial distribution over plasmid dissemination and the role of noise during the infectious cycle. Interestingly, the analysis reveals the crucial effect of spatial segregation of populations on the dissemination dynamics and the robustness of the system against noise. Finally, this study also highlights the signal inheri-

tance phenomenon, which interferes with the quorum sensing systems dynamics of bacteria colonies growing in solid surfaces.

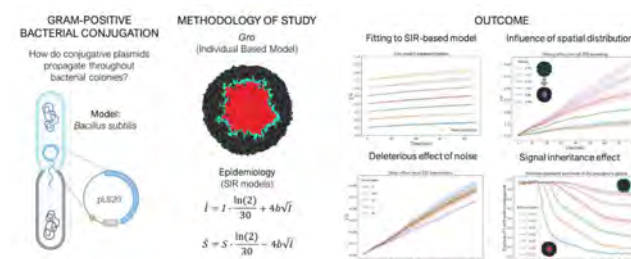


Fig. 1. Bacterial conjugation, snapshot of a colony simulation, simplified epidemic modeling of conjugation plasmid spread, and main outcomes from simulations and their comparison with the epidemic model.

- [1] W.J. Meijer, D.R. Boer, S. Ares, C. Alfonso, F. Rojo, J.R. Luque-Ortega, and L.J. Wu, *Multiple layered control of the conjugation process of the *Bacillus subtilis* plasmid pLS20*. *Frontiers in Molecular Biosciences* **8**, 648468 (2021).

Virus-host protein co-expression networks reveal temporal organization and strategies of viral infection

Jacobo Aguirre¹ and Raúl Guantes²,

¹Centro de Astrobiología (CAB), CSIC-INTA, ctra. de Ajalvir km 4, 28850 Torrejón de Ardoz, Madrid, Spain.

²Department of Condensed Matter Physics, Universidad Autónoma de Madrid, 28049 Cantoblanco, Madrid, Spain

Viral infection is a very complex process where, apart from replication of the viral machinery, many host cell proteins change their abundance, localization and modifications. Traditionally, the global effect of viral infection on the host cell proteome has been investigated using protein-protein interaction networks, which provide only static information of physical interactions between proteins. However, viral infection is a dynamic event, since viruses can hijack different cellular processes at different times of their replicative cycle.

Here, we take advantage of a recent technique to quantify the global proteome of virus and host cells across time, *Quantitative Temporal Viromics*[1], to reconstruct in detail the protein co-expression networks for different virus/host systems. These complex networks reveal that the viral infection can be seen as a dynamical process where a relatively small but strongly connected network (the virus proteome) activates different modular components of a larger network (the host proteome), Fig. 1. We take advantage of a formal framework, the *theory of interacting networks* [2, 3, 4], to describe the viral replicative cycle as a dynamic interaction between complex protein networks, where perturbations induced by viral proteins spread to hijack the host proteome for the virus benefit. Our methodology provides useful insights into the virus and host temporal organization and strategies, key protein nodes targeted by the virus and dynamical bottlenecks during the course of the infection.

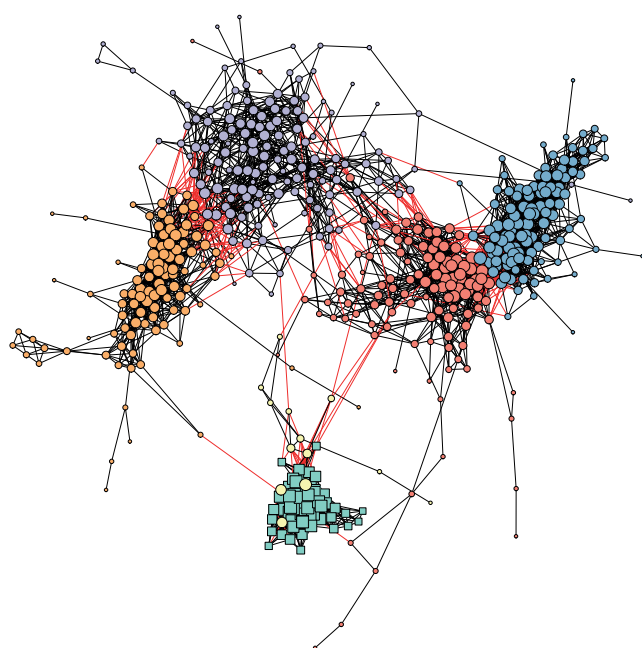


Fig. 1. Protein co-expression network of Epstein-Barr virus infection. Green squares: viral proteins. Circles: Host proteins. Colors correspond to different communities.

-
- [1] A. Fletcher-Etherington and M.P. Weeks, *Quantitative Temporal Viromics*, Annual Review of Virology **8:1**, 159-181 (2021).
 - [2] J. Aguirre, D. Papi and J.M. Buldú, *Successful strategies for competing networks*, Nat. Phys. **9**, 230-234 (2013).
 - [3] J. Iranzo, J.M. Buldú and J. Aguirre, *Competition among networks highlights the power of the weak*, Nat. Commun. **7**, 13273 (2016).
 - [4] J.M. Buldú, F. Pablo-Martí and J. Aguirre, *Taming out-of-equilibrium dynamics on interconnected networks*, Nat. Commun. **10**, 5314 (2019).

Segregation dynamics in granular suspensions

Rubén Gómez González¹ and Vicente Garzó²,

¹Departamento de Física, Universidad de Extremadura, E-06006 Badajoz, Spain

²Departamento de Física and Instituto de Computación Científica Avanzada (ICCAEx), Universidad de Extremadura, E-06006 Badajoz, Spain

The comprehension of the physical mechanisms involved in segregation is likely one of the most challenging problems in the realm of granular mixtures. Segregation has garnered significant attention in the context of dry granular mixtures as it constitutes a nice and interesting application stemming from the derivation of the diffusion transport coefficients. Among the various segregation phenomena, the Brazil-nut effect (BNE) stands out as a prominent example of size-based segregation in vertically vibrated mixtures. In the BNE, a relatively large particle, known as the intruder, tends to ascend to the uppermost region of the sample against the force of gravity. Conversely, alternative experimental investigations have reported a contrasting phenomenon of reverse buoyancy known as the reverse Brazil-nut effect (RBNE), wherein the intruder may sink to the bottom of the container under specific conditions. In this work, we want to study the segregation induced by a thermal gradient and/or gravity. We assume with this aim that gravity and the thermal gradient point in parallel directions (i.e., the bottom plate is hotter than the top plate). The main target is to assess the impact of the interstitial gas surrounding the particles on the segregation criterion previously obtained in the absence of the gas phase [1].

We consider a set of intruders immersed in a granular gas of smooth inelastic hard spheres (grains). The starting point of the present work is the (inelastic) Enskog-Lorentz kinetic equation. The effect of the interstitial gas on solid particles is accounted for in the kinetic equation through two different terms: (i) a viscous drag force proportional to the particle velocity and (ii) stochastic Langevin-like term defined in terms of the background temperature. To obtain the segregation phase diagrams, the kinetic equation is solved by means of the Chapman–Enskog method conveniently adapted to account for the inelasticity of collisions. The transport coefficients are obtained as the solutions of a set of coupled linear integral equations recently derived for binary granular suspensions with arbitrary concentration [2]. Using those results, we consider here the tracer limit of the linear integral equations obeying the corresponding diffusion transport coefficients.

The main goal of the present work is twofold. Firstly, we aim to solve the aforementioned equations to determine the diffusion transport coefficients up to the second Sonine approximation, which involves considering two terms in the Sonine polynomial expansion of the distribution function. Secondly, we intend to evaluate the accuracy of the Sonine approximations by solving the Enskog equation through the direct simulation Monte Carlo (DSMC) method. We use the Einstein relation to compute the tracer diffusion coefficient as a function of the coefficients of (normal) restitution. Although some deviations between the Sonine approximations are noticeable when the grains possess a greater mass and size compared to the intruders, these discrepancies are

smaller than those observed in dry granular systems [3]. Notably, the second Sonine approximation enhances the theoretical predictions of the first Sonine approximation, resulting in excellent agreement with the simulation results.

As an application, we study the segregation dynamics of the mixture. In the absence of gravity, our results (see Fig. 1) show that the effect of the gas phase on segregation is in general significant for large mass and/or diameter ratios. The main effect of the surrounding gas is to increase the size of the RBNE region (intruders attempt to accumulate near the hot plate) with respect to the one observed in the absence of the gas phase. Conversely, in scenarios where segregation is predominantly influenced by gravity (namely, when thermal gradient can be neglected) the phase diagrams with and without gas phase are practically identical. In addition, as for dry granular mixtures, the influence of inelasticity of

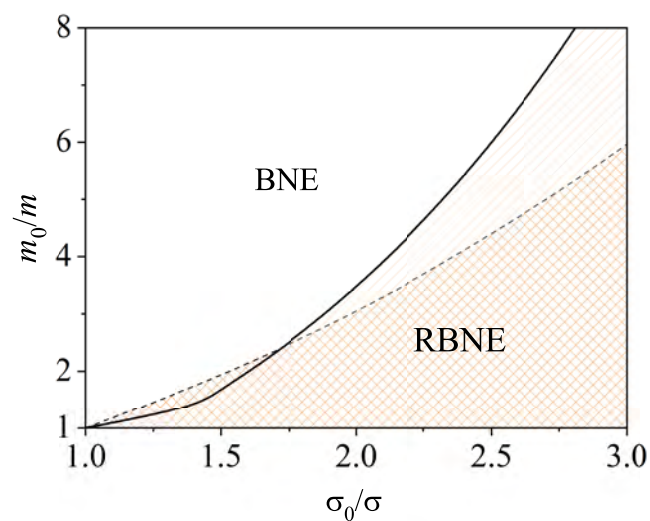


Fig. 1. Segregation phase diagram as a function of the intruder-grain mass (m_0/m) and size (σ_0/σ) ratios. We consider a common coefficient of (normal) restitution ($\alpha = \alpha_0 = 0.8$) in the absence of gravity. The solid line corresponds to the segregation criterion for granular suspensions while the dashed line refers to the one derived for dry granular mixtures.

- [1] V. Garzó, *Thermal diffusion segregation in granular binary mixtures described by the Enskog equation*, New J. Phys. **13**, 055020 (2011).
- [2] R. Gómez González, N. Khalil, and V. Garzó, *Enskog kinetic theory for multicomponent granular suspensions*, Phys. Rev. E **101**, 012904 (2020).
- [3] V. Garzó, *Granular Gaseous Flows* (Springer Nature, Cham, 2019).

Modelo mecánico del proceso de adsorción de “k-meros”

Tomás de Navascués¹, Marcelo Pasinetti², Antonio Ramirez-Pastor², Eugenio Vogel^{3,4}, Martín Maza-Cuello¹, Diego Maza

¹ Departamento de Física y Matemática Aplicada, Facultad de Ciencias, Universidad de Navarra, E-31080 Pamplona, España.

² Departamento de Física, Instituto de Física Aplicada (INFAP), Universidad Nacional de San Luis-CONICET, Argentina.

³ Centro para el Desarrollo de la Nanociencia y Nanotecnología (Cedenna), Santiago, Chile.

⁴ Departamento de Ciencias Físicas, Universidad de La Frontera, Temuco, Chile.

En este trabajo presentamos resultados experimentales preliminares sobre la posibilidad de explorar la dinámica y estados de equilibrio de un gas de “k-meros” en un símil mecánico, donde el material sustrato se modela con una base acanalada y los “k-meros” por varillas de longitud variable. Presentamos también algunos resultados numéricos que permiten predecir la dinámica esperable en el sistema.

Así, el sistema consta de una base en la cual se han trazado canaletas equiespaciadas una distancia de 5 mm con una configuración cuadriculada. Las canaletas tienen una profundidad de 1 mm y en ella pueden quedar atrapadas varillas que en principio se han elegido de 20 mm de longitud. Las varillas son cilindros rectos de grafito de 0.7 mm de diámetro.

La base se encuentra colocada sobre un vibrador vertical que produce oscilaciones armónicas en la dirección vertical. Las aceleraciones alcanzadas, tanto en la vertical como los posibles residuos en los otros ejes son medidas con un acelerómetro de 3 ejes insertado en el centro de la base. En principio pueden modificarse tanto la frecuencia como la amplitud de las oscilaciones. En este trabajo, se ha fijado la frecuencia de oscilación en 40 Hz y se ha variado la aceleración de la base hasta valores superiores a las 4 g's. Todo el sistema puede verse en la Fig. 1.

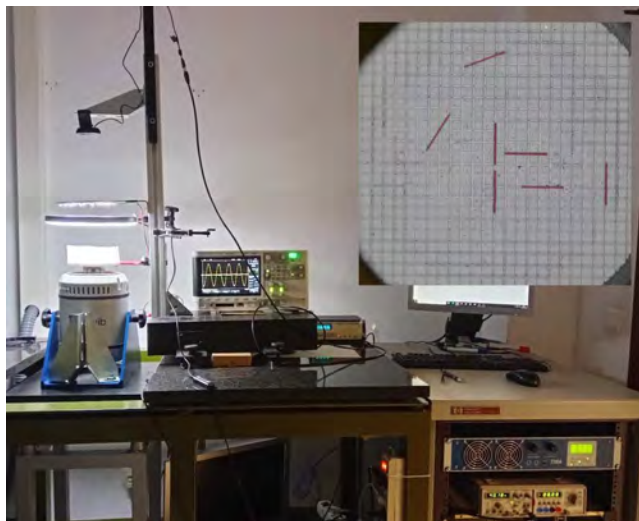


Fig. 1. Vista general del sistema experimental. Detalle: Imagen obtenida por la cámara cenital donde se ve el sistema acanalado con varillas adsorbidas y desorbidas.

En una primera etapa se exploró la dinámica de una única varilla para estudiar su dinámica sobre el sustrato así como para conocer las probabilidades tanto de adsorción como de desorción de las mismas en función de la aceleración adimensional $\Gamma = \frac{Aw^2}{g}$. Se comprobó así que para conseguir tiempos donde las varillas permanecieran en estados tanto adsorbidos como desorbidos. Se pudieron estimar estas probabilidades asumiendo un comportamiento Markoviano donde la adsorción de una varilla luego de aplicar N oscilaciones está dada por una PDF geométrica, es decir $(1 - p)^{N-1} p$.

Se estudió también la evolución espacial de las varillas en el régimen desorbido, donde se comprobó que los movimientos superficiales eran tales que una varilla podía visitar cualquier sitio de la red antes de ser adsorbida. Más importante aún, se comprobó que estos movimientos poseen una distribución de probabilidad de saltos dada por una distribución Gamma, compatible con un proceso difusivo tipo Levy.

Todos estos resultados resultan compatibles con la aproximación numérica lo que validaría el sistema para estudiar su evolución hacia estados más densos. La simulación numérica GCMC a una temperatura T y presión P , considera el estado adsorbido de un conjunto de varillas, es decir, cuando cada una de estas se encuentran atrapadas en las canaletas y sin posibilidades de solaparse entre sí. Los resultados experimentales resultan compatibles con la aproximación numérica lo que validaría el sistema para estudiar su evolución hacia estados más densos.

[1] Nematic-disordered phase transition in systems of long rigid rods on two-dimensional lattices. Joyjit Kundu, R. Rajesh, Deepak Dhar, and Jürgen F. Stilck, *Phys. Rev. E* **87**, 032103 (2013). Sequence of phase transitions in a model of interacting rods. Juliane U. Klamser, Tridib Sadhu, and Deepak Dhar, *Phys. Rev. E* **106**, L052101 (2022)

[2] Entropy-driven phases at high coverage adsorption of straight rigid rods on two-dimensional square lattices, P. M. Pasinetti, A. J. Ramirez-Pastor, E. E. Vogel, and G. Saravia, *Phys. Rev. E* **104**, 054136 (2021).

Thermal brachistochrone: Minimizing connection times between equilibrium states in harmonically confined Brownian particles

Carlos A. Plata

Física Teórica, Universidad de Sevilla, Apartado de Correos 1065, E-41080 Sevilla, Spain

We are used to apply a predictive approach in physical problems: specific external conditions are considered and the evolution of the physical system is derived. However, it is not uncommon to wonder what the external protocol should be to impose in order to drive the system in a certain desired evolution. Inverse engineering techniques and, more generally, (optimal) control theory provide a robust framework to address such problems. In the last decade, the use of control theory has been proven as a productive strategy in the context of quantum mechanics, where a number of shortcut methods have been successfully applied [1].

More recently, these strategies have been brought to the field of classical statistical mechanics [2], exploiting the analogy between the mathematical descriptions of both realms. In this contribution, we present an exact shortcut within a paradigmatic model system in non-equilibrium statistical mechanics. Specifically, we consider a d -dimensional overdamped harmonically confined Brownian particle in contact with a thermal bath, in which the temperature can be externally manipulated. Therein, we obtain the shortest protocol connecting two equilibrium states at different temperatures.

The Gaussian character of the position distribution persists along the whole evolution, which reduces the problem to a system of first-order differential equations for the d variances in each dimension where the temperature appears linearly in all the equations. Direct application of Pontryagin's principle leads us to obtain that the protocol giving the shortest connection time is a bang-bang protocol for the temperature between the bounds of the control, i.e., the temperature takes constant values switching between the bounds. Remarkably, the problem in the limit of spherical symmetry is singularly different from the one-dimensional case: there is an unavoidable time cost to connect systems with higher dimension as shown in Fig. 1.

We have looked into this problem of the thermal brachistochrone in detail, studying the effect of finite power to heat and cool, that is, considering finite bounds for the temperature of the thermal bath. Furthermore, the thermodynamic length and the thermodynamic cost are investigated for the optimal protocol, delving into the role of information geom-

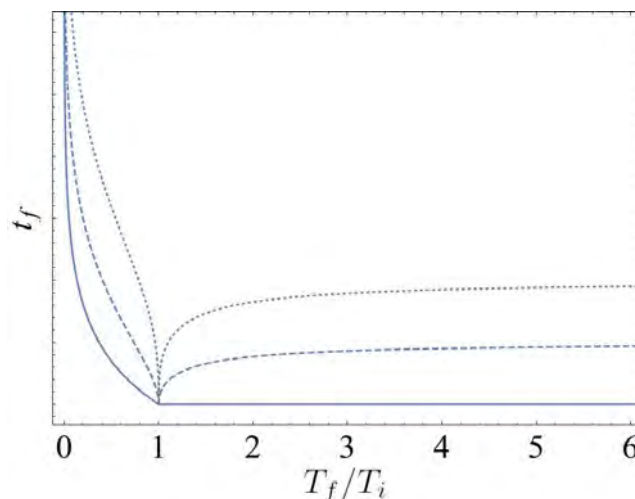


Fig. 1. Shortest time t_f for connecting two equilibrium states of a d -dimensional Brownian harmonic oscillator with a ratio T_f/T_i between the final and initial temperature for $d = 1$ (solid), $d = 2$ (dashed), and $d = 3$ (dotted). An unavoidable cost of time emerges despite the fact that the limit of spherical symmetry is assumed.

etry quantities within the field of stochastic thermodynamics.

-
- [1] D. Guéry-Odelin, A. Ruschhaupt, A. Kiely, E. Torrontegui, S. Martínez-Garaot, and J. G. Muga, *Shortcuts to adiabaticity: Concepts, methods, and applications*, Rev. Mod. Phys. **91**, 045001 (2019).
- [2] D. Guéry-Odelin, C. Jarzynski, C. A. Plata, A. Prados, and E. Trizac, *Driving rapidly while remaining in control: classical shortcuts from Hamiltonian to stochastic dynamics*, Rep. Prog. Phys. **86**, 035902 (2023).
- [3] A. Patrón, A. Prados, and C. A. Plata, *Thermal brachistochrone for harmonically confined Brownian particles*, Eur. Phys. J. Plus **137**, 1011 (2022).

Self-similarity of turning avalanches in schooling fish

Andreu Puy¹, Elisabet Gimeno², David March¹, M. Carmen Miguel^{2,3}, and Romualdo Pastor-Satorras¹

¹ Departament de Física, Universitat Politècnica de Catalunya, Campus Nord B4, 08034 Barcelona, Spain

² Departament de Física de la Matèria Condensada, Universitat de Barcelona, Martí i Franquès 1, 08028 Barcelona, Spain

³ Institute of Complex Systems (UBICS), Universitat de Barcelona, Barcelona, Spain

Groups of animals are observed to transmit information across them with propagating waves or avalanches of behaviour. These behavioral cascades often display scale-free signatures in their duration and size, ranging from activating a single individual to the whole group, signatures that are commonly related to critical phenomena from statistical physics. A particular example is given by turning avalanches, where large turns in the direction of motion of individuals are propagated [1]. Employing experimental data of schooling fish, we examine characteristics of spontaneous turning avalanches and their dependency with schools of different number of individuals. We report self-similar properties in the avalanche duration, size and inter-event time distributions, as well as in the avalanche shape [2]. We argue that turning avalanches are a result of collective decision-making processes to select a new direction to move. They start with the group having low speed and decreasing the coordination, but once a direction is chosen, speed

increases and coordination is restored. We report relevant boundary effects given by wall interactions and by individuals at the border of the group. We conclude investigating spatial and temporal correlations using the concept of aftershocks from seismology. Contrary to earthquakes, turning avalanches display statistically significant clustered events only below a given time scale and follow an Omori law for aftershocks with a faster decay rate exponent than that observed in real earthquakes [2].

[1] J. Múgica, J. Torrents, J. Cristín, A. Puy, M.C. Miguel and R. Pastor-Satorras, *Scale-free behavioral cascades and effective leadership in schooling fish*, Scientific Reports **12**, 10783 (2022).

[2] A. Puy, E. Gimeno, D. March, M.C. Miguel and R. Pastor-Satorras, *Self-similarity of turning avalanches in schooling fish*, Preprint available here: <http://arxiv.org/abs/2309.16455>

Immersing in a rigid particle flow versus immersing in a soft particle flow

Jing Wang¹, Bo Fan², Tivadar Pongó^{3,4}, Tamas Borzsonyi², Ralf Stannarius¹ and Raúl Cruz Hidalgo³

¹Institute of Physics, Otto von Guericke University, Magdeburg, Germany

²Institute for Solid State Physics and Optics, Wigner Research Centre for Physics, Budapest, Hungary

³Física y Matemática Aplicada, Facultad de Ciencias, Universidad de Navarra, Pamplona, Spain

⁴Collective Dynamics Lab, Division of Natural and Applied Sciences, Duke Kunshan University, Kunshan, China

In this work, we have shown that a sphere suspended in a discharging silo experiences mechanical forces from the weight of the overlaying layers and the friction of the surrounding moving granular material. In experiments and simulations with hard frictional glass particles, the force on the obstacle was nearly uninfluenced by the flow velocity. Its value remained unaltered during a large part of the discharge process and depended linearly on the obstacle diameter. The simulations indicate that during the discharge, the pressure of the granular bed at the obstacle's surface scales with the size as $p(z') \sim 1/R$, which is congruent with a force proportional to the diameter of the obstacle. Besides, the mean pressure gradient acting on the obstacles was practically the same for all the explored orifices and did not vary significantly in the discharge process. It is worth mentioning that when the outflow of GLS was interrupted, the force on the ball remained nearly unchanged, indicating the predominantly static nature of the interaction. On the other hand, in flowing frictionless soft particles, noticeable drag is added to the gravitational forces on the suspended obstacles. As confirmed by our micromechanical analysis, the obstacle experienced a total force from the top as if immersed in a dynamic hydrostatic pressure profile, but practically without acting from below. Irrespective of the low friction, the particle collisions generate a noticeable drag force. It increases with velocity up to a certain speed, but then reaches saturation. We argue that at high discharge rates, the local packing density drops, thus reducing the drag force and compensating for the effects of increased velocity.

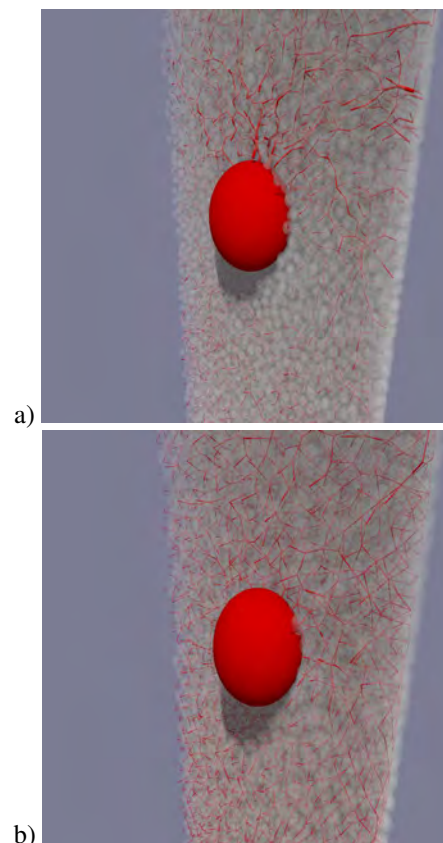


Fig. 1. Force network acting on an obstacle with 40 mm diameter submerged in GLS (a) and in HGS (b)

On the formation of coral reefs

Miguel Álvarez-Alegría, Manuel A. Matías and Damià Gomila
Instituto de Física Interdisciplinar y Sistemas Complejos, IFISC (CSIC-UIB)

Coral reefs are incredibly captivating ecosystems found in our world. The vast array of diverse species that inhabit them, combined with their intricate and vibrant formations, have earned them the nickname "the rainforests of the sea". Beyond the interactions within the reef's entire ecosystem, the biology of corals itself is filled with intricate phenomena. For instance, they engage in a symbiotic relationship with microalgae called *Zooxanthellae*, and exhibit remarkable properties like synchronized sexual events that occur under specific conditions. Additionally, individual polyps within coral colonies display self-organization, forming distinct structures such as massive, branching, and table corals. While there are solitary species, coral polyps generally gather together in colonies of the same species, creating the aforementioned structures. When colonies of corals exist in the same area, they form a reef. These coral animals have the ability to synthesize aragonite, a form of calcium carbonate, during their clonal growth, which contributes to the development of a sturdy external skeleton. As one colony dies, a new polyp can settle on the remnants of the former colony's solid structure, initiating the formation of a new colony. Over centuries, this cycle repeats, leading to the creation of large aragonite structures that exhibit

recognizable patterns found worldwide. These patterns encompass closed atolls, parallel stripes, and collections of closed atolls with smaller halos inside, demonstrating a remarkable example of self-similarity within this coral reef system.

In this study, we present a novel model that successfully replicates the observed formations of coral reefs. Our proposed model is based on partial differential equations and incorporates the wealth of knowledge accumulated over the past decades regarding the physical and ecological interactions occurring at the micro- and mesoscales within these systems. These interactions include clonal growth, facilitation, the uptake of resources by corals, and the supply of these resources by ocean water currents, among others. Through the mathematical analysis of this model using bifurcations theory, we uncover that the interplay of only a few parameters of the model is sufficient to elucidate the emergence of various reef shapes found in nature. This includes the formation of fringing reefs, closed atolls, and the inner structures within closed atolls. Our findings provide valuable insights into the underlying mechanisms driving the diverse morphologies observed in coral reefs.

Sub-cellular description of cardiac action potential propagation with gap junctions dynamics.

Jean Bragard¹, and Blas Echebarria²

¹Department of Physics & Applied Math., School of Sciences, University of Navarra. 31008 Pamplona. Spain.

²Dept Física, Universitat Politècnica de Catalunya.

We study the propagation of the cardiac action potential in a one-dimensional fiber, where cells are electrically coupled through gap junctions (GJs) [1]. We integrate the dynamical equations at the sub-cellular level. We consider gap junctional gate dynamics that depend on the intercellular potential. We find that different GJs in the tissue can end up in two different states: a low conducting state and a high conducting state. We first present evidence of the dynamical multistability that occurs by setting specific parameters of the GJ dynamics. Subsequently, we explain how the multistability is a direct consequence of the GJ stability problem by reducing the dynamical systems dimensions. The conductance dispersion usually occurs on a large time scale, i.e., thousands of heartbeats [2, 3]. That is highly relevant in studying diseases that develop on a large time scale compared to the basic heartbeat. As in the brain, plasticity and

tissue remodeling are crucial parameters in determining the action potential wave propagations stability.

-
- [1] R. M. Shaw, and Y. Rudy, *Ionic Mechanisms of Propagation in Cardiac Tissue: Roles of the Sodium and L-Type Calcium Currents During Reduced Excitability and Decreased Gap Junction Coupling*, *Circulation Research* **81**(5), 727–741 (1997).
 - [2] C. Hawks, J. Elorza, A. Witt, D. Laroze, I. R. Cantalapiedra, A. Penaranda, B. Echebarria, and J. Bragard, *Gap Junction Dynamics Induces Localized Conductance Bistability in Cardiac Tissue*, *Int. J. of Bifurcation and Chaos* **29**,1930021 (2019).
 - [3] J. Bragard, A. Witt, D. Laroze, C. Hawks, J. Elorza, I.R. Cantalapiedra, A. Penaranda, B. Echebarria, *Conductance heterogeneities induced by multistability in the dynamics of coupled cardiac gap junctions*, *Chaos* **31**, 073144 (2021).

Dynamics of an inelastic tagged particle under strong confinement

Pablo Maynar Blanco^{1,2}, María Isabel García de Soria^{1,2}, and J. Javier Brey^{1,2}

¹Física Teórica, Universidad de Sevilla, Apartado de Correos 1065, E-41080, Sevilla, Spain

²Institute for Theoretical and Computational Physics. Facultad de Ciencias. Universidad de Granada, E-18071, Granada, Spain

The dynamics of a tagged particle immersed in a fluid of particles of the same size but different mass is studied when the system is confined between two hard parallel plates separated a distance smaller than twice the diameter of the particles. The collisions between particles are inelastic while the collisions of the particles with the hard walls inject energy in the direction perpendicular to the wall, so that stationary states can be reached in the long-time limit. The velocity distribution of the tagged particle verifies a Boltzmann-Lorentz-like equation that is solved assuming that it is a spatially homogeneous gaussian distribution with two different temperatures (one associated to the motion parallel to the wall and another associated to the perpendicular direction). It is found that the temperature perpendicular to the wall diverges when the tagged particle mass approaches a critical mass from below, while the parallel temperature remains fi-

nite. Molecular Dynamics simulation results agree very well with the theoretical predictions for tagged particle masses below the critical mass. The measurements of the velocity distribution function of the tagged particle confirm that it is gaussian if the mass is not close to the critical mass, while it deviates from gaussianity when approaching the critical mass. Above the critical mass, the velocity distribution function is very far from a gaussian, being the marginal distribution in the perpendicular direction bimodal and with a much larger variance than the one in the parallel direction [1].

-
- [1] P. Maynar, M. I. García de Soria, and J. J. Brey, *Dynamics of an inelastic tagged particle under strong confinement*, Physics of Fluids **34**, 123321 (2022).

A pattern-formation mechanism arising from pulsed interaction signals

Eduardo H. Colombo¹, Cristóbal López², and Emilio Hernández-García²,

¹Center for Advanced Systems Understanding (CASUS), Helmholtz-Zentrum Dresden Rossendorf (HZDR), Görlitz, Germany.

²Instituto de Física Interdisciplinar y Sistemas Complejos (IFISC), CSIC-UIB, Palma de Mallorca, Spain

Many physical, chemical or biological systems experience instabilities that create spatially periodic distributions of substances or energy out of a homogeneous initial state. Several mechanisms have been identified for such *pattern-forming* processes, being the most well-known the Turing mechanism, in which a fast-diffusing *inhibitor* substance controls the growth of a slow-diffusing *activator*, leading to modulated distributions. This process is usually modeled with reaction-diffusion equations, so that interactions between substances occur locally in space.

Another mechanism that has been identified in the context of vegetation patterns [1] and cluster crystals [2] is *competitive clustering*, in which biological competition or repulsive interactions lead to spatially periodic arrangements of substances or of clusters of particles. This mechanism is often modeled in terms of non-local equations, in which interactions occur at finite distances within an interaction range.

A timely question is to assess if such non-local interactions can be obtained from more fundamental models, in which the action-at-a-distance is just an approximate description of interactions of substances or signals that are released by the agents and act locally, but at time-scales that are very fast, justifying their elimination from the description.

Here [3] we show that pattern formation of the competitive-clustering type may be obtained from local interactions between substances released by agents, but only if the release occurs in a pulsed and intermittent manner. This pulsed or flashing signal dynamics creates a route to pattern formation alternative to the most studied ones arising from Turing-like mechanisms.

Our finding is obtained by studying a general activator-inhibitor (population-signal) model, where a biological population interacts through the release of harmful signals with a fine-scale dynamics which is explicitly modeled. For slow signal dynamics (with timescales similar to those of the population), we recover standard reaction-diffusion dynamics which, for a broad set of population and signal dynamics, does not exhibit Turing instability for any values of model parameters. For the same system dynamics, but with sufficiently fast flashing signals, the system can be described by a single integrodifferential equation, where the toxic effects are captured by a competitive nonlocal spatial interaction. In this limit, and for a suitable class of signal dynamics, spatial instability can occur leading to pattern formation. Thus, our approach identifies a novel mechanism of pattern formation, which relies on the fine-scale and fast dynamics of signals of pulsed character, and bridges the reaction-diffusion and the integrodifferential description in adequate limit cases.

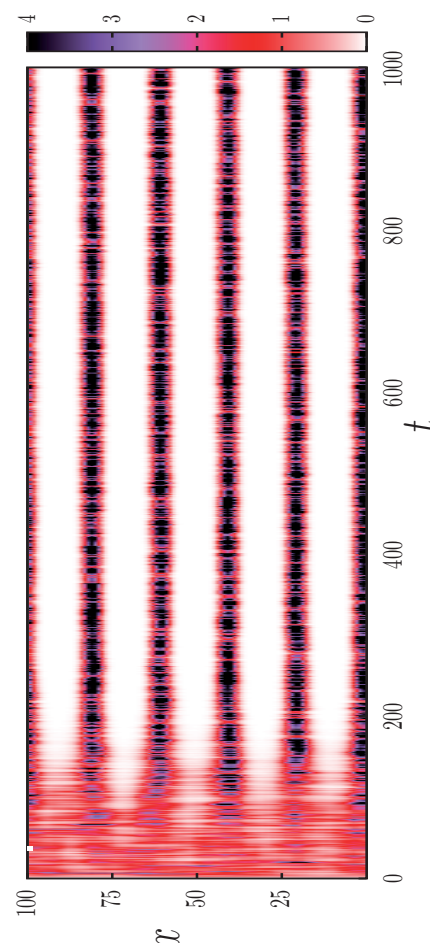


Fig. 1. Spatiotemporal representation of the density of a one-dimensional population of organisms releasing toxins in a pulsed way, leading to a spatially periodic pattern. Space is represented in the horizontal and time runs in the vertical.

-
- [1] R. Martínez-García, C. Cabal, J.M. Calabrese, E. Hernández-García, C.E. Tarnita, C. López, J.A. Bonachela, *Integrating theory and experiments to link local mechanisms and ecosystem-level consequences of vegetation patterns in drylands*, *Chaos Solitons and Fractals* **166**, 112881 (2023).
- [2] J-B. Delfau, C. López, E. Hernández-García, *Active cluster crystals*, *New Journal of Physics* **19**, 095001 (2017).
- [3] E.H. Colombo, C. López, E. Hernández-García, *Pulsed interaction signals as a route to biological pattern formation*, *Physical Review Letters* **130**, 058401 (2023).

Impact of overlapness on dynamical systems with higher-order interactions

Santiago Lamata-Otn^{1,2,*}, Federico Malizia^{2,3,*}, Mattia Frasca⁴, Vito Latora^{3,5,6}, and Jesús Gómez-Gardeñes^{1,2}

¹Department of Condensed Matter Physics, University of Zaragoza, 50009 Zaragoza, Spain

²GOTHAM lab, Institute of Biocomputation and Physics of Complex Systems (BIFI), University of Zaragoza, 50018 Zaragoza, Spain

³Department of Physics and Astronomy, University of Catania, 95125 Catania, Italy

⁴Department of Electrical, Electronics and Computer Science Engineering, University of Catania, 95125 Catania, Italy

⁵School of Mathematical Sciences, Queen Mary University of London, London E1 4NS, United Kingdom

⁶Complexity Science Hub Vienna, A-1080 Vienna, Austria

* These two authors contributed equally

Higher-order structures are the most widely used framework to embody group interactions, and the influence of these structures on dynamical processes has been extensively addressed in recent years. In this panel we propose a metric which characterizes the overlapping between groups, i.e. hyperedges, from the perspective of the individual, i.e. node.

The surrounding environment of a node is determined by the hyperedges to which it is connected. In the case of pairwise interactions, each of them accounts for a different neighbour. However, in presence of higher order interactions, a node may have coincident nodes in different hyperedges. Thus, we introduce, for each node i , the *local overlapness* $T_i^{(m)}$ of the m -order hyperedges. This metric measures the normalized difference between the number of unique neighbours $\mathcal{S}_i^{(m)}$ the node has, and the minimum number of neighbours $\mathcal{S}_i^{(m),-}$ the node must have, given its value of connectivity $k_i^{(m)}$. The expression reads

$$T_i^{(m)} = 1 - \frac{\mathcal{S}_i^{(m)} - \mathcal{S}_i^{(m),-}}{\mathcal{S}_i^{(m),+} - \mathcal{S}_i^{(m),-}}, \quad (1)$$

where $\mathcal{S}_i^{(m),+}$ is the maximum number of unique neighbors a node must have given its generalized degree $k_i^{(m)}$. In the definition, we consider the subtraction to 1 in order to set $T_i^{(m)} = 0$ when there is no local overlapness at all, and $T_i^{(m)} = 1$ for the maximum overlapping scenario. Once defined the set of local metrics, we introduce the *global overlapness* as the weighted mean $\mathbf{T}^{(m)}$. In this panel we are going to restrict to just to pairs (1-hyperedges) and triplets (2-hyperedges), and thus our control parameter is $\mathbf{T} = \mathbf{T}^{(2)}$. We have studied the relevancy of this metric on real data sets, obtaining a broad range of metric values.

Henceforth, we focus on its impact on contagion and synchronization dynamics by means of a synthetic structure. For the sake of simplicity, as contagion dynamics we consider an Higher-order Susceptible-Infected-Susceptible (HO SIS) compartmental model. According to it, the contagion may occur through both pairs and triplets with two distinct transmission ratios rescaled by the recovery rate, $\lambda^{(1)}$ and $\lambda^{(2)}$ respectively. On the other hand, as synchronization dynamics we contemplate the higher-order Kuramoto model, where oscillators associated to each node evolve according to a individual natural frequency and to the coupling with pairs and triplets. The strength of the former is named $\lambda^{(1)}$ and the strength of the latter is $\lambda^{(2)}$.

Our results show that the order of both contagion and synchronization transitions changes depending on the level of overlapness. We characterize in Fig 1 and Fig 2 the phase diagrams of both dynamics as a function of the strength of the pairwise interactions and the overlapness. The similarity between the diagrams indicates universality in our find-

ings: when higher-order structures are not locally congregated and connect all regions of the structure, explosiveness arises. However, in case they just enforce locally several nodes subsets, the phenomenology changes and a second order transition is obtained. These reasoning are validated by microscopic analysis based on effective frequencies and local synchronization on Kuramoto dynamics.

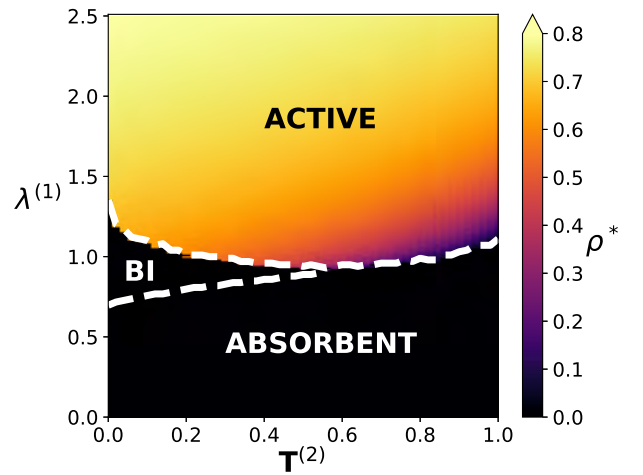


Fig. 1. SIS dynamics phase diagram is shown for $\lambda_T = 3$. Three phases emerge: absorptive phase where epidemic dies out, active phase where an endemic stationary state is reached, and a bi-stable region where the outcome depends on the initial conditions.

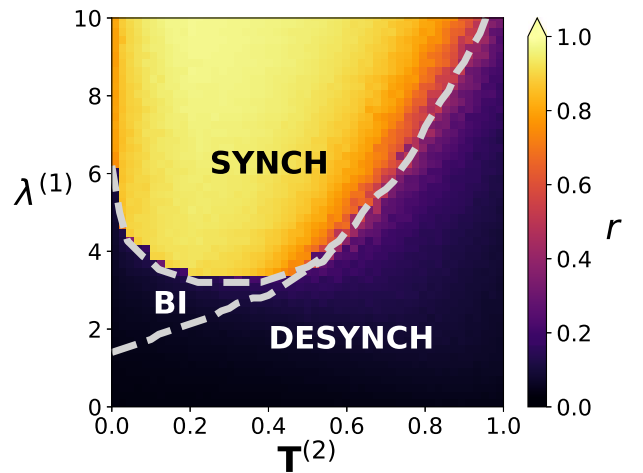


Fig. 2. Kuramoto dynamics phase diagram is shown for 2-hyperedges coupling $\lambda^{(2)} = 3$. Three regions emerge: synchronization where all oscillators are locked, desynchronization where are unlocked, and a bi-stable regime.

Inverse percolation by removing straight semirigid rods from bilayer square lattices

L.S. Ramirez^{1,2}, F.M.L. Pimentel³, N. De La Cruz Felix^{2,3}, and A. J. Ramirez-Pastor²

¹Instituto de Física Interdisciplinar y Sistemas Complejos (IFISC), Campus Universitat Illes Balears, España

²Departamento de Física, Instituto de Física Aplicada (INFAP), Universidad Nacional de San Luis CONICET, San Luis, Argentina

³Instituto de Física (IFIS), Facultad de Ciencias, Universidad Autónoma de Santo Domingo-FONDOCYT, República Dominicana

Numerical simulations and finite-size scaling analysis have been carried out to study the problem of inverse percolation by removing semirigid rods from a $L \times L$ square lattice that contains two layers (and $M = L \times L \times 2$ sites). The process starts with an initial configuration where all lattice sites are occupied by single monomers (each monomer occupies one lattice site) and, consequently, the opposite sides of the lattice are connected by nearest-neighbor occupied sites. Then the system is diluted by removing groups of k consecutive monomers according to a generalized random sequential adsorption (RSA) mechanism. The study is conducted by following the behavior of two critical concentrations with size k : (1) jamming coverage $\theta_{j,k}$, which represents the concentration of occupied sites at which the jamming state is reached; and (2) inverse percolation threshold $\theta_{c,k}$, which corresponds to the maximum concentration of occupied sites for which connectivity disappears. The obtained results indicate that (1) the jamming coverage exhibits an increasing dependence on the size k . It rapidly increases for small values of k and asymptotically converges towards a definite value for infinitely large k -sizes $\theta_{j,k \rightarrow \infty} \approx 0.2701$; and (2) the in-

verse percolation threshold is a decreasing function of k in the range $1 \leq k \leq 17$. For $k \geq 18$, all jammed configurations are percolating states (the lattice remains connected even when the highest allowed concentration of removed sites is reached), and consequently, there is no nonpercolating phase. This finding contrasts with the results obtained in literature for a complementary problem, where straight rigid k -mers are randomly and irreversibly deposited on a square lattice forming two layers. In this case, percolating and nonpercolating phases extend to infinity in the space of the parameter k and the model presents percolation transition for the whole range of k . The results obtained in the present study were also compared with those reported for the case of inverse percolation by removing of rigid linear k -mers from a square monolayer. The differences observed between monolayer and bilayer problems were discussed in terms of vulnerability and network robustness. Finally, the accurate determination of the critical exponents ν , β , and γ reveals that the percolation phase transition involved in the system has the same universality class as the standard percolation problem.

Disregulation of tissue homeostasis in a two cell-type system

A. Alsina¹, D. Soriano-Paños¹, R. Martins¹, M. Pires¹, M. Soares¹ and P. Sartori¹
¹Instituto Gulbenkian de Ciência, Rua da Quinta Grande 6, 2780-156, Oeiras, Portugal

Biological systems operate far from thermodynamic equilibrium, relying on the exchange of matter and energy with the environment to perform specific functions. Despite operating in noisy environments, biological systems can maintain physiological variables in an optimal operational regime, a property known as homeostasis. Nevertheless, homeostatic properties can be altered in response to certain conditions, such as disease. It is thus crucial to understand the disregulation of homeostasis in order to be able to steer recovery after a perturbation like disease.

Here, we study the disregulation of tissue homeostasis resulting from intrinsic and extrinsic perturbations using a combination of theoretical and experimental approaches. In particular, we focus on an established *in vitro* minimal model of a tissue, corresponding to co-cultures of fibroblasts and macrophages, two cell types found in most mammalian tissues that form stable circuits [1, 2]. In addition to growth factors secreted by the other cell type, these cells require micronutrients supplied as part of the cell culture medium in order to grow and proliferate.

A crucial micronutrient required for proper mitochondrial function, and hence for proliferation, is iron. However, free (labile) iron is highly reactive, becoming toxic unless stored in a non-reactive form, a task performed by ferritin, a molecule that stores iron in a non-reactive form and is able to release it when required for cellular functions [3].

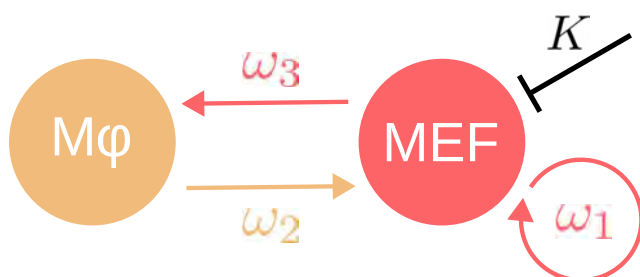


Fig. 1. Cartoon of the theoretical model depicting the interactions between fibroblasts (MEF) and macrophages (M ϕ).

In this work we study the disregulation of homeostasis in the fibroblasts-macrophages cell circuit resulting from intrinsic and extrinsic perturbations, corresponding respectively to ferritin knock-outs and to the addition of supplemental iron to the cell culture media. Our experimental results show that when both cell types lack ferritin iron toxicity leads to the extinction of both cell types. However,

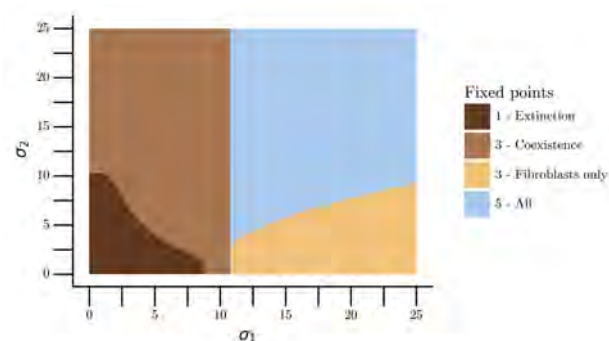


Fig. 2. Phase diagram of the system as a function of the strength of the ferritin-mediated regulation of the intracellular iron pool of fibroblasts σ_1 and macrophages σ_2 . Color indicates the number of fixed points of the dynamics with non-negative concentration of fibroblasts and macrophages.

when only fibroblasts lack ferritin, the dynamics are rescued by the interactions between the two cell types, reaching a steady-state characterised by the coexistence of fibroblasts and macrophages.

Our experimental findings are supported by theoretical modelling of the dynamics of the concentration of fibroblasts, macrophages and their respective intracellular free iron pools (Fig. 1). We show that the steady-state of the dynamics is determined by two effective parameters corresponding to the asymptotic death to proliferation ratios of fibroblasts and macrophages. Furthermore, for biologically-sensible values of the model parameters, our model phenomenologically reproduces the outcome of the different experimental conditions by adequately tuning the strength of the ferritin-mediated regulation of the intracellular iron pool. (Fig. 2).

Taken together, we have shown using a combination of a minimal *in vitro* system and theoretical modelling, how cellular interactions can lead to the restoration of tissue homeostasis even in the presence of strong intrinsic and extrinsic perturbations.

- [1] X. Zhou et al., *Circuit design features of a stable two-cell system*, Cell **172**(4), (2018).
- [2] M. Adler et al., *Endocytosis as a stabilizing mechanism for tissue homeostasis*, PNAS **115**(8), (2018).
- [3] B. Blankenhau et al., *Ferritin regulates organismal energy balance and thermogenesis*, Molecular Metabolism **24**, (2019).

Macroscopic active particles driven by light

Sára Lévy¹, Iker Zuriguel¹, and Raúl Cruz Hidalgo¹

¹Dpto. de Física y Mat. Apl., Fac. de Ciencias, Universidad de Navarra, 31080 Pamplona, España

The self-organization of bird flocks, the formation of human stampedes, the motion of molecular motors, or the collective cell migration can all be considered ensembles of self-propelling active particles. The study of such ensembles is getting increased interest [1] due to the broad range of its applications in physics, biology, chemistry, and robotics. It has been observed that, regardless of the type of particles in question, active systems share certain properties at the group level. Accordingly, several models have been developed to describe the emergence of collective behavior [2, 3].

In self-propelled particles, some kind of energy is converted into directed mechanical motion. Indeed, the energy can come from the particle itself (e.g. bird flocks), or from an external source, acting locally or at the boundary (e.g. moving or shaking boundaries in the case of granular systems). In our work, we focus on the response to a stimulus, called taxis. We present novel, macroscopic self-propelled agents excited by light.

The agents are small robots called Hexbugs [4] with photovoltaic cells mounted on their top (see Fig. 1 right). Using this configuration the behavior of the agents can be influenced by changing the light intensity. Fig. 1 shows the sketch of the experimental setup, while Fig. 2 represents the trajectories of four particles obtained with homogeneous illumination.

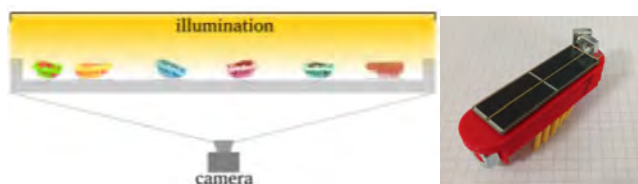


Fig. 1. Left: Sketch of the experimental setup. Right: Hexbug with a 3D printed cover holding the photovoltaic cell.

On the one hand, the macroscopic size of the particles allows us to explore the limit case of more sophisticated microscopic systems and isolate the contribution of some physical variables regarding the emergence of collective motion.

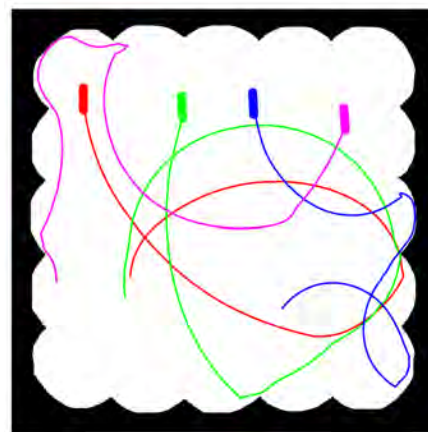


Fig. 2. Sample particle trajectories recorded with homogeneous illumination.

On the other hand, using a fully controllable illumination panel, we are able to change the illumination intensity spatially and temporally. E.g. by imposing spatial gradients of activity, we aim studying the diffusion, mixing, and clustering of the particles.

In this poster, we present the first results about the collective behavior of the photosensitive agents.

-
- [1] C. Bechinger, R. Di Leonardo, H. Löwen, C. Reichhardt, and G. Volpe, *Active particles in complex and crowded environments*, *Rev. Mod. Phys.* **88**, 045006 (2016).
 - [2] T. Vicsek, A. Czirók, E. Ben-Jacob, I. Cohen, and O. Shochet, *Novel type of phase transition in a system of self-driven particles*, *Phys. Rev. Lett.* **75**, 1226, (1995).
 - [3] T. Vicsek and A. Zafeiris, *Collective motion*, *Phys. Rep.* **517**, 71-140 (2012).
 - [4] E. Altshuler, J. M. Pastor, A. Garcimartín, I. Zuriguel, and D. Maza, *Vibrot, a simple device for the conversion of vibration into rotation mediated by friction: preliminary evaluation*, *PLoS One* **8**, e67838 (2013).

Interacting particle systems with mobility and demographic dynamics as biological models

Alejandro Almodóvar, Tobias Galla, and Cristóbal López
IFISC, Instituto de Física Interdisciplinar y Sistemas Complejos (CSIC-UIB),
Campus Universitat de les Illes Balears, E-07122 Palma de Mallorca, Spain

The behaviour of active matter has been intensively investigated in the last decades partly because of its many applications to living systems. In this work, we add stochastic birth-death dynamics to a system of particles with volume exclusion. This is a simple, but general biological ingredient which has not been studied in detail before. The number of particles in the system at long times depends on the birth and death rates, and on a parameter characterising the activity. We find liquid, solid and hexatic phases in the absence of activity. Which one of these phases is realised depends

on the birth and death rates [1]. When self-propulsion is considered, we also observe these phases depending on the activity. We will also analyse what happens when there are two types of particles of different sizes. We will study the conditions to find coexistence.

-
- [1] Almodvar, A., Galla, T., Lpez, C., *Liquid-hexatic-solid phases in active and passive Brownian particles determined by stochastic birth and death events.*, Phys. Rev. E , **106(5)**, 054130, 2022.

Phase Separation of Proteins: Finding the Disordered Regions that Drive it

Esteban Meca¹, Anatol W. Fritsch², Juan M. Iglesias-Artola², Simone Reber³, and Barbara Wagner⁴

¹Departamento de Física Aplicada, Radiología y Medicina Física, Universidad de Córdoba, 14014 Córdoba (Spain).

²Max Planck Institute of Molecular Cell Biology and Genetics, Pfotenhauerstraße 108, 01307 Dresden, Germany.

³IRI Life Sciences, Humboldt-Universität zu Berlin, 10115 Berlin, Germany.

⁴Weierstrass Institute Berlin, Mohrenstraße 39, 10117 Berlin, Germany.

Liquid-liquid phase separation of proteins (LLPS) is increasingly being recognized as a fundamental mechanism within the cell. This phase transition is behind the formation of numerous organelles in cells (nucleoli, P-granules, stress granules, ...). Also, its importance for the process of heterochromatin compartmentalization is currently emerging[1].

LLPS occurs typically for intrinsically disordered proteins (IDP), i.e. proteins without a defined secondary structure. IDPs are extremely common, and this is likely related with the ubiquity of Functional LLPS. Intrinsically disordered proteins usually contain one or more intrinsically disordered regions (IDR), which have also been identified as the main drivers for LLPS

The important role of these regions begs the question of whether the description of this regions is enough to predict the phase behavior of the whole protein. This has been observed in numerous cases but remains a contentious topic.

Despite its enormous importance, it remains a challenge to predict the phase behavior of a protein directly from its sequence and the solvent environment. Molecular dynamics cannot really be applied to a large ensemble of proteins. Hence, coarse-grained approaches are necessary. Our approach will be based on the Random Phase Approximation (RPA), an asymptotic approximation to the full partition function[2].

Here we present the phase diagram of two proteins, derived using a thermodynamically consistent mean-field theory that includes salt concentration as a variable. We build the free energy by adding an entropic part and a part stemming from the electrostatic interaction between charged residues, with the particularity that only one IDR is used at a time to compute the electrostatic part of the free energy. We validate the results by comparing them to experimental data that has been obtained for the whole protein.

We have studied the proteins PGL-3 (*C. elegans*) and fused in sarcoma (FUS). By using structure-predicting software we have identified the longest IDR in each protein and computed the phase diagrams using the RPA free energy. We have studied the temperature/protein concentration as well as the salt/protein concentration phase diagrams and have found good agreement with the theory (Fig. 1).

For FUS, which has two long IDRs, we have obtained the additional insight that only one of the IDRs is responsible for

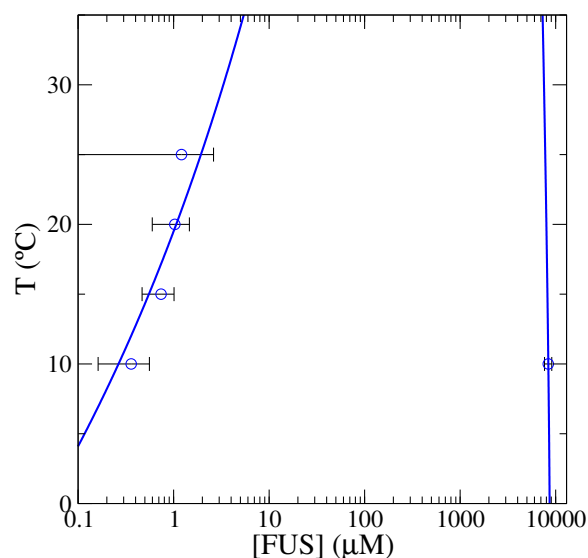


Fig. 1. Predicted temperature-concentration phase diagram using the N1 IDR of FUS, for 150 mM KCl.

LLPS. It contains a low-complexity prion-like domain, but we argue that the charged residues in its vicinity are critical for phase separation, a result that agrees with experiments.

Additionally we have studied the effect of salt, finding that the condensed phase must have a higher salt concentration than the dilute phase, a result that awaits experimental confirmation[3].

[1] H. Zhang, W. Qin, H. Romero, H. Leonhardt, and M.C. Cardoso, *Heterochromatin organization and phase separation*, *Nucleus* **14**, 1 (2023).

[2] Y.H. Lin, J.D. Forman-Kay, and H.S. Chan, *Sequence-specific polyampholyte phase separation in membraneless organelles*, *Phys. Rev. Lett.* **117**, 178101 (2016).

[3] E. Meca, A.W. Fritsch, J.M. Iglesias-Artola, S. Reber, and B. Wagner, *Predicting disordered regions driving phase separation of proteins under variable salt concentration*, *accepted in Frontiers in Physics* (2023).

Parte IX

Sesión Póster 2. Jueves 26 Tarde

The role of averaging in multidimensional symbolic dynamics

Juan Gancio¹, Giulio Tirabassi¹ and Cristina Masoller¹

¹Universitat Politècnica de Catalunya

Different data analysis tools have been developed, and applied with different rates of success, to deal with sets of time series (TS) that represent the evolution in time of some variable in different points of space (or channels), such as electroencephalograms (EEG), satellite data, or functional magnetic resonance imaging (f-MRI). One of these successful tools is Permutation Entropy (PE) [3]. Originally, PE was developed to analyse one-dimensional TS, constructing symbols from the relative magnitude of the TS at different times [1]. Different strategies have been proposed to generalise PE to deal with higher order TS, such as using all the available data across channels to calculate a single value of PE. This operation is known as pooling, and the value of PE calculated by pooling is called Pooled PE (PPE) [2]. However, many works use some average, either in time or space, to generalise PE to their data without explicitly mentioning what is the consequence of this operation, from an information theory perspective, or how the value of PE reported relates to PPE. Here, we extend the work done by Keller & Lauffer [2], who introduced PPE and studied its relation with averaged PE, by exchanging the role of space and time. As Keller and Lauffer obtained a measure of heterogeneity in the symbol distribution of different channels, we report here a new measure of the heterogeneity in time of the symbol distribution in space. Such measure can be used

to detect non-stationarity in the system. We discuss what kind of structures in the data would each measure be able to detect, and applied them in synthetic systems close to bifurcation, coding them in both usual PE symbols and spatial PE (SPE) symbols [4]. We found that, for these synthetic systems, these measures of heterogeneity are able to anticipate the bifurcation, and can successfully detect non-stationary TS.

-
- [1] Bandt, C., & Pompe, B. (2002). Permutation entropy: a natural complexity measure for time series. *Physical review letters*, 88(17), 174102..
 - [2] Keller, K., & Lauffer, H. (2003). Symbolic analysis of high-dimensional time series. *International Journal of Bifurcation and Chaos*, 13(09), 2657-2668.
 - [3] Leyva, I., Martínez, J. H., Masoller, C., Rosso, O. A., & Zanin, M. (2022). 20 years of ordinal patterns: Perspectives and challenges. *Europhysics Letters*, 138(3), 31001.
 - [4] Schlemmer, A., Berg, S., Shajahan, T. K., Luther, S., & Parlitz, U. (2015, August). Quantifying spatiotemporal complexity of cardiac dynamics using ordinal patterns. In 2015 37th Annual International Conference of the IEEE Engineering in Medicine and Biology Society (EMBC) (pp. 4049-4052). IEEE.

Estadística Regional en Pacientes con Fibrilación Auricular

Leire Moriones¹, Susana Ravassa², and Jean Bragard¹

¹Departamento de Física y Matemática Aplicada, Universidad de Navarra, Pamplona, España

²Departamento de Enfermedades Cardiovasculares, CIMA, Pamplona, España

La fibrilación auricular (FA) es una de las patologías cardíacas más prevalentes, asociada al envejecimiento, a un alto riesgo de morbilidad y mortalidad y a un elevado gasto socio-sanitario debido a las complicaciones clínicas derivadas y a los costes de su tratamiento. Por lo tanto, existe una necesidad médica de fenotipar con precisión las alteraciones electroanatómicas de la aurícula izquierda presentes en pacientes con FA [1, 2].

Este trabajo propone caracterizar la remodelación eléctrica de la aurícula mediante mapas de voltaje de alta densidad (HDvM). A partir de ellos, se extraen valores de voltaje, entre otros, como biomarcadores eléctricos con los que se realizan cálculos estadísticos.

Utilizando una técnica reciente, se divide la aurícula izquierda de cada uno de los 122 pacientes participando al estudio en 24 regiones 'estándar' [3]. Con ellas, el objetivo principal es refinar el cálculo del voltaje medio en cada una de las regiones para el estudio de la Fibrilación Auricular.

La metodología propuesta parte de la regionalización en 24 regiones y la incluye en la geometría original de la aurícula. En ella se estudian las posibles controversias que puedan existir, como el error producido en la traslación de regiones desde el mapa de 2D al de 3D y el fallo en la determinación de donde se produce realmente la ablación, para la posterior quemadura de la zona dañada (Figura 1).

El método facilita una limpieza de los datos con la que se corrige dicha falta de etiquetas basada en anillos de vecindad. Estos anillos son el punto determinante para establecer el criterio de corrección. Se definen en torno a 7 anillos de vecindad, 4 con gran prioridad en la limpieza y otros 3 como secundarios para apoyo en la misma.

Además, el algoritmo se valida y compara con otro método, que se asume como 'ground truth' en el que las regiones están perfectamente determinadas, de forma que cada una de las áreas no contiene anomalías. Junto a esa validación, se determina una última región, llamada 25 (Figura 1) con la que se establecen los últimos componentes del mapa en 3D, las cuales no aparecen en el primero de los mapas estudiados, el de 2D.

Por último, determinar que el método propuesto es correcto en su utilización y los datos extraídos son satisfactorios para posteriores análisis estadísticos regionales. Los valores extraídos tras el análisis son la determinación del valor medio de voltaje en cada una de ellas (V_m), el cálculo del área que abarcan (A), los errores asociados a las medidas (Std.Error) o las discrepancias que puedan existir como

errores entre el método desarrollado y el establecido como 'ground truth'.

En resumen, se determina un algoritmo con el que se detallan de forma más precisa y fiable los biomarcadores eléctricos de los datos extraídos tras la ablación como tratamiento de la Fibrilación Auricular.

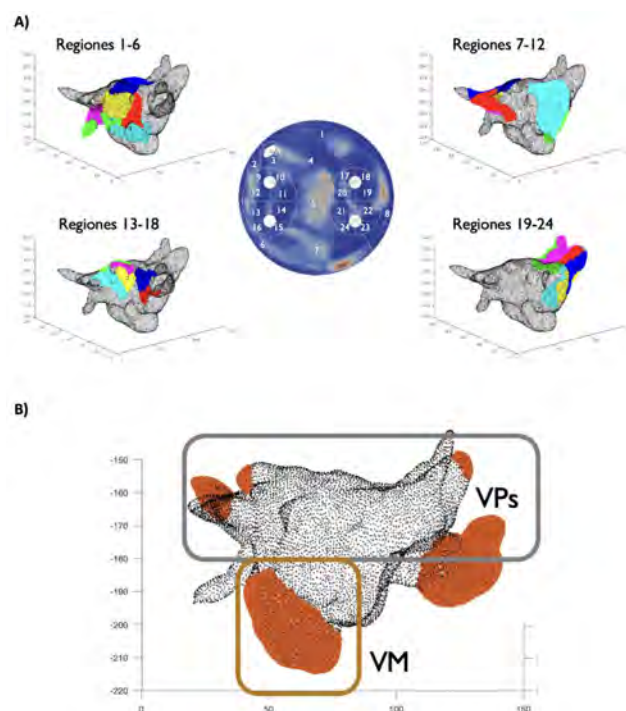


Fig. 1. Representación de las 25 regiones en 2D y 3D. A) primeras 24 regiones para ambas dimensiones y B) región 25 detallada en 3D

- [1] Ballesteros G., Ravassa S., Bragard J., et al., *Association of left atrium voltage amplitude and distribution with the risk of atrial fibrillation recurrence and evolution after pulmonary vein isolation* J. Cardiovasc. Electrophysiol. 2019; 30,1231-1240.
- [2] Byagishita A., Sparano D., Cakulev I., et al. *Identification and electrophysiological characterization of early left atrial structural remodeling as a predictor for AFR after pulmonary vein isolation* J. Cardiovasc. Electrophysiol. 2017; 28, 642-650
- [3] Tobon-Gomez, Catalina, et al. *Standardised unfold map of the left atrium: regional definition for multimodal image analysis* Journal of Cardiovascular Magnetic Resonance 17.1 (2015): 1-3.

Dynamics of a confined and ultraconfined vibrated granular system

M. Mayo¹, J. Javier Brey², Juan C. Petit³, M. I. García de Soria⁴, and P. Maynar⁵

¹Universidad de Sevilla, mmayo@us.es

²Universidad de Sevilla, brey@us.es

³German Aerospace Center, jcpetit@gmail.com

⁴Universidad de Sevilla, gsoria@us.es

⁵Universidad de Sevilla, maynar@us.es

A granular system is an ensemble of macroscopic particles, characterised by dissipative interactions. This means that, when two particles interact, part of the kinetic energy of the center of mass of the two particles is transferred to another internal degree of freedom. Many elements of nature can be identified with granular matter: from dessert to interstellar dust or planetary rings, and they are also relevant because of its technological applications [1]. From a theoretical point of view, granular systems are especially interesting because, due to its dissipative character, they are intrinsically out of equilibrium. Although, Stationary states of a granular medium can be reached experimentally in a simple way in order to compare theoretical predictions with experimental results. This is achieved, for example, by vibrating the walls that contains the system. In stationary states, the energy that is injected compensates for the energy dissipated in the collisions. The price to pay is that the stationary state becomes highly inhomogeneous [2, 3]. However, there exist a granular systems that allows to simplify the analytical study. This is a dilute granular gas confined into vibrating box.

This work will be focused on studying one of the main outcomes derived in the context of the kinetic theory of

gases, the Boltzmann equation, which will be adapted in order to describe granular systems. Complementary, a dynamic equation for confined systems will be derived by using a simplified model consisting of a gas of inelastic hard spheres confined between two plane-parallel plates. These plates are spaced a distance H . Both plates vibrates in a manner that injects kinetic energy into the system in the normal direction allowing to reach a non-trivial stationary state. From the proposed kinetic equation, closed evolution equations for the horizontal and vertical temperatures are derived, assuming spatial homogeneity. An acceptable agreement between the theoretical predictions and Molecular Dynamics simulation results is obtained.

[1] Campbell, C S, *Rapid Granular Flows*, Annual Review of Fluid Mechanics, **22**,1,(1990).

[2] J. J. Brey y D. Cubero, *Hydrodynamic transport coefficients of granular gases*, Granular Gases (Springer, 2001), pgs. 59-78.

[3] Brey, J. Javier and Dufty, James W. and Kim, Chang Sub and Santos, Andrés, *Hydrodynamics for granular flow at low density*, Phys. Rev. E **58**,4638 (1998).

Modeling a primordial, non-enzymatic RNA replication in the early Earth

Carla Alejandre¹, Adrián Aguirre-Tamaral², Carlos Briones¹ and Jacobo Aguirre^{1,3}

¹Centro de Astrobiología, CSIC-INTA, Madrid, Spain

²Centro de Biotecnología y Genómica de Plantas (CBGP), UPM-INIA, Madrid, Spain

³Grupo Interdisciplinar de Sistemas Complejos (GISC), Madrid, Spain

Life appeared on Earth around 3.800 million years ago, not long after our planet became habitable. The hypothesis of the *primordial soup* describes a very young planet in which prebiotic chemistry could have progressively increased the available molecular complexity in several out-of-equilibrium environments such as surface lakes, sea coasts, water-mineral interfaces, oceanic hydrothermal vents, etc. In some of those scenarios, the accumulation of organic compounds and the availability of energetic sources laid the foundations for the emergence of life.

One of the widely accepted hypothesis related to the origin of life, widely supported by experimental data, is the *RNA world*. It suggests that life was originated in an environment in which informational and functional RNA molecules were able to self-replicate (through the activity of RNA ribozymes). Later evolution of these primordial RNA populations would give rise to the decoupling of genotype and phenotype in the RNA/protein and DNA/RNA/protein worlds [1]. However, the sophisticated machinery associated with current RNA polymerase enzymes could not emerge randomly from those initial organic compounds that were available in the stage of prebiotic chemistry. Instead, a step-wise, ligation-based modular evolution of short RNA sequences seems a more plausible pathway for the appearance of the first RNA molecules with enzymatic properties [2]. Nevertheless, even modular evolution of RNA requires the presence of an up-to-now unknown replicative mechanism to guarantee the availability of copies of specific RNA sequences (oligoribonucleotides) in which selection can act.

In this work we describe the development of a computational model to simulate the polymerization of single ribonucleotides and a subsequent non-enzymatic, template-dependent replication mechanism for the primordial RNA molecules. These processes would have arisen in a confined space such as the interphase between an aqueous solution and the interlayers of clay minerals, an environment known

to favor RNA polymerization [3, 4]. In our simulations, two RNA polymerization processes are described: (i) surface-dependent, random polymerization of ribonucleotides, and (ii) template-dependent polymerization thanks to RNA complementary base pairing (RNA replication). This conceptually simple in silico model allows us to test how environmental conditions can affect the length and fidelity of RNA copies, as well as to study how the efficiency of the RNA replicative phenomenology depends on the parameters of the system, such as the amount of available ribonucleotides, size of genetic alphabet, the strength of chemical bonds or environmental fluctuations. Our results point towards oscillatory environments as necessary requirements for the formation of efficient copies of long enough RNA sequences, in agreement with recent works in the field that suggest that fluctuating environments were necessary for life to emerge [5].

-
- [1] K. Ruiz-Mirazo, C. Briones, and A. de la Escosura, *Prebiotic systems chemistry: New perspectives for the origins of life*, *Chemical Reviews* **114**, 285-366 (2014).
 - [2] C. Briones, M. Stich, and SC. Manrubia, *The dawn of the RNA World: toward functional complexity through ligation of random RNA oligomers*, *RNA* **15**, 743749 (2009).
 - [3] W. Huang, and J.P. Ferris, *One-Step, Regioselective Synthesis of up to 50-mers of RNA Oligomers by Montmorillonite Catalysis*, *J. Am. Chem. Soc.* **128**, 89148919 (2006).
 - [4] H. Kaddour, S. Gerislioglu, P. Dalai, T. Miyoshi, C. Wesdemitis, and N. Sahai, *Nonenzymatic RNA Oligomerization at the Mineral/Water Interface: An Insight into the Adsorption/Polymerization Relationship*, *J. Phys. Chem. C* **122**, 29386-29397 (2018).
 - [5] H. Boigenzahn, and J. Yin, *Glycine to Oligoglycine via Sequential Trimetaphosphate Activation Steps in Drying Environments*, *Origins of Life and Evolution of Biospheres* **52**, 249261 (2022).

Language shift dynamics: Role of size and coupling strength of communities with different preferences

Pablo Rosillo-Rodes¹, Maxi San Miguel¹, and David Sánchez¹

¹Institute for Cross-Disciplinary Physics and Complex Systems IFISC (UIB-CSIC),
Campus Universitat de les Illes Balears, E-07122, Palma, Spain

Language shift is a multifaceted phenomenon characterised by the change from one language to another within a community. The effect is driven by a diverse array of sociolinguistic factors and constitutes a paradigmatic example of social collective phenomena. One of these key factors is language ideologies, which encompass individuals' values regarding language and its usage. In practice, ideologies exert influences on language shift through the formation of language preferences. For example, the standardisation of a language promotes overt prestige, encouraging speakers to adhere to linguistic norms. Conversely, there exists a covert prestige, which embraces a preference for socially perceived lower forms due to cultural attachment or group identity [1]. Our aim is to investigate the effects of both preference and prestige in the dynamics of language shift.

Our work [2] extends previous research [3, 4] on binary agent communities with diverse states. Let X and Y , respectively, be two possible languages or varieties. We label with 1 the speakers that prefer X and with 2 the speakers that prefer Y . Therefore, our model considers the proportion of individuals x_1, x_2, y_1 , and y_2 as sketched in Fig. 1. The transition rates for variety adoption incorporate the influence of surrounding individuals, including the prestige associated with each variety (s_1 and s_2). Notably, the agents possess an internal fixed preference determined by their language ideologies: $\alpha = x_1 + y_1$. Further, since covert and overt prestiges are generally not the same, we take $s_2 < s_1$, where s_1 (s_2) is for the standard (vernacular) variety.

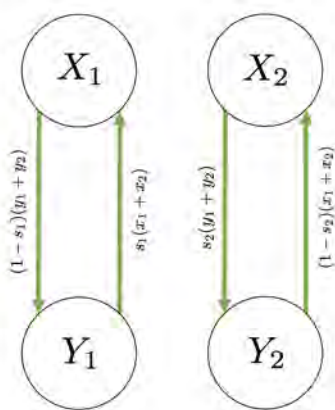


Fig. 1. Four groups of speakers differentiated by the spoken variety (X , standard, or Y , vernacular) and their internal preference (1: standard variety and 2: vernacular variety). Language shift is described with four transition rates. The proportion of speakers of each group is represented in lowercase x or y .

Additionally, we consider coupling between communities

with different preferences. We define γ as the proportion of active links between different communities. We find several phase transitions (see Fig. 2) and compute the sets of parameters which allow for them to exist. The coupling of communities can drive the system from coexistence to standard dominance, going through vernacular dominance and coexistence. Finite-size fluctuations take the system to an absorbing state of dominance of one of the varieties in a survival time that scales exponentially with system size.

Our approach to examining language shift in relation to language ideologies not only finds the role of the preference of the speakers as a counterforce to the prestige of the languages but also reveals the coupling between different communities as a key feature in the study of the different phases of coexistence or dominance.

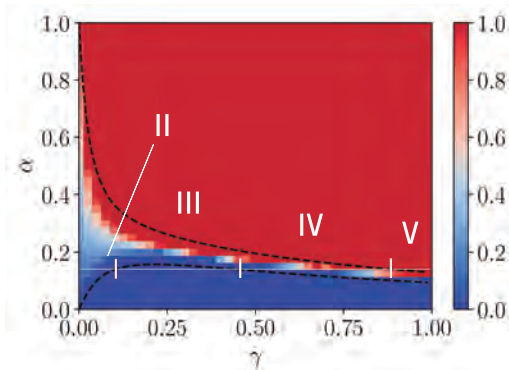


Fig. 2. Analytical and simulated phase diagrams in the parameter space α - γ for $s_1 = 0.58$ and $s_2 = 0.51$. The colour plot refers to the value of the unique steady state for the total proportion of standard speakers. Depending on the parameter configuration we may find several phase transitions. For example, for $\alpha = 0.15$ we find five different phases: I) no coupling (a vertical line for $\gamma = 0$), II) coexistence, III) vernacular dominance, IV) coexistence and V) standard dominance.

-
- [1] W. Labov. *Sociolinguistic Patterns*, Philadelphia: University of Pennsylvania Press, 1972.
- [2] P. Rosillo-Rodes, D. Sánchez and M. San Miguel, *Modelling language ideologies for languages in contact*, in preparation, 2023.
- [3] X. Castelló, V. M. Eguíluz, and M. San Miguel, *Ordering dynamics with two non-excluding options: bilingualism in language competition*, *New Journal of Physics* **8**, 308-322 (2006).
- [4] A. Carro, R. Toral, and M. San Miguel, *Coupled dynamics of node and link states in complex networks: A model for language competition*, *New Journal of Physics* **18**, 113056 (2016).

Diffusion and Release of Cargo from Collapsed Microgels: A Theoretical Framework

Adri Escañuela-Copado¹, José López-Molina¹, Matej Kanduč², Arturo Moncho-Jordá^{1,3} and Irene Adroher-Benítez¹

¹Biocolloid and Fluid Physics Group, University of Granada, 18071 Granada, Spain

²Jožef Stefan Institute, SI-1000 Ljubljana, Slovenia

³Institute Carlos I for Theoretical and Computational Physics, 18071 Granada, Spain

Microgels are soft colloidal particles made of crosslinked polymer networks suspended in a liquid. Their size can be controlled by adjusting various factors, such as temperature. When the temperature of the liquid decreases, the polymer chains interact to increase their separation. The free volume inside each particle allows the microgels to absorb molecules. When the temperature rises, the polymers shrink, trapping the absorbed molecules in a dense mesh. This mesh enables the slow and controlled diffusion of the cargo molecules.

Previous studies have proposed a theoretical model that successfully predicts the molecule release kinetics of hollow microgels, as demonstrated in both simulations and experiments [1, 2]. However, this model fails to capture the behavior observed in dense homogeneous distributions of polymers. In this work, we aim to develop a theoretical framework that accurately describes the release of cargo from collapsed microgels. Diffusion through a dense polymer network has been shown to exhibit a different behavior from what is expected at lower polymer concentrations. The former process is governed by fluctuations happening in the microgel structure, while the latter is described by singular events of limited obstruction. This difference is the main reason for the discrepancy observed between the two scenarios [3].

In collapsed microgels, the spherical symmetry and high network density neutralize cargo-monomer interactions, except at the interface. This interface sets the boundary for the quasi-constant potential barrier, thereby making interactions crucial in determining the release time. The high concentration of polymers in collapsed microgels significantly restricts the movement of the cargo, leading to preferred diffusion directions dictated by the cargo's geometry. This situation has a notable effect over the diffusion coefficient and the depth of the potential barrier.

In this study, we have employed dynamical density functional theory (DDFT) to generate numerical results of the mean passage time for both repulsive and attractive microgels. This technique has been proven successful in previous works [1, 2]. These results have been accurately replicated by an analytic model, confirming the validity of our theoretical framework. Consequently, this work provides a robust and practical method for predicting the mean release time of anisotropic cargo from collapsed microgels.

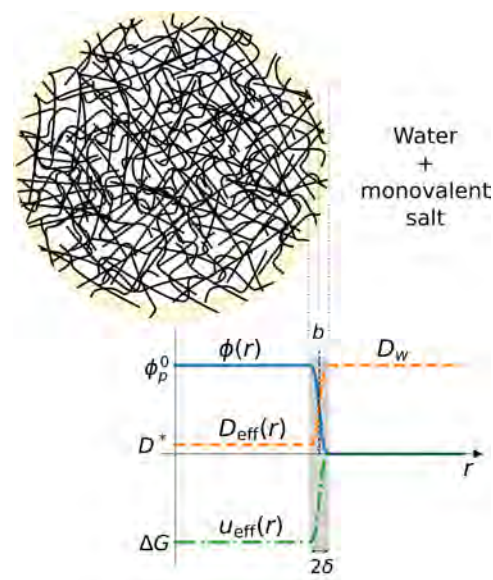


Fig. 1. Model of a collapsed microgel used in this study. The radius of the particle is denoted by b , and the interface width is 2δ . Three important system functions are illustrated: $\phi(r)$, representing the polymer packing fraction within the microgel; $D_{\text{eff}}(r)$, depicting the molecule effective diffusion coefficient which varies from D^* inside the microgel to D_w in bulk; and $u_{\text{eff}}(r)$, the effective microgel-molecule interaction, which assumes the value ΔG at the center of the colloidal particle.

-
- [1] A. Moncho-Jordá, A. Germán-Bellod, S. Angioletti-Uberti, I. Adroher-Benítez, J. Dzubiella, *Nonequilibrium Uptake Kinetics of Molecular Cargo into Hollow Hydrogels Tuned by Electrosteric Interactions*, ACS Nano **13**, 1603 (2019).
- [2] A. Moncho-Jordá, A. B. Jódar-Reyes, M. Kanduč, A. Germán-Bellod, J. M. López-Romero, R. Contreras-Cáceres, F. Sarabia, M. García-Castro, H. A. Pérez-Ramírez, G. Odriozola, *Scaling Laws in the Diffusive Release of Neutral Cargo from Hollow Hydrogel Nanoparticles: Pacilataxel-Loaded Poly(4-vinylpyridine)*, ACS Nano **14**, 15227 (2020).
- [3] M. Kanduč, W. K. Kim, R. Roa, J. Dzubiella, *How the Shape and Chemistry of Molecular Penetrants Control Responsive Hydrogel Permeability*, ACS Nano **15**, 614 (2021).

Modelling the behaviour of functional nanoparticles in polymer melts by Molecular Dynamics simulation

Adri Escañuela-Copado¹, J. Javier Burgos-Mármol² and Alessandro Patti^{1,3}

¹Department of Applied Physics, The University of Granada, Av. Fuentenueva s/n, 18071 Granada, Spain

²Institute of Systems, Molecular and Integrative Biology, Crown Street, Liverpool L69 7BE, University of Liverpool, UK

³Department of Chemical Engineering, The University of Manchester, Booth St East, Manchester M13 9PL, UK

Polymers hosting nanoparticles (NPs), referred to as polymer nanocomposites (PNCs), are paving the path for next-generation smart nanomaterials to meet the demand of upcoming technologies that are expected to be of remarkable industrial and societal benefit. PNCs are hybrid materials comprising a polymer matrix that hosts organic or inorganic NPs. The incorporation of NPs, usually between 1 and 5 wt%, allows one to improve the macroscopic response of a polymer, including its thermal and mechanical resistance and viscoelastic behaviour. However, formulating PNCs that are more suitable to target applications than their engendering polymers is not trivial as it depends on an intricate network of correlated factors that pivot around the interactions established at the polymer/NP interface.

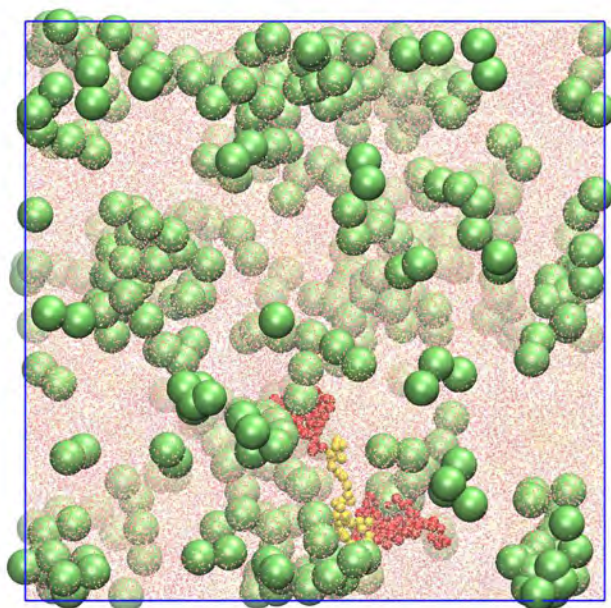


Fig. 1. Initial configuration of 800 chains of a triblock copolymer incorporating 215 nanodimers at 298 K. Blocks of type A and B are respectively shown in red and yellow, while nanodimers in light green. For clarity, only one polymer chain and nanodimers are magnified, while all other chains are point-like.

In this work, we present recent molecular simulation results that try to clarify the role of some of these factors and how they can be employed to control the behaviour of NPs and polymer chains at the small scale and influence the PNCs response at the macroscopic scale [1, 2, 3, 4]. Starting from simple models, where NPs are represented as soft spheres, we will show how manipulating the NP surface chemistry and shape anisotropy, one can better control their distribution and orientation in the polymer matrix. We will discuss how coupling NPs' functionalisation to an accurate choice of the polymer architecture can provide a powerful tool to fine-tune the material properties, including its viscosity. Finally, we will see how the use of block copolymers, able to self-assemble into ordered mesophases, offers an opportunity to drive the arrangement of functional NPs into precise nanodomains, where specific functions can be activated.

Acknowledgments A. E.-C. and A. P. acknowledge financial support from the U. S. Army Research Office under grant agreement 80692-CH-INT.

-
- [1] A. Patti, *Molecular Dynamics of Spherical Nanoparticles in Dense Polymer Melts*, J. Phys. Chem. B **118**, pp. 3731–3742 (2014).
- [2] J. J. Burgos-Mármol and A. Patti, *Unveiling the impact of nanoparticle size dispersity on the behavior of polymer nanocomposites*, Polymer, **113**, pp. 92–104 (2017).
- [3] J. J. Burgos-Mármol, Ó. Álvarez-Machancoses and A. Patti, *Modeling the Effect of Polymer Chain Stiffness on the Behavior of Polymer Nanocomposites*, J. Phys. Chem. B, **121**, pp. 6245–6256 (2017).
- [4] J. J. Burgos-Mármol and A. Patti, *Molecular Dynamics of Janus Nanodimers Dispersed in Lamellar Phases of a Block Copolymer*, Polymers, **13**, pp. 1524–1539 (2021).

Tuning the depletion forces among colloidal particles using external magnetic fields

Joan J. Cerdà¹, Josep Batle², Carles Bona-Casas¹, Joan Massó¹, Tomàs Sintes³

¹ Departament de Física UIB i Institut d'Aplicacions Computacionals de Codi Comunitari (IAC3),
Campus UIB, 07122 Palma de Mallorca, Spain.

² Centre de Recerca Independent, Sa Pobla, Mallorca

³ Dpt. de Física UIB i Instituto de Física Interdisciplinar y Sistemas Complejos (IFISC),
Campus UIB, E-07122 Palma de Mallorca

Using Langevin Dynamics simulations the pair-depletion interactions between two non-magnetic soft colloidal particles immersed in a suspension of magnetic colloidal polymers have been studied. We have focused on systems corresponding to quasi-two dimensional geometries which are representative of interfaces between two fluids. The depletion force profiles obtained are observed to present magnetic field modulable regions of attraction and repulsion leading in some cases to the existence of stable points, i.e. local potential wells. It is observed that the use of an external magnetic field allows to shift the location of those regions

and enhance the attractive and repulsive regimes observed in the depletion profiles, as well as the number of stable points present in the force profiles. Our results show that these interfaces have the potential for allowing to control the distance between the two non-magnetic colloidal particles, which is a step forward to the creation of magnetic colloidal tweezers.

[1] J.J. Cerd, J. Batle, C. Bona-Casas, T. Sintes, J. Mass, Colloidal depletion interactions at interfaces induced by magnetic colloidal polymers, (submitted).

The following network of Olympic athletes

Jorge P. Rodríguez^{1,2}, and Lluís Arola-Fernández²

¹CA UNED Illes Balears, Universidad Nacional de Educación a Distancia, Palma, Spain

²Instituto de Física Interdisciplinar y Sistemas Complejos (IFISC), CSIC-UIB, Palma, Spain

Professional sport is an activity that enhances social interaction among the athletes through meetings such as training groups, large-scale competitions and sponsored events. Within these, the Olympic games represent the largest international competition, having a unique global impact. This event is assumed to promote international cooperation through the values of sport, becoming an opportunity for creating global connections between athletes.

Here we want to understand the properties of the following activity, an indicator of the information flows, between highly successful Olympic athletes both at microscopic and macroscopic scales. Thus, we built a database including the Twitter usernames of Olympic medalists in Tokyo 2020, using it for creating the follower-followee network, a directed network representing who is following whom in this social network. From our database of 1061 athletes, we found 7326 connections between 964 athletes. The most popular athletes, those with highest in-degree (*i.e.*, number of followers), were Kevin Durant (basketball, USA), Allyson Felix (athletics, USA), Teddy Riner (judo, France), Alex Morgan (football, USA) and Simone Biles (gymnastics, USA). The macro-scale network structure displayed organized patterns by sports and countries and microscopic –node– properties showed a higher activity among female athletes, with a strong sex assortativity. We quantified these properties comparing them with randomly expected values keeping fixed either the in- and out- degrees or the group sizes, revealing the underlying assortativity patterns (Fig. 1). Finally, we performed a link prediction task, quantifying the importance of follower and followee’s metadata to predict the existence of a link between any two athletes.

Our network describes the following activity, which captures the interest of athletes besides real acquaintance or friendship, as well as it shows the information flows, which

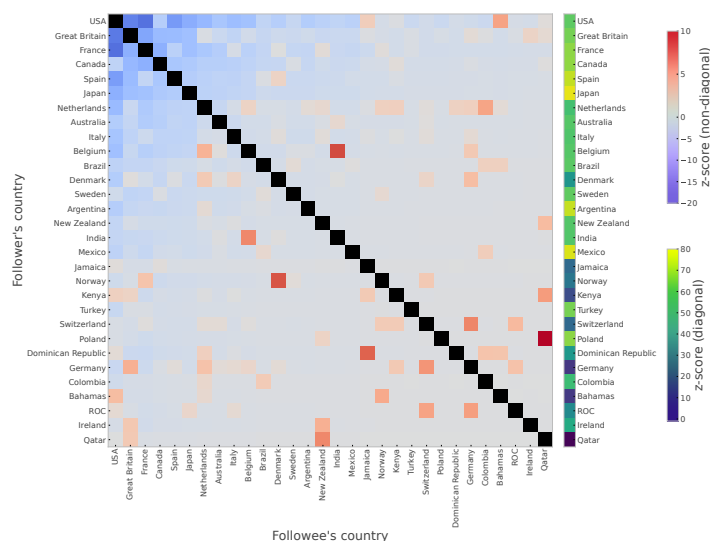


Fig. 1. Normalized following patterns among the top-30 Olympic countries with highest in-degree. Colors represent the z-score obtained comparing the observed number of following links from i to j , E_{ij}^o , with the statistics of 10^4 shufflings of the athlete’s networks keeping the in- and out-degrees, average links E_{ij}^s and standard deviation σ_{ij}^s , leading to $z_{ij} = \frac{E_{ij}^o - E_{ij}^s}{\sigma_{ij}^s}$. The diagonal interactions have a different scale, so they are represented in the lateral bar.

can be crucial for the inference of influential spreaders. We suggest that datasets built thanks to the high public exposure of the professional sport community can serve as a proxy to investigate interesting aspects of many complex socio-cultural systems at different scales.

Inferring the connectivity of coupled oscillators from sequences of intervals between events

R. P. Aristides¹, G. Tirabassi², H. Cerdeira¹ and C. Masoller²,

¹Instituto de Física Teórica, Universidade Estadual Paulista, São Paulo, Brazil

²Departament de Física, Universitat Politècnica de Catalunya, Terrassa, Spain

The Kalman filter is a well-known technique to infer the parameters of a model given uncertain observations. We have recently used a nonlinear version, the unscented Kalman filter (UKF), to infer the connectivity of a small network of coupled Izhikevich neurons [1], where the links between neurons were given in terms of an adjacency matrix, A_{ij} , and their intensity was controlled by a global coupling parameter, K . Assuming that we had full information about the temporal dynamics of the different neurons [i.e., the time series $x_i(t)$ and $y_i(t)$ obtained by simulating the Izhikevich model], we have shown that UKF allows to infer the structural connectivity, i.e., to recover the matrix KA_{ij} , even if the network is directed and evolves in time.

However, usually we do not have full information of the neurons' variables, as we can only detect the spikes. Therefore, here we assume that for each neuron i , we only know the sequence of time intervals between spikes, $\{\Delta T_i(1), \Delta T_i(2), \dots\}$ (obtained by simulating coupled Izhikevich neurons, as in [1]). Then, a natural question is, can we infer the network connectivity, i.e., the matrix KA_{ij} , from the analysis of the N spike sequences of the N neurons?

To address this problem, we first obtain, from each sequence, $\{\Delta T_i(1), \Delta T_i(2), \dots\}$, a continuous instantaneous phase, $\phi_i(t)$, by simply assuming that $\phi_i(t)$ increases linearly between 0 and 2π in each ISI (Fig. 1).

Then, we use the UKF to fit the set of N phases time series, $\{\phi_1(t) \dots \phi_N(t)\}$, to N Kuramoto phase oscillators,

$$\dot{\phi}_i = \omega_i + \sum_j m_{i,j} \sin(\phi_j - \phi_i) + \sigma \xi_i. \quad (1)$$

The last step to recover the adjacency matrix is to apply a clustering algorithm (k-means) and transform the set of $m_{i,j}$ values into a set of 0s and 1s, which are the coefficients of the recovered adjacency matrix (Fig. 2, top panel).

To evaluate the performance of the UKF approach we use the F_1 score [$F_1 = 2TP/(2TP + FN + FP)$, where TP is the number of true positives, FP , the number of false positives and FN , the number of false negatives]. We find that UKF performance is maximized for intermediate coupling strength (Fig. 2, bottom panel).

A natural next step is to test the performance of the UKF method on experimental data. We therefore used data freely available recorded from 28 electronic chaotic oscillators [2] and addressed the challenge of inferring the connectivity of sets of 3 oscillators (i.e., classify the 3 possible links as existing or nonexisting). We used the Hilbert transform to obtain the time series of the instantaneous phase of each oscillator, and finally, used UKF to fit the evolution of the phases to the Kuramoto model. Preliminary results (not shown) suggest that UKF is able to differentiate between existing and nonexisting links, in spite of the fact that the 3 oscillators are linked to other, unobserved oscillators. Ongoing efforts are devoted to develop efficient methods for inferring the

connectivity of larger sets of oscillators, and to compare the performance of UKF with other well-known methods for inferring the network connectivity (cross-correlation, mutual information, etc.)

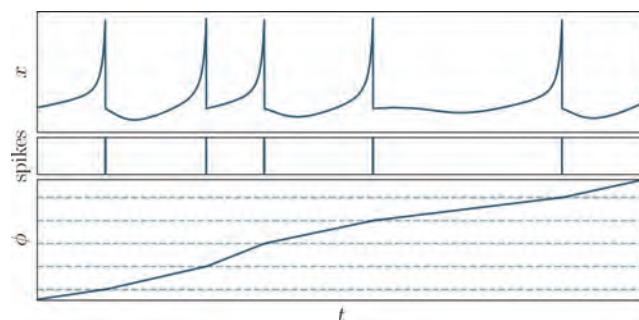


Fig. 1. (top) Simulated spike sequence, (middle) only the spike times are analyzed, (bottom) from the spike times, the time series of the instantaneous phase is obtained.

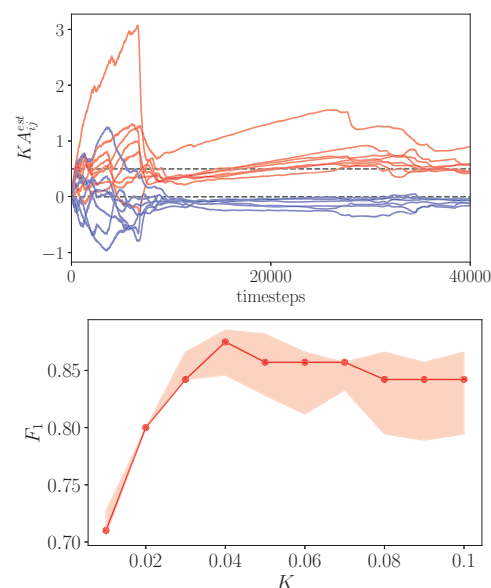


Fig. 2. (top) Estimation of the coupling coefficients. (bottom) Performance of UKF for inferring the connectivity of a network of Izhikevich neurons measured with F_1 score (15 networks were simulated, each with 6 neurons and 8 links, for each network, F_1 was averaged over 100 simulations).

[1] R. P. Aristides et al., *Parameter and coupling estimation in small groups of Izhikevichs neurons*, *Chaos* **33**, 043123 (2023).

[2] R. Sevilla-Escoboza and J. M. Buldu, *Synchronization of networks of chaotic oscillators: Structural and dynamical datasets*, *Data in Brief* **7**, 1185 (2016). Session Poster 2, p2.10

Characterizing social information spreading by using event-synchronization and causality measures

Lucio Garcia¹, Giulio Tirabassi², Cristina Masoller², and Pablo Balenzuela¹

¹Departamento de Física, Universidad de Buenos Aires, Argentina

²Departament de Física, Universitat Politècnica de Catalunya, Terrassa, Spain

Understanding the diffusion of information is a fundamental challenge of complexity science. Here we analyze 28000 news articles published in Argentina in the period 26/05/2022 - 26/09/2022 in six main cities, and classify them in 20 non-orthogonal topics (Fig. 1). Then, we obtain a time series for each topic, $n = 1, \dots, 20$, in each city, $i = 1, \dots, 6$, by adding the number of articles per day.

Next, we use two causality measures, Granger causality, GC, and pseudo Transfer Entropy, pTE [2] to study how the information about a topic that appears in the local press in one city, spreads to news articles published in other cities. GC and pTE, however, have the drawback that assume stationarity. Therefore, we also use event synchronization measures, Q_s and Q_a , as proposed in [3]. To calculate Q_s and Q_a we count the number of events, c_{ij} , that occur in one time series, j , after an event occurred in a time series i , allowing for a lag of up to 3 days. The events are detected by using two thresholds, one to detect when media attention grows above a certain value, and another, to detect when media attention decays, and then, a different event may occur latter. These thresholds are defined in terms of the relative importance of a topic.



Fig. 1. Unsupervised distribution of articles in 20 topics.

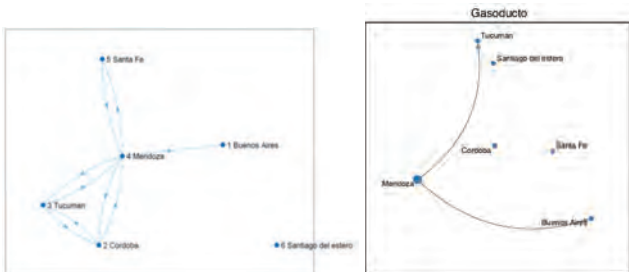


Fig. 2. Links obtained for topic *Gasoducto* from (left) event synchronization measures and (right) causality measures.

Finally, the process of information spreading is represented as a multiplex network, in which the different topics represent the layers, the six cities in Argentina represent the nodes, and the links are defined by thresholding the values of (GC and pTE) or (Q_s and Q_a). Figure 2 shows, as an example, the links obtained for topic *Gasoducto*, and Fig. 3 displays the corresponding time series.

Figure 4 displays the causal layers obtained from the 20

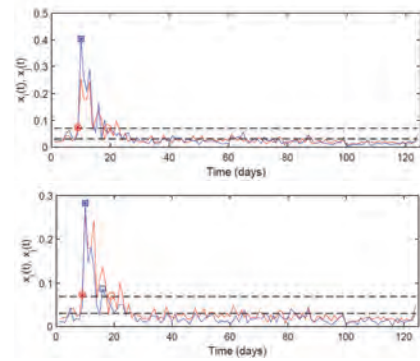


Fig. 3. Examples of time series obtained for topic *Gasoducto*. Top: Mendoza (red) and Buenos Aires (blue); Bottom: Mendoza (red) and Tucuman (blue). Empty (solid) symbols indicate not-synchronized (synchronized) events.

topics analyzed. In this talk/poster, the results obtained with different event-detection criteria and with different synchronization/causality measures will be compared and discussed.

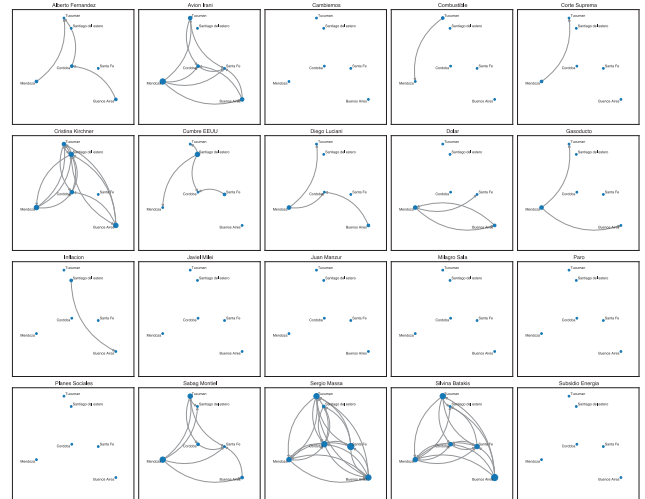


Fig. 4. Layers obtained by thresholding the values of GC and pTE . Some layers do not have links, which also happens when thresholding Q_s and Q_a .

[1] S. Pinto et al., *Quantifying time-dependent Media Agenda and public opinion by topic modeling*, *Physica A* **524**, 614 (2019).

[2] R. Silini and C. Masoller, *Fast and effective pseudo transfer entropy for bivariate data-driven causal inference*, *Sci. Rep.* **11**, 8423 (2021).

[3] R. Quian Quiroga, T. Kreuz, and P. Grassberger, *Event synchronization: A simple and fast method to measure synchronicity and time delay patterns*, *Phys. Rev. E* **66**, 041904 (2002).

Topological Defects in the Non-Reciprocal XY Model

Ylann Rouzairé^{1,2,3} and Demian Levis^{1,2} and Ignacio Pagonabarraga^{1,2,3}

¹ Departament de Física de la Materia Condensada, Universitat de Barcelona, Martí i Franques 1, E08028 Barcelona, Spain

²UBICS University of Barcelona Institute of Complex Systems, Martí i Franques 1, E08028 Barcelona, Spain

³CECAM, Centre Européen de Calcul Atomique et Moléculaire, Ecole Polytechnique Fédérale de Lausanne (EPFL), Lausanne, Switzerland

Non-reciprocal interactions are fundamental for crowd dynamics and animal flocking collective phenomena, where limited vision cones result in influences that are not necessarily mutual. To study the consequences of non-reciprocity, in particular on topological defects, we propose a new generic framework based on the 2D XY model.

At equilibrium, the actual shape of a defect (whether it is a source, a sink or a vortex for instance) is rather irrelevant as its charge q alone faithfully describes its behaviour. Here, we demonstrate that for a system with non-reciprocal interactions, the shape μ of a defect becomes crucial for its dynamics in the xy -plane. While in the critical phase of XY Model, pairs of defects always attract, defects in the non-reciprocal XY model exhibit shape-dependent complex motion patterns, including rapid annihilation or prolonged stabilization, challenging the Kosterlitz-Thouless scenario and paving the way to a refined control on topological structures.

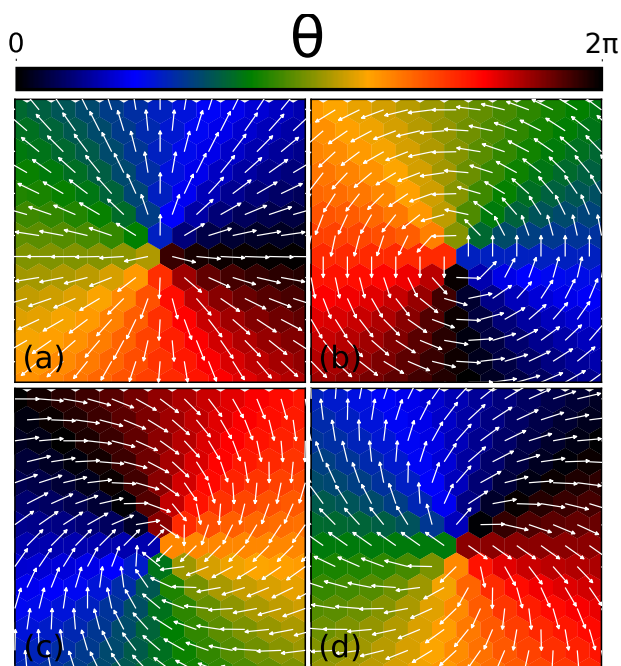


Fig. 1. Four defects with identical $q = +1$ topological charge but with different shapes $\mu_+ = 0, \pi/2, 4, 5.6$ from (a) to (d).

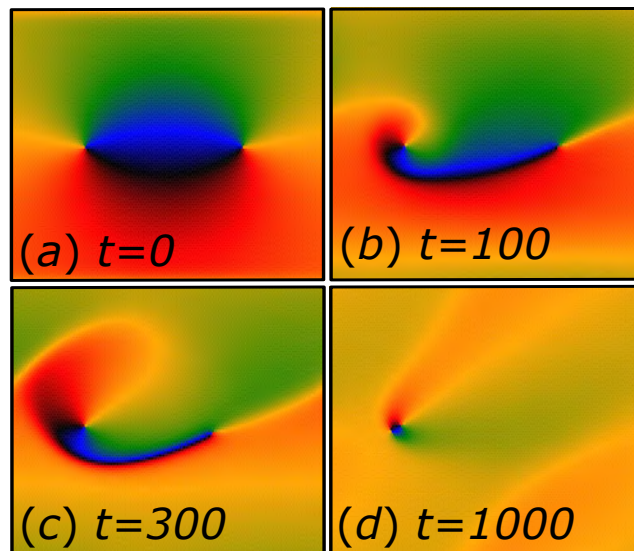


Fig. 2. Some shape combinations lead to new defect pair interactions, far from the classical XY scenario. Here four snapshots over time of a 200×200 spin system. Same cyclic colorcode as in Fig. 1 for the phase θ of individual spins.

Sampling rare trajectories in stochastic processes

Sara Oliver¹, Javier Aguilar¹, Tobias Galla¹, and Raúl Toral¹

¹Instituto de Física Interdisciplinar y Sistemas Complejos IFISC (CSIC-UIB), Palma, Spain

Despite their infrequent occurrence, rare events in stochastic processes can lead to the most catastrophic outcomes. Examples where an unlikely combination of events with a large impact occurs include natural disasters such as earthquakes or volcanic eruptions, stock market crashes, fade-outs of epidemics and species extinctions. Much interest has recently been focused on the sampling of rare trajectories and the quantification of their statistics in models of stochastic phenomena. This problem is computationally demanding if conventional sampling methods are used, so specific rare-trajectory sampling techniques must be developed to deal with it.

The renowned Wentzel-Kramers-Brillouin (WKB) method constitutes a tool to characterise most likely paths describing rare events, but it is only valid in the limit of small noise. A recently proposed backtracking sampling method that overcomes this limitation consists of working with so-called stochastic bridges, which are trajectories that are constrained to have fixed start and end points. The novelty of this method is that stochastic bridges are generated backwards in time [1]. The aim of our work is to employ the backtracking method to sample rare trajectories in stochastic models belonging to a wide variety of disciplines. We are specially interested in the study of problems with absorbing states, from which the system cannot escape once it reaches them.

To illustrate the power of the backtracking method, let us focus on the escape of a Brownian particle from the potential $U(x) = (x^2 - 1)^2/4$, which has two minima at $x = \pm 1$ separated by a barrier of height $1/4$. The deterministic dynamics of the particle is governed by:

$$\frac{dx(t)}{dt} = -\frac{\partial U(x)}{\partial x}. \quad (1)$$

This system has three fixed points: the wells $x = \pm 1$ (attracting) and the origin (repelling). Transitions of the particle from one well to the other passing through the intermediate repelling point $x = 0$ are forbidden in the deterministic limit, but become possible if stochasticity is taken into account. In such case, the mean time required for the particle to escape from one well increases exponentially with the inverse noise strength of the system. For small noise amplitudes D it is therefore difficult to observe escape paths from one well to the other in direct simulations of the stochastic process. Figure 1 shows a set of stochastic bridges, constructed using the backtracking method, representing such rare trajectories. On the other hand, the WKB formalism is incapable of describing the most likely path connecting the two wells, but only characterises the optimal transition path from one well to the repelling state $x = 0$, as can be seen in Figure 2. This figure also shows a set of stochastic bridges at finite noise amplitude, which fluctuate around the WKB most probable path valid in the small-noise limit.

Our current research focuses on further exploiting the

backtracking method, which we propose as a simpler and more comprehensive method for the sampling of rare trajectories to those already existing in the literature. On the other hand, we are exploring the backtracking method as a technique to study the influence of the nature of the noise on the transition paths between different states in rare events. In particular, we want to determine whether quantities such as jump times between states or path fluctuations are affected by the type of noise considered.

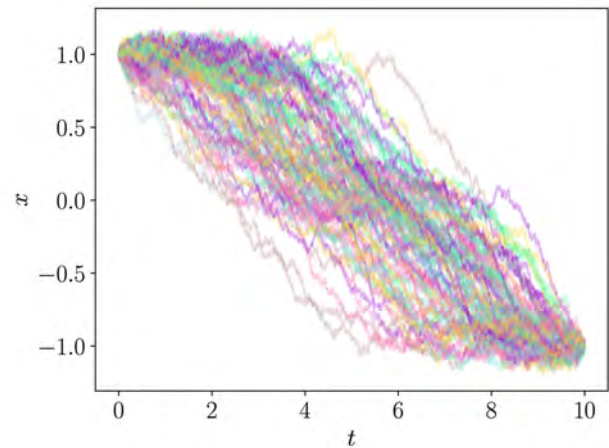


Fig. 1. Sample of 100 transition paths from one well to the other of a Brownian particle moving in a quartic double-well potential.

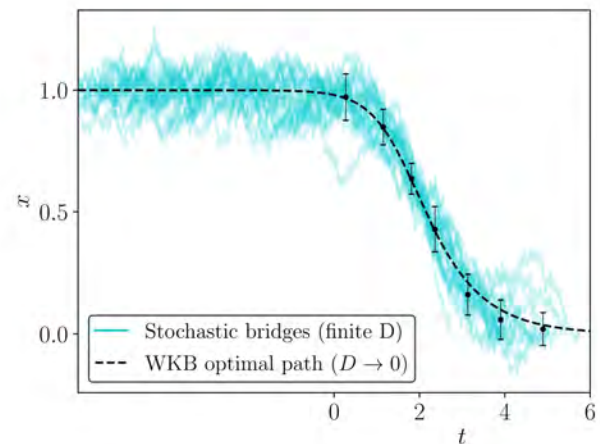


Fig. 2. WKB most likely transition path from one well to the origin, valid at the small-noise limit, together with a set of stochastic bridges at finite noise amplitude.

A spectrum of complexity uncovers Dunbar's number and other leaps in social structure

Martín Saavedra^{1,2}, Jorge Mira³, Alberto P Muñuzuri^{1,2} and Luís F Seoane^{4,5}

¹Group of Nonlinear Physics. Universidade de Santiago de Compostela, 15782, Santiago de Compostela, Spain.

²Galician Center for Mathematical Research and Technology (CITMAGA), 15782 Santiago de Compostela, Spain

³Departamento de Física Aplicada and iMATUS, Universidade de Santiago de Compostela, 15782, Santiago de Compostela, Spain.

⁴Systems Biology Department, Spanish National Center for Biotechnology (CSIC), C/ Darwin 3, 28049 Madrid, Spain.

⁵Grupo Interdisciplinar de Sistemas Complejos (GISC), Madrid, Spain.

How do societies become more complex? Are there specific scales at which they are reorganized into emergent entities? Social dynamics are shaped by each person's actions, as well as by collective trends that emerge when individuals are brought together. Features like population size, polarization, cohesion, or hierarchy add nuance and complexity to social structure, and might be present, or not, for societies of different sizes. Here we show that, while societal complexity increases monotonically with population, there are specific scales at which complexity builds up faster, one of them, similar to Dunbar's number (an estimation of the number of meaningful relationships that individuals can sustain). We have observed this by measuring, as a probe across populations of varied sizes, the sociolinguistic process that has unfolded over decades within the Spanish region of Galicia. For this, we have developed a methodological tool (social complexity spectrum, Fig 1), inspired by theoretical considerations about dynamics on complex networks, that could be applied in further study cases.

In this paper, published in *Chaos, Solitons and Fractals* [1] we have put forward the *social complexity spectrum*, a computational tool to study how certain social dynamics change as a function of the size of the interaction network within which they happen. One of our hypotheses is that the sociolinguistic dynamics of Galician and Castilian Spanish coexistence proceed faster when the web of interactions between speakers is simpler. Our second hypothesis is that population centers with more inhabitants foster more complex social networks. All our empirical results are consistent with what we might expect if these hypotheses hold true.

Our method quantifies how larger population centers are, indeed, on average, more complex than smaller ones. This is indicated by sustained negative correlations between the speed of the sociolinguistic dynamics and our measure of urbanity. Additionally, singular points at which correlation becomes saliently more negative suggest prominent population sizes at which social complexity builds up more rapidly.

One of these singular scales is observed when considering a linear relationship between dynamic rates and urbanity, $c \propto \alpha u$ (with $\alpha < 0$ a regression coefficient). This outstanding scale falls near the threshold of 5 000 inhabitants. Anecdotally, this is also known as Plato's number—Plato identified 5 040 as an ideal number of citizens in a Polis. Another singular scale appears when trying a power-law relationship. This prominent scale ($\hat{\theta}_u^\dagger = 183$ inhabitants, close to Dunbar's number) is the most salient one throughout all our spectrograms.

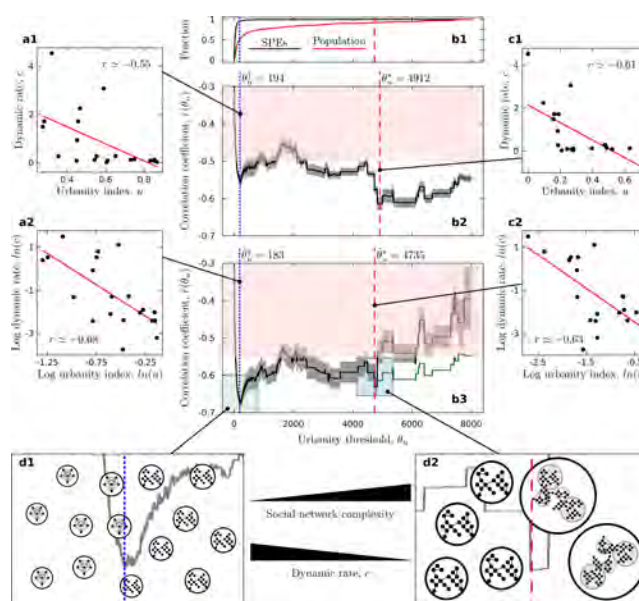


Fig. 1. Social complexity spectra. **a** Examples of correlations between urban indexes and dynamic rates, taking θ_u as the local minima in the prominent dip at low population sizes. The red plot marks the fraction of Galician population living in SPEs sized less than θ_u . This panel shows that nothing suspicious, which could trivially explain the properties of our spectra, happens at the outstanding scales (marked with vertical lines). **b2** Social complexity spectrum (black curve) assuming the straightforward, linear relationship $c \propto u$. Standard deviation of the spectrum (gray shading) was estimated by 10-fold jackknifing. **b3** Same for the logarithmic spectrum, which assumes $c \propto u^\beta$. **c** Same as in **a**, but for the spectral dip at large population size. **d** Cartoons illustrating the main implications of our hypotheses: A scale at which social complexity builds up very quickly segregates simpler from more complex social networks. Dynamics being slower in more complex networks would result in a good, negative correlation between dynamics rates within a region and that region's urbanity. We portray two distinct jumps in complexity to suggest that the social complexity buildup at around $\hat{\theta}_u^\dagger$ (**d1**) is likely very different from the one around θ_u^* (**d2**).

[1] Martín Saavedra, Jorge Mira, Alberto P. Muñuzuri and Luís F. Seoane *A spectrum of complexity uncovers Dunbar's number and other leaps in social structure*. *Chaos, Solitons & Fractals*, **170**, 113389, 2023.

Emerging collective behavior in many particles systems

Umair Rehman Raffi¹, Martin Maza-Cuello¹, and Diego Maza¹

¹Granular Media Lab.

University of Navarra, Pamplona, Spain

The flow of grains through an orifice has always been of interest due to their numerous industrial applications as hoppers and silos. The previous works have been done with only solid particles exiting the silo in a dry state [1].

This project is a natural extension of the "dry" problem to study the particles dispersion within a fluid matrix. Therefore, the starting point will be the study of the flow of particles in orifices and sizes of particles already studied in the "dry" case, but now with the existence of an interstitial fluid. In this study we are analyzing and monitoring a newer system, for clogging and jamming frequencies, in which the particles exit the silo against the flow of a liquid. This interaction of solid particles and fluids creates a complex system with their own macroscopic and microscopic behavior [2].

It has been decided to work with water as an interstitial medium due to its easy obtaining and handling. The particles used will be 1 mm aluminum balls, which will allow us to compare the results achieved with previous studies in the absence of liquid. In subsequent stages, however, it is expected to explore the role of the material using PVC balls.

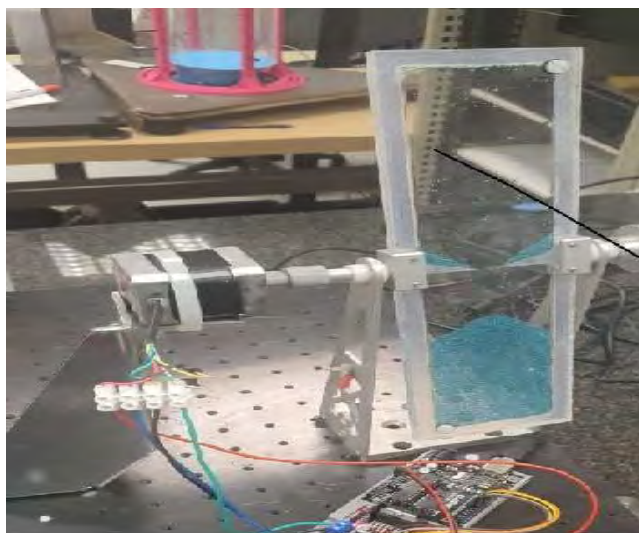


Fig. 1. Experimental setup.

Currently, in this study an automated lab scale silo has been set up with a stepping motor which is controlled by an Arduino board through MATLAB, as shown in Fig 1, and a camera is being used to capture and analyze videos of the exiting behaviors of the solid particles against the fluid. Image processing will be used to analyze the video frames and then track particles and measure velocities of the particles in this system. Also, the sedimentation rates and avalanches will be studied and measured. The major problem that currently needs solving is the elimination of bubbles as the bubbles choke the system.

25-27 de octubre de 2023, Pamplona

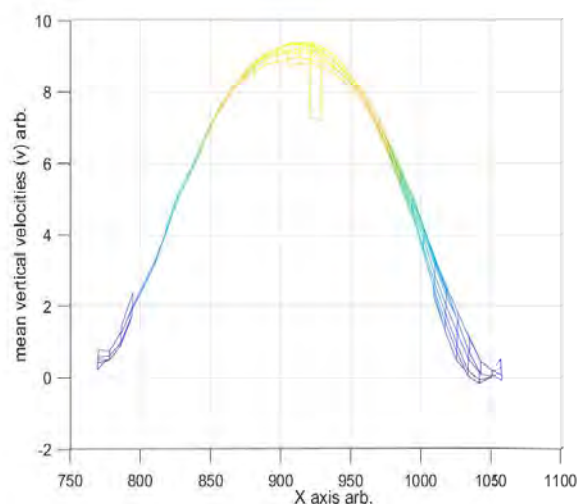


Fig. 2. Mean vertical velocity calculated using PIVLab.

In this work PIVLab (Particle Image Velocimetry) is being used to analyze the mean flow velocities at the orifice, as shown in Fig 2. The graph represents the average velocities of the particles, at the orifice, as the fluid interacts with the particles. Fig 2 shows that the system displays higher mean velocities at the center of the orifice and the lower values as we move away from the center.

Acknowledgements: The authors thanks the grant number PID2020-114839GB-I00 funded by MCIN/AEI/10.13039/501100011033 and the European Union NextGenerationEU/PRTR for the fellowship.

- [1] I. Zuriguel, D. R. Parisi, R.C. Hidalgo, C. Lozano, A. Janda, P. Gago, J.P. Peralta, I. Ferrer, I.A. Pagnaloni, E. Clment, D. Maza, I. Pagonabarraga y A. Garcimartn, clogging transition of many-particle systems flowing through bottlenecks, *Scientific reports* (2014).
- [2] N. Delouche, J.M. Van doorn, T.R. Kodger, A.B. Schofield, J. Sprakel, H. Tabuteau, the contribution of colloidal aggregates to the clogging dynamics at the pore scale, *journal of membrane science*(2021).

Modelling the phase behaviour of nematic liquid crystals by Molecular Dynamics simulation

A. Díaz Acosta¹, I. Adroher-Benítez¹, and A. Patti^{1,2}

¹Department of Applied Physics, University of Granada, Avenida Fuente Nueva s/n, 18071 Granada, Spain

²Department of Chemical Engineering, The University of Manchester, Oxford Road, Manchester M13 9PL, UK

Liquid crystals (LCs) are a fascinating state of matter with properties in between those of crystalline solids and liquids. They are employed in a wide spectrum of applications, including smart windows and lens and, especially, in displays. LCs flow like liquids, but exhibit a degree of internal order that resembles the organisation typically found in crystals. If this ordering is only orientational, nematic LCs are observed, otherwise a degree of positional ordering in one or two dimensions leads to more complex systems, such as smectic and columnar LCs. In particular, uniaxial nematics (N_U) are characterised by the presence of a single optic axes, whereas biaxial nematics (N_B) exhibit two optic axes. The N_B phase has been observed experimentally in micellar [1] and colloidal [2] systems, but its existence at the molecular scale is still debated.

Motivated by the impact that molecular N_B phases would generate on display technology and in light of our recent work on colloidal biaxial nematics [3], in this contribution we discuss the phase behaviour of a family of molecules that have been indicated as promising candidates to form N_B phases [4]. More specifically, these molecules consist of a rigid anthraquinone core decorated by four heavily substituted groups with lateral and/or terminal aliphatic chains. By employing an atomistic model and the General Amber Force Field (GAFF), we perform Molecular Dynamics simulation to map the pressure vs temperature phase diagrams of these systems and locate the order-to-disorder

phase transition. We characterise the LCs observed at equilibrium by computing positional and orientational pair correlation functions to assess the eventual presence of positional and orientational ordering, respectively. Our results indicate that, in a range of temperatures and pressures, these molecules are able to form especially aligned N_U phases, with an especially large nematic order parameter [5] and in qualitative agreement with experimental results.

-
- [1] L. J. Yu and A. Saupe, *Observation of a Biaxial Nematic Phase in Potassium Laurate-1-Decanol-Water Mixtures*, Phys. Rev. Lett. **45**, 1000 (1980).
 - [2] E. van den Pol, A. V. Petukhov, D. M. E. Thies-Weesie, D. V. Byelov, and G. J. Vroege, *Experimental Realization of Biaxial Liquid Crystals Phases in Colloidal Dispersions of Boardlike Particles*, Physical Review Letter, **103**, 258301 (2009).
 - [3] A. Cuetos, M. Dennison, A. Masters and A. Patti, *Phase behaviour of hard board-like particles*, Soft Matter, **13**, 4720 (2017).
 - [4] M. Lehmann, S. Maisch, N. Scheuring, J. Carvalho, C. Cruz, P. J. Sebastião and R. Y. Dong, *From molecular biaxiality of real board-shaped mesogens to phase biaxiality? On the hunt for the holy grail of liquid crystal science*, Soft Matter, **15**, 8496 (2019).
 - [5] P. R. ten Wolde, D. W. Oxtoby, and D. Frenkel, *Coil-globule transition in gas-liquid nucleation of polar fluids.*, Physical review letters, **81**, 3695 (1998)

Navier–Stokes transport coefficients of a granular gas of inelastic and rough Maxwell particles

A. Santos¹, and G. M. Kremer²

¹Departamento de Física and Instituto de Computación Científica Avanzada (ICCAEx),
Universidad de Extremadura, E-06006 Badajoz, Spain

²Departamento de Física, Universidade Federal do Paraná, Curitiba, Brazil

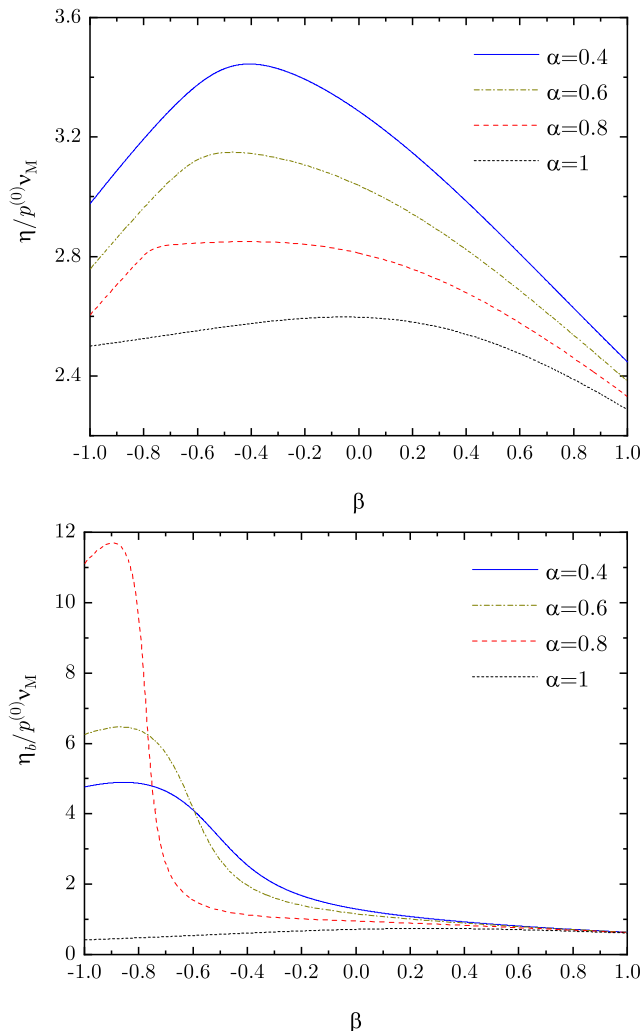


Fig. 1. Plot of the shear (η) and bulk (η_b) viscosities as functions of β for $\alpha = 0.4, 0.6, 0.8$, and 1.

The most widely used model for a granular gas is the inelastic hard-sphere model (IHSM), where the grains are as-

sumed to be perfectly smooth spheres colliding with a constant coefficient of normal restitution α [1, 2]. A much more tractable model is the inelastic Maxwell model (IMM), in which the velocity-dependent collision rate is replaced by an effective mean-field constant [3]. This simplification has been taken advantage of by many researchers in the past to find a number of exact results within the IMM. On the other hand, both the IHSM and IMM neglect the impact of roughness on the dynamic properties of a granular gas. This is remedied by the inelastic rough hard-sphere model (IRHSM), where, apart from the coefficient of normal restitution, a constant coefficient of tangential restitution β is introduced [4].

In parallel to the simplification carried out when going from the IHSM to the IMM, we have recently proposed an inelastic rough Maxwell model (IRMM), as a simplification of the IRHSM, and derived the corresponding exact expressions for the most relevant collisional moments [5]. The aim of the present work is to apply the IRMM to the derivation of the exact Navier–Stokes transport coefficients predicted by the model.

As an example, Fig. 1 shows the shear and bulk viscosities as functions of β for $\alpha = 0.4, 0.6, 0.8$, and 1. As we can see, both coefficients are nonmonotonic functions of both α and β .

-
- [1] N. V. Brilliantov, T. Pöschel, *Kinetic Theory of Granular Gases* (Oxford University Press, Oxford, 2004).
- [2] V. Garzó, *Granular Gaseous Flows. A Kinetic Theory Approach to Granular Gaseous Flows* (Springer Nature, Switzerland, 2019).
- [3] A. V. Bobylev, J. A. Carrillo, and I. M. Gamba, *J. Stat. Phys.* **98**, 743–773 (2000).
- [4] J. T. Jenkins and M. W. Richman, *Phys. Fluids* **28**, 3485–3494 (1985).
- [5] G. M. Kremer and A. Santos, *J. Stat. Phys.* **189**, 23, pp. 1–24 (2022).

A journey through ecosystems: the complexity of interaction networks in the gut microbiome

Adrián Aguirre-Tamaral¹, Sandra Ferreiro¹, and Jaime Iranzo¹

¹Centro de Biotecnología y Genómica de Plantas (CBGP, UPM-INIA)

Microbial communities, known as microbiomes, are everywhere in nature: in the environment, in our food and even in our bodies. They play an important role in ecosystems and also influence our health. Understanding the physical and chemical interaction network of microbiomes under different conditions is therefore a key objective for academic and medical reasons.

A perfect example is the human gut microbiome, as the intricate competitive and cooperative interactions between its microbial inhabitants play a crucial role in maintaining host health (Fig. 1, A). Indeed, several studies have correlated alterations of the gut microbiome (dysbiosis) with diseases such as inflammatory bowel diseases (e.g. Crohn's disease), colorectal cancer or type 2 diabetes [1, 2]. However, the causes underlying sudden changes in microbiome composition under pathological conditions still have several open questions, such as the effect of microbial order of cooperation on health.

Consequently, to better understand the intestinal cooperative network in different environments and pathological conditions, we reconstructed metabolic models from a longitudinal study of the human intestinal microbiome in patients with inflammatory bowel disease (HMP2, [3]), incorporating the diverse metabolic capabilities of individual species and simulating their potential interactions. Finally, we used flux balance analysis to compute the cooperation of reconstructed and curated [4, 5] metabolic models of microbial communities.

Our results indicate that there is a remarkable prevalence of cooperative interactions of higher order than two, which are also essential in certain environments (Fig. 1, B). These results provide insights into the composition of the microbiome in different media and contribute to a deeper understanding between health and microbial interactions in the gut ecosystem.

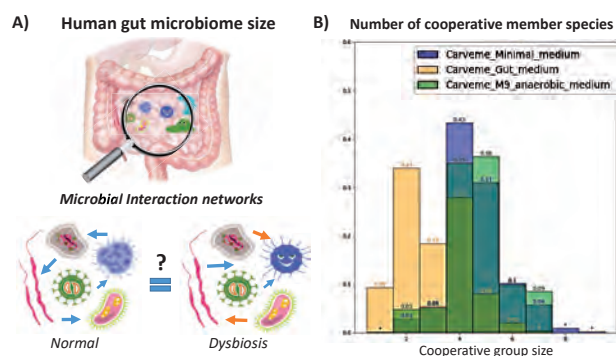


Fig. 1. The human gut microbiome: A) Schematic view of the microbial interaction networks under normal and dysbiosis conditions. B) Size of the cooperative community in different environments.

-
- [1] J. Sung, et. al, *Global metabolic interaction network of the human gut microbiota for context-specific community-scale analysis*, Nature **8**, 15393 (2016).
- [2] J. Lloyd-Price, et. al, *Multi-omics of the gut microbial ecosystem in inflammatory bowel diseases*, Nat. Commun. **569**, 655662 (2019).
- [3] <http://ibdmdb.org/>
- [4] S. Magnsdottir, et. al, *Generation of genome-scale metabolic reconstructions for 773 members of the human gut microbiota*, Nat. Biotech. **35**, 8189 (2017).
- [5] T. Blasco, et. al, *An extended reconstruction of human gut microbiota metabolism of dietary compounds*, Nat. Commun. **12**, 4728 (2021).

Shaping coral reef growth. The role of nutrient diffusion and erosion

Tomás Sintés¹, and Eva Llabrés¹

¹ Instituto de Física Interdisciplinar y Sistemas Complejos, IFISC (UIB-CSIC).
Campus Universitat de les Illes Balears, 07122 Palma de Mallorca.

Coral reefs are some of the most biodiverse and productive ecosystems in the world, providing habitats for a vast array of marine species and supporting the livelihoods of millions of people [1]. However, coral reefs are facing increasing threats from climate change, pollution, and overfishing [2]. Understanding how these ecosystems grow and function is crucial for effective conservation efforts.

One key aspect of coral reef ecosystems is their spatial patterns, which can provide important insights into how these ecosystems form and persist [3]. Remote sensing data and satellite imagery have revealed that coral reefs often exhibit distinct patterns in their morphology, such as the arrangement of coral colonies and the formation of reef structures [4]. These patterns can reflect a combination of biological and physical processes, including water flow, nutrient availability, and competition among coral colonies and reefs [3].

To better understand the mechanisms underlying coral reef pattern formation, a range of theoretical and numerical models based on reaction diffusion equations have been used to explore the roles of competition, predation, and other ecological factors in shaping coral reef communities [5]. Other models have focused on the physical processes that influence reef growth, such as hydrodynamics and sediment transport [6]. However, many of these models have limitations in terms of their ability to capture the

complexity of coral reef ecosystems. While some of them overlook the importance of specific ecological interactions or physical processes, others are overly simplified, ignoring the heterogeneity of coral reef habitats or assuming uniform conditions across the reef.

We will propose a novel model that aims to address some of actual limitations by incorporating both biological and physical factors into a single framework. Specifically, we will focus on the role of nutrient diffusion and erosion in shaping the spatial patterns of coral reefs.

-
- [1] D. R. Bellwood et al. *Confronting the Coral Reef Crisis*, Nature **429**, 827-33 (2004).
 - [2] T. P. Hughes et al. *Global warming and recurrent mass bleaching of corals*, Nature **543**, 373-377 (2017).
 - [3] T. P. Hughes et al. *Global warming impairs stockrecruitment dynamics of corals*, Nature **568**, 387-390 (2019).
 - [4] P. Mumby and R. S. Steneck, *Coral reef management and conservation in light of rapidly evolving ecological paradigms*, Trends in Ecology & Evolution **23**, 555-563 (2008).
 - [5] N. Shigesada et al. *Modeling Stratified Diffusion in Biological Invasions*, The American Naturalist, **146**, 229-250 (1995).
 - [6] L. Alvarez-Filip et al., *Shifts in coral-assembly composition do not ensure persistence of reef functionality*. Scientific Reports, **3** 3486 (2013).

Unveiling the highly nonlinear dynamics of KCN molecular system using Lagrangian descriptors

F. Revuelta¹, F.J. Arranz¹, R.M. Benito¹, and F. Borondo^{2,3}

¹ Grupo de Sistemas Complejos, Escuela Técnica Superior de Ingeniería Agronómica, Alimentaria y de Biosistemas, Universidad Politécnica de Madrid, Avda. Puerta de Hierro 2-4, 28040 Madrid, Spain

² Departamento de Química, Universidad Autónoma de Madrid, Cantoblanco, 28049 Madrid, Spain

³ Instituto de Ciencias Matemáticas (ICMAT), Cantoblanco, 28049 Madrid, Spain

In this work [1], we identify the phase-space structures which are responsible for the chaotic dynamics observed in KCN molecular system using the Lagrangian descriptors [3]. We show that the vibrational dynamics of this molecule is strongly determined by the invariant manifolds associated with a particular stretching periodic orbit previously described [2]. Likewise, the representation of these invariant manifolds on a Poincaré surface of section shown in Fig. 1 is also studied, concluding that the intricate depiction that is observed has its origin in the complex behavior of the manifolds, which is a consequence of the strong anharmonicities in the potential energy surface, as inferred from visual inspection of Fig. 2.

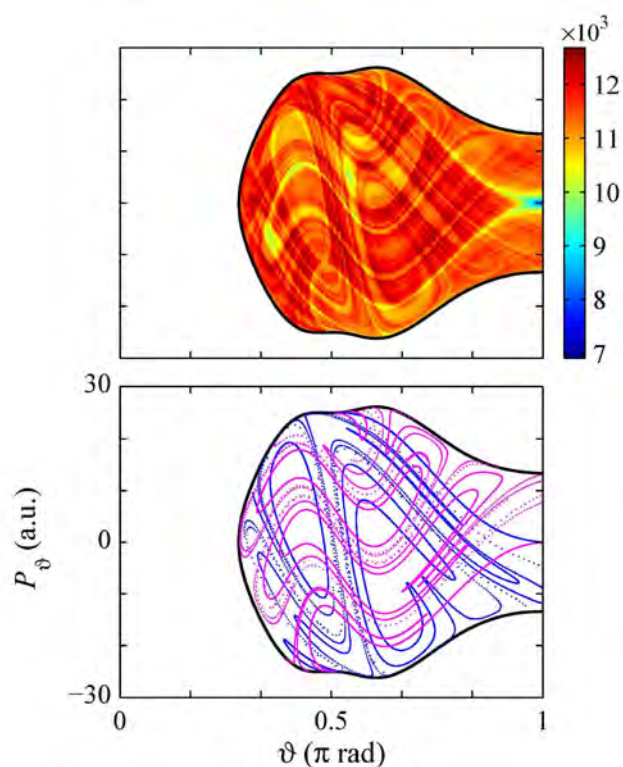


Fig. 1. Cuts of the phase space of the KCN molecular system along the Poincaré surface for a vibrational energy $E=1300\text{cm}^{-1}$. (Top) The Lagrangian descriptors integrated over 437.5 fs are able to unravel the homoclinic tangle (bottom) formed by the intersection of the stable (blue) and the unstable (pink) manifolds.

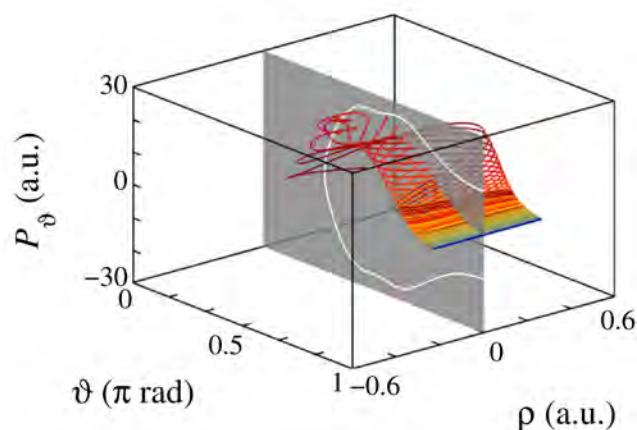


Fig. 2. The invariant manifolds of KCN molecular system are linear close to a stretching periodic orbit (blue line), but they get strongly distorted at larger distances due to the anharmonicities.

[1] F. Revuelta, F.J. Arranz, R.M. Benito, and F. Borondo, *Unraveling the highly nonlinear dynamics of KCN molecular system using Lagrangian descriptors*, Commun. Nonlinear Sci. Numer. Simul. **123**, 107265 (2023).

[2] H. Párraga, F. J. Arranz, R. M. Benito, and F. Borondo, *Above Saddle-Point Regions of Order in a Sea of Chaos in the Vibrational Dynamics of KCN*, J. Phys. Chem. A **122**, 343341 (2018).

[3] C. Lopesino, F. Balibrea-Iniesta S. Wiggins, and A. M. Mancho, *Lagrangian descriptors for two dimensional, area preserving, autonomous and nonautonomous maps*, Commun. Nonlinear Sci. Numer. Simul. **27**, 4051 (2015).

Two diverse types of criticality in neural network models

Carles Martorell^{1,2}, Rubén Calvo^{1,2}, Miguel A Muñoz^{1,2}, and Alessia Annibale³

¹Departamento de Electromagnetismo y Física de la Materia, Universidad de Granada E-18071, Granada, Spain

² Instituto Carlos I de Física Teórica y Computacional, Universidad de Granada E-18071, Granada, Spain

³Department of Mathematics, Kings College London, SE11 6NJ London, United Kingdom

The idea that biological and artificial learning systems may extract crucial functional advantages by exploiting collective effects, in general, and critical phenomena, in particular, has been gaining more and more momentum in the last decades. At the edge of a phase transition, between order and chaos, the system can exploit the combined advantages of stability (order) and responsiveness to perturbations (chaos) without saturating and obtaining an optimal computational performance. From a biological point of view, it has been suggested that computational capabilities of brain networks stem from that delicate balance between order and disorder [1].

Recent works in neuroscience has underscored the dichotomy between two types of phase transitions in neural network dynamics: Type-I criticality, consisting on a transition to a synchronous state; and Type-II criticality, a transition to a non-synchronous and chaotic regime [2]. Both types of criticality can be characterized by the shape of the spectral distribution -the probability distribution of eigenvalues- of the adjacency matrix, which encodes the topological structure of the network. Hence, Type-I is related with the emergence of a dominant eigenvalue, also called "outlier"; while Type-II is characterized by a bulk of eigenvalues (see Figure 1).

Here, we aim to shed further light on these issues by studying one of the simplest possible neural network models, very similar to the classical model of Sompolinsky, Crisanti, and Sommers [3]. In particular, our goal is to establish a correspondence between the Ising and spin-glass transitions in statistical physics and type-I and type-II criticality in simple neural-network models.

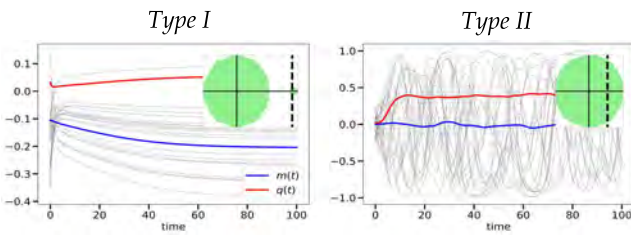


Fig. 1. **Type I vs Type II criticality.** Two different realizations for system (1) at the Ferromagnetic (F) and Spin-Glass (SG) regimes, respectively. The inset shows the spectra distribution for the adjacency matrix, gJ .

Our model consists of a fully-connected network with N neurons, each one described by its time-dependent rate, $x_i(t)$, with $i = 1, 2, \dots, N$, whose dynamics obeys the following set of coupled stochastic differential equations

$$\dot{x}_i = -x_i + \tanh \left(g \sum_j J_{ij} x_j \right), \quad i = 1, \dots, N \quad (1)$$

where the synaptic weights, J_{ij} , are quenched Gaussian random variables with mean J_0 and variance J (convenient

scaled to guarantee the convergence in the infinite-network-size limit). To study analytically this problem we use a Dynamical Mean Field (DMF) approach leading to a self-consistent stochastic equation for the dynamics of a representative neuron,

$$\dot{x}(t) = -x(t) + \tanh[J_0 g M(t) + \phi(t)], \quad (2)$$

where $M(t) = \langle x(t) \rangle$ is the first moment, and $\phi(t)$ is a white-noise process with zero mean and $\langle \phi(t)\phi(t') \rangle = J^2 g^2 \langle x(t)x(t') \rangle$. This simple equation is equivalent to the well-known Sherrington-Kirkpatrick model for spin-glasses, within a replica symmetric ansatz, on which $1/g$ plays the role of the temperature. The main result is shown in Figure 2, on which the first moment (M) and the second moment (q) are plotted as a function of the parameters $\phi_1 = J_0/J$ and $\phi_2 = 1/gJ$. We proved analytically that three different regimes emerge (paramagnetic (P), ferromagnetic (F) and spin-glass (SG), by analogy), where Type-I criticality is characterized as a transition from P to F regimes, while Type-II is defined as a transition from P to SG regimes.

This work serves as an initial point to study the emergence of criticality for more sophisticated neural networks – for biological-plausible architectures: for instance, implementing the Dale's principle– by means of DMF framework.

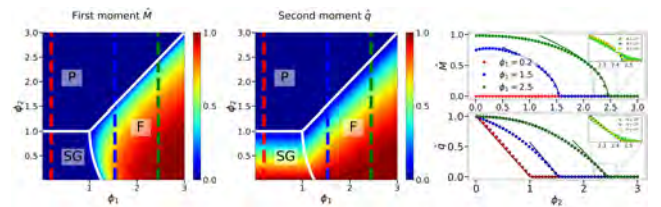


Fig. 2. **Left and middle:** Heat map of the time-averaged mean activity \hat{M} (left) and mean square activity \hat{q} (middle) obtained from simulations, as a function of the parameters ϕ_1, ϕ_2 . The white line shows the theoretically predicted critical lines separating the paramagnetic, ferromagnetic and spin-glass phases for fixed point solutions. **Right:** Symbols show \hat{M} (top) and \hat{q} (bottom) obtained from simulations, versus ϕ_2 . Full lines show the theoretically predicted asymptotic behaviour around the critical point. The inset shows the effect of increasing the system size.

[1] Miguel A. Muñoz, *Colloquium: Criticality and dynamical scaling in living systems*, Rev. Mod. Phys. 90, 031001 (2018).

[2] D. Dahmen, S. Grn, M. Diesmann and M. Helias, *Second type of criticality in the brain uncovers rich multiple-neuron dynamics*, PNAS 116 26 13051-13060 (2019).

[3] H. Sompolinsky, A. Crisanti, and H. Sommers, *Chaos in random neural networks*, Phys. Rev. Lett. 61, 259 (1988).

Stick-Slip Behavior: Evolution of a Condensation Pattern with a Humidity Sink

Mathan K. Raja, and Wenceslao González-Viñas

Dept. of Physics and Applied Mathematics, Universidad de Navarra, Pamplona, Spain

Breath figures (BF) are patterns of condensed droplets on a substrate in contact with supersaturated vapor. Its dynamics has been studied long ago [1]. If we set, prior to the condensation, a hygroscopic NaCl drop on the substrate, the salty drop acts as a humidity sink absorbing most of the available water vapor in the surroundings [2]. The depleted humidity near the salty droplet inhibits the growth of pure water droplets and defines the region of inhibited condensation (RIC). Previous studies attempted to understand the complex interplay between the growth of salty and water droplets experimentally [2]. Here, we report numerical simulations validated against the interpretation of experimental findings. Our model enables us to simulate the controllable characteristics and conditions in contrast to constraints that arise from the experimental setup.

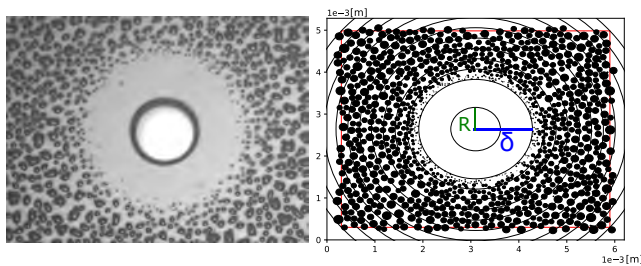


Fig. 1. (Left) Experimental image of breath figure with the salty droplet in the center [2] captured from the top with a horizontal field of view of 4.4 mm, and (right) numerical simulation with δ region of inhibited condensation (RIC) and radius R of the salty droplet.

The initial conditions of the simulation are set by experimentally derived parameters such as the flow rate of humid air and the rate of nucleation. The substrate design is modeled with periodic boundary conditions, and additional droplets are included near the boundary to eliminate edge effects. The coalescence events take place in parallel to the simulation event on the droplet population recursively when any droplets overlap. The state of all the components in the simulation for any given time step is captured for further detailed analysis.

Competition for resources: In our simulations, physical objects operate independently but are interconnected through resource availability and previous outcomes. The availability of humidity estimated using interpolation of shared vapor concentration by the existing population governs the nucleation model, growth of salty and water droplets. Nucleation events are contingent on nucleation rates determined by the resource availability of the seed site, selected from a random pool.

Stick-slip-like dynamics: Dilution of the salty droplet alters the region's vapor concentration profile, affecting the growth dynamics of the droplet population. This change is

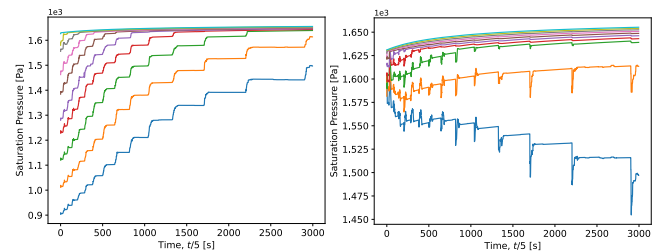


Fig. 2. Eulerian observation(left) of adaptive humidity reveals increased availability away from the salt droplet. Lagrangian observation(right) of δ evolution demonstrates BF's effect on humidity profiles. Forefront rings (green, orange, blue) capture reduced saturation pressure when facing the salty droplet.

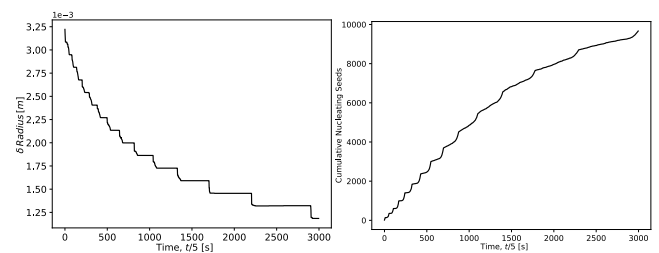


Fig. 3. In our simulation, the cumulative nucleating seeds (right) and the evolution of the δ (left) display regular stick-slip-like dynamics, similar to what was observed in [2], but the underlying cause remains unexplained.

not gradual or evenly distributed. Initially, there is a rapid decline in δ , followed by prolonged plateaus (fig. 3). Water droplets compete for resources, diminishing the sink effect of the salty droplet over the period. Even with constant humid airflow, regular stick-slip-like dynamics manifest in both experimental and simulation models.

In conclusion, our presentation will provide additional analysis to elucidate the intricate interplay among the key components based on our simulation results [3].

This work was partly supported by the Spanish MCIN/AEI/10.13039/501100011033 (Grant PID2021-129066NA-I00) and by "ERDF A way of making Europe".

- [1] D. Beysens, *Dew nucleation and growth*, C. R. Phys. 7, 1082 (2006), and references therein.
- [2] J. Guadarrama-Cetina, R.D. Narhe, D.A. Beysens, W. González-Viñas, *Droplet pattern and condensation gradient around a humidity sink*, Phys. Rev. E 89, 012402 (2014).
- [3] Mathan K. Raja, R. García-García, W. González-Viñas. *In preparation*

Virus-cytokine arms race in mammalian cell tissue

Sabalic A¹, Nguyen DH², Li P², and Garcia-Ojalvo J¹

¹Department of Medicine and Life Sciences, Universitat Pompeu Fabra, Dr. Aiguader 88, 08003, Barcelona, Spain

²Department of Biology, Massachusetts Institute of Technology, 31 Ames Street Cambridge, MA, USA

After an initial infection occurs in mammalian tissue, a cascade of immune system processes is triggered with the primary objective of safeguarding the host and eliminating the pathogen. However, the molecular mechanisms underlying these processes are still not fully understood. In this study, we develop a mathematical model to propose a novel mechanism of viral response that operates autonomously within single cells. The model is constrained by experimental observations in fibroblast cultures, which reveal a bistable response in individual cells. We focus on the influenza A virus (IAV), whose primary targets include epithelial cells of the upper respiratory tract [1]. One of the most important cellular responses to this virus is the production and secretion of interferon by the infected host cells to the surrounding tissue. Interferon induces the expression of hundreds of interferon-stimulated genes (ISGs), which block virus replication at many levels [2]. In that way, virus and interferon compete to gain control of the tissue - the virus attempts to replicate and spread its genetic material, while interferon aims to suppress viral replication.

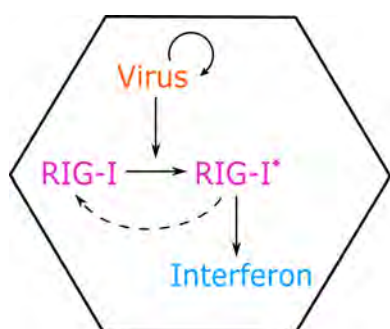


Fig. 1. **Schematic representation of the antiviral response.** Once the virus enters the cell it provokes an instant antiviral response causing the sensor RIG-I to turn to its active state, RIG-I*. When there is a sufficient concentration of active sensor, the cell is able to produce and subsequently secrete interferon.

To understand the mechanisms of interferon expression within the cell, we propose a simple circuit that consists of viral molecules, interferon, and active and inactive RIG-I sensor. RIG-I serves as a sensor for viral infections, playing a crucial role in triggering the activation of type I interferons and other genes that collectively establish a host response with antiviral properties [3]. Following viral entry, the instant antiviral response causes sensor RIG-I to convert to its active state, RIG-I*. Crucially, we assume that active RIG-I stimulates the production of the inactive sensor. Finally, the active sensor triggers the production of interferon within the cell, which will afterwards be secreted to the surrounding tissue. The schematic representation of the proposed antiviral response mechanism is given in Fig. 1. To avoid hyperinflammation, only a small portion of infected cells will

indeed induce interferon, therefore it was of great importance to establish a bistable system that would be able to model the stochastic nature of RIG-I activation. To explore the interferon production, we have built a simple stochastic two-variable model that consists of active and inactive RIG-I sensor. As shown by Eq. (1), once the virus v is detected within the cell, the inactive sensor R will turn active R_a . Next, as given in Eq. (2), when there is enough active sensor, the cell will produce more inactive sensor.

$$\frac{dR_a}{dt} = K_r v R - \delta_r R_a \quad (1)$$

$$\frac{dR}{dt} = \frac{\alpha R_a^n}{K_i^n + R_a^n} - \delta_r R - K_r v R \quad (2)$$

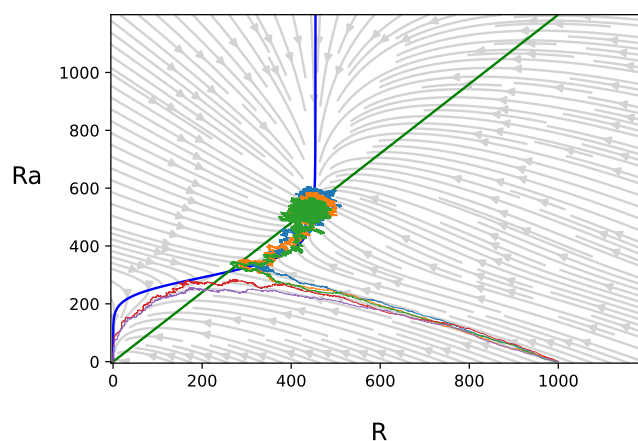


Fig. 2. **Phase portrait.** The system shows the bistable behaviour observed experimentally, where only a portion of cells activates the sensor to produce interferon.

The proposed model produces a bistable response, showing the distribution of active and inactive sensor observed experimentally (Fig. 2). As expected, only a fraction of infected cells activates the sensor leading to the production of interferon. In summary, this study characterizes the relationship between the cellular sensor machinery and interferon production, contributing to a better understanding of the antiviral response within a single-cell environment.

[1] Chen, X., Liu, S., Goraya, M., Maarouf, M., Huang, S. & Chen, J. Host immune response to influenza A virus infection. *Frontiers In Immunology*. **9**, 1-13 (2018)

[2] Schneider, W., Chevillotte, M. & Rice, C. Interferon-stimulated genes: A complex web of host defenses. *Annual Review Of Immunology*. **32** pp. 513-545 (2014)

[3] Liu, G., Lu, Y., Raman, S., Xu, F., Wu, Q., Li, Z., Brownlie, R., Liu, Q. & Zhou, Y. Nuclear-resident RIG-I senses viral replication inducing antiviral immunity. *Nature Communications*. **9** (2018) Sesión Póster 2, P2.24

Hallmarks of habituation: a biochemically-plausible model

M. S. Vidal-Saez¹, L. Eckert², Z. Zhao², J. Gunawardena², R. Martinez-Corral^{3,4}, and J. Garcia-Ojalvo¹

¹Department of Medicine and Life Sciences, Universitat Pompeu Fabra, 08003 Barcelona, Spain.

²Department of Systems Biology, Harvard Medical School, 02115 Boston MA, USA.

³Barcelona Collaboratorium for Modelling and Predictive Biology, 08005 Barcelona, Spain.

⁴Centre for Genomic Regulation, 08003 Barcelona, Spain.

Living systems have complex information processing capabilities. Arguably the most remarkable is learning, which enables organisms to modify their behavior in response to past stimuli. In this work we focus on habituation, one of the non-associative forms of learning. Habituation is commonly defined as a progressive decrease in response upon repetitive sensory stimulation (Fig. 1). A multitude of different organisms, behaviors, and experimental approaches have been used to study habituation, but still surprisingly little is known about the underlying mechanisms [1].

There are several characteristics of habituation that are widely conserved from single cell organisms to invertebrates and vertebrates. For example, the dynamics of habituation is not solely determined by the number of stimuli but additionally depends on the frequency and intensity of stimulation. These hallmarks are called frequency and intensity sensitivity [2].

Frequency sensitivity means more frequent stimulation produces more rapid and/or more pronounced habituation. On the other hand, more intense stimuli generates less rapid and/or less pronounced response decrement (intensity sensitivity).

In this study we have set a biochemically-plausible mechanistic model that can account for the frequency and intensity sensitivity hallmarks of habituation in a unified framework, which has not been done yet to our knowledge.

Following an idea of a habituation model in a discrete time setting [3], we show that concatenation of two incoherent feedforward motifs (IFF) can explain the central effects of the stimulation frequency on the dynamics of habituation, *i.e.*, frequency sensitivity. The primary characteristic lies in the different timescales of the two cascaded motifs, resulting in a distinct pattern of memory formation based on the frequency of stimulation. Additionally, our concatenated IFF model comprehensively obeys the intensity sensitivity hallmark of habituation.

On the other hand, we have also examined a negative feedback architecture (NF), which has been previously suggested as a possible circuit underlying habituation [4]. As with the IFF model, we concatenated two NF circuits. We have found a region in the parameters' space that exhibits

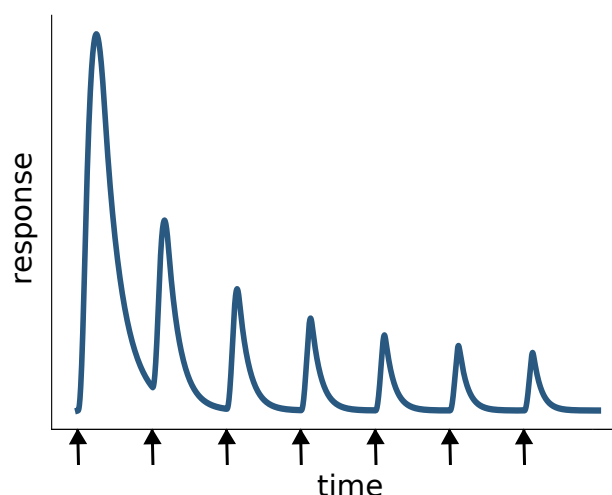


Fig. 1. Schematic illustration of habituation. The response diminishes upon repeated stimuli (black arrows). For additional properties of habituation, see [2].

robust solutions, which account for the nontrivial hallmarks of frequency and intensity sensitivity.

Our biochemically inspired model of habituation sheds some light on the possible mechanisms underlying the well-conserved frequency and intensity sensitivity hallmarks.

-
- [1] S. Schmid, D. A. Wilson and C. H. Rankin, *Habituation mechanisms and their importance for cognitive function*, *Frontiers in integrative neuroscience* **8,97** (2015).
 - [2] C. H. Rankin *et al.*, *Habituation revisited: an updated and revised description of the behavioral characteristics of habituation*, *Neurobiology of learning and memory* **92,2** (2009).
 - [3] J. E. R. Staddon, *On rate-sensitive habituation*, *Adaptive Behavior* **1,4** (1993).
 - [4] J. E. R. Staddon and J. J. Higa, *Multiple time scales in simple habituation*, *Psychological Review* **103,4** (1996).

Transiciones estocásticas y deterministas en juegos evolutivos en redes

Nagi Khalil¹, I. Leyva^{1,2}, J.A. Almendral^{1,2}, and I. Sendiña-Nadal^{1,2}

¹Complex Systems Group & GISC, Universidad Rey Juan Carlos, Móstoles, 28933 Madrid, Spain

²Center for Biomedical Technology, Universidad Politécnica de Madrid, Pozuelo de Alarcón, 28223 Madrid, Spain

En este trabajo se investiga el comportamiento crítico de diferentes juegos evolutivos con entornos estructurados, utilizando para ello un enfoque teórico y de simulación Monte Carlo. La población de jugadores se modela como un sistema de partículas en una red, cada una en dos posibles estados (cooperación y defección). Tras cada ronda del juego, cada jugador recibe una ganancia que depende de su estrategia, de la de sus vecinos y de los parámetros del juego en cuestión. El resultado del juego determina la evolución del sistema: se elige un jugador al azar, un vecino de éste también al azar, y la diferencia de ganancias determina la probabilidad de que el primero copie la estrategia del segundo. Dicha probabilidad viene modulada por una temperatura efectiva θ , de modo que si $\theta = 0$ entonces el cambio resulta determinista.

La teoría desarrollada y los resultados de simulación muestran la existencia de distintos estados posibles para los que la densidad de cooperación ρ es estacionaria: de estrategia absorbente (todos los jugadores llegan a una situación en la que sus estrategias no cambian con el tiempo), cuasi-absorbente (una parte de los jugadores fija su estrategia y la otra cambia con el tiempo) y mixta (los jugadores cambian continuamente sus estrategias). Además, la teoría es capaz de predecir la naturaleza (continua o discontinua) de las transiciones a medida que se cambian los parámetros del juego y la temperatura efectiva.

En particular, cuando el proceso de decisión es determinista ($\theta = 0$), el sistema es muy propenso a sufrir transiciones discontinuas a medida que cambian los parámetros del juego (ver figura). La localización de dichas transiciones, que depende de la distribución de grado de la red, ha sido predicha teóricamente. Además, resulta que las transiciones pueden aparecer para cualquier tamaño del sistema. Sin embargo, éstas tienen a desaparecer para $\theta > 0$.

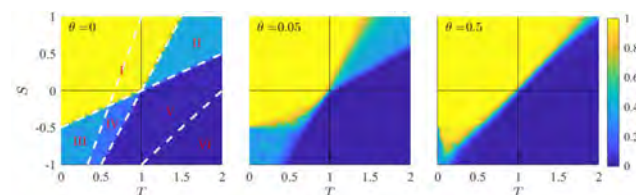


Fig. 1. Diagrama de fases determinado por dos parámetros del juego S y T (los otros dos son $P = 0$ y $R = 1$), según la definición habitual [1, 2], para distintos valores de la temperatura efectiva θ . La escala de colores determina la densidad de cooperación: $\rho = 0$ corresponde a defección (azul) y $\rho = 1$ a cooperación (amarillo). Las líneas blancas a trazos son teóricas y los colores son resultados de simulación.

Los resultados de simulación muestran la existencia de otras transiciones continuas y discontinuas para temperaturas efectivas positivas $\theta > 0$, cuando el sistema se hace grande. La mayoría de dichas transiciones pueden ser explicadas teóricamente mediante un análisis tipo campo medio. Finalmente, para algunos parámetros del juego, encontramos "temperaturas sociales" óptimas que maximizan o minimizan la densidad de cooperación.

[1] A. Zhuk, I. Sendiña-Nadal, I. Leyva, D. Musatov, A. Raigorodskii, M. Perc, and S. Boccaletti, *Predicting transitions in cooperation levels from network connectivity*, *New J. Phys.* **23** 093040 (2021).

[2] Nagi Khalil, I. Leyva, J. A. Almendral, and I. Sendiña-Nadal, *Deterministic and stochastic cooperation transitions in evolutionary games on networks*, *Phys. Rev. E* **107** 054302 (2023).

SARS-CoV-2 Genotype Network

Iker Atienza-Diez^{1,2}, Luís F Seoane^{1,2}, and Susanna Manrubia^{1,2},

¹ Systems Biology Department, Centro Nacional de Biotecnología (CSIC), Madrid, Spain

² Grupo Interdisciplinar de Sistemas Complejos (GISC), Madrid, Spain

Genotype networks are powerful representations of great aid in the interpretation of evolutionary processes, especially for highly heterogeneous molecular populations [1]. These networks can be constructed at different scales, for instance by deep-sequencing evolving in-vitro populations [2] or through geographically extended data of a circulating pathogen [3]. In this contribution, we present the SARS-CoV-2 (SARS2) genotype network (GN) reconstructed from genomic data spanning from December 2019 to March 2023, with Wuhan-Hu-1 strain (GenBank: MN908947.3) as wild-type (WT) reference sequence [4].

SARS2 genome is about 30,000 base-pairs long. The reconstruction of the network using whole genomes is computationally unfeasible, so we have selected the Receptor Binding Domain (RBD) section of the viral Spike protein. The RBD contains 223 amino acids (S:319-541) involved in the recognition of the human ACE2 receptor, and thus in cell entry of the virus [5]. Its location in SARS2 genome is illustrated in Figure 1.

A haplotype is any sequence that differs from the WT. After curating the original dataset, we analyse 5,799,310 complete genomes to extract the set of different haplotypes in the RBD section of interest; we identify 28,686 unique haplotypes with an abundance ranging from 1 to 1,915,492 sequences. Each identified haplotype is a node in our GN, and two nodes are connected through an edge if their sequences differ by a single mutation: SARS2 GN has 27,634 nodes and 56,122 edges. Fig. 1 shows the obtained GN with nodes colored according to the number of mutations accumulated with respect to the WT, as specified in the legend. Our analysis of the topological properties of this GN reveals that it is weakly disassortative and has an average degree $\langle k \rangle \simeq 4$.

Since genomes in the dataset are labelled according to the variant they belong to, an analysis using the subset of haplotypes in each variant is possible. Since our study is limited to the RBD, there is some degeneracy in this classification, with 916 (3.31%) multi-variant haplotypes, that is, sequences that can be classified in two or more variants. All variants of concern, except Omicron, are relatively close to the WT (< 5 mutations). Omicron-labelled haplotypes are more diverse in terms of mutations, suggesting that this variant has explored a larger region of genotype space. Our analysis supports as well that the fitness landscape around this variant is flatter, since its associated subnetwork has a significantly larger number of nodes with high degree, consistently leading to a less disassortative pattern than that of previous variants. Interestingly, the SARS2 GN contains a large number of cycles, pointing at a non-uniqueness of evolutionary pathways linking different haplotypes within and between variants.

We have also explored the temporal appearance of different haplotypes and found, first, a burst of haplotype diversity (12/2021-01/2022) associated to the emergence of Omicron and, second, a waxing and waning pattern in haplotype

abundance caused by the sequential emergence of new successful variants. We observe that some early-explored, but not fixed, haplotypes re-emerge when Omicron arises, possibly due to other accompanying mutations out of the RBD region.

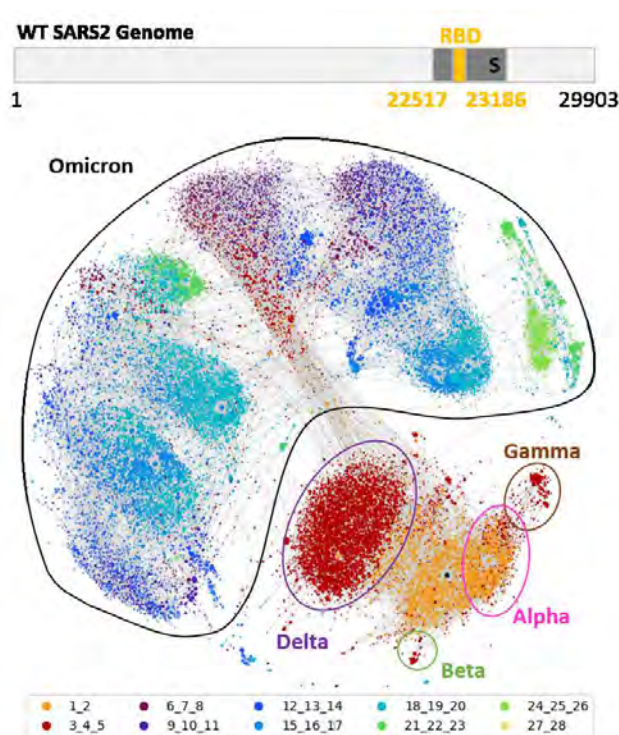


Fig. 1. SARS-CoV-2 genome and RBD Genotype Network. Above: schematic of SARS2 genome highlighting the position of the spike protein and its RBD motif. Below: SARS2 GN. Node size is proportional to (the logarithm of) haplotype abundance and node color indicates the number of mutations accumulated by each particular haplotype. Colors stand for the number of mutations, as indicated in the legend, ranging from 1-2 mutations (orange) to 27-28 (yellow) when compared to the WT RBD sequence (black node).

- [1] J. Aguirre, P. Catalán, JA. Cuesta, and S. Manrubia. *Open Biol.* **81** (2018).
- [2] A. Villanueva, H. Secaira-Morocho, LF Seoane, E. Lzaro and S. Manrubia. *Biophysica* **2(4)**, 381-399 (2022).
- [3] A. Wagner. *Proc. R. Soc. B.* **281** (2014).
- [4] <https://docs.nextstrain.org/en/latest/>
- [5] Y. Huang, C. Yang, Xf. Xu, W. Xu and SW. Liu. *Acta. Pharmacol. Sin.* **41**, 11411149 (2020).
- [6] RA. Neher. *Virus Evolution*, **8(2)** (2022).

A statistical model for codon optimization

D. Luna Cerralbo^{1,2}, I. Blasco Machn³, E. Broset³, J. Martinez³ and P. Bruscolini^{1,2}

¹Department of Theoretical Physics, University of Zaragoza.

²Institute for Biocomputation and Physics of Complex Systems (BIFI), University of Zaragoza.

³Department of RNA Design, Certest Pharma.

The degeneracy of the codon alphabet allows different codons to translate to the same amino acid, and it is well-known that different species show different statistics of codon usage. However, the reasons why a species adopts a particular statistics are not clear, even if protein yield, production speed, and RNA stability are believed to play a role in the choice. In this context, codon optimization involves adjusting the codon sequence for a target protein, to mimic the natural choice a given species would make, to produce that protein. However, conventional methods used for codon optimization are often simplistic (e.g., resorting just to the importance of each codon), or phenomenological, using the observed average frequency of codon pairs as input, instead of obtaining it as a result. Using large databases of human proteins, we propose a statistical-physics model, where the

probability of any codon sequence is related to the interactions between neighboring codons. We have adjusted the model's parameters to maximize the dataset's probability. We have applied the method to the case of Luciferase, as a simple test protein, optimizing the codon sequence by Simulated Annealing, and comparing the results to those obtained by conventional methods.

[1] Genome Reference Consortium Human Build 38 patch release 13 (GRCh38.p13)

[2] National Center for Biotechnology Information (NCBI)
<https://www.ncbi.nlm.nih.gov/>

[3] ViennaRNA Package 2.0 doi:10.1186/1748-7188-6-26

Nest site selection in honeybee swarms: The colony as a cognitive unit

David March^{1,2}, Julia Mugica¹, Ezequiel Ferrero² and Carmen Miguel²

¹ Departament de Física, Universitat Politècnica de Catalunya, Campus Nord, Mdul B4, 08034 Barcelona, Espanya

² Departament de Física de la Materia Condensada, Universitat de Barcelona, Av. Diagonal 645, 08028, Barcelona, Espanya

Collective decision making is a broad and interdisciplinary field of study where statistical physics, biology and social sciences meet. In our group we study collective decision making in groups formed by social agents in complex environments. We observe these processes constantly on social groups: from humans taking part in elections, social mammals herds or schooling fish moving together or insect colonies moving to a food source or a new settlement. Information flow is crucial to the outcome of a decision making process, and the extent to which group members are able to individually explore the available options, to assess their benefit for the group or to acknowledge the information that their colleagues have gathered are some of the most relevant factors mediating this process.

We study a particular decision making process inspired by real honeybee swarms seeking a new nest site. Each spring bee colonies split and half of the colony seeks a new place to establish their nest, in a process that involves exploring the environment and exchanging information with other members of the group. The key factors influencing the outcome of this decision process are the cost or difficulty to discover the possible sites and the honeybees capacity to assess the sites' qualities and to announce effectively their findings. A characteristic feature of this process is that bees announce their discoveries via a *waggle dance*, a dance that is livelier and longer the better quality the of the site is estimated to be. Other bees may explore, and consequently advertise, an already announced site instead of individually seeking in the environment a new discovery which to advertise. Favouring the best findings via longer advertisement periods allows an information cascade to be built and a collective, decentralized decision to be taken for the best possible option, to the extent on how easy it is to discover, how different in quality it is related to other options or how trustful are bees to one another.

The approach we follow is based on computer simulations of an agent-based model first presented in [1], and further studied in [2]. This model accounts for the cost and quality of the options and the group ability to either independently explore the environment or trust other members opinions. We study how the interplay of these factors results in a beneficial or detrimental choice for the group or even a stalemate between the options.

Interestingly, a honeybee swarm faced with such a scenario can be thought of as a single cognitive unit faced with a sensory discriminatory task [4]. Originally, the relationship between stimulus intensity (sound loudness, image brightness, time duration, for instance) and its perception was studied only in the domain of the human brain.

Over the years it has been shown that results valid on the human brain are also valid for other organisms at different levels of complexity, from other mammals to fish or insects. Consequently, psychophysical laws that, for instance, relate the difference between stimuli intensity that can be properly discriminated (Weber's Law) or the reaction time necessary to correctly discriminate between different stimuli (Piron's Law) have been established at the individual level. It has only been in the last years that efforts have been made to explore the validity of these laws in the swarm level [3], inspired by the behavior of real honeybees. By means of the model under study we explore the applicability of these laws at the colony level, relating the stimuli intensity to the sites' qualities between which the swarm has to choose.

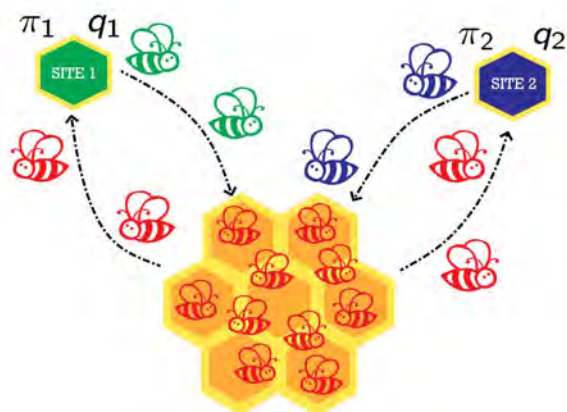


Fig. 1. Schematic representation of the model under study. The members of the group (bees) explore the environment and discover options (nest sites) with a probability π_i . They advertise their finding to the rest of the group for a time period relative to the site quality, q_i . Following the initial discoveries, bees will follow other bees advertisements with a probability λ .

[1] List, C. and Elsholtz, C. and Seeley, T. D, Philos. Trans. R. Soc. Lond., B, Biol. Sci. **364**, 1518, 755-762 (2009)

[2] Galla T, J. Theor. Biol., **262**, 1, 186-196 (2010)

[3] Reina, A., Bose, T., Trianni, V., Marshall, J. A. R. Sci. Rep., **8**(1), Article 1. (2018)

[4] Passino, K., Seeley, T., Visscher, P. (2008). Behav. Ecol. Sociobiol., **62**, 401414.

Enhancing Multi-Physics Microwave Heating Simulation of a Packed Bed of Spheres: Insights from Tangency-Preserving DEM Simulations

Carlos González Niño¹, and Miguel Ángel Castán Lascorz¹

¹Fundación CIRCE, Avenida Ranillas, Edificio Dinamiza 3D, 50018 Zaragoza, Spain

Microwave heating offers a promising avenue for renewable and efficient heating processes by directly transferring heat into the core of matter. However, certain materials may be transparent to the electromagnetic waves due to their low permittivity values. In such cases, the utilization of a susceptor material such as silicon carbide (SiC) becomes necessary, which absorbs the power of the waves and subsequently transfers the generated heat to the surrounding material. This work delves into the investigation of microwave heating in a packed bed of SiC spheres where emphasis is placed on accounting for the concentration of the electromagnetic field at the tangent points between spheres, a well-known characteristic of such systems.

In the present study, the position of the SiC spheres was obtained by using the open-source DEM software LIGGGHTS, with the aim of exporting the resulting packed bed geometry and importing it into COMSOL Multiphysics to carry out a radio-frequency simulation of the MW heating. However, this approach proved unsuccessful due to the presence of small interpenetrations in the DEM simulation results, rendering the construction of the COMSOL geometry unfeasible.

To overcome these limitations, an algorithm was developed in Python to modify the DEM-generated geometry, allowing for slight repositioning and small changes in the sizes of the spheres to achieve a fully tangent geometry. The algorithm employs a grid-based technique to partition the space and takes into account the number of spheres surrounding each given sphere, imposing constraints to determine its new position and radius. Python automatically generates the necessary Java code for the fully tangent geometry generation, which can be executed through COMSOL's built-in application builder.

This algorithm is useful when setting up MW simulations of packed beds with a reduced number of spheres. However, this approach becomes impractical when simulating tens of thousands of spheres, leading to computationally unfeasible simulations. To address this limitation, we developed a novel method based on existing literature [1] to calculate the permittivity of a bulk material with dielectric properties equivalent to those of a real unit cell. Initially, the permittivity for a unit cell was calculated using the constitutive relation $\mathbf{D} = \epsilon\mathbf{E}$ and obtaining an average permittivity in the unit cell by integrating volumetrically \mathbf{D} and \mathbf{E} over it before division [2]. Unlike previous cases examined in the literature, the packing configuration considered in our study was not isotropic, but a realistic arrangement of particles. As a result, the calculated permittivity obtained in this manner takes the form of a tensor of phasors.

Based on the permittivity value obtained through detailed simulations (Fig. 1) using the equation mentioned earlier, a

parametric study of a bulk material is conducted in which both the real (ϵ') and imaginary (ϵ'') parts of the permittivity are varied in a range around the obtained permittivity ϵ_0 . The objective is to determine the combination of ϵ' and ϵ'' that minimizes errors by calculating electromagnetic losses and the time-averaged electrical energy in the material. Thus, the problem is reduced to a multi-objective optimization that can be automated.

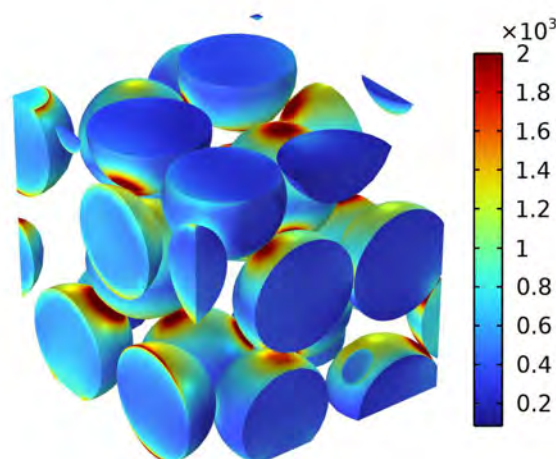


Fig. 1. Electric field distribution in the unit cell [V/m].

The procedure was repeated for a wide range of temperatures to account for the temperature dependency of the permittivity of the SiC. This enables the calculation of a time-dependent permittivity for the bulk material, which can then be utilized in radio-frequency simulations and even coupled with turbulent flow simulations in a porous material.

Furthermore, it becomes possible to accurately model chemical reactions in a flowing phase within a microwave-heated packed bed of susceptor spheres. In this way, there is no longer a need to mesh the detailed packed bed geometry, which for a great number of spheres results in unfeasible meshes and memory errors.

-
- [1] R.M. Costa Mimoso, J.M. da Silva, and J.C. Fernandes *Computational Method for Calculating the Effective Permittivity of Complex Mixtures*, J. Microw. Power. Electromagn. Energy. **49**, 2, 85-99 (2015).
- [2] H. Goyal, and D.G. Vlachos, *Multiscale modeling of microwave-heated multiphase systems*, Chem. Eng. J. **397**, 125262 (2020).

Preserving Tangencies in Postprocessed DEM Results: Enabling FEM Electromagnetic Simulation

Carlos González Niño¹, and Miguel Ángel Castán Lascorz¹

¹Fundación CIRCE, Avenida Ranillas, Edificio Dinamiza 3D, 50018 Zaragoza, Spain

Microwave heating has gained prominence as a versatile and efficient technique with the potential to significantly contribute to the decarbonization efforts in various industrial and scientific sectors, particularly in Europe. Among the commonly employed equipment in these industries, packed-bed reactors stand out as widely utilized units. Expanding on the versatility of microwave heating, the particles of catalyst within these reactors can serve a dual purpose by not only facilitating catalytic reactions but also potentially acting as effective heating agents for the fluid, depending on their dielectric properties.

However, a distinctive characteristic of such configurations is that, when subjected to a varying electromagnetic field, the concentration of electric field and the resulting electromagnetic losses, which drive the heating process, tend to occur predominantly at the tangent points between the particles [1], and so preserving these is of the outmost importance for microwave heating process simulation.

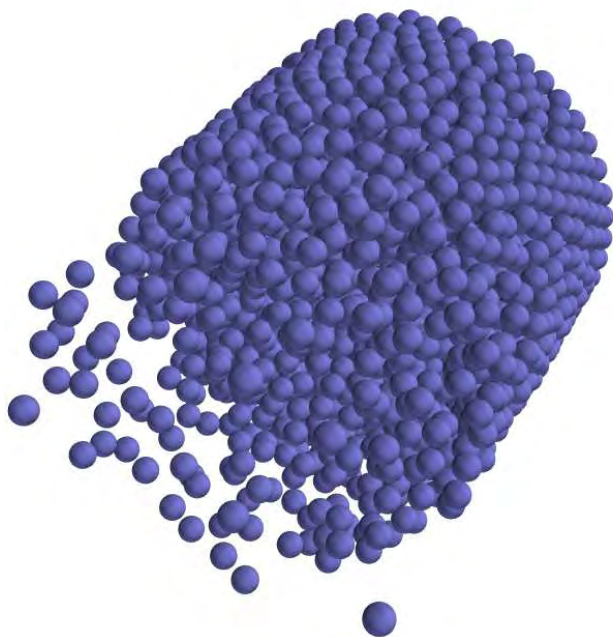


Fig. 1. Packed-bed distribution of spheres generated by DEM simulation.

In our study, we depart from the conventional approach of utilizing an artificially ideal arrangement of particles, such as the commonly referenced FCC packing found in the literature [2]. Instead, we employ Discrete Element Method (DEM) simulations to model a realistic packing within a fixed-bed reactor. However, this approach presents a challenge as the DEM simulations result in small interpenetrations between the particles, hindering the import of the geometry into Finite Element Method (FEM) software for MW heating simulation.

To overcome these challenges, we have devised an algorithm that facilitates minor repositioning and size adjustments for each sphere, resulting in tangent geometries. These modified geometries can be seamlessly imported and meshed using FEM software, enabling us to conduct precise simulations of microwave heating in the packed bed system. Our iterative algorithm utilizes a combination of trigonometric calculations and equation-solving to come up with the tangent geometry.

The algorithm we have developed incorporates a partition scheme that divides the space into cells, enabling efficient checks for tangencies between spheres within the current cell and its surrounding cells. This partitioning strategy avoids the need for unnecessary distance checks between separate spheres, resulting in a significant computational time reduction.

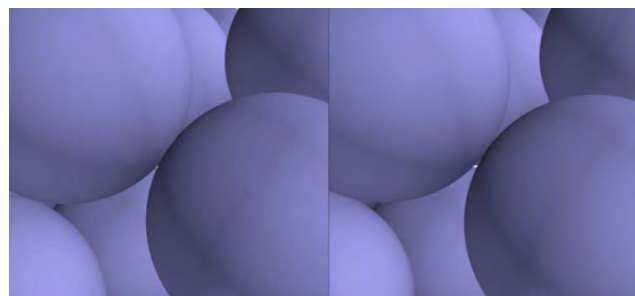


Fig. 2. Details of the initial (left) and final (right) particle arrangements. The algorithm provides a tangency point in a previously interpenetrating position.

Given the high density of spheres present in the real-world applications, the relocation of spheres is a process that must be carried out in iterative stages, as the movement of one sphere can affect those around it. Due to the high computational cost of the calculation process, which grows exponentially with the number of spheres, it is necessary to parallelize the separation algorithm so it can be performed within a reasonable time frame. The proposed methodology includes this parallelization, which involves generating sets of spheres that can be processed independently and are based on unsupervised clustering algorithms. This approach allows for the distribution of the separation algorithm, leading to computational time savings that are almost proportional to the number of clusters.

[1] N. Haneishi, S. Tsubaki, E. Abe *et al.*, *Enhancement of Fixed-bed Flow Reactions under Microwave Irradiation by Local Heating at the Vicinal Contact Points of Catalyst Particles.*, *Sci. Rep.* **9**, 222 (2019).

[2] H. Goyal, and D.G. Vlachos, *Multiscale modeling of microwave-heated multiphase systems*, *Chem. Eng. J.* **397**, 125262 (2020).
Sesión Póster 2, P2.31

Transición vítrea en un fluido molecular con fuerzas de arrastre no lineales

B. Sánchez-Rey¹, A. Patrón², and A. Prados²

¹Dpto. Física Aplicada I, EPS, Universidad de Sevilla

²Física Teórica, Universidad de Sevilla

Un vidrio estructural se puede definir como un líquido que no fluye, es decir, es un material que se halla en un estado de no equilibrio intermedio entre el estado líquido y el del sólido cristalino. Por una parte, tiene propiedades mecánicas similares a la del sólido, pero por otra parte, sus átomos o moléculas presentan un desorden estructural semejante al de un líquido. Usualmente un vidrio se forma enfriando de manera suficientemente rápida un líquido por debajo de su punto de fusión. En lugar de cristalizar, a partir de una cierta temperatura T_g llamada temperatura de transición vítrea, el fluido se queda “congelado”. A partir de dicha temperatura aumentan muy rápidamente la viscosidad y los tiempos de relajación, se reducen bruscamente las posibilidades de realizar reajustes configuracionales, y se forma el vidrio. A pesar de los numerosos trabajos dedicados al problema de la transición vítrea en las últimas décadas, éste continúa siendo un problema abierto [1]. No hay aún una teoría completa que de cuenta de forma satisfactoria de toda la fenomenología característica del comportamiento vítreo.

En este trabajo estudiamos la emergencia de la transición vítrea en un fluido molecular con una fuerza viscosa no lineal, cuando la temperatura del baño T_s con el que está en contacto disminuye linealmente en el tiempo con una velocidad r_c . La dinámica de la función de distribución de velocidades del fluido $f(\mathbf{v}, t)$ está descrita por una ecuación de Fokker-Planck no lineal [2], de la cual podemos deducir una jerarquía de ecuaciones diferenciales para los momentos $M_l \equiv \langle c^l \rangle$, siendo

$$\mathbf{c} \equiv \frac{\mathbf{v}}{\sqrt{2k_B T(t)/m}} \quad (1)$$

una velocidad adimensional, $T(t)$ la temperatura del fluido, k_B la constante de Boltzmann y m la masa de las partículas. Mediante una teoría perturbativa de capa límite, demostramos que la temperatura final a la que el fluido se queda congelado escala con la velocidad de enfriamiento como $r_c^{2/3}$, y que los momentos de la distribución de velocidades del estado congelado son independientes de r_c .

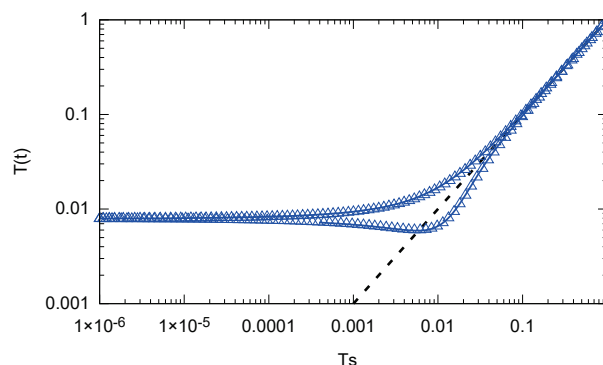


Fig. 1. Ciclo de histéresis experimentado por el fluido molecular. Primero lo enfriamos hasta que experimenta la transición vítrea y se queda “congelado”. Después calentamos desde el estado congelado hasta alcanzar de nuevo el equilibrio con el baño térmico, representado por la línea negra discontinua.

Además, obtenemos expresiones analíticas aproximadas para las capas externa e interna que ajustan muy bien los resultados de la simulación numérica de la ecuación de Fokker-Planck.

Mostramos asimismo que si, tras quedar el sistema congelado, volvemos a calentar el fluido, emerge un ciclo de histéresis característico, como el que se puede ver en la figura 1, que igualmente podemos describir muy bien con nuestra teoría perturbativa.

[1] Debenedetti, P. G. and Stillinger, F. H. *Supercooled liquids and the glass transition*. Nature 410, 259267 (2001).

[2] A. Patrón, B. Sánchez-Rey, A. Prados *Strong nonexponential relaxation and memory effects in a fluid with nonlinear drag*, Physical Review E 104 (6), 064127 (2021).

Global non-equilibrium attractor for non-linear Fokker-Planck systems

A. Patrón¹, B. Sánchez-Rey² and A. Prados¹

¹Física Teórica, Universidad de Sevilla, Apartado de Correos 1065, E-41080 Sevilla, Spain

²Departamento de Física Aplicada I, E.P.S., Universidad de Sevilla, Virgen de África 7, E-41011 Sevilla, Spain

Stochastic processes are ubiquitous in physics. Systems of interest are usually not isolated but in contact with a much larger environment. What makes their dynamics stochastic is the interaction with the environment (thermal bath): the integration over its degrees of freedom entails that the “force”—understood in a generalised sense—acting on the system becomes effectively random. It is in this approach, often called mesoscopic, that the Langevin or Fokker-Planck equations emerge.

Let us consider a physical system whose mesoscopic states are described by $\mathbf{r} \equiv \{x_1, \dots, x_d\}$. A prototypical example is a colloidal particle confined in a d -dimensional potential well. We assume the dynamics of \mathbf{r} to be Markovian and governed by the following “fully non-linear” Fokker-Planck equation for the probability distribution function $P = P(\mathbf{r}, t)$ in the ensemble picture [1],

$$\partial_t P = \nabla_{\mathbf{r}} \cdot \left[\mathbf{A}(\mathbf{r})P + \frac{1}{2} B^2(\mathbf{r}) \nabla_{\mathbf{r}} P \right]. \quad (1)$$

Our terming “fully non-linear” for the Fokker-Planck equation stresses the fact that, in general, not only the “force” $\mathbf{A}(\mathbf{r})$ but also the diffusivity $B^2(\mathbf{r})$ are non-linear functions of \mathbf{r} . The dynamics of the system is stochastic due to its contact with a thermal bath at temperature T . We assume that detailed balance holds, so the fluctuation-dissipation relation

$$2\mathbf{A}(\mathbf{r}) = \beta B^2(\mathbf{r}) \nabla H(\mathbf{r}). \quad (2)$$

is verified, $H(\mathbf{r})$ being the system’s “Hamiltonian” and $\beta = (k_B T)^{-1}$. In certain contexts, $H(\mathbf{r})$ would not be the Hamiltonian of the system but the function playing its role: e.g., for an overdamped Brownian particle, $H(\mathbf{r})$ would be the confining potential, with \mathbf{r} being the spatial coordinates, while for a molecular fluid within the context of kinetic theory, $H(\mathbf{r})$ would be the kinetic energy, with \mathbf{r} now accounting for the velocities of the particles of the fluid [2]. Eq. (2) entails that the canonical distribution, proportional to $e^{-\beta H(\mathbf{r})}$, is the stationary solution of the Fokker-Planck equation.

In the long-time limit, systems evolving under stochastic dynamics typically relax to equilibrium at the bath temperature. The equilibrium state is thus a global attractor, reached from an arbitrary initial condition, of the system dynamics. A relevant question is whether it is only the final equilibrium state that is independent of the initial preparation or there appears a previous global non-equilibrium attractor, already independent of the initial preparation. In the latter case, relaxation to equilibrium would proceed in two stages: first, the system would approach the universal non-equilibrium

state and, second, this non-equilibrium state would tend to equilibrium.

Here we show—under general assumptions—that there emerges such a universal non-equilibrium state for a wide class of systems described by a non-linear Langevin equation, when quenched to low enough temperatures. This state, which we term long-lived non-equilibrium state (LLNES), is a global attractor of the dynamics for an intermediate time scale, over which initial conditions are already forgotten but the system is still far from equilibrium. In particular, the probability distribution function exhibits a Dirac-delta shape within the LLNES [1], as shown in Fig. 1.

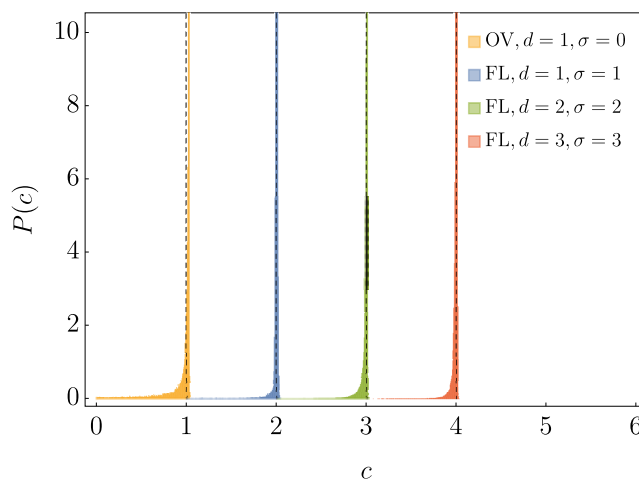


Fig. 1. Scaled probability distribution function at the LLNES for different physical situations. Plots for both (OV) an overdamped particle in a non-harmonic potential and (FL) a molecular fluid with non-linear drag, in different dimensions. For the former, $\mathbf{c} = \mathbf{r}/\langle r \rangle$ stands for the scaled spatial position of the confined overdamped particle; while for the latter, $\mathbf{c} = \mathbf{v}/\langle v \rangle$ accounts for the scaled velocities of the particles of the molecular fluid. In order to appreciate the universal Dirac-delta shape, each probability distribution function is shifted an amount σ to the right, as indicated in the legend.

[1] A. Patrón, B. Sánchez-Rey, E. Trizac and A. Prados, *Non-equilibrium attractor for non-linear stochastic dynamics*, Phys. Rev. Lett. (Under review)

[2] A. Patrón, B. Sánchez-Rey, and A. Prados, *Strong non-exponential relaxation and memory effects in a fluid with non-linear drag*, Phys. Rev. E **104**, 064127 (2021).

Polarization measures in multi party elections

Samuel Martin-Gutierrez^{1, 2}, Juan C. Losada¹, and Rosa M. Benito¹

¹Grupo de Sistemas Complejos, Escuela Técnica Superior de Ingeniería Agronómica, Alimentaria y de Biosistemas, Universidad Politécnica de Madrid, Av. Puerta de Hierro 2-4, 28040 Madrid, Spain

²Network Inequality Group, Complexity Science Hub Vienna, Josefstädter Str. 39, 1170 Wien, Austria

Social polarization is a pervasive phenomenon that has been observed in a wide variety of contexts like elections, referenda and around controversial issues. Polarization has been traditionally studied in binary conflicts where two groups support opposite ideas.

In this work, we introduce new polarization metrics for multidimensional scenarios and develop a methodology that extracts the ideological structure of multipolar contexts from social networks. We use our framework to model multiparty democracies by considering each party as an opinion pole. If there are n opinion poles, we place each pole at the vertex of a regular simplex of dimension $n - 1$, being each pole at the same distance of the others.

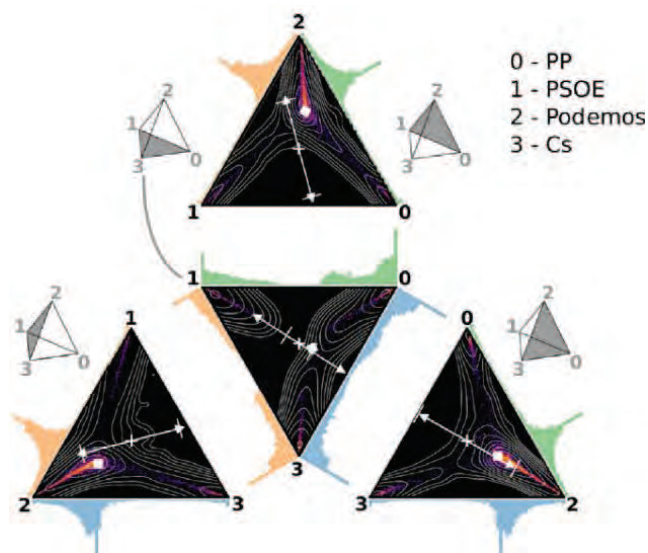


Fig. 1. Quadripolar opinion distribution of the Spanish general elections of the 20 of December, 2015.

Our multidimensional opinion inference technique is a generalization of a bipolar (one-dimensional) methodology [1] based on models of opinion dynamics. The process consists in building a network of social interactions from empirical data, identifying the opinion leaders and their respective ideological positions [2]. Then, we use the model to propagate the leaders' opinions throughout the rest of the nodes. Finally, we take the model's outputs (the converged opinions) as the inferred opinions of the nodes. To characterize and measure the polarization of the inferred opinion distribution we propose different metrics based on the covariance matrix [3], which is the multidimensional generalization of the variance, a quantity often adopted as a one-dimensional measure of polarization. In particular, we use the trace of the covariance matrix (the total variation) as a global measure of opinion extremeness, and its eigendecomposition to quantify pole alignment (a multipolar analogue of opinion

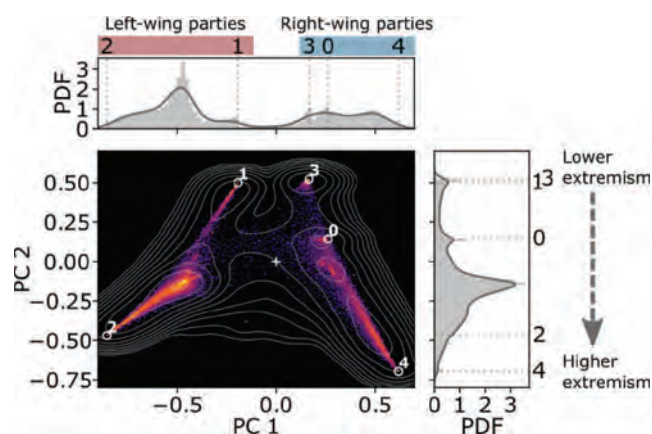


Fig. 2. Inferred ideological space of the Spanish general elections of 28 of April 2019. The 5 opinion poles are labeled from 0 to 4 and correspond to the main political parties (0-PP, 1-PSOE, 2-Podemos, 3-Cs, 4-Vox)

alignment), obtaining the direction of maximum polarization in the ideological space by principal components (PC).

We have applied this methodology to empirical Twitter data from multi-party elections: the Spanish general elections of 2015 (four poles) and 2019 (five poles).

Figure 1 shows the opinion space in the case of the 2015 Spanish general elections. Projections of the opinion distribution onto the simplex faces of the tetrahedron are shown as heat maps and contour plots. The centers of mass of the projected opinion distributions are represented as white squares and the projection of the direction of maximum polarization (PC 1), as a double-headed arrow. 1D projections onto each edge of the simplex are shown on the sides of the triangles.

Figure 2 shows the two-dimensional heatmap and contour plot corresponding to the projection of the inferred opinion distribution onto the first two PCs. The top and right plots respectively show the one-dimensional projection of the opinion distribution onto the first and second PCs. The parties are spontaneously sorted along the left-wing / right-wing axis in the first PC and according to their perceived extremeness in the second PC.

[1] Morales AJ, Borondo J, Losada JC, Benito RM. *Measuring political polarization: Twitter shows the two sides of Venezuela*. *Chaos* **25** (3) 033114 (2015).

[2] Borondo J, Morales A, Benito R, Losada J. *Multiple leaders on a multilayer social media*. *Chaos Solitons Fractals* **72** 908 (2015).

[3] Martin-Gutierrez, S, Losada, JC, Benito, RM. *Multipolar social systems: Measuring polarization beyond dichotomous contexts*. *Chaos Solitons and Fractals* **169** 113244 (2023).

Evolutionary Kuramoto Dilemma: Coevolution of Synchronization and Cooperation in Costly Networked Interactions

Alberto Antonioni¹, and Alessio Cardillo²

¹ Grupo Interdisciplinar de Sistemas Complejos (GISC), Universidad Carlos III de Madrid, Leganés, Spain

² Universitat Oberta de Catalunya, Internet Interdisciplinary Institute (IN3), UOC Campus Poblenou, Barcelona, Spain

The phenomenon of synchronization in coupled oscillating systems has been a subject of substantial interest, given its pervasive nature across a variety of fields [1]. From the rhythmic flashing of fireflies, circadian rhythms, to the periodic oscillations in mechanical, electrical, and quantum systems, synchronization finds diverse applications [2]. The patterns of interaction among individual oscillators are commonly modeled as a network or a graph, significantly impacting the genesis of the synchronized state [3]. Over the years, significant research efforts have delved into understanding the evolution of synchronization in populations of oscillators configured within a network [4]. These networks, representing the intricate web of interactions, are integral to dissecting the complexities of these dynamical systems.

However, many studies assume that the transition of an oscillator's state, necessary for achieving synchronization, is costless. While this assumption is convenient for theoretical modeling, it seems somewhat unrealistic. A more practical hypothesis would involve acknowledging that the modification of an oscillator's state involves a certain cost. This hypothesis brings forth a dichotomous scenario: an oscillator may decide to bear the cost necessary to alter its state, aligning it with the others, or it may remain in its current state, anticipating that the other oscillators will adjust their rhythm [5]. Interpreting this from a game-theoretic perspective, the former choice mirrors an act of cooperation, while the latter represents a choice of defection [6].

Complex networks play a vital role in the emergence of cooperative behavior, especially the presence of highly connected nodes, or hubs, in scale-free networks. Given this, it becomes essential to explore the mechanisms responsible for the onset of synchronization in a network of oscillators where each node must choose whether to cooperate by synchronizing their states with those of their neighbors or not. This line of inquiry leads us towards a coevolutionary approach, intertwining the dynamics of synchronization with game theory [7].

In this talk, I will present a novel coevolutionary model, which is built upon the combination of Kuramoto oscillators playing an evolutionary game [8]. We delve into the emergence of cooperation and synchronization in three different network topologies: Erdős-Rényi random graphs (ER), Random Geometric Graphs (RGG), and Barabási-Albert scale-free networks (BA). This comprehensive analysis provides a detailed view of the coevolutionary dynamics, revealing the principles that govern the behavior of these fascinating oscillating systems [9].

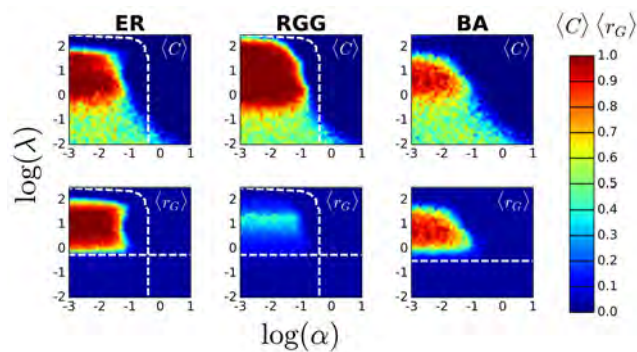


Fig. 1. Emergence of cooperation and synchronization at global scale. The top (bottom) row illustrates the average level of cooperation (synchronization) $\langle C \rangle$ ($\langle r_G \rangle$) as a function of the coupling λ and relative cost α . Each column corresponds to a different topology, namely, ER, RGG, and BA. Results are averages over 50 different realizations.

- [1] Pikovsky, A., Rosenblum, M., & Kurths, J. (2001). *Synchronization: A universal concept in nonlinear sciences*. Cambridge University Press.
- [2] Strogatz, S. H. (2003). *Sync: How order emerges from chaos in the universe, nature, and daily life*. Hyperion.
- [3] Arenas, A., Díaz-Guilera, A., Kurths, J., Moreno, Y., & Zhou, C. (2008). Synchronization in complex networks. *Physics Reports*, 469(3), 93-153.
- [4] Boccaletti, S., Latora, V., Moreno, Y., Chavez, M., & Hwang, D. (2006). Complex networks: Structure and dynamics. *Physics Reports*, 424(4-5), 175-308.
- [5] Abrams, D. M., Mirollo, R., Strogatz, S. H., & Wiley, D. A. (2008). Solvable model for chimera states of coupled oscillators. *Physical Review Letters*, 101(8), 084103.
- [6] Nowak, M. A. (2006). Five rules for the evolution of cooperation. *Science*, 314(5805), 1560-1563.
- [7] Szabó, G., & Fáth, G. (2007). Evolutionary games on graphs. *Physics Reports*, 446(4-6), 97-216.
- [8] Kuramoto, Y. (1975). Self-entrainment of a population of coupled non-linear oscillators. In H. Araki (Ed.), *International Symposium on Mathematical Problems in Theoretical Physics* (pp. 420-422). Springer.
- [9] Antonioni, A., & Cardillo, A. (2017). *Coevolution of Synchronization and Cooperation in Costly Networked Interactions*. *Physical Review Letters*, 119, 238301.

Topologically-induced suppression of explosive synchronization on graphs

Manuel Miranda¹, Mattia Frasca^{2,3} and Ernesto Estrada¹

¹ Institute of Cross-Disciplinary Physics and Complex Systems, IFISC (UIB-CSIC), 07122 Palma de Mallorca, Spain.

² Department of Electrical, Electronics and Computer Science Engineering, University of Catania, Italy.

³ Istituto di Analisi dei Sistemi ed Informatica A. Ruberti, Consiglio Nazionale delle Ricerche (IASI-CNR), Roma, Italy.

The transition from a disordered state to the one in which all the nodes oscillates with the same phase typically occurs in a gradual way, which is characteristic of second order transitions. Therefore, the discovery of explosive synchronization on the networked Kuramoto model [1] when there is a correlation between degree (topological feature) and natural frequency (dynamical feature) marked a tipping point in this field.

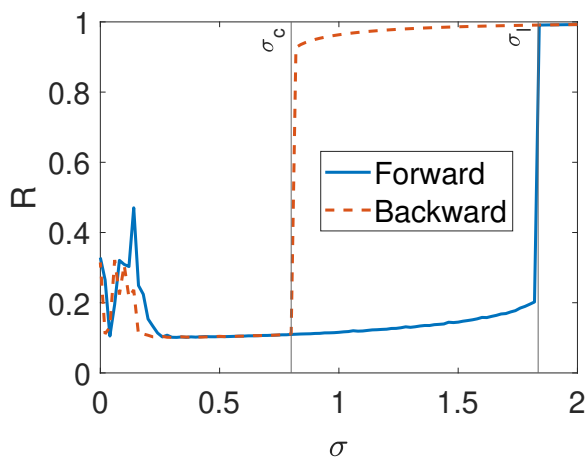


Fig. 1. Transition diagram on a star graph using the classic Laplacian.

For that purpose, we investigated how modifying the Kuramoto model by using degree-biased Laplacians [2] affects the explosive synchronization.

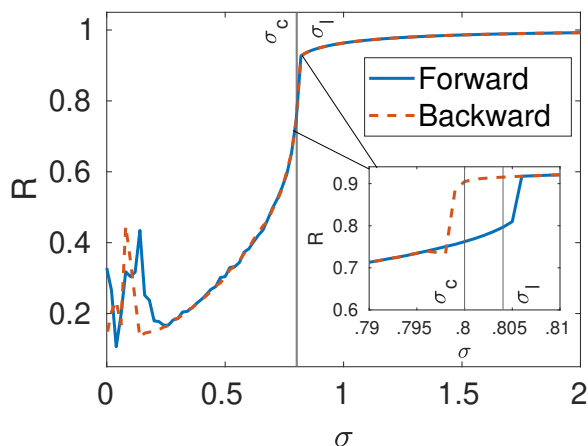


Fig. 2. Transition diagram on a star graph using the hubs-attracting Laplacian.

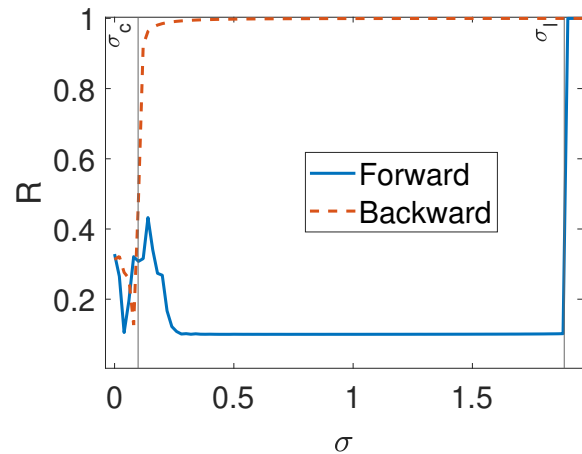


Fig. 3. Transition diagram on a star graph using the hubs-repelling Laplacian.

In this poster there will be shown the results in our latest article [3]. There we report how explosive synchronization is modified by these kind of operators, changing the points at which the transition occurs. Moreover, due to the heavy dependence between the operators and the network topology, we observed that the explosive synchronization happens on tree-like graphs, while it disappears for scale-free ones. Therefore, there is a transition between explosive synchronization in a branched acyclic system to normal one once cycles emerge in the system. This transition may represent a potential mechanism with which a neuronal system can synchronize explosively individual neurons, and returning to normal synchronization when the neuronal network is formed to avoid pathological states like epilepsy or chronic pain.

[1] J. Gmez-Gardenes, S. Gmez, A. Arenas, Y. Moreno. Explosive synchronization transitions in scale-free networks. *Physical review letters*, 106(12), 128701. (2011).

[2] M. Miranda, E. Estrada. Degree-biased advection-diffusion on undirected graphs/networks. *Mathematical Modelling of Natural Phenomena*, 17, 30. (2022).

[3] M. Miranda, M. Frasca, E. Estrada. Topologically induced suppression of explosive synchronization. *Chaos*, 33 (5): 053103. (2023)

D-Mercator: multidimensional hyperbolic embedding of real networks

Robert Jankowski^{1,2}, Antoine Allard^{3,4}, Marián Boguñá^{1,2} & M. Ángeles Serrano^{1,2,5}

¹Departament de Física de la Matèria Condensada, Universitat de Barcelona, Martí i Franquès 1, E-08028 Barcelona, Spain

²Universitat de Barcelona Institute of Complex Systems (UBICS), Universitat de Barcelona, Barcelona, Spain

³Département de physique, de génie physique et d'optique, Université Laval, Québec (Québec), Canada G1V 0A6

⁴ Centre interdisciplinaire en modélisation mathématique, Université Laval, Québec (Québec), Canada G1V 0A6

⁵ ICREA, Passeig Lluís Companys 23, E-08010 Barcelona, Spain

Summary

One of the pillars of the geometric approach to networks has been the development of model-based mapping tools that embed network topologies in their latent geometry. In particular, Mercator [1] embeds real networks into the hyperbolic plane. However, some real networks are better described by the multidimensional formulation of the underlying geometric model [2]. Here, we introduce *D*-Mercator [3], an embedding method that goes beyond Mercator to produce multidimensional maps of real networks into the $D + 1$ hyperbolic space where the similarity dimension is represented in a D -sphere. We evaluated the quality of the embeddings using synthetic S^D networks. We also produced multidimensional hyperbolic maps of real networks that provide more informative descriptions than their two-dimensional counterparts and reproduce their structure more faithfully. Having multidimensional representations will help to reveal the correlation of the dimensions identified with factors known to determine connectivity in real systems and to address fundamental issues that hinge on dimensionality, such as universality in critical behavior. *D*-Mercator also allows us to estimate the intrinsic dimensionality of real networks in terms of navigability and community structure, in good agreement with embedding-free estimations.

Multidimensional network model

Our approach assumes that real networks are well described by the geometric soft configuration model in D similarity dimensions, the S^D/H^{D+1} model [4], which is a multidimensional generalization of the S^1 model. In the S^D model, a node i is endowed with a hidden variable representing its popularity, influence, or importance, denoted κ_i and named hidden degree, and with a position \mathbf{v}_i in the D -dimensional similarity space, represented as a vector in a D -dimensional sphere. The connection probability between a node i and a node j takes the form of a gravity law:

$$p_{ij} = \frac{1}{1 + \chi_{ij}^\beta}, \quad \text{with } \chi_{ij} = \frac{R\Delta\theta_{ij}}{(\mu\kappa_i\kappa_j)^{1/D}}. \quad (1)$$

The separation $\Delta\theta_{ij} = \arccos\left(\frac{\mathbf{v}_i \cdot \mathbf{v}_j}{\|\mathbf{v}_i\| \|\mathbf{v}_j\|}\right)$ represents the angular distance between nodes i and j in the D -dimensional similarity space. The parameter β , named inverse temperature, calibrates the coupling of the network topology with the underlying metric space and controls the level of clustering, which grows with the increase of β . Finally, the parameter μ controls the average degree of the network.

Multidimensional maps of real world networks

Real networks can be embedded in any dimensions within the limits of *D*-Mercator. We compiled data for several real-world complex networks from different domains and embedded them in different dimensions. More specifically, here we present Add-health [5] network, which describes the friendships between high school students. In this case, the best embedding dimension is $D = 2$ such that the similarity subspace can be easily visualized in three dimensions as a 2-sphere.

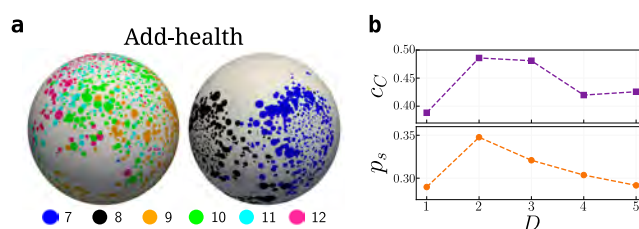


Fig. 1. Embeddings of Add-health network. (a) Two views of the *D*-Mercator embedding in $D = 2$. The size of a node is proportional to its expected degree. Nodes are colored based on their communities, i.e., a grade the student belongs to. Panel (b) shows the performance of geometric community concentration c_C and the success rate of greedy routing (p_s) in different embedded dimension.

-
- [1] García-Pérez, G., Allard, A., Serrano, M., and Boguñá M. Mercator: uncovering faithful hyperbolic embeddings of complex networks. *New Journal Of Physics*. **21**, 123033 (2019)
- [2] Almagro, P., Bogu, M. & Serrano, M. Detecting the ultra low dimensionality of real networks. *Nature Communications*. **13**, 6096 (2022,10,15), <https://doi.org/10.1038/s41467-022-33685-z>
- [3] Jankowski, R., Allard, A., Boguñá, M. & Serrano, M. *D*-Mercator: multidimensional hyperbolic embedding of real networks. *arXiv Preprint arXiv:2304.06580*. (2023)
- [4] Serrano, M., Krioukov, D. & Boguñá, M. Self-similarity of complex networks and hidden metric spaces. *Physical Review Letters*. **100**, 078701 (2008)
- [5] Moody, J. Peer influence groups: identifying dense clusters in large networks. *Social Networks*. **23**, 261-283 (2001)

Socioeconomic determinants of Stay-at-Home Policies during the First COVID-19 Wave

Pablo Valgañón^{1,3,a)}, David Soriano-Paños^{2,3}, Andrés F. Useche⁴, Gourab Ghoshal⁵ and Jesús Gómez-Gardeñes^{1,3}

¹Department of Condensed Matter Physics, University of Zaragoza, 50009 Zaragoza (Spain).

²Instituto Gulbenkian de Ciência (IGC), 2780-156 Oeiras (Portugal).

³GOTHAM lab, Institute for Biocomputation and Physics of Complex Systems (BIFI), University of Zaragoza, 50018 Zaragoza (Spain).

⁴Department of Industrial Engineering, School of Engineering, Universidad de Los Andes, 111711 Bogotá (Colombia).

⁵Department of Physics and Astronomy, University of Rochester, NY 14627 Rochester (United States).

The COVID-19 pandemic has had a significant impact on public health and social systems worldwide. In the absence of vaccines, the most widespread reaction to stop the spread of the disease was the implementation of lockdowns or stay-at-home policies. In spite of the reported usefulness of such policies, their efficiency was highly constrained by socioeconomic factors determining their feasibility and their outcome in terms of mobility reduction and the subsequent limitation of social activity. My talk will consist of two studies that aim to assess the impact of the socioeconomic class of the population in both following the restrictions and curbing the pandemic, at two different scales. First, we take a look at the efficacy of the policies implemented in 42 different countries, quantifying the *social permeability* which reflects the inability of individuals to remain in confinement and continue social mixing allowing the spread of the virus. After calibrating the model to incidence and mobility data, our results show (Fig.2) low-income countries have a harder time slowing the advance of the pandemic, even if the virus did not initially propagate as fast as in wealthier countries. The study highlights the disparities between countries in their ability to mitigate the spread of the disease and the impact on vulnerable populations. In the second part [1], we turn to a smaller scale and focus on the three largest cities of Colombia: Bogotá, Medellín and Cali, where we have shown that the first policies were not successful in containing the virus due to the social permeability. Here we investigate the impact of these restrictions on the mobility patterns of different socioeconomic classes in the mentioned cities during the first wave of the COVID-19 pandemic. In global terms, we find a consistent positive correlation between the reduction in mobility levels and the economic stratum of the population in every city, implying that those with lower incomes were less capable of adopting the aforementioned policies (Fig.1). Our analysis also suggests a strong restructuring of the mobility network of lowest socioeconomic strata during the lockdown, which increased their mixing while hampering their connections with wealthiest areas due to sharp reduction in long-distance trips.

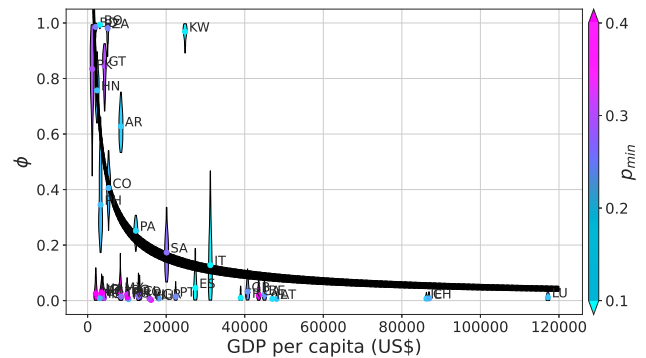


Fig. 1. Posterior distribution obtained for the permeability parameter ϕ as a function of the GDP per capita of the country in which the model is calibrated. The color represents the minimum mobility recorded during this time frame. The Spearman correlation coefficient ρ_S between both variables is $\rho_S = -0.590$ with p -value $< 10^{-4}$.

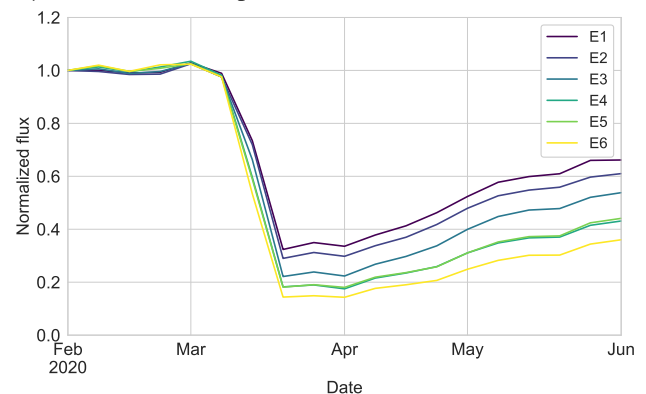


Fig. 2. Time evolution of the aggregated number of trips for each socioeconomic stratum (color code) in the city of Bogotá, re-scaled to a reference value set on 2020-02-02, corresponding to the pre-pandemic scenario.

[1] P. Valgañón, Andrés F. Useche, D. Soriano-Paños, Gourab Ghoshal and J. Gómez-Gardeñes, *Quantifying the heterogeneous impact of lockdown policies on different socioeconomic classes during the first COVID-19 wave in Colombia*, arXiv:2304.05746 [physics.soc-ph].

Structural properties of hard-disk fluids under single-file confinement

Ana M. Montero¹ and Andrés Santos^{1,2}

¹Departamento de Física, Universidad de Extremadura, E-06006 Badajoz, Spain.

²Instituto de Computación Científica Avanzada (ICCAEx), Universidad de Extremadura, E-06006 Badajoz, Spain

We consider a fluid of hard disks of unit diameter confined between two parallel walls separated by a distance $w = 1 + \epsilon \leq 1 + \sqrt{3}/2$ such that each disk can only interact with its two nearest neighbors. This highly confined system can be treated as a quasi one-dimensional (Q1D) system, where its longitudinal properties can be studied from an exact statistical-mechanical perspective.

In this work, we study the structural properties by means of a mapping of the original system onto a one-dimensional polydisperse mixture of non-additive hard rods [1], with all species in the mixture having equal chemical potential. The main idea of this mapping is that the transverse coordinate of each disk, $-\epsilon/2 < y < \epsilon/2$ represents the dispersity parameter and the longitudinal separation at contact, $a(y - y') = \sqrt{1 - (y - y')^2}$ is the hard-core distance of two ‘species’ (y and y'). A schematic representation of this mapping is shown in Fig. 1.

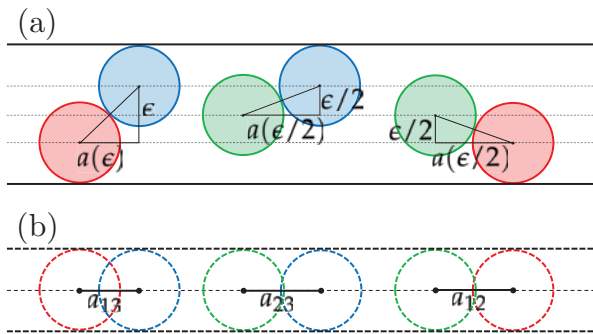


Fig. 1. Schematic representation of the mapping of (a) the original Q1D system onto (b) a 1D mixture of non-additive hard rods.

Standard liquid theory of mixtures is then used as a starting point to derive exact thermodynamic and structural properties, such as the structure factor, the radial distribution function (RDF) or the correlation length, of the mapped one-dimensional system. Comparisons with Monte Carlo simulation methods performed in the original Q1D system show an excellent agreement in all studied quantities. Figure 2 shows the longitudinal RDF for several values of the linear

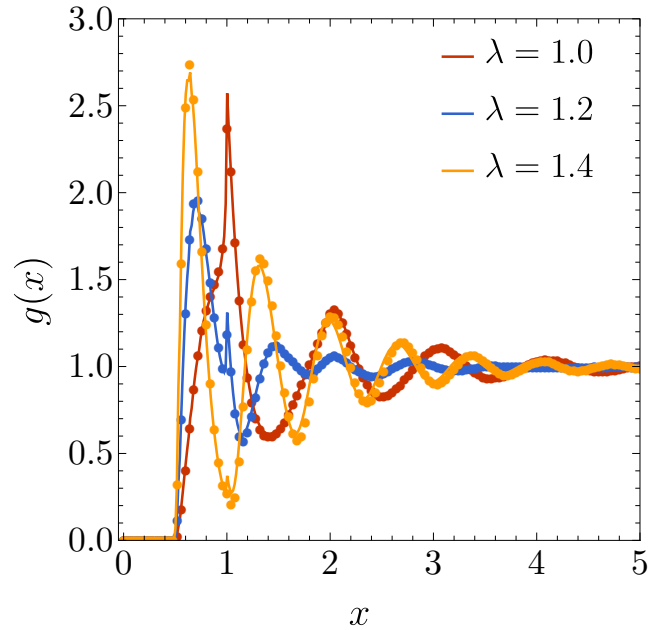


Fig. 2. RDF $g(x)$ for different values of density at $\epsilon = \sqrt{3}/2$. Solid lines are out theoretical results, while symbols are MC data from Ref. [2].

density λ for the maximum possible value of the channel width.

We have also analyzed the scaling form of the disappearance of defects in the zigzag configuration at high pressures. Moreover, by studying the nonzero poles of the Laplace transform of the RDF, we have obtained the translational correlation length and the asymptotic oscillation frequency, which show that a *structural crossover* takes place at a certain crossing pressure, where the asymptotic oscillation frequency experiences a discontinuous jump.

[1] A. M. Montero, and A. Santos, *Equation of state of hard-disk fluids under single-file confinement*, J. Chem. Phys. **158**, 154501 (2023).

[2] S. Varga, G. Balló, and P. Gurin, *Structural properties of hard disks in a narrow tube*, J. Stat. Mech. **2011**, 11006 (2011).

El complejo efecto de un obstculo al desatascar un silo con vibraciones

A. Garcimartín, R. Caitano, I. Zuriguel

Depto. de Física y Mat. Apl., Facultad de Ciencias, Universidad de Navarra, E-31080 Pamplona, Spain

Cuando se coloca un obstculo antes de la salida de un silo lleno de material granular, se crean menos arcos que taponen la salida y se atasca menos [1]. Pero si el silo se agita o se somete a vibraciones (un mtodo empleado frecuentemente para deshacer los atascos [2]), se desconoce cul puede ser el efecto combinado de ambas estrategias. En este trabajo experimental, examinamos qu ocurre al colocar un obstculo encima de la salida en un silo cuya base se somete a una vibracin (Fig. 1).

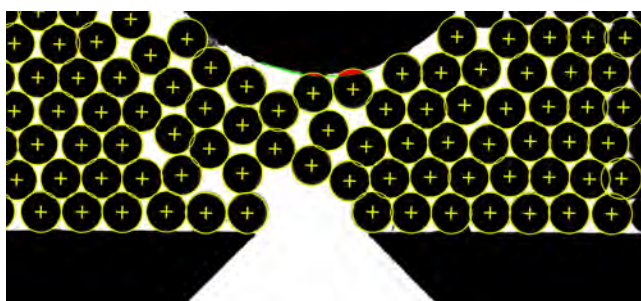


Fig. 1. Fotografía del orificio de salida del silo. Las dos piezas que conforman la base estn sometidas a una vibracin. El obstculo circular, colocado sobre la base, se muestra parcialmente. Las esferas tienen 1 mm de diámetro y se han detectado mediante análisis de imagen (sus centros se indican con una cruz amarilla). Las bolas que tocan el obstculo encima del orificio tienen una marca de color rojo.

Los resultados indican que el obstculo produce un doble efecto en un silo vibrado. Por un lado, los arcos ms dbiles se destruyen con ms rapidez que si no hubiera obstculo, lo cual contribuye a mejorar el flujo. Pero por otro lado, aparecen algunos arcos ms robustos que duran mucho tiempo aun cuando se les aplique una vibracin. As, los efectos beneficiosos que tienen la vibracin y el obstculo separadamente no se refuerzan mutuamente de manera simple.

Las mediciones que apoyan esa conclusin se muestran de manera condensada en la Fig. 2. En ella se comparan las distribuciones de las duraciones de los atascos entre el caso sin obstculo (\bar{O}) y con un obstculo (O) mediante grficos cuantil-cuantil. Se proporcionan las mediciones para seis valores de

intensidad de la vibracin, caracterizada mediante el parmetro $S = \frac{A \cdot \omega}{\sqrt{g \cdot l}}$, donde A y ω son la amplitud y la frecuencia angular de la vibracin, g la aceleracin de la gravedad y l el diámetro de una bola. Para S pequea, los atascos con un obstculo duran menos que si no est presente. Cuando aumenta S , los arcos de corta duracin (los ms dbiles) se destruyen antes, pero los atascos ms robustos duran incluso ms que si no hay obstculo (el grfico cuantil-cuantil atraviesa la bisectriz).

Probablemente eso se debe a que hay configuraciones que se apoyan en el obstculo y se incrementa la resistencia mec-

nica a la vibracin.

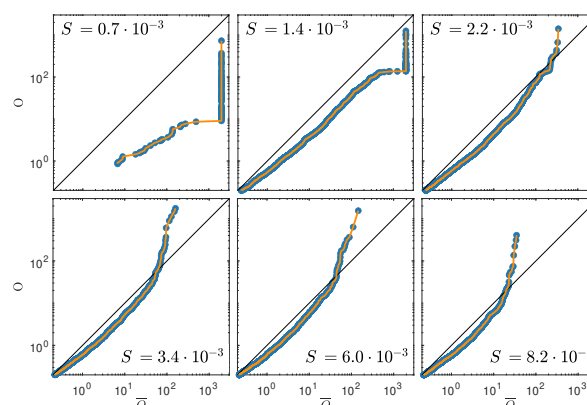


Fig. 2. Grficos cuantil-cuantil, que comparan las distribuciones de los tiempos que duran los atascos con obstculo (O) y sin obstculo (\bar{O}), para seis intensidades diferentes de la vibracin, indicada por S . Ntese la escala logarítmica.

[1] I. Zuriguel, A. Janda, A. Garcimartín, C. Lozano, R. Arvalo, and D. Maza, *Silo clogging reduction by the presence of an obstacle*, Phys. Rev. Lett. **107**, 278001 (2011)

[2] R. Caitano, B.V. Guerrero, R.E.R. González, I. Zuriguel, and A. Garcimartín, *Characterization of the clogging transition in vibrated granular media*, Phys. Rev. Lett. **127**, 148002 (2021)

Patient-specific beam delivery times in a synchrotron-based proton pencil beam scanning (PBS) system

Javier Burguete¹, Marina Garcia-Cardosa¹, P. Borja Aguilar², Elena Antolin² and Juan Diego Azcona².

¹ Department of Physics and Applied Mathematics, School of Sciences, Universidad de Navarra, Pamplona, Spain

² Department of Radiophysics and Radiological Protection, Clínica Universidad de Navarra, Madrid, Spain

Purpose: A proton beam therapy system is based on the Bragg peak effect: each proton interacts with the patient mainly along a straight pathway and delivers most of its energy on a specific location, whose depth depends on the initial energy of the incoming proton. This effect allows a much more accurate dose administration on tumors, avoiding healthy tissues. A treatment is delivered by a series of different bunches (spots) of protons with the same initial energy sent along straight lines (pencil beam). These series of spots can be distributed (modifying the initial energy and so the range) covering the tumor volume. The protontherapy system of the Clínica Universidad de Navarra consists on a synchrotron that can prepare a large cloud of protons (spill) that can be accelerated to different energies and redirected to the patient using a rotating gantry that can place these protons in any position inside the patient using magnets.

The purpose of this work is to characterize the beam delivery times for a group of 12 individual patients in a Hitachi synchrotron-based proton PBS system. Our goal is to derive a model that can achieve accurate predictions on the temporal sequences for individual plans. A secondary goal is to retrieve patient-specific temporal sequences to achieve time resolved dose calculations (blood circulation, breathing).

Materials and Method: The treatment plan establishes global requirements for the dose delivery that can be modified on the actual treatment delivery. Our system [1] is a ProBeat-CR (Hitachi) synchrotron that produces beams with 98 different energies, between 70.2 and 228.7 MeV. Values of relevant parameters such as dose rate (MU/s), spot, switch energy and spill change times, are specified by the manufacturer.

The irradiation times are obtained using a digital signal from the PBS console that indicates when the beam extraction is on. The signal is recorded using an oscilloscope with a 100MHz filter and a 31kHz sampling rate. The whole treatment plan is recorded, from the start of the first field to the end of the last field. The retrieved data are compared to the treatment plan, to verify the field sequence, and the timing for the different energy levels, spots and spills. The MU rate is reconstructed from the measured spot time compared to the intended treatment time. The number of spots per spill and energy levels per spill are estimated.

Results: A preliminary analysis in a group of 12 patients reveals that all the parameters are within the manufacturer specifications. Using these data we can derive patient-specific temporal sequences to achieve time resolved dose calculations (blood circulation, breathing). We have analyzed 31 Beams, 95 Energy values (with more than 1500 realizations), 650 Spills and more than 185000 spots.

Conclusions: We verified, on a daily and monthly ba-

sis using regular QA procedures, that the system delivered dose complied with the planned dose. Dose and MU delivery accuracy is ensured by the nozzle monitor chambers. Using the data recovered from the Console and the Hitachi Control Room we can record the specific delivery sequence for individual patients. Different signals can be analyzed (for instance, Beam On and Monitor Chamber) that provide data from different time scales. A model has been built to deal with the prediction of delivery times. Using this data we can model the time-resolved dose received by individual patients using on-purpose single energy layer dose distributions computed from Monte Carlo, and can be used to achieve accurate dose determination on circulating blood or breathing cycles.

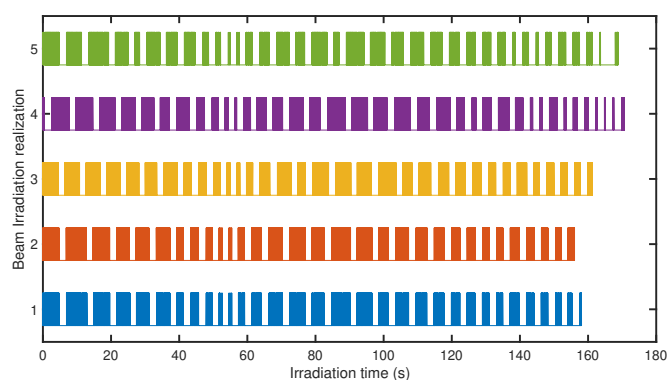


Fig. 1. Different realizations of the same field. Each band in a single realization corresponds to a different spill. The total irradiation time differs between realizations.

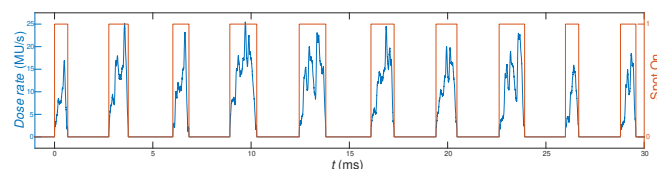


Fig. 2. Real dose rate delivered inside each spot.

[1] JD Azcona, B Aguilar, A Perales, R Polo, D Zucca, L Irazola, A Viñals, P Cabello, JM Delgado, D Pedrero, R Bermeiz, R Fayos-Solá, C Huesa-Berral, J Burguete, *Rad. Phys. and Chem.* **204**, 110708 (2023)

[2] Link to the group webpage:
<https://me-qr.com/T938BIDS>

Propulsion from energy bursts for nitromethane in water

Arnau Jurado Romero¹, Carles Calero Borrallo², and Rossend Rey Oriol¹

¹Universitat Politècnica de Catalunya, Jordi Girona, 1-3. B5, 08034 Barcelona

²Universitat de Barcelona, Martí i Franquès, 1, 11, 08028 Barcelona

Energy dissipation is of interest for the accurate generation and control of movement in micro and nano-particles. Studying molecular relaxation after a vibrational excitation has potential applications in multiple fields.

We consider the nitromethane molecule, whose energy relaxation after vibrational excitation has already been studied in argon gas [1, 2].

Prompted by the amphiphilic nature of nitromethane we study its relaxation in liquid water. We perform high energy excitations (200 kJ/mol) of individual modes and study energy relaxation via all-atom molecular dynamics simulations.

Our results show that, as expected, some normal modes relax considerably faster than others. These faster modes have associated motions related to the nitro group, which is to be expected due to the hydrophilic nature of the functional group.

To get more insight into the relaxation mechanisms we also studied the work performed by the nitromethane molecule on the surrounding water molecules [3]. Our main finding is that energy relaxation is remarkably asymmetric, favoring the nitro side (30% more work is performed to the nitro side).

To our knowledge this is the smallest molecule for which a marked asymmetry has been found, irrespective of the excited mode.

A combination of fast relaxation, asymmetry and translational work result in a short time impulse for select mode excitations. Repeated excitations result in enhanced diffusion.

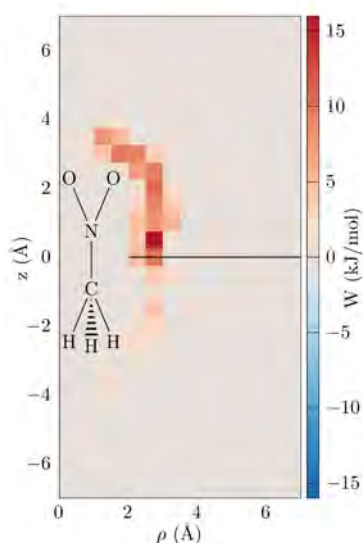


Fig. 1. Spatial distribution of the net work exerted by a nitromethane molecule on its liquid water environment once vibrational relaxation is complete, averaged over a set of microcanonically distributed excitations of 200 kJ/mol.

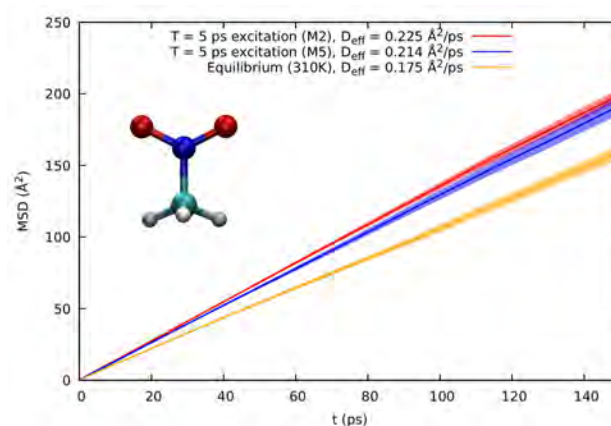


Fig. 2. Mean square displacement for repeated excitations of select normal modes of nitromethane and for equilibrium.

[1] Rivera-Rivera, L. A., Wagner, A. F., Sewell, T. D., and Thompson, D., *J. Chem. Phys.* **142**, 014303 (2015).

[2] Rivera-Rivera, Luis A. and Wagner, Albert F. and Perry, Jamin W., *J. Chem. Phys.* **151**, 034303 (2019).

[3] Rossend Rey and James T. Hynes, *PCCP* **14**, 6332 (2012).

[4] Calero, C., Sibert E. L. III, and Rey, R. *Nanoscale* **12** 7557 (2020)

[5] Jurado Romero, A., Calero, C., Sibert, E. L. III, and Rey, R., *J. Chem. Phys.* **158**, 194501 (2023).

On the binomial method for the generation of stochastic trajectories

Raúl Toral¹, Javier Aguilar¹ and Jose J. Ramasco¹

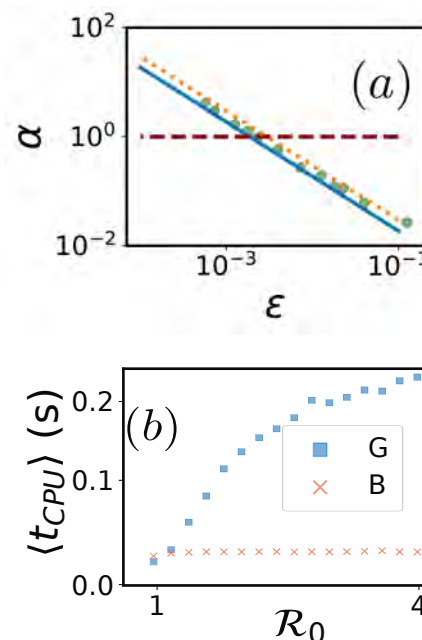
¹Instituto de Física Interdisciplinar y Sistemas Complejos IFISC (CSIC-UIB), Campus UIB, 07122 Palma de Mallorca, Spain.

Stochastic processes are one of the main pillars of complexity science [1]. Indeed, the list of fruitful applications is endless and we can name some paradigmatic examples like the study of population dynamics in ecology, gene expression, metabolism in cells, finances and market crashes, epidemiology, telecommunications, chemical reactions, quantum physics and active matter, to name a few [2]. As models become more intricate, there arises a technical challenge of producing numerically stochastic trajectories in feasible computation times, since unbiased methods that generate unbiased realizations of stochastic trajectories may become unpractical due to lengthy computations. Alternatively, approximate numerical methods are one of the most used strategies to extract information from many-interacting-agents systems. In particular, the binomial method is of extended use to deal with epidemic, ecological and biological models, when unbiased methods like the Gillespie algorithm can become unpractical due to high CPU time usage required. However, some authors have criticized the use of this approximation and there is no clear consensus about whether unbiased methods or the binomial approach is the best option [3, 4].

In this work, we analyze the issue on whether the binomial method is competitive compared to unbiased methods [5]. We proof, through both numerical and analytical evidence, that the systematic errors of the binomial method scale linearly with the discretization time. Using this result, we can establish a rule for selecting the optimal discretization time and number of simulations required to estimate averages with a fixed precision while minimizing CPU time consumption. Furthermore, we derive a rule of simple and practical use that can tell us in which cases the binomial method is superior to unbiased algorithms. In general, the advantage of using the binomial method depends on the target precision: the use of unbiased methods becomes more optimal as the target precision increases. We quantify the relative efficiency of the binomial versus the unbiased method as the ratio α of CPU times taken by each method to achieve a desired precision ϵ . In particular, values of $\alpha < 1$ indicate that the unbiased method is more effective than the binomial. We plot in panel (a) of the figure the ratio α as a function of the precision ϵ in the case of a simulation of an all-to-all connected Susceptible-Infected-Susceptible model. The dots are the results of the numerical simulations using the binomial method with the obtained optimal values for the discretization step and number of realizations, while the solid and dotted lines are theoretical result obtained from our scaling analysis. In panel (b) of the same figure we fix the precision $\epsilon = 0.01$, and plot the CPU-time to generate the ensemble of trajectories for different values of the basic reproductive number \mathcal{R}_0 for both the binomial (B) and the Gillespie (G) methods. Except for $\mathcal{R}_0 \approx 1$, where they perform similarly, the binomial method takes always less time

than the Gillespie algorithm.

In summary, this work provides a solution for the existing debate regarding the use of the binomial approximation to sample stochastic trajectories. The discretization time of the binomial method needs to be chosen carefully since large values can result in errors beyond the desired precision, while low values can produce extremely inefficient simulations. A proper balance between precision and CPU time consumption is necessary to fully exploit the potential of this approximation and make it useful. The efficiency of the binomial method is superior to the unbiased approaches only when the target precision is above a certain threshold value.



-
- [1] A. Argun, A. Callegari and G. Volpe, *Simulation of Complex Systems* (IOP Publishing, 2021)
 - [2] S. Thurner, R. Hanel and P. Klimek, *Introduction to the theory of complex systems* (Oxford University Press, 2018).
 - [3] S. Gómez, J. Gómez-Gardenes, Y. Moreno and A. Arenas, Nonperturbative heterogeneous mean-field approach to epidemic spreading in complex networks, *Phys. Rev.* **E84**, 036105 (2011).
 - [4] P.G.Fennell, G. Peter, S. Melnik and J.P. Gleeson, Limitations of discrete-time approaches to continuous-time contagion dynamics, *Phys. Rev.* **E94**, 052125 (2016).
 - [5] J. Aguilar, José J. Ramasco, Raúl Toral, Numerical methods for stochastic simulations: application to contagion processes arXiv:2305.02902.

The role of major signaling pathways in vertebrate neurogenesis

Mario Ledesma-Terrón^{1,2}, Diego Pérez-Dones^{1,2} and David G. Míguez^{1,2},

¹ Depto de Física de la Materia Condensada and IFIMAC, Universidad Autónoma de Madrid, Spain

² Centro de Biología Molecular Severo Ochoa, Universidad Autónoma de Madrid, Spain

The study of developmental processes often relies on image analysis, given the key influence of spatial cues such as morphogenes or contact inhibition in the regulation of stem cell differentiation. Unfortunately, imaging these dense three-dimensional developing organs results in reduced resolution, and reliable quantification of these images becomes very challenging.

To overcome these limitations, we have developed a novel Object Segmentation, Counter and Analysis Resource (OSCAR) specifically designed to quantify three-dimensional images from densely packed biological samples, such as developing organs in vertebrates.

In this contribution, we will explain the basics of how our tools is able to outperform other commercial solutions, and apply OSCAR to study the zebrafish developing retina, providing a quantitative characterization of the dynamics of the vertebrate retinogenesis in space and time with unprecedented accuracy.

Combined with small molecule inhibition treatment and a branching process mathematical formalism, we are able to unveil the role of major signaling pathways, such as HH, Wnt and Notch, in the regulation of the balance between proliferation and differentiation of neural stem cells into terminally differentiated neurons.

Our framework is not only valid for retinas of smaller vertebrates, and it is also very capable of extracting the number and location of all cells in other types of 3D cultures, such as neurospheres from mouse cerebral cortex cultured *in vitro* (see Fig. 1 for an example) or even retinal organoids from human iPS cells.

In the context of the developing retina, our results show that the Sonic Hedgehog pathway, a master regulator in the formation of potentially all organs in vertebrates, induces

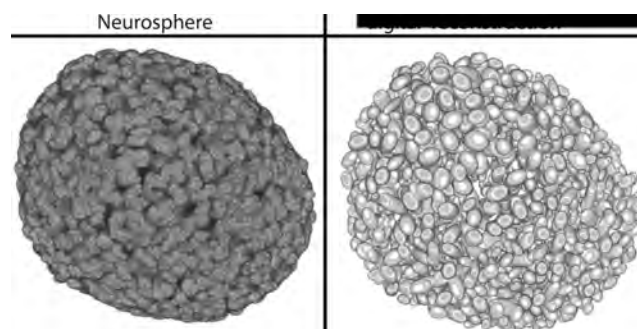


Fig. 1. Example of the capabilities of our framework OSCAR in extracting the location of each cell in a crowded three-dimensional tissue such as a neurosphere. Left) Original 3D image. Right) Digital representation using OSCAR output.

differentiation and cell cycle progression, while the Wnt-Frizzles pathway (Wnt) promotes cell cycle progression without affecting the cell cycle. Another major regulator of developmental processes, the Notch-Delta pathway, strongly reduces differentiation when inhibited, but it does so via arresting cell in the cell cycle. Overall, the combination of our image analysis and our branching process mathematical model allows us to obtain a clear picture of the role of each major signaling pathway in vertebrate neurogenesis.

[1] Mario Ledesma-Terrón, Diego Pérez-Dones and David G. Míguez, *In preparation* (2023).

[2] <https://www.cbm.uam.es>

A theoretical approach to the complex chemical evolution of phosphorus in the interstellar medium

Marina Fernández-Ruz^{1,2}, Jacobo Aguirre^{1,2}, and Izaskun Jiménez-Serra¹

¹Centro de Astrobiología CSIC-INTA, Madrid, Spain

²Grupo Interdisciplinar de Sistemas Complejos (GISC), Madrid, Spain

Phosphorus (P) chemistry in the Interstellar Medium (ISM) has become a topic of growing interest within the Astrobiology community [1]. P is present in many organic biomolecules such as phospholipids, nucleotides, and the energetic molecules ATP and GTP. On the other hand, many P-bearing species have been observed in astrophysical environments that cover a wide range of physical conditions, from cold molecular dark clouds to hot cores. Some of these molecules could have been introduced in the early Earth during the Late Heavy Bombardment that took place 4 billion years ago -inside asteroids or comets-, and importantly enriched prebiotic chemistry. This idea is supported by the recent discovery of certain P-bearing molecules in the comet 67P/Churyumov-Gerasimenko [2].

In particular, special attention has been recently paid to the abundances of PO and PN because, while most existing theoretical models lead to $PO/PN < 1$, high-sensitivity observations have revealed that PO is substantially more abundant than PN in many different environments [3], a question that has been informally named as the *interstellar phosphorus problem*.

In order to shed light on the interstellar phosphorus problem, in this work [4] we introduce a mathematical model for the time evolution of the P chemistry in an interstellar molecular cloud and analyze its associated chemical network as a complex dynamical system composed of 17 ODEs and 14 different chemical species. We obtain explicit mathematical expressions that describe the abundance evolution of all the P-bearing species involved in the network, whose interactions are represented in the sub-network shown in Fig. 1. Despite the approximations applied, our mathematical solution of the system agrees with very high precision with the numerical results, for all different species and for all values of time (Fig. 2).

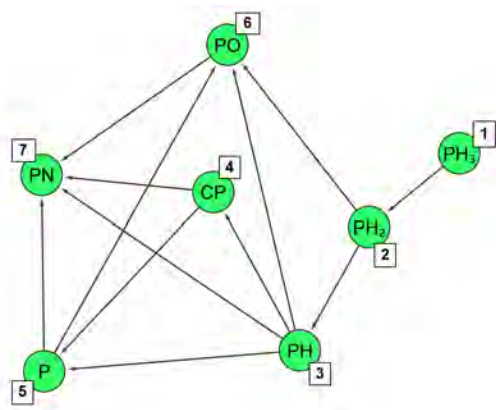


Fig. 1. Sub-network that sketches the theoretically solved system of the time evolution of P chemistry in an interstellar molecular cloud.

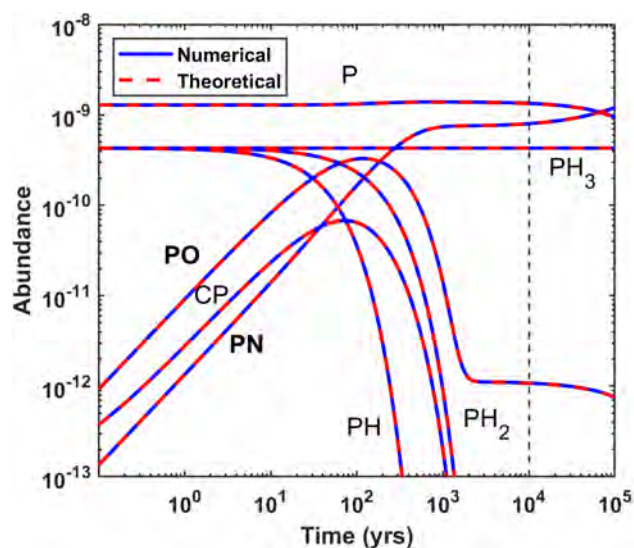


Fig. 2. Evolution of the abundances relative to H of the P-bearing molecules of a molecular cloud. A dashed vertical line remarks the typical cloud age, $t = 10^4 - 10^5$ yrs. This case represents a simulation at $T=10$ K.

Furthermore, our theoretical results allow much faster computation times than available numerical methods, being our model very powerful to analyze in detail the dependence of the chemical species abundances on the parameters. In particular, we focus on the rate coefficients of the chemical reactions involved in the model because most of them have not been calculated or measured and therefore their values are highly uncertain. Interestingly, we find that the formation of PO and PN is governed by a few critical reactions and we clearly show that the value of PO/PN is highly dependent on their rate coefficients, thus identifying a source that is significantly contributing to the PO/PN disagreement between models and real data. Next, we apply Bayesian inference to constrain the values of the most influential rate coefficients, obtaining results of $PO/PN > 1$ that match the observations and suggesting a plausible solution for the interstellar phosphorus problem.

[1] I. Jiménez-Serra, S. Viti, D. Quénard, and J. Holdship, *The Astrophysical Journal* **862**(2), 128 (2018).

[2] V.M. Rivilla *et al.*, *Monthly Notices of the Royal Astronomical Society* **492**, 1180 (2020).

[3] M. Sil *et al.*, *The Astronomical Journal* **162**, 119 (2021).

[4] M. Fernández-Ruz, I. Jiménez-Serra, and J. Aguirre, *A theoretical approach to the complex chemical evolution of phosphorus in the interstellar medium*, submitted.

Diffusion in colloidal monolayers: bridging the gap between two and three spatial dimensions

Alvaro Domínguez
 Universidad de Sevilla
 dominguez@us.es

It is well established that, unlike for a three-dimensional fluid, particle interactions prevent the hydrodynamic transport coefficients from being defined for a two-dimensional fluid due to the notorious “long-time tail” feature of the velocity autocorrelation.

A colloidal monolayer formed at a fluid interface builds a bridge between these two limiting cases, and it provides insight on the transition from three down to two spatial dimensions: the positions of the colloidal particles are constrained to a plane and the colloid thus resembles a two-dimensional fluid. But the exchange of particle momentum takes place in three-dimensional space because it is mediated by the ambient fluid in the form of hydrodynamic interactions.

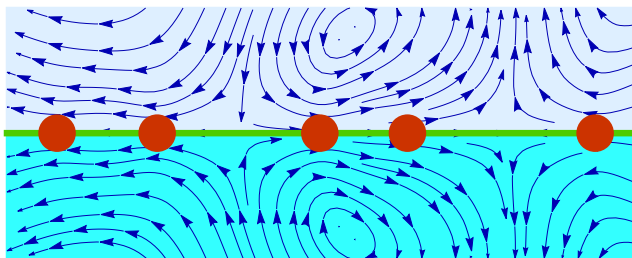


Fig. 1. Side view of a colloidal monolayer formed at the interface between two fluids, and sketch of the three-dimensional flows responsible for the hydrodynamic interactions.

Here we study the behavior of the colloidal diffusivity, which is the only hydrodynamic transport coefficient for the

two-dimensional colloidal fluid. The starting point is the Smoluchowski equation, i.e., the Fokker-Planck equation for the colloidal particles in the overdamped regime with due account of the hydrodynamic interactions. We show that the diffusivity exhibits an intermediate behavior between purely two-dimensional and fully three-dimensional fluid: on the one hand, Fick’s law, which pertains to *collective diffusion*, breaks down altogether [1, 2, 3], as confirmed experimentally [4]. On the other hand, the coefficient of *self-diffusion* (or single-particle diffusion) is finite [5], but the transitional nature of the monolayer shows up in a non-analytic dependence on the colloidal packing fraction [6], at odds with the case of a fully three-dimensional colloid.

-
- [1] J. Bleibel, A. Domínguez, F. Günther, J. Harting, M. Oettel, *Soft Matter* **10**, 2945 (2014).
 - [2] S. Panzuela, R. P. Peláez, R. Delgado-Buscalioni, *Physical Review E* **95**, 012602 (2017).
 - [3] J. Bleibel, A. Domínguez, M. Oettel, *Physical Review E* **95**, 032604 (2017).
 - [4] B. Lin, B. Cui, X. Xu, R. Zangi, H. Diamant, S. A. Rice, *Physical Review E* **89**, 022303, (2014).
 - [5] R. P. Peláez, F. Balboa Usabiaga, S. Panzuela, Q. Xiao, R. Delgado-Buscalioni, A. Donev, *Journal of Statistical Mechanics: Theory and Experiment*, 063207 (2018).
 - [6] A. Domínguez, in preparation (2023).

Universal fluctuations of global measurements in planar clusters

S. N. Santalla^{1,5}, I. Álvarez Domenech^{2,5}, D. Villarrubia^{3,5}, R. Cuerno^{3,5}, and J. Rodríguez-Laguna⁴

¹ Dep. de Física, Universidad Carlos III de Madrid, Spain.

² Dep. de Física Matemática y de Fluidos, UNED, Spain.

³ Dep. de Matemáticas, Universidad Carlos III de Madrid, Spain.

⁴ Dep. de Física Fundamental, UNED, Spain.

⁵ Grupo Interdisciplinar de Sistemas Complejos.

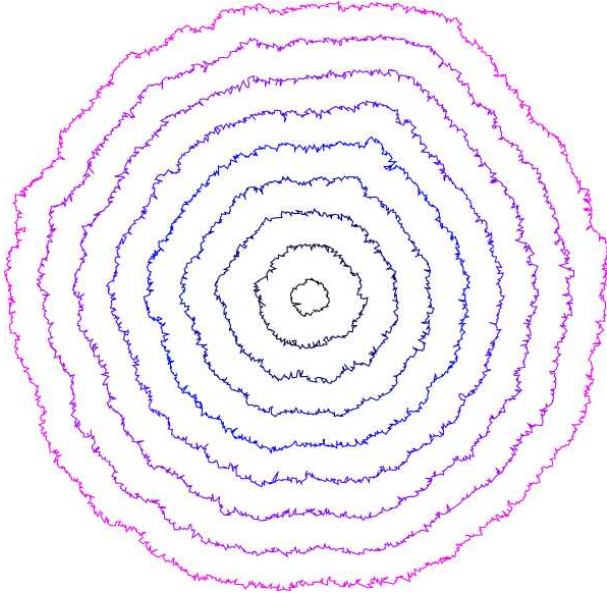


Fig. 1. Example of balls of increasing radii of a random metric.

The growth of interfaces in a noisy environment is, under broad conditions, described by the renowned Kardar-Parisi-Zhang (KPZ) universality class. Recently, a deep relation

between the KPZ class and random geometry was shown in the study of balls on random two-dimensional riemannian manifolds whose metric field is, in average, flat and presents only short-range correlations [1]. Moreover, it was shown that the choice of background manifold was crucial for the nature of the fluctuations: when the manifold is a cylinder, the radial fluctuations follow the TW-GOE distribution, while the distribution becomes TW-GUE when the manifold is a cone of any opening angle, or a plane [2].

Our aim in this work is to describe the statistical characterization of key geometric observables within the random metrics paradigm of the KPZ class, such as the area, length or position of the center of mass of the balls as those shown in the figure 1. These are all *global* observables of a given ball, as opposed to local ones, such as the radial fluctuations. As we will show, the fluctuations in all these global observables present a scaling behavior, with exponents associated to those of the KPZ class.

[1] S.N. Santalla, J. Rodríguez-Laguna, T. LaGatta and R. Cuerno, *Random geometry and the KardarParisiZhang universality class*, New J. Phys. **17** 033018 (2015).

[2] S.N. Santalla, J. Rodríguez-Laguna, A. Celi and R. Cuerno, *Topology and the KardarParisiZhang universality class*, J. Stat. Mech. 023201 (2017).

Impact of economic inequality on the emergence of intolerance in reputation-based societies

Luis A. Martínez-Vaquero^{1,2,3}

¹Grupo de Sistemas Complejos (GSC), Universidad Politécnica de Madrid, 28040 Madrid, Spain

²DEFE, Escuela Técnica Superior de Arquitectura, Universidad Politécnica de Madrid, 28040 Madrid, Spain

³Grupo Interdisciplinar de Sistemas Complejos (GISC), Madrid, Spain

Economic inequality has been reducing among nations during the last decades, however the difference between economic classes within countries has been continuously rising. Increasing evidence indicates that inequality could be one of the key causes of the emergence and expansion of intolerance, at least at the same level as the absolute economic income. On the other hand, modern societies have become highly dependent on public reputation systems, which shape their social dynamics.

Taking an evolutionary game theoretical perspective, this work studies how economic inequality impacts the emergence of intolerance [1]. A previous model of indirect reciprocity based on reputations [2] has been adapted to include inequality and intolerance. In indirect reciprocity, individuals assign other individuals reputations following the actions they witness and base future decisions on that reputation. The so-called *leading eight* strategies were found evolutionarily stable, with high payoffs, promoters of cooperation and robust against errors and cheating in this framework [3, 4]. In order to account for the effect of inequality in the current model, the population is also divided into two groups with different economic power, which limit their resources to cooperate. In addition, individuals are considered tolerant, if they follow a base leading eight strategy regardless the group of the others, and intolerant, if they always assign bad reputation to individuals from the opposite group, refuse to help them and assign bad (good) reputation to anyone who helps (refuses to help) someone from that opposite group. In this setup, it is studied under what circumstances intolerant behaviours can evolutionarily invade tolerant populations and under what conditions tolerance can be restored.

Results show that inequality is a powerful catalyser of intolerance. When inequality is significant, initial discriminatory behaviours escalate to the whole population even without introducing new intolerant individuals in the other group. It also changes the behaviour of individuals that manage to remain tolerant, especially among disfavoured minorities. Some of these individuals opt to behave as cooperatively as possible with their own in order to avoid the spread of bad reputation originated by the scarcity of resources, but reducing the punishment also against individuals that have fairly acquired bad reputation. On the other hand, disfavoured strategists that remain more strict tend to help more to wealthier individuals than to their own kind even if they receive discrimination in return.

This work also studies the efficacy of the redistribution of wealth as a mechanism to avoid intolerance (see Fig. 1). Results show that this policy can be successful, but only if it increases equality and, for a significant amount of scenarios, if it is applied before intolerance invades part of the population.

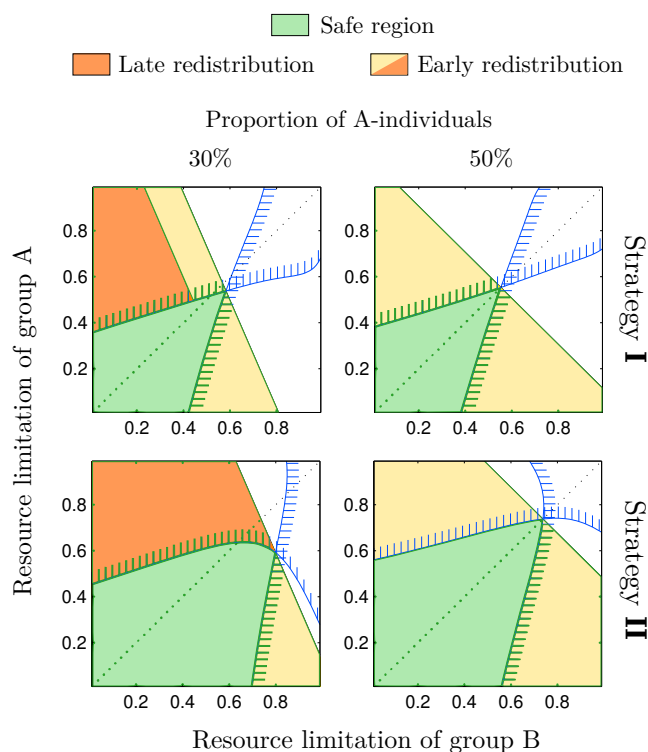


Fig. 1. Redistribution of wealth capacity to prevent intolerance for different proportions of individuals belonging to each group, resource limitations and base strategies. The area in green is safe from an invasion of intolerance while the yellow population can prevent intolerance through redistribution of wealth only if applied before intolerance appears. Redistribution of wealth can restore tolerance in the orange region, even after intolerance has invaded one group. Blue lines limit the parameter regions where intolerance can successfully invade a subpopulation.

- [1] L.A. Martínez-Vaquero, *Inequality leads to the evolution of intolerance in reputation-based populations*, Chaos **33**, 033119 (2023).
- [2] L.A. Martínez-Vaquero, J.A. Cuesta, *Spreading of intolerance under economic stress: Results from a reputation-based model*, Phys. Rev. E **90**(2), 022805 (2014).
- [3] L.A. Martínez-Vaquero, J.A. Cuesta, *Evolutionary stability and resistance to cheating in an indirect reciprocity model based on reputation*, Phys. Rev. E **87**(5), 052810 (2013).
- [4] H. Ohtsuki, Y. Iwasa, *The leading eight: Social norms that can maintain cooperation by indirect reciprocity*, J. Theor. Biol. **239**, 435444 (2006).

Un nuevo método personalizado de cálculo de la dosis recibida por la sangre circulante en los principales vasos en radioterapia de protones y fotones

M. Garcia-Cardosa¹, P. B. Aguilar², R. Meiriño³, M. Vidorreta⁴,
E. Antolin², J. D. Azcona², F. A. Calvo³ & J. Burguete¹.

¹Departamento de Física y Matemática Aplicada, Universidad de Navarra, Pamplona, España.

²Departamento de Radiofísica y Protección Radiológica, Clínica Universidad de Navarra, Madrid, España.

³Departamento de Oncología Radioterápica, Clínica Universidad de Navarra, Madrid, España.

⁴Siemens Healthineers, Madrid, España.

Se ha desarrollado un método novedoso que permite cuantificar la dosis administrada a la sangre circulante en los principales vasos sanguíneos durante un tratamiento de radioterapia. Este método es personalizado a cada paciente, justo al contrario de otros casos de la literatura [1, 2] que trabajan con modelos.

Este método trabaja con datos del propio paciente: la vasculatura, las lesiones tumorales, el campo de velocidad del flujo sanguíneo, los mapas de dosis de los niveles de energía usados para irradiar al paciente y la estructura temporal de la entrega del haz de radiación.

Un experto contornea los vasos sanguíneos y las lesiones tumorales utilizando la señal de amplitud de una secuencia de resonancia magnética de contraste de fase.

La estructura temporal de la irradiación se obtiene utilizando MonteCarlo en RayStation, se calcula un mapa de dosis para cada capa de energía que participa en cada campo de irradiación y se obtiene el tiempo de inicio y de fin de cada de cada capa de energía. Estos tiempos se miden a través de la consola del operador que trabaja con el acelerador.

Para poder representar el volumen de sangre de una manera fidedigna, se discretiza el volumen total de una persona y se divide en $5.5 \cdot 10^6$ partículas de sangre que tendrán un tamaño de 1mm^3 . Estas partículas de sangre viajan a lo largo de la vasculatura con un enfoque lagrangiano y se propagan con una velocidad medida.

La velocidad se ha medido utilizando una secuencia de resonancia magnética de contraste de fase. Hay que especificar que el campo de velocidad adquirido es una media temporal del flujo pulsátil y el desplazamiento de los vasos. Debido a este hecho, es necesario aplicar un método de corrección que acabe proporcionando un campo de velocidad que cumpla con la condición de que el flujo es incompresible, $\nabla \cdot \vec{v} = 0$, ya que el campo de velocidad promediado no cumple con la condición comentada, ver Figura 1.

Con esta información podemos obtener la dosis recibida por campo y por fracción en cada elemento de sangre para después acumular todas las fracciones con dos tipos de estrategias: pesimista y aleatoria. Llegados a este punto, se puede realizar un análisis estadístico: media, dosis, Histograma Dosis-Volumen (DVH), etc. Los resultados preliminares muestran que en un paciente el 2.5% del volumen sanguíneo recibió más de 0.1Gy, siendo la dosis más alta 0.72Gy para el 0.004% del volumen sanguíneo. Todo lo anterior, puede complementarse con un estudio

de robustez analizando el desplazamiento de los vasos, la determinación imprecisa del diámetro de los vasos y las incertidumbres del gasto cardíaco.

Por lo tanto, es factible tener y realizar un enfoque personalizado y específico para cada paciente que tenga como objetivo el determinar la dosis recibida en vasos y sangre durante un tratamiento de radioterapia de protones y fotones en la práctica clínica.

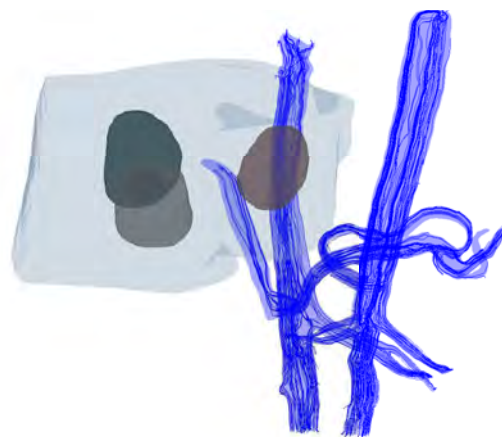


Fig. 1. Se representan las trayectorias (en color azul) creadas con el campo de velocidad procesado, $\nabla \cdot \vec{v} = 0$, las cuales visitan todos los lugares de la vasculatura para que las partículas sanguíneas puedan viajar. También se ilustran las lesiones tumorales de un paciente (en color verde oscuro, gris oscuro y marrón) y el mapa de dosis total (5% del máximo) que corresponde a todas las capas de energía que participan durante el tratamiento (en color gris claro).

[1] S. Xing et al, *A dynamic blood flow model to compute absorbed dose to circulating blood and lymphocytes in liver external beam radiotherapy*, Physics in Medicine & Biology 67.4 (2022): 045010.

[2] A. Hammi, H. Paganetti, and C. Grassberger, *4D blood flow model for dose calculation to circulating blood and lymphocytes*, Physics in Medicine & Biology 65.5 (2020): 055008.

[3] Link a la página web de nuestro grupo:
<https://me-qr.com/T938BIDS>

Prediction of the liquid-crystal phase behavior of hard right triangles from fourth-virial density functional theories

Yuri Martínez-Ratón¹ and Enrique Velasco²

¹Grupo Interdisciplinar de Sistemas Complejos, Departamento de Matemáticas, Universidad Carlos III de Madrid.

²Departamento de Física Teórica de la Materia Condensada, Universidad Autónoma de Madrid.

Two-dimensional fluids of nonregular polygons can stabilize liquid-crystal phases of exotic symmetries where entropy plays a subtle role. In these fluids particles tend to form local clusters of oriented particles that can be viewed as ‘superparticles’, with symmetries sometimes very different from that of the ‘monomers’ and therefore from the symmetry of the bulk liquid-crystal phase that would trivially follow from the monomers. Such is the case in fluids made of low-aspect-ratio rectangles, which tend to form highly stable square clusters that stabilise a global 4-atic phase (invariant over $2\pi/n$ rotations, with $n = 4$). The basic understanding of this phase lies in the excluded area between particles (second-order virial coefficient), an essential ingredient of the Scaled-Particle Theory (SPT) extension of classical Onsager theory. Three-body correlations can be incorporated into the theory through the third-order virial coefficients, and the ensuing corrections are important: the stability region of the 4-atic phase is extended to larger aspect ratios and lower densities.

Recently we have studied a fluid made of hard right-angle triangles (HRT) [1]. Motivated by Monte Carlo (MC) simulations by Gantapara et al. [2], we analysed the fluid using the standard SPT theory, based on the second virial coefficient (which is analytic), and an extension that includes the third-virial coefficient, calculated using MC integration. It turns out that none of these theories can reproduce the behaviour predicted from the simulations: as the isotropic fluid is compressed, clustering of particles in clusters of various shapes give rise to strong 8-atic correlations, and an orientational distribution function with 4-atic symmetry but high secondary peaks at 45° with respect to the main peaks results. The equilibrium orientational distribution function from the theories, by contrast, shows no hint of the high-order 8-atic symmetry. In a previous work we speculated [1] that a theory based on four-body correlations (i.e. on the fourth virial coefficient) might give some indication as to whether high-order particle correlations, involved in clus-

tering tendencies of the particles, might be important to understand the equilibrium structure of the fluid.

In the present work we show the predictions of such a theory. A resummed SPT theory is developed using the standard technique, which allows to systematically incorporate an arbitrary number of virial coefficients. These objects are generalised virial coefficients in the sense that they are functionals of the orientational distribution function. The third and fourth virial coefficients are computed numerically, and the instability of the isotropic (I) phase against orientational orders of different symmetries is investigated. This process allows to analyse the effect of increasing low-order, from two- to four-, particle correlations on the onset of bulk orientational order. Focusing on the 8-atic (or octatic) orientational symmetry, we explore the tendency of the fluid to stabilise orientational order through a bifurcation analysis. Our conclusion is that four-particle correlations do enhance octatic symmetry (see the table).

Bifurcation	I-2-atic	I-4-atic	I-6-atic	I-8-atic
η from SPT	0.8249	0.9928	0.9821	0.9444
η from B_3 -SPT	0.7325	0.9794	0.9328	0.8353
η from B_4 -SPT	0.7281	0.9681	0.8631	0.7399
η from B_5^* -SPT	0.7255	0.9590	0.8304	0.7091

Table 1. Values of the packing fractions η at I-2-atic, I-4-atic, I-6-atic and I-8-atic bifurcations from the SPT, B_3 -SPT, B_4 -SPT and B_5^* -SPT theories, the later implemented with a value of B_5 calculated by the extrapolation of $\{B_2, B_3, B_4\}$.

[1] Y. Martínez-Ratón and E. Velasco, Phys. Rev. E **104**, 054132 (2021).

[2] A. P. Gantapara, W. Qi and M. Dijkstra, Soft Matter **11**, 8684 (2015).

Modelado de Osciladores Biológicos con Retroalimentación Dual: Un Análisis de Ecuaciones Diferenciales con Retardo

Christian Cortés^{1,2,3}, Marcos Wappner⁴, Ernesto Nicola, Luis G. Morelli^{4,5}, Saúl Ares^{1,3}

¹Centro Nacional de Biotecnología (CNB) - CSIC, Madrid, España.

²Departamento de Matemáticas, Universidad Carlos III de Madrid, Madrid, España.

³Grupo Interdisciplinar de Sistemas Complejos (GISC)

⁴Instituto de Investigación en Biomedicina de Buenos Aires (IBioBA) - CONICET - Partner Institute of the Max Planck Society, Buenos Aires, Argentina.

⁵Departamento de Física, Universidad de Buenos Aires, Buenos Aires, Argentina.

Este trabajo se centra en el análisis de modelos matemáticos de osciladores biológicos con retroalimentación dual - positiva y negativa. Estos osciladores son relevantes en numerosos contextos biológicos, incluyendo ritmos cardíacos y ciclos celulares. Una característica clave de estos osciladores es su capacidad para variar en un amplio rango de frecuencias mientras mantienen una amplitud casi constante [1, 2, 3].

Centramos nuestra atención en dos modelos de ecuaciones diferenciales ordinarias unidimensionales con retardo temporal [4], que ofrecen un marco simplificado pero potente para investigar la formación de oscilaciones con amplitud constante. Estos modelos, aunque simplificados, capturan las características esenciales de los sistemas biológicos oscilantes, proporcionando así una base sólida para nuestro análisis.

El primer modelo que consideramos involucra la interacción de retroalimentación positiva y negativa, cuyo equilibrio determina la cota superior de las soluciones. En este caso, descubrimos que la bifurcación SNIC y Neimark-Sacker son esenciales para lograr las oscilaciones deseadas.

Por otro lado, el segundo modelo, derivado a partir de un *represillator* en que las variables están acotadas [1], logra una amplitud constante en sus soluciones ondulatorias a

través de una cota superior constante. Aquí, una bifurcación de Hopf es suficiente para obtener el comportamiento oscilatorio requerido.

Este trabajo no solo ofrece una visión más profunda de los osciladores biológicos, sino que también subraya la utilidad de las ecuaciones diferenciales con retardo en el modelado de estos complejos sistemas. Nuestro análisis ofrece nuevas herramientas y perspectivas para la comprensión de los ritmos biológicos.

-
- [1] T.Y.C. Tsai, Y.S. Choi, W. Ma, J.R. Pomeroy, C. Tang, and J.E. Ferrell Jr, *Robust, tunable biological oscillations from interlinked positive and negative feedback loops*, *Science*, **321**, 126 (2008).
 - [2] K. Maeda, and H. Kurata, *Long negative feedback loop enhances period tunability of biological oscillators*, *Journal of Theoretical Biology*, **440**, 21 (2018).
 - [3] J.I. Marrone, J.A. Sepulchre, and A.C Ventura, *A nested bistable module within a negative feedback loop ensures different types of oscillations in signaling systems*. *Scientific Reports*, **13**, 529 (2023)
 - [4] P. Amster, P. *Ecuaciones diferenciales con retardo*, *Cursos y Seminarios de Matemática - Serie B* (2017).

Non-equilibrium dynamics of microbial ecosystems

José Camacho-Mateu¹, Aniello Lampo¹, and José A Cuesta^{1,2}

¹ Grupo Interdisciplinar de Sistemas Complejos (GISC), Departamento de Matemáticas, Universidad Carlos III de Madrid, Leganés, Spain

² Instituto de Biocomputación y Física de Sistemas Complejos (BIFI), Universidad de Zaragoza, Zaragoza, Spain

Understanding the ecological forces that shape microbial communities is a fundamental problem in ecology. In this context, macroecology has established itself as an important top-down approach to connect such mechanisms with the statistical patterns of coexistence, abundance and diversity. In this work, we unveil some of the mechanistic consequences of the Ecological Forces upon the emergence of macroecological patterns. For this purpose, we advanced a population dynamics model which explicitly takes into account microbial interactions and resources fluctuations:

$$\dot{x}_i = \frac{x_i}{\tau_i} \left(1 - \frac{x_i}{K_i} + \sum_{j \neq i}^S a_{ij} x_j \right) + x_i \xi_i(t) \quad (1)$$

where x_i is the abundance of species i , S is the total number of species, τ_i is the time scale of basal population growth, K_i is the maximum carrying capacity, $(a_{ij}) = \hat{A}$ is the Lotka-Volterra interaction matrix and ξ_i is a zero-mean Gaussian noise with correlations $\langle \xi_i(t) \xi_j(t') \rangle = w_{ij} \delta(t-t')$ —aimed to describe environmental fluctuations—.

Experimental evidence suggests modelling *biotic* interactions through matrix \hat{A} , which describes a weighted and directed network whose nodes represent species and edges represent interactions strength and direction. On the other hand, *abiotic* factors are encoded in the diffusion matrix, $\hat{D} = (w_{ij} x_i x_j)$. When $i \neq j$, w_{ij} describes the resource preference of the pair of species (i, j) , thus if $w_{ij} > 0$ species have a preference for the same resources/environmental conditions, whereas they have an opposite preference if $w_{ij} < 0$.

Both types of ecological forces have gathered significant attention in recent works [1, 2, 3]. Direct species interactions \hat{A} , for instance, play a pivotal role in reproducing abundance correlations [1], while the response of species to environmental fluctuations, \hat{D} , can yield correlations based on phylogenetic closeness [2]. However, the dynamics of ecosystems remains understudied when both types of interactions coexist. In our work, we unveil the intricate interplay between biotic and abiotic forces, elucidating non-trivial effects that elude comprehension through the analysis of each force type in isolation. For instance, the single-species patterns [3] are independent of resource fluctuations when considered alone but produce alterations when considered at the same time with interactions. Even though, closed analytical solutions of equation (1) can not be obtained, it can be solved using a mean field approximation, which is accurate

enough for a wide range of parameters.

Finally, the interplay of ecological forces maintains the ecosystem out of thermodynamic equilibrium, which we elucidate through the synthesis of four distinct dynamical forces (see Fig. 1 for a two-dimensional example). Equilibrium (detailed balance is fulfilled) is only achieved when the magnitudes of biotic and abiotic factors are equal yet opposing in direction. Importantly, we establish that under such a regime, model equation (1) is equivalent to the "stochastic consumer-resource" model, a well-established framework widely employed in the study of microbial ecosystems. Our findings demonstrate that our proposed model serves as a concrete instantiating of the established one, providing further validation and applicability to the field.

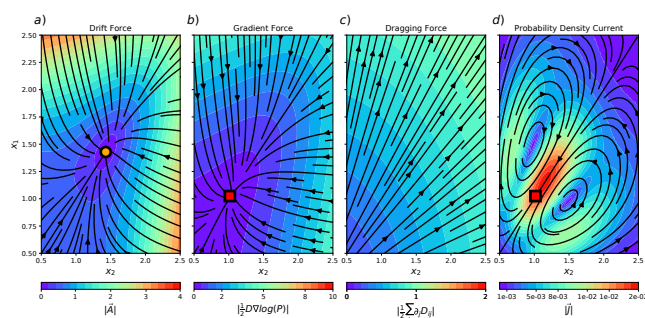


Fig. 1. Non-equilibrium dynamics of a two species ecosystems. The existence of a non-vanishing probability flux at steady state, panel **d**), indicates that the detailed balance is broken. The driving force of equation (1), panel **a**), can be decomposed into a part that is the negative gradient of a non-equilibrium potential, panels **b**) and **c**), and a part involving a rotational curl, panel **d**).

-
- [1] J. Camacho-Mateu, A. Lampo, M. Sireci, MA. Muñoz and J. Cuesta, *Species interactions reproduce abundance correlations patterns in microbial communities*, arXiv:2305.19154.
- [2] M. Sireci, MA. Muñoz, J. Grilli, *Environmental fluctuations explain the universal decay of species-abundance correlations with phylogenetic distance*. *bioRxiv*, 2022-07.
- [3] J. Grilli, *Macroecological laws describe variation and diversity in microbial communities*. *Nature communications*, 11(1), 4743.

Nonequilibrium properties of granular gases of rough particles

Alberto Megías¹, and Andrés Santos²

¹ Departamento de Física, Universidad de Extremadura, E-06006 Badajoz, Spain

² Instituto de Computación Científica Avanzada (ICCAEx), Universidad de Extremadura, E-06006 Badajoz, Spain

Granular matter, under rapid flow conditions, follows a gas-like behavior with dissipative interactions, in which classical kinetic-theory tools can be used as the proper theoretical framework. The simplest way of describing these particles and their interactions consists in considering hard disks or spheres colliding inelastically with a constant coefficient of normal restitution, α . However, recent experiments [1] highlight the importance of the implementation, in the collisional models, of the surface roughness of the granular particles to improve the theoretical predictions.

In this work, we study a monodisperse and dilute granular gas of inelastic and rough hard particles, with certain reduced moment of inertia κ , with and without external energy injection, from theory and computer simulations. The original inelastic model is improved by accounting for the effect of roughness via a constant coefficient of tangential restitution, β . We characterize the nonequilibrium properties of a homogeneous granular gas in terms of the violation of equipartition via the rotational-to-translational temperature ratio θ , and the nonGaussianities of the long-time-limit velocity distribution function (VDF), by means of the first nontrivial cumulants (a_{20} , a_{02} , a_{11} in the case of hard disks) and the marginal high-velocity tails (HVT).

In free evolution, the homogeneous system collapses to the homogeneous cooling state (HCS), where all the system evolution is driven through the temperature decay due to energy dissipation. The nonequilibrium properties of the HCS are much stronger than in the smooth case (see Fig. 1), where a divergence of an infinite set of velocity moments appears as a consequence of a scale-free HVT of the HCS marginal VDF of angular velocities [2] (see Table 1). These results are even more important for hard disks, which can be the consequence of recently reported strong instabilities of the hydrodynamic description of the system [3, 4].

On the other hand, we consider the homogeneous and driven case in terms of a thermostat that injects energy to the translational and rotational degrees of freedom. The system reaches a nonequilibrium steady state (NESS), in which the mean granular temperature depends on the whole energy injection, but the rest of nonequilibrium properties are only subjected to the fraction of rotational energy injected with respect to the total, ε . Whereas the violation of equipartition is still important, the nonGaussian features of the NESS VDF are much softer than in the HCS case, as novel results of the first nontrivial cumulants (see Fig. 2) and the HVT of the translational and rotational marginal VDF show. The cumulant divergences vanish, as own by the form of the HVT for this case (see Table 1). Moreover, the description of the transient states in terms of a Maxwellian approximation fits very well with simulation results, and the emergence of memory effects is essentially based on the nonequipartition [5].

Those predictions show a good agreement with results from direct simulation Monte Carlo (DSMC) and event-driven molecular dynamics (EDMD) algorithms (see [2] for

the HCS case), and with recent experimental results [6].

Table 1. Theoretical HVT for the marginal VDF

Marginal VDF	HCS	NESS
Translational $f_t(\mathbf{c})$	Exponential $e^{-\gamma c}$	Stretched exponential $e^{-\lambda c^{3/2}}$
Rotational $f_r(\mathbf{w})$	Scale-free $w^{-\gamma w}$	Exponential $e^{-\lambda w}$

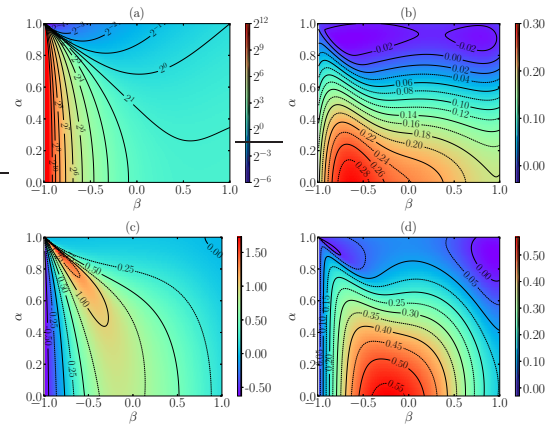


Fig. 1. Theoretical HCS values of (a) θ , (b) a_{20} , (c) a_{02} , and (d) a_{11} for hard disks with $\kappa = 1/2$, versus α and β .

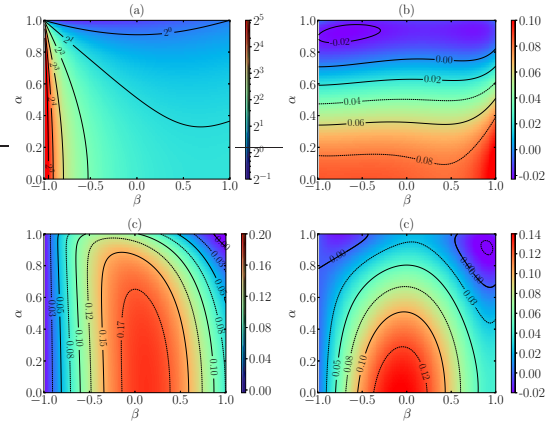


Fig. 2. Same as Fig 2, but for the NESS with $\varepsilon = 1/2$.

[1] P. Yu, M. Schröter, and M. Sperl, Phys. Rev. E **124**, 208007 (2020).

[2] A. Megías and A. Santos, arXiv:2303.00057 (2023).

[3] A. Megías and A. Santos, Phys. Rev. E **104**, 034901 (2021).

[4] A. Megías and A. Santos, Phys. Rev. E **104**, 034902 (2021).

[5] A. Megías and A. Santos, Front. Phys. **10**, 971671 (2022).

[6] J-B. Gorce and E. Falcon, Phys. Rev. E **107**, 034903 (2023).

Amplitude modulation control of spatiotemporal chaos in starlike networks of damped-driven pendula

R. Chacón¹, A. Martínez García-Hoz² and F. Palmero³,

¹ Departamento de Física Aplicada, Escuela de Ingenierías Industriales, Universidad de Extremadura, Apartado Postal 382, E-06006 Badajoz, Spain and Instituto de Computación Científica Avanzada (ICCAEx), Universidad de Extremadura, E-06006 Badajoz, Spain

² Departamento de Física Aplicada, E. T. S. de Ingenieros Agrónomos, Universidad de Castilla-La Mancha, E-13071 Ciudad Real, Spain

³ Departamento de Física Aplicada I, Escuela Técnica Superior de Ingeniería Informática, Universidad de Sevilla, Avda Reina Mercedes s/n, E-41012 Sevilla, Spain

Introduction

Applying amplitude modulations to a parametrically excited damped pendulum is shown to be a reliable method to control (suppress or enhance) its chaotic behaviour. Analytical (Melnikov analysis) and numerical (Lyapunov exponents and bifurcation diagrams) results show an effective control scenario. The method's effectiveness at suppressing spatiotemporal chaos of starlike networks of sinusoidally coupled chaotic pendula is demonstrated where effective regularization is obtained under localized control on an increasing number of pendula.

A single pendulum case

We consider the equation of a dissipative pendulum whose pivot is subjected to a vertical oscillation having a small resonant amplitude modulation:

$$\ddot{\theta} + \sin \theta = -\delta \dot{\theta} - \gamma [1 + \varepsilon \cos(\Omega t + \phi)] \cos(\omega t) \sin \theta, \quad (1)$$

where $-\gamma \varepsilon \cos(\Omega t + \phi) \cos(\omega t) \sin \theta$, is the control excitation. When the control excitation is absent ($\varepsilon = 0$), we assume that the pendulum has a chaotic attractor for a given set of the remaining parameters. A summary of some of the results is shown in Fig. 1.

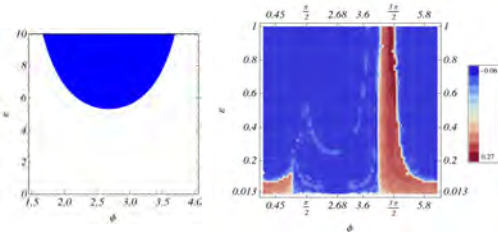


Fig. 1. Typical boundary function encircling the regularization regions where homoclinic bifurcations are frustrated obtained from Melnikov analysis (left) and maximal Lyapunov exponent obtained numerically (right) in the $\phi - \varepsilon$ parameter plane. The quantities plotted are dimensionless.

Controlling chaos in starlike networks

We will study the application of the above control scenario to a topology consisting of a starlike network (one hub and $N - 1$ peripheral leaves) where each node is occupied by a chaotic pendulum and where the CC excitation is solely applied to a number, M , of pendula:

$$\begin{aligned} \ddot{\theta}_i + \sin \theta_i &= -\gamma [1 + \sigma_H F_c(t)] \cos(\omega t) \sin \theta_i \\ &\quad - \delta \dot{\theta}_i + \lambda \sin(\theta_H - \theta_i), \\ \ddot{\theta}_H + \sin \theta_H &= -\delta \dot{\theta}_H - \gamma [1 + \sigma_H F_c(t)] \cos(\omega t) \sin \theta_H \\ &\quad - \lambda \sum_{i=1}^{N-1} \sin(\theta_i - \theta_H), \end{aligned} \quad (2)$$

$i = 1, \dots, N - 1$. These equations describe the dynamics of a highly connected node (or hub), θ_H , and $N - 1$ linked pendula (or leaves), θ_i , with $F_c(t) \equiv \varepsilon \cos(\Omega t + \varphi)$ being the (local) CC excitation, while σ_H (σ_i) is equal to 1 when the CC excitation acts on the hub (leaf i) and 0 otherwise, while λ is the coupling constant. Main results are shown in Figs. 2 and 3.

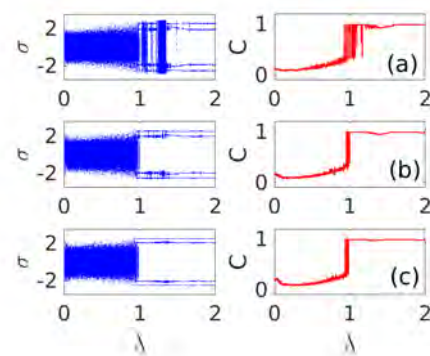


Fig. 2. Typical bifurcation diagrams of the average velocity σ and correlation function C as functions of the coupling parameter λ ($N = 10$, and the hub being the node 10). (a) $M = 1$. (b) $M = 2$. (c) $M = 3$. The quantities plotted are dimensionless and all pendula are initially desynchronized.

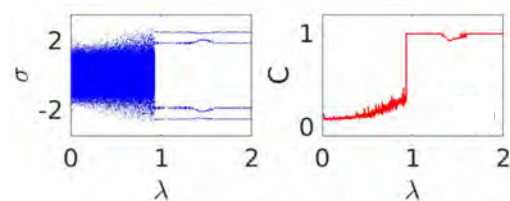


Fig. 3. Typical bifurcation diagrams of the average velocity σ and correlation function C as functions of the coupling parameter λ for $N = 10$. All pendula are asynchronous at $t = 0$. The hub (node 10) is the single pendulum subjected to multiplicative control. The quantities plotted are dimensionless.

Conclusions

We have shown theoretically and numerically that the application of suitable amplitude modulations is a reliable procedure to control (suppress and enhance) the chaotic behaviour of both isolated parametrically excited damped pendula and starlike networks of them subjected to sinusoidal coupling.

Emergence of chaos in complex networks of damped-driven nonlinear systems

Ricardo Chacón¹, Pedro J. Martínez²

¹Departamento de Física Aplicada, E.I.I., Universidad de Extremadura, Apartado Postal 382, E-06006 Badajoz, Spain and Instituto de Computación Científica Avanzada (ICCAEx), Universidad de Extremadura, E-06006 Badajoz, Spain

²Departamento de Física Aplicada, E.I.N.A., Universidad de Zaragoza, E-50018 Zaragoza, Spain

Characterizing the emergence of chaotic dynamics of complex networks is an essential task in nonlinear science with potential important applications in many fields such as neural control engineering, microgrid technologies, and ecological networks. Here, with the aid of a hierarchy of low-dimensional effective models, we theoretically characterize the interplay among heterogeneous connectivity, variation of the impulse transmitted by a homogeneous periodic excitation, and its driving period in the emergence and persistence of spatio-temporal chaos in starlike networks of damped-driven bistable systems, while they exhibit regular behavior when uncoupled. Numerical experiments fully confirmed the theoretical predictions showing how the onset and strength of chaos undergo resonancelike behaviors because of the conjoint effects of the connectivity degree and

the driving impulse, on one hand, and the conjoint effects of the connectivity degree and the driving period, on the other, both in the significant weak-coupling regime in which the networks present asynchronous states. Remarkably, scale-free networks of the same systems retain the main features of the starlike network scenario, thus suggesting its universal character.

-
- [1] S. P. Cornelius, W. L. Kath, and A. E. Motter, *Nat. Commun.* **4**, 1942 (2013).
- [2] I. Klickstein, A. Shirin, and F. Sorrentino, *Phys. Rev. Lett.* **119**, 268301 (2017).

Una técnica para la estimación de umbrales de percolación en sistemas de redes: Aplicación a un problema de flujo granular a través de un orificio

A. A. Torres¹, R. Caitano², and A. J. Ramirez-Pastor¹

¹Departamento de Física, Instituto de Física Aplicada, Universidad Nacional de San Luis-CONICET, Ejército de Los Andes 950, D5700BWS San Luis, Argentina

²Departamento de Física y Mat. Apl., Facultad de Ciencias, Universidad de Navarra, E-31080 Pamplona, Spain

Desde su introducción en la década de 1950 propuesta por Hammersley y Broadbent, el problema de la percolación ha sido de gran interés en la física estadística y de la materia condensada. Aunque se originó en el estudio del flujo de fluidos en medios porosos, la percolación se ha aplicado a diversos campos científicos donde la conectividad y la agrupación son importantes. En este estudio, se propone una nueva técnica, en la cual llamamos de *Multiple Effective Thresholds* (MET), para estimar umbrales de percolación en sistemas de redes [1]. Esta técnica complementa el método de Yonezawa, Sakamoto y Hori (YSH), y permite una determinación precisa de los umbrales de percolación en el límite termodinámico sin requerir conocimiento completo de las funciones de probabilidad. Se validó la técnica mediante el análisis de percolación en redes cuadradas y se aplicó al análisis de transiciones de obstrucción en un silo bidimensional con la base vibrada. Con el cual se describe la transición entre un estado atascado y un estado desatascado. El sistema experimental se describe y analiza en [2].

El método YSH se basa en la definición de las probabilidades $R_L^X(p)$ para encontrar un cluster de percolación de tipo X en una red finita de tamaño L [X puede ser horizontal (H), vertical (V), promedio (A), intersección (I) o unión (U)]. Las funciones $R_L^X(p)$ se obtienen mediante simulación. A continuación, los umbrales efectivos de percolación $p_c^X(L)$ se calculan a partir de las posiciones de los puntos de inflexión de las funciones de probabilidad (ver Fig. 1). Una vez que se determinan estos valores para varios tamaños de red, se puede realizar un análisis de escalamiento para calcular el umbral de percolación en el límite termodinámico $p_c^X(\infty)$:

$$p_c^X(L) = p_c^X(\infty) + A^X L^{-1/\nu}, \quad X \equiv \{U, I, A\} \quad (1)$$

donde A^X es una constante no universal y ν es el exponente crítico de la longitud de correlación, que se muestra analíticamente igual a $\nu = 4/3$ en el caso de percolación aleatoria.

Con el método MET, se pueden obtener múltiples umbrales efectivos $p_c^{X,r}(L)$ para cada criterio X a partir de la condición $R_L^X(p) = r$ (donde r es un parámetro que varía entre 0 y 1 (ver Fig. 1)). Los valores resultantes $p_c^{X,r}(L)$ siguen la conocida ley de escalamiento en la ecuación 2.

$$p_c^{X,r}(L) = p_c^{X,r}(\infty) + A^{X,r} L^{-1/\nu}, \quad X \equiv \{U, I, A\} \quad (2)$$

Los valores de $p_c^{X,r}(\infty)$ obtenidos a partir de las extrapolaciones dadas por la ecuación 2 permiten una determinación muy precisa del umbral de percolación en el límite termodinámico.

El método MET se aplicó a un conjunto de series temporales obtenidas de los experimentos estudiados en [2]. Estas series se caracterizan por los tiempos de obstrucción y flujo, para diferentes, niveles de vibración y tamaños de orificios.

A través de este análisis, hemos demostrado que la transición de fase observada en el sistema granular puede ser comprendida en términos de la transición de fase de percolación. En el régimen de obstrucción, el paso de partículas a través del orificio de descarga se caracteriza por períodos cortos de flujo interrumpidos por obstrucciones. Esto se traduce en la existencia de pequeños grupos finitos desconectados entre sí (región no percolante). En contraste, en el régimen de desobstrucción se observa un flujo continuo de material, similar a la existencia de un grupo percolante que conecta las regiones extremas del sistema (región percolante). Los resultados demuestran la eficacia de esta nueva técnica para calcular umbrales de percolación en diferentes escenarios, indicando que el método MET es una herramienta útil tanto para sistemas estructurados como para sistemas reales con información limitada.

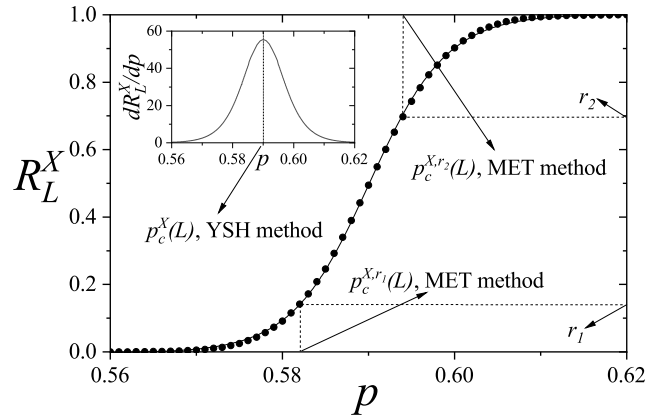


Fig. 1. Curva típica de $R_L^X(p)$ para una red finita de tamaño lineal L . Los símbolos y la línea representan los datos de simulación y la curva de ajuste (utilizando la función de error), respectivamente. A partir de la condición dada por $R_L^X(p) = r$ ($0 \leq r \leq 1$), se pueden obtener múltiples umbrales efectivos $p_c^{X,r}(L)$ (método MET). El inserto en la figura ilustra el cálculo del umbral efectivo a partir del punto de inflexión en $dR_L^X(p)/dp$ (método YSH).

[1] A. A. Torres, R. Caitano and A. J. Ramirez-Pastor *A Technique for the Estimation of Percolation Thresholds in Lattice Systems: Application to a Problem of Granular Flow Through an Orifice*. Available at SSRN: <https://ssrn.com/abstract=4415862> or <http://dx.doi.org/10.2139/ssrn.4415862> (2023).

[2] R. Caitano, B. V. Guerrero, R. E. R. González, I. Zuriguel, and A. Garcimartín, *Characterization of the Clogging Transition in Vibrated Granular Media*, Phys. Rev. Lett. **127**, 148002 (2021).

Making rare events typical in chaotic maps

Ricardo Gutiérrez¹, Adrián Canella-Ortiz², and Carlos Pérez-Espigares^{2,3}

¹Grupo Interdisciplinar de Sistemas Complejos (GISC), Departamento de Matemáticas,
Universidad Carlos III de Madrid, 28911 Leganés, Madrid, Spain

²Departamento de Electromagnetismo y Física de la Materia, Universidad de Granada, Granada 18071, Spain

³Institute Carlos I for Theoretical and Computational Physics, Universidad de Granada, Granada 18071, Spain

Dynamical fluctuations or rare events associated with atypical trajectories in chaotic maps due to specific initial conditions can be very relevant, as they may lead to stability islands or regions in phase space with other features of interest. Yet, finding such initial conditions is a daunting task precisely because of the chaotic nature of the system. In this work, we circumvent this problem by proposing a framework for finding an effective topologically-conjugate map whose typical trajectories correspond to atypical ones of the original map. This is illustrated by means of examples which focus on counterbalancing the instability of fixed points and periodic orbits, as well as on the characterization of a dynamical phase transition involving the finite-time Lyapunov

exponent. The procedure parallels that of the application of the generalized Doob transform in the stochastic dynamics of Markov chains, diffusive processes and open quantum systems, which in each case results in a new process having the prescribed statistics in its stationary state. This work thus brings chaotic maps into the increasing family of systems whose rare fluctuations can be characterized and controlled by means of a large-deviation formalism.

[1] R. Gutiérrez, A. Canella-Ortiz, and C. Pérez-Espigares, *Making rare events typical in chaotic maps*, arXiv:2304.13754 (2023).

Reentrant odd diffusion in a 2D chiral fluid, and its rotational scales

Francisco Vega Reyes^{1,2}, Álvaro Rodríguez-Rivas², and Miguel A. López-Castaño¹

¹Departamento de Física, Universidad de Extremadura, Avda. Elvas s/n 06071 Badajoz, Spain

²Instituto de Computación Científica Avanzada (ICCAEx), Universidad de Extremadura, Avda. Elvas s/n 06071 Badajoz, Spain

³Department of Physical, Chemical and Natural Systems, Pablo de Olavide University, 41013, Sevilla, Spain

Chiral fluids constitute a class of active matter characterized by persistent rotations. The state of the art of the study of active matter is now being heavily focused on this class of soft matter [1]. One major reason for this is the fact that chiral particles are present in most relevant processes of developmental biology and, by extension, in diverse systems of active matter [1, 2].

Within this context, diffusion in chiral fluids has recently brought renewed interest. This is partly due to the intriguing peculiar properties that diffusion in chiral fluids shows, and which are not present in other complex fluids nor elsewhere, like odd diffusion [3, 4], oscillatory correlations [6] and, in the case of glassy states, a reentrant diffusive regime [5] (the diffusion coefficient has been found to display a highly non-monotonous behavior, with an increasing trend at large rotational velocities).

With respect to the latter example, however, new intriguing experimental results have put in evidence that a non-monotonous behavior and a reentrant regime of the diffusion coefficient are present not only for chiral glassy states but also for chiral fluids in general [7]. See Figure 1 for a graphical depiction of this diffusive behavior. The predominant rotational scale of autocorrelation oscillations (ω_c , Y-axis) coincides with the average of particle spin ($\langle \mathbf{w} \rangle$, X-axis), which results in a linear behavior with unity slope (dashed line) for this representation. The values of ω_c have been extracted from the first peak of the fast Fourier transform (FFT) (blue curves in the insets) of the particle spin autocorrelation function (red curves in the insets). Because of the existence of a predominant rotational scale (Figure 1 a), a chiral flow with average vorticity $\bar{\omega}$ emerges [4]. This vorticity appears in fact as the control parameter of the diffusion coefficient D (Figure 1 (b), main panel). Three different regimes appear for D , as the main panel of Figure 1 (b) shows (where these regimes appear separated by vertical dashed lines). Additionally, the inset shows the evolution of the mean square displacement for a representative set of experiments. As it can be seen, these curves do not show the plateau that is typical of glassy states.

These new results may cast more light on the physical meaning of the rotational scales that induce this behavior, and the underlying mechanism for a reentrant diffusive regime to appear. Moreover, analysis of the diffusive regimes in a chiral fluid would remain incomplete unless the antisymmetric part of the corresponding diffusion ten-

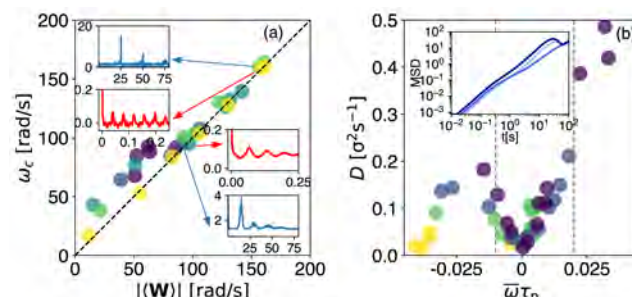


Fig. 1. (a) Critical frequencies of spin autocorrelation oscillations vs. $|\langle \mathbf{w} \rangle|$. Insets: spin autocorrelation (red) vs. time (in seconds) and its FFT (blue curve, X axis in Hz); packing fraction: $\phi = 0.03$ (upper half insets) and $\phi = 0.45$ (lower half). (b) Diffusion coefficient D vs. reduced time $\bar{\omega}\tau_p$, with $\tau_p = (m\sigma^2/T_r^*)$ (m is particle mass, T_r^* is the average of the fluctuating rotational kinetic energy).

sor (represented by the counterintuitive odd diffusion coefficient) is also analyzed.

We will discuss these matters in the present work.

-
- [1] M. J. Bowick, N. Fakhri, M. C. Marchetti and S. Ramaswamy, *Symmetry, Thermodynamics, and Topology in Active Matter*, Phys. Rev. X 12, 010501 (2022).
 - [2] B. Liebchen and D. Levian, *Chiral active matter*, EPL, 139 67001 (2022).
 - [3] C. Hargus, J. M. Epstein and K. K. Mandadapu, *Odd diffusivity of chiral random motion*, Phys. Rev. Lett. 127, 178001 (2021).
 - [4] F. Vega Reyes, M. A. Lpez-Castao. and A. Rodriguez-Rivas *Diffusive regimes in a two-dimensional chiral fluid*. Commun. Phys. 5, 256 (2022).
 - [5] V. E. Debets, H. Löwen and L. M. C. Janssen, *Glassy Dynamics in Chiral Fluids*, Phys. Rev. Lett. 130, 058201 (2023).
 - [6] M. A. López-Castaño, A. Márquez Seco, A. Márquez Seco, A. Rodríguez-Rivas and F. Vega Reyes, *Spin and velocity correlations in a confined two-dimensional fluid of disk-shaped active rotors*. Phys. Fluids 35, 033321 (2023).
 - [7] F. Vega Reyes, M. A. López-Castaño, and A. Rodriguez-Rivas *Comment on "Glassy Dynamics in Chiral Fluids"*. submitted to Phys. Rev. Lett. (2023).

Optimising search processes through heterogeneous stochastic resetting

Gregorio García-Valladares¹, Carlos A. Plata¹, Antonio Prados¹ and Alessandro Manacorda²

¹Física terica, Universidad de Sevilla, Apartado de Correos 1065, E-41080 Sevilla, Spain

²Department of Physics and Materials Science, University of Luxembourg, L-1511 Luxembourg

Stochastic resetting was introduced as a mechanism in the context of Brownian search processes [1, 2]. At certain random times, the considered system restarts its natural dynamics, forgetting the past and beginning to search again until it reaches the target—see Fig. 1 for an example of a single realisation. Specifically, working on the simplest case (one-dimensional free diffusion process between resets), it is proved that the average time to hit a fixed target, also known as the mean-first passage time (MFPT), becomes finite when a Poissonian reset process with constant rate r is incorporated.

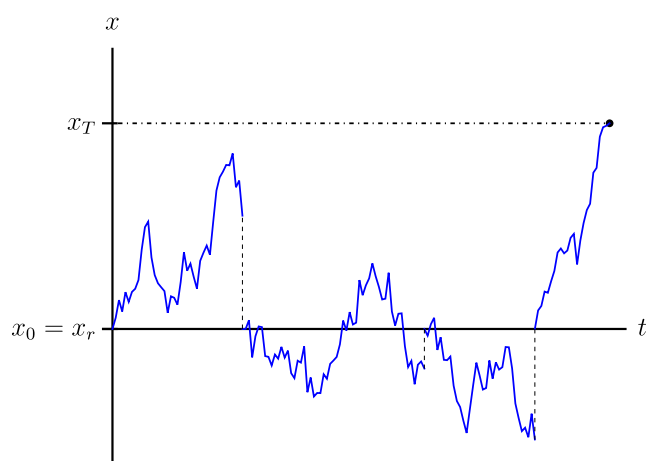


Fig. 1. Single trajectory of a free Brownian particle under the effect of stochastic resetting. The positions x_0 , x_r and x_T correspond to the initial, reset and target position, respectively.

The ability of making the MFPT finite is an appealing property that has arisen the interest of the statistical physics community, since an optimisation problem appears—the MFPT diverges in both the limits of no resetting ($r = 0$) and of infinitely frequent resetting ($r = \infty$) [1]. Further-

more, broadly speaking, search processes with stochastic resetting have many applications in a wide range of contexts beyond theoretical physics, such as animal foraging, site-binding search of biomolecules of chemical reactions [2].

Previous works about stochastic resetting usually considers a target at a fixed position for all realisations of the search process, *i.e.* a single target remains at the same position for all realisations of the search process. Nevertheless, from a fundamental point of view, the searcher (for instance, an animal [3]) does not know where its objective (food) is, *i.e.* there is some degree of randomness in the search process that renders every instance thereof unique. It is then natural to wonder how the information about the target position distribution (disorder) can guide a searcher

In this work, we address search processes with quenched (or static) disorder, *i.e.* the position of the target follows a certain static spatial distribution $p_T(x_T)$. This raises two questions: how does disorder affect the search process? Is it possible to define clever strategies for a global optimisation of MFPT, *e.g.* find an optimal space-dependent reset $r(x)$ given the target position distribution $p_T(x_T)$? This questions define an optimal control problem and its solution opens the door to new strategies for search processes of Brownian particles [4].

-
- [1] M. R. Evans and S. N. Majumdar, *Diffusion with optimal resetting*, J. Phys. A.: Math. Theor. **44**, 435001 (2011).
 - [2] M. R. Evans, S. N. Majumdar and G. Schehr, *Stochastic resetting and applications*, J. Phys. A. **53**, 193001 (2020).
 - [3] O. Berger-Tal and S. Bar-David, *Recursive movement patterns: review and synthesis across species*, Ecosphere **6**, 149 (2015).
 - [4] G. Garca-Valladares, C. A. Plata, A. Prados and A. Manacorda *Optimal resetting strategies for search processes in heterogeneous environments*, arXiv:2305.14245 (submitted to New J. Phys.).

Local balance reveals major historical events in signed networks of international relations

Fernando Diaz-Diaz¹, Paolo Bartesaghi², and Ernesto Estrada¹

¹ Institute for Cross-Disciplinary Physics and Complex Systems (IFISC, UIB-CSIC)

Campus Universitat de les Illes Balears E-07122, Palma de Mallorca, Spain

² Department of Statistics and Quantitative Methods, University of Milano - Bicocca,
Via Bicocca degli Arcimboldi 8, Milano, 20126, Italy

Structural balance [1], the tendency of graphs to avoid conflictual situations (modelled as cycles with negative parity), is widely regarded as the most important property of signed networks. Although real-world networks are rarely perfectly balanced, their deviation from balance significantly impacts their structural and dynamical properties. As such, researchers have developed indices, such as the Estrada-Benzi balance index [2], to measure the level of balance in such networks. However, an important question that has been overlooked is which nodes contribute more to the network's unbalance. This issue is particularly significant in international relations, as unbalanced nodes are often key players in international conflicts.

In this work [3], we address this question by developing a local balanced index κ_v for each node v of a signed graph with adjacency matrix A : $\kappa_v = (e^A)_{vv} / (e^{|A|})_{vv}$. This index is well-suited for understanding the role of nodes in network unbalance due to its connection with the statistical mechanics of network ensembles and its mathematical properties. For instance, it has bounds $0 < \kappa_v \leq 1$, and $\kappa_v = 1$ for every node v if and only if the network is perfectly balanced.

Equipped with this statistical-mechanical framework, we turn our attention to the network of international relations between the years 1814 and 2014 and analyze the time series of the local balance index of each country. We find that the drops in the local balance time series are strongly correlated not only with armed conflicts between countries, but also with systemic instabilities within a country, even in the absence of war (figure 1). This is the case of the revolutionary wave of 1848, where several European countries suddenly reduce their local balance despite the absence of explicit interstate conflict between them.

This index not only identifies unbalanced nodes in a network, but also sheds light on the structural causes of geopolitical instability. For example, we find that cliques made up of negative edges significantly reduce the balance of all nearby nodes, even those not directly connected to the clique. We observe the existence of these negative cliques in various regions during periods of deep crises, such as Europe in 1941, Yugoslavia through the 1990s, and the Middle East in 1961 (figure 2).

Overall, our work highlights how unbalanced subgraphs are at the core of many geopolitical conflicts. Moreover, it emphasizes the role of the networked structure of international relations in the emergence of conflicts.

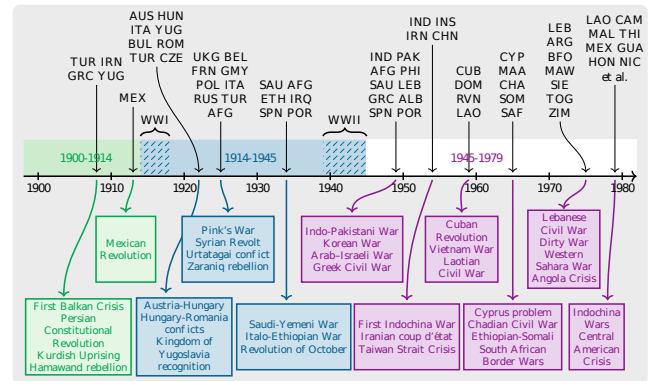


Fig. 1. Timeline of significant local balance drops. The upper half indicates the affected countries. Most balance drops correspond to important historical events (wars, revolutions, political and economic crises...).

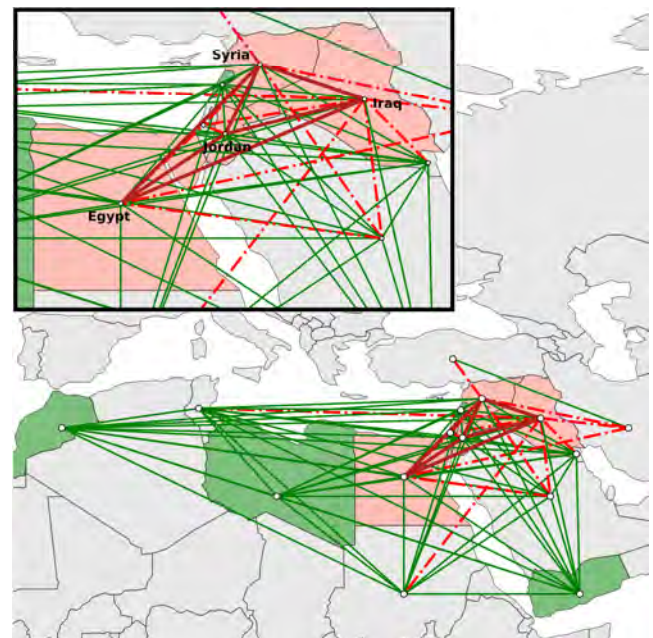


Fig. 2. Signed network depicting the international relations in the Middle East in 1961. Despite the abundance of positive links, the involved countries show a low balance index due to the presence of a negative clique, indicating that the region is highly unstable.

[1] Cartwright, Dorwin, and Frank Harary. Psychological review 63.5 (1956): 277.

[2] Estrada, Ernesto, and Michele Benzi. Physical Review E 90.4 (2014): 042802.

[3] Diaz-Diaz, Fernando, Paolo Bartesaghi, and Ernesto Estrada. "Network theory meets history. Local balance in global international relations." arXiv preprint arXiv:2303.03774 (2023). 25-27 de octubre de 2023, Pamplona

Communicability geometry reveals antagonistic factions in signed networks

Fernando Diaz-Diaz¹, and Ernesto Estrada¹

¹ Institute for Cross-Disciplinary Physics and Complex Systems (IFISC, UIB-CSIC)
Campus Universitat de les Illes Balears E-07122, Palma de Mallorca, Spain

The study of signed networks is becoming increasingly popular over the last years. One of the key challenges in this field lies in generalizing network properties while simultaneously preserving the signed nature of the edges. Specifically, the notion of distance between nodes is not clearly defined in the presence of negative connections, since the shortest-path distance ceases to be positive definite. Another significant problem in the field is the determination of the effective relation between any pair of nodes; i.e., whether they act as effective allies or adversaries. This question was answered by Harary in 1953 [1] for the case of balanced graphs (graphs where nodes can be grouped into two factions, with positive edges within the same faction and negative edges across factions). However, the question remains unsolved for the case of unbalanced graphs.

In this work, we propose a novel approach that unifies these seemingly unrelated questions through the introduction of the signed communicability, G , which is defined as the exponential of the adjacency matrix of the graph, A : $G(A) = e^A$. This function has been explored in depth for the case of unsigned networks [2], yet no extension to signed networks was done until this work. We have proved that, by taking into account all walks between two given nodes, the communicability function is able to measure the effective level of alliance or conflict between them. Additionally, it induces an Euclidean distance [3] that remains valid for signed graphs, overcoming the limitations of the traditional shortest path distance. Moreover, we have also proved that the communicability distance induces an embedding of the signed network into a high-dimensional hypersphere.

On the other hand, we have defined a communicability angle between nodes of a signed network, and mathematically proved that this angle provides better insights into the network's mesoscopic structure than other measures (figure 1). Guided by this insight, we devised a clustering technique to categorize nodes into opposing factions that works even when the network is unbalanced. Finally, we applied this technique to analyze voting patterns within the European Parliament, revealing that structural factions in this political entity diverge from conventional political party delineations.

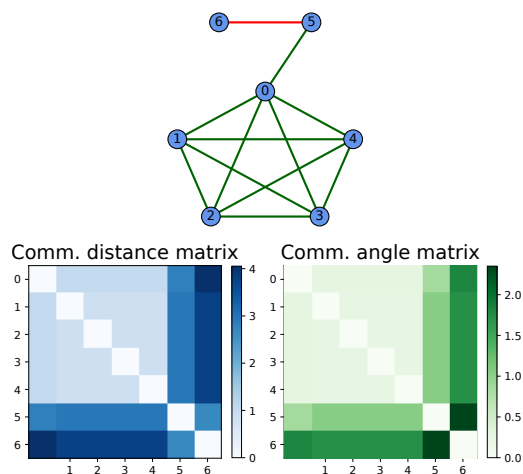


Fig. 1. Example that highlights the superiority of the communicability angle over the communicability distance (green colors represent positive edges and red colors, negative ones). The drawn graph is balanced and one of the factions is composed only by node 6, so any reliable distance measure should conclude that node 6 is farther from all other nodes compared to the distance between the remaining nodes themselves. However, the communicability distance matrix (lower left plot) situates nodes 5 and 6 closer than nodes 5 and 1. On the other hand, the communicability angle matrix (lower right plot) correctly identifies that nodes 5 and 6 are more separated than nodes 5 and 1. Consequently, the communicability angle is a more reliable distance measure.

-
- [1] Harary, Frank. "On the notion of balance of a signed graph." *Michigan Mathematical Journal* 2.2 (1953): 143-146.
- [2] Estrada, Ernesto, and Naomichi Hatano. "Communicability in complex networks." *Physical Review E* 77.3 (2008): 036111.
- [3] Estrada, Ernesto. "The communicability distance in graphs." *Linear Algebra and its Applications* 436.11 (2012): 4317-4328.

Parte X

Asistentes al Congreso

Lista de Participantes

Enrique Abad Jarillo
Centro Universitario de Mérida, Universidad de Extremadura
eabad@unex.es

Miguel Aguilar Janita
Complex Systems Group, Universidad Rey Juan Carlos,
28933 Móstoles, Madrid, Spain
miguel.aguilar@urjc.es

Javier Aguilar Sánchez
Instituto de física interdisciplinar y sistemas complejos
jvrglrshcz@gmail.com

Jacobo Aguirre Araujo
Centro de Astrobiología (CAB), CSIC-INTA, Ctra de Torrejón a Ajalvir km 4, 28850 Torrejón de Ardoz
jaguirre@cab.inta-csic.es

Adrian Aguirre-Tamaral
Centro de Biotecnología y Genómica de Plantas (CBGP, UPM-INIA)
adrian.aguirre@upm.es

Carla Alejandre Villalobos
Centro de Astrobiología (CAB), CSIC-INTA, Madrid, España
calejandre@cab.inta-csic.es

José Antonio Almanza Marrero
Institute for Cross-Disciplinary Physics and Complex Systems
joseantonio@ifisc.uib-csic.es

Alejandro Almodovar
IFISC, Instituto de Física Interdisciplinar y Sistemas Complejos (CSIC-UIB)
alex.adp.96@gmail.com

Sergio Alonso
Departamento de Física, Universitat Politècnica de Catalunya
s.alonso@upc.edu

Laciel Alonso Llanes
Departamento de Física y Matemática Aplicada, Facultad de Ciencias, Universidad de Navarra
lalonsollan@unav.es

Adolfo Alsina Lopez
Instituto Gulbenkian de Ciência
aalsina@igc.gulbenkian.pt

Edgar Alvarez Galera
Departament de Física, Universitat Politècnica de Catalunya, B4-B5 Campus Nord UPC, 08034 Barcelona
edgar.alvarez.galera@upc.edu

Miguel Álvarez-Alegría
Instituto de Física Interdisciplinar y de Sistemas Complejos (IFISC)
malvarez@ifisc.uib-csic.es

Alberto Antonioni
GISC, Universidad Carlos III de Madrid
alberto.antonioni@uc3m.es

Alex Arenas
URV
alexandre.arenas@urv.cat

Saúl Ares
Grupo Interdisciplinar de Sistemas Complejos (GISC) y Centro Nacional de Biotecnología (CNB) - CSIC
saul.ares@csic.es

Iker Atienza Diez
Centro Nacional de Biotecnología (CNB-CSIC)
iatienza@cnb.csic.es

Laia Barjuan Ballabriga
Departament de Física de la Matèria Condensada, Universitat de Barcelona
laia.barjuan@ub.edu

Guillermo Barrios Morales
Departamento de Electromagnetismo y Física de la Materia, Universidad de Granada
guillermobm@onsager.ugr.es

Carlos Miguel Barriuso Gutierrez
Universidad Complutense de Madrid - Facultad de Física - Dpto. EMFTEL, GISC
carbarri@ucm.es

Rosa María Benito Zafrilla
Universidad Politécnica de Madrid
rosamaria.benito@upm.es

Stefano Boccaletti
CNR - Institute of Complex Systems
stefano.boccaletti@gmail.com

Jean Bragard
Dept. Física y Mat. Aplicada, Facultad de Ciencias, Universidad de Navarra
jbragard@unav.es

Pierpaolo Bruscolini
Dep. de Física Teórica & Instituto BIFI, Universidad de Zaragoza, Zaragoza
pier@unizar.es

Gorka Buenvarón Campo
IFISC, CSIC-UIB, Palma, Mallorca
gbuenvaron96@gmail.com

Javier Burguete
Departamento Física y Matemática Aplicada, Universidad de Navarra
javier@unav.es

Oriol Cabanas Tirapu
Universitat Rovira i Virgili, Departament d'Enginyeria
Química
oriol.cabanas@urv.cat

Rodrigo Caitano Barbosa da Silva
Departamento de Física y Mat. Apl., Facultad de Ciencias,
Universidad de Navarra, E-31080 Pamplona
rcaitanobar@alumni.unav.es

Rubén Calvo Ibáñez
Instituto Carlos I de Física Teórica y Computacional, Uni-
versidad de Granada
rubencio1797@gmail.com

Jose Manuel Camacho Mateu
Universidad Carlos III de Madrid
joscamac@math.uc3m.es

Jaume Casademunt Viader
Universitat de Barcelona - UBICS (Universitat de Barcelona
Institute of Complex Systems)
jaume.casademunt@ub.edu

Miguel Ángel Castán Lascorz
Fundación CIRCE
macastan@fcirce.es

Mario Castro Ponce
Instituto de Investigación Tecnológica, Universidad Pontificia
Comillas
marioc@comillas.edu

Joan Josep Cerdà Pino
Universitat de les Illes Balears, Dpt. Física , IAC3
jj.cerda@uib.cat

Ricardo Chacón García
Departamento de Física Aplicada, Escuela de Ingenierías In-
dustriales, UEx e ICCAEx
rchacon@unex.es

Miguel Ángel Chamorro Burgos
Departamento de Física Atómica, Molecular y Nuclear, Uni-
versidad de Sevilla
ma.chamorro.burgos@outlook.com

Pere Colet Rafecas
Instituto de Física Interdisciplinar y Sistemas Complejos,
IFISC (CSIC-UIB)
pere@ifisc.uib-csic.es

alvaro corral cano
Centre de Recerca Matematica
acorral@crm.cat

Christian Cortes Garcia
Departamento de Biología de Sistemas, Centro Nacional de
Biotecnología, Madrid - España
chriscort05@gmail.com

Raul Cruz Hidalgo
Departamento de Física y Matemática Aplicada, Universidad
de Navarra
raulcruz@unav.es

Rodolfo Cuerno Rejado
Departamento de Matematicas y GISCI, Universidad Carlos
III de Madrid
cuerno@math.uc3m.es

José A. Cuesta Ruiz
Universidad Carlos III de Madrid
cuesta@math.uc3m.es

Mar Cuevas Blanco
Instituto de Física Interdisciplinar y Sistemas Complejos
marcuevas@ifisc.uib-csic.es

Juan De Gregorio
Instituto de Física Interdisciplinar y Sistemas Complejos
(IFISC, UIB-CSIC)
juan@ifisc.uib-csic.es

Tomás de Navascués
Departamento de Física y Matemática Aplicada de la Uni-
versidad de Navarra
tdenavascue@alumni.unav.es

Serena Di Santo
Universidad de Granada
serenadisanto@ugr.es

Adrián Díaz Acosta
Departamento de física aplicada, Universidad de Granada
adacosta@ugr.es

Javier Díaz Brañas
Departament de Física de la Matèria Condensada, Universi-
tat de Barcelona
jdiazbranas@ub.edu

Fernando Diaz Diaz
Instituto de Física Interdisciplinar y Sistemas Complejos
fernandodiaz@ifisc.uib-csic.es

Albert Diaz-Guilera
Universitat de Barcelona Institute of Complex Systems
(UBICS)
albert.diaz@ub.edu

Alvaro Domínguez
Dpto. Física Atómica, Molecular y Nuclear, Universidad de
Sevilla
dominguez@us.es

Blas Echebarria Dominguez
Departament de Física, Universitat Politècnica de Catalunya
blas.echebarria@upc.edu

Adri Escañuela Copado
Universidad de Granada
escanuela.copado@gmail.com

Pau Esteve Ferrer
Institute for Cross-Disciplinary Physics and Complex Systems (IFISC)
pesteveferrer@gmail.com

Fernando Falo Forniés
Dpto Física de la Materia Condensada, Universidad de Zaragoza
fff@unizar.es

Marina Fernández Ruz
Centro de Astrobiología CSIC-INTA
mfernandez@cab.inta-csic.es

Alessandro Fiasconaro
Depto de Física de la Materia Condensada - Universidad de Zaragoza
afiascon@unizar.es

Rosa Flaquer Galmés
Universitat Autònoma de Barcelona
rosa.flaquer@uab.cat

Mario Floría Peralta
Universidad de Zaragoza
mario.floria@gmail.com

Javier Galeano Prieto
Grupo de Sistemas Complejos, Universidad Politécnica de Madrid
javier.galeano@upm.es

Amparo Galindo
Department of Chemical Engineering, Imperial College London
a.galindo@imperial.ac.uk

Juan Gancio Vazquez
Universitat Politècnica de Catalunya
juan.gancio@upc.edu

Lucía García
UPM estudiante doctorado sistemas complejos
luciagarciaregueiro@yahoo.es

Reinaldo García García
Departamento de Física y Matemática Aplicada, Facultad de Ciencias, Universidad de Navarra
regarciag@unav.es

Gregorio García Valladares
Física Teórica, Departamento de Física Atómica, Molecular y Nuclear. Universidad de Sevilla
ggvalladares@us.es

Marina Garcia-Cardosa
Departamento de Física y Matemática Aplicada, Universidad de Navarra, Pamplona, España
mgarciacard@alumni.unav.es

Jordi Garcia-Ojalvo
Universidad Pompeu Fabra
jordi.g.ojalvo@upf.edu

Angel Garcimartín Montero
Dpto. de Física y Mat. Apl., Facultad de Ciencias, Universidad de Navarra
angel@unav.es

Vicente Garzó Puertos
Departamento de Física and Instituto de Computación Científica Avanzada (ICCAEx)
vicenteg@unex.es

Alex Giménez Romero
Instituto de Física Interdisciplinar y Sistemas Complejos
alex@ifisc.uib-csic.es

Jesús Gomez Gardeñes
Universidad de Zaragoza
gardenes@gmail.com

Miguel Ángel González Casado
Grupo Interdisciplinar de Sistemas Complejos (GISC), Universidad Carlos III de Madrid
miguelangel.gonzalezc@outlook.es

Carlos González Niño
Fundación CIRCE
cgonzalez@fcirce.es

Eva González Noya
Instituto de Química-Física Blas Cabrera, CSIC
eva.noya@iqf.csic.es

Wenceslao González-Viñas
Depto. Física y Matemática Aplicada, Facultad de Ciencias, Universidad de Navarra
wens@unav.es

Clara Granell
Departament d'Enginyeria Informàtica i Matemàtiques. ETSE. Universitat Rovira i Virgili
clara.granell@urv.cat

Raul Guantes
Departamento de Física de la Materia Condensada, Universidad Autónoma de Madrid
raul.guantes@uam.es

Ricardo Gutiérrez
Grupo Interdisciplinar de Sistemas Complejos, Dpto. Matemáticas, Universidad Carlos III de Madrid
rigutier@math.uc3m.es

Dariel Hernández Delfin
BCAM, Basque Center for Applied Mathematics
dhernandez@bcamath.org

Emilio Hernandez-Garcia
IFISC (CSIC-Universitat de les Illes Balears), Palma de Mallorca
emilio@ifisc.uib-csic.es

Pablo Ignacio Hurtado Fernández
Departamento de Electromagnetismo y Física de la Materia,
Universidad de Granada
phurtado@onsager.ugr.es

Robert Jankowski
Departament de Física de la Matèria Condensada, Universitat de Barcelona
robert.jankowski@ub.edu

Arnau Jurado Romero
Universitat Politècnica de Catalunya
arnau.jurado.romero@gmail.com

NAGI KHALIL RODRÍGUEZ
Complex Systems Group & GISC, Universidad Rey Juan Carlos, Móstoles, 28933 Madrid, Spain
cpfimt@gmail.com

Adrià Labay Mora
Institute for Cross Disciplinary Physics and Complex Systems (IFISC) UIB-CSIC
alabay@ifisc.uib-csic.es

Santiago Lamata Otín
Departamento de Física de la Materia Condensada, Universidad de Zaragoza
santiagolaot@gmail.com

Antonio Lasanta Becerra
Departamento de Álgebra. Facultad de Educación, Economía y Tecnología de Ceuta Universidad de Granada
alasant@ugr.es

Teresa Lázaro Sánchez
Universitat Rovira i Virgili
teresa.lazaro@urv.cat

Sára Lévy
Departamento de Física y Matemática Aplicada, Facultad de Ciencias, Universidad de Navarra
slevay@unav.es

Jaume Llabres Rubio
Institute for Cross-Disciplinary Physics and Complex Systems
jaumellabresr@gmail.com

Juan Manuel López Martín
Instituto de Física de Cantabria, CSIC-UC
lopez@ifca.unican.es

Javier López Pedrares
Grupo de Física No Lineal (Universidade de Santiago de Compostela)
javierlopez.pedrares@usc.es

Álvaro López-Maroto Quiñones
Centro Nacional de Biotecnología
alvaro.lopez.maroto.quinones@gmail.com

Juan Carlos Losada
Grupo de Sistemas Complejos. Universidad Politécnica de Madrid
juancarlos.losada@upm.es

David Luna Cerralbo
Universidad de Zaragoza
dluna@unizar.es

Susanna Manrubia Cuevas
Centro Nacional de Biotecnología (CSIC)
smanrubia@cnb.csic.es

David March Pons
Universitat Politècnica de Catalunya, Computer Simulation in Condensed Matter Research Group. SIMCON
david.march@upc.edu

Alvaro Marin
Physics of Fluids, University of Twente, Enschede, Netherlands
a.marin@utwente.nl

María Martínez Barbeito
Instituto de Física Interdisciplinar y Sistemas Complejos (IFISC)
maria@ifisc.uib-csic.es

Yuri Martínez Ratón
Departamento de Matemáticas, Universidad Carlos III de Madrid
yuri@math.uc3m.es

Luis Alberto Martínez Vaquero
Grupo de Sistemas Complejos y ETS Arquitectura, Universidad Politécnica de Madrid
l.martinez.vaquero@upm.es

Carles Martorell Argemí
INSTITUTO CARLOS I DE FÍSICA TEÓRICA Y COMPUTACIONAL, Universidad de Granada
carlesma@ugr.es

Cristina Masoller
Universitat Politècnica de Catalunya
cristina.masoller@upc.edu

Manuel A. Matias
Instituto de Física Interdisciplinar y Sistemas Complejos, IFISC (CSIC-UIB), Palma de Mallorca
manuel@ifisc.uib-csic.es

Pablo Maynar Blanco
Física Teórica. Universidad de Sevilla
maynar@us.es

Manuel Mayo León
Universidad de Sevilla
mmayo@us.es

Martin Maza Cuello
Departamento de Física y Matemática Aplicada, Facultad de
Ciencias, Universidad de Navarra
mmaza@unav.es

Diego M Maza Ozcoidi
Granular Media Lab. Dpto. de Física y Matemática Apli-
cada, Fac. de Ciencias, Universidad de Navarra
dmaza@unav.es

Juan José Mazo Torres
Universidad Complutense de Madrid
jmazo@ucm.es

Esteban Meca Álvarez
Departamento de Física Aplicada, Radiología y Medicina
Física, Universidad de Córdoba
esteban.meca@uco.es

Jorge Medina Hernández
Instituto de Física Interdisciplinar y Sistemas Complejos
(UIB-CSIC)
jorgemedina@ifisc.uib-csic.es

Alberto Megías Fernández
Departamento de Física, Universidad de Extremadura
albertom@unex.es

Carlos Mejía Monasterio
Universidad Politécnica de Madrid
carlos.mejia@upm.es

Gustavo Eduardo Mereles Menesse
Departamento de Electromagnetismo y Física de la materia -
Facultad de Ciencias - UGR
mereles930@gmail.com

M. Carmen Miguel
Universitat de Barcelona
carmen.miguel@ub.edu

david Míguez gomez
Universidad Autónoma de Madrid, departamento de física de
la materia condensada
davidgmiguez@gmail.com

Ana P Millan
Universidad de Granada
apmillan@ugr.es

Manuel Miranda Barrado
Instituto de Física Interdisciplinar y Sistemas Complejos
m2bmanu@gmail.com

Juan Pablo Miranda López
Universidad Complutense de Madrid, Departamento EMF-
TEL
juanpami@ucm.es

Ana María Montero Martínez
Departamento de Física, Universidad de Extremadura
anamontero@unex.es

Javier Moreno Gordo
Universidad de Zaragoza
jmorenogordo@gmail.com

Leire Moriones Imirizaldu
Universidad de Navarra
lmorionesi@unav.es

Jaume Ojer Ferrer
Departament de Física, Universitat Politècnica de Catalunya,
Campus Nord, 08034 Barcelona, Spain
jaume.ojer@upc.edu

Sara Oliver Bonafoux
Instituto de Física Interdisciplinar y Sistemas Complejos
saraoliver@ifisc.uib-csic.es

Antonio Patrón Castro
Universidad de Sevilla
apatron@us.es

Alberto Pérez Cervera
Universidad Complutense de Madrid
alberp13@ucm.es

Carlos Pérez Espigares
Departamento de Electromagnetismo y Física de la Materia.
Universidad de Granada
carlosperez@ugr.es

Hugo Pérez Martínez
Departamento de Física de la Materia Condensada, Univer-
sidad de Zaragoza
h.perez@unizar.es

Vicente Pérez Muñuzuri
Grupo de Física No Lineal. Facultad de Físicas. Universidad
de Santiago de Compostela
vperezm.usc@gmail.com

Irina Pi Jaumà
Universitat de Barcelona
ipijauma@ub.edu

Paula Pirker Díaz
Universitat de Barcelona - University of Potsdam
paula.pirker@gmail.com

Carlos A. Plata
Física Teórica, Universidad de Sevilla, Apartado de Correos
1065, E-41080 Sevilla, España
cplata1@us.es

Mihail Nicolae Popescu
Theoretical Physics, Department of Atomic, Molecular, and
Nuclear Physics, University of Sevilla
mpopescu@us.es

Antonio Prados
Física Teórica, Universidad de Sevilla
prados@us.es

Antonio Manuel Puertas López
Departamento de Química y Física. Universidad de Almería
apuertas@ual.es

Umair Rehman Raffi
Departamento de Física y Mat. Apl., Facultad de Ciencias,
Universidad de Navarra, E-31080 Pamplona
umairrehmanraffi@yahoo.com

Mathan K. Raja
Depto. Física y Matemática Aplicada, Facultad de Ciencias,
Universidad de Navarra
mraja@alumni.unav.es

Lucia Ramirez
Instituto de Física Interdisciplinar y Sistemas Complejos
luciamirez@ifisc.uib-csic.es

David Reguera López
Departament de Física de la Matèria Condensada & UBICS,
Universitat de Barcelona
dreguera@ub.edu

Fabio Revuelta Peña
Grupo de Sistemas Complejos, ETSIAAB, Universidad
Politécnica de Madrid
fabio.revuelta@upm.es

Jorge P. Rodríguez
Instituto de Física Interdisciplinar y Sistemas Complejos
(IFISC), CA UNED Illes Balears
jorge@ifisc.uib-csic.es

Juan Manuel Rodríguez Parrondo
Dep. Estructura de la Materia, Física Térmica y Electrónica-
GISC. Universidad Complutense de Madrid
parrondo@fis.ucm.es

Álvaro Rodríguez Rivas
Dpto. de Sistemas Físicos, Químicos y Naturales. Área de
Química Física. Universidad Pablo de Olavide
arodriguezrivas@upo.es

José Manuel Romero Enrique
Departamento de Física Atómica, Molecular y Nuclear, Fac-
ultad de Física, Universidad de Sevilla
enrome@us.es

Pablo Rosillo Rodes
Institute for Cross-Disciplinary Physics and Complex Sys-
tems IFISC (UIB-CSIC)
prosillo@ifisc.uib-csic.es

Ylann Rouzairé
Universitat de Barcelona, Martí i Franquès 1, Barcelona,
Spain
rouzairé.ylann@gmail.com

Miguel Ángel Rubio Álvarez
Departamento de Física Fundamental, Facultad de Ciencias,
UNED
mar@fisfun.uned.es

Miguel Ruiz Garcia
Universidad Complutense de Madrid
miguel.ruiz.garcia@ucm.es

Juan Jesus Ruiz Lorenzo
Departamento de Física. Universidad de Extremadura
ruiz@unex.es

Natalia Ruiz Pino
Universidad de Sevilla
nruiz1@us.es

Martín Saavedra López
Group of Nonlinear Physics, Faculty of Physics, University of
Santiago de Compostela. CITMAGA
martin.saavedra.lopez@usc.es

Alda Sabalic
Department of Medicine and Life Sciences, Universitat Pom-
peu Fabra
alda.sabalic@upf.edu

Alejandro Sáinz-Agost
Departamento de Física de la Materia Condensada, Univer-
sidad de Zaragoza
asainz@unizar.es

Maxi San Miguel
IFISC (UIB-CSIC), Instituto de Física Interdisciplinar y Sis-
temas Complejos
maxi@ifisc.uib-csic.es

Anxo Sánchez
GISC, Matemáticas, Universidad Carlos III de Madrid
anxo@math.uc3m.es

Silvia Santalla
Departamento de Física y GISC. Universidad Carlos III de
Madrid
silvia.santalla@uc3m.es

Andrés Santos Reyes
Departamento de Física, Universidad de Extremadura, 06006
Badajoz
andres@unex.es

Irene Sendiña Nadal
Complex Systems Group & GISC, Universidad Rey Juan
Carlos, 28933 Móstoles, Madrid, Spain
irene.sendina@urjc.es

Tomas Sintés Olives
Instituto de Física Interdisciplinar y Sistemas Complejos
(IFISC, UIB-CSIC)
tomas@ifisc.uib-csic.es

David Soriano Paños
Instituto Gulbenkian de Ciência
sorianopanos@gmail.com

Joan Térmens Cascalló
Departament de física de la materia condensada, Facultat de
física, Universitat de Barcelona
joan.termens@ub.edu

Giulio Tirabassi
Universitat Politècnica de Catalunya
giulio.tirabassi@upc.edu

Raul Toral
IFISC (Instituto de Física Interdisciplinar y Sistemas Com-
plejos), Universidad de las Islas Baleares
raul@ifisc.uib-csic.es

Joaquín J. Torres Agudo
Instituto Carlos I de Física Teórica y Computacional, Uni-
versidad de Granada, Facultad de Ciencias
jtorres@ugr.es

Ruddy Eglee Urbina Sulbarán
Universidad de Navarra, Grupos PHYSMED y Sistemas Com-
plejos
rurbina@alumni.unav.es

Pablo Valgañón
Departamento de Física de la Materia Condensada, Univer-
sidad de Zaragoza
pablovalgaruiz@gmail.com

Sylvana Varela
BFlow- Universitat Rovira i Virgili
sylvana.varela@b-flow.es

Francisco Vega Reyes
Departamento de Física e Instituto de Computación Científica
Avanzada, de Universidad de Extremadura
fvega@unex.es

Rafael Vida
Grupo Interdisciplinar de Sistemas Complejos (GISC). UC3M
rvida@math.uc3m.es

Maria Sol Vidal Saez
Department of Medicine and Life Sciences, Universitat Pom-
peu Fabra
mariasol.vidal@upf.edu

Roberta Zambrini
IFISC (Institute for Cross-Disciplinary Physics and Complex
Systems) , CSIC-UIB
roberta@ifisc.uib-csic.es

Iker Zuriguel
Departamento de Física y Matemática Aplicada, Universidad
de Navarra
iker@unav.es

